

A Structure-Function Analysis of the Φ X174 DNA Piloting Protein

by

Aaron Roznowski

Copyright © Aaron Roznowski 2019

A Dissertation Submitted to the Faculty of the

GRADUATE INTERDISCIPLINARY PROGRAM IN GENETICS

In Partial Fulfillment of the Requirements

For the Degree of

DOCTOR OF PHILOSOPHY

In the Graduate College

THE UNIVERSITY OF ARIZONA


2019

THE UNIVERSITY OF ARIZONA
GRADUATE COLLEGE


As members of the Dissertation Committee, we certify that we have read the dissertation prepared by *Aaron Roznowski*, titled *A Structure-Function Analysis of the Φ X174 DNA Piloting Protein* and recommend that it be accepted as fulfilling the dissertation requirement for the Degree of Doctor of Philosophy.




Dr. Magdalene So Date: 3/29/2019



Dr. William Montfort Date: 3/29/2019



Dr. Samuel Campos Date: 3/29/2019



Dr. Koenraad Van Doorslaer Date: 3/29/2019



Dr. Bentley Fane Date: 3/29/2019

Final approval and acceptance of this dissertation is contingent upon the candidate's submission of the final copies of the dissertation to the Graduate College.

I hereby certify that I have read this dissertation prepared under my direction and recommend that it be accepted as fulfilling the dissertation requirement.



Magdalene So
Professor
Immunobiology Date: 3/29/2019



STATEMENT BY AUTHOR

This dissertation has been submitted in partial fulfillment of the requirements for an advanced degree at the University of Arizona and is deposited in the University Library to be made available to borrowers under rules of the library.

Brief quotations from this dissertation are allowable without special permission provided that an accurate acknowledgement of the source is made. Request for permission for extended quotation from or reproduction of this manuscript in whole or in part may be granted by the copyright holder.

SIGNED: Aaron Roznowski

ACKNOWLEDGEMENTS

I would like to thank my advisor, Bentley Fane, and my former lab mate, Sarah Doore, for their help, encouragement, and infinite tolerance of my shortcomings and shenanigans.

I would also like to thank YeRin Kim for preparing the figures in chapter one and for choosing to team up with me for the remainder of our time.

TABLE OF CONTENTS

LIST OF FIGURES	7
LIST OF TABLES	9
ABSTRACT	10
INTRODUCTION	12
1.1 Problem Definition	12
1.2 Literature Review	14
1.2.1 The <i>Cystoviridae</i>	16
1.2.2 The <i>Corticoviridae</i>	20
1.2.3 The <i>Leviviridae</i>	21
1.2.4 The <i>Inoviridae</i>	23
1.2.5 The <i>Tectiviridae</i>	26
1.2.6 Order <i>Caudovirales</i> : The <i>Myo</i> -, <i>Podo</i> -, and <i>Siphoviridae</i>	27
1.2.6.1 The <i>Myoviridae</i>	28
1.2.6.2 The <i>Siphoviridae</i>	30
1.2.6.3 The <i>Podoviridae</i>	31
1.2.7 The <i>Microviridae</i>	34
1.2.8 Summary	37
1.3 Dissertation Format	39
1.4 References	41
1.5 Figure Legends	54
CHAPTER 2: STRUCTURE-FUNCTION ANALYSIS OF THE ΦX174 DNA PILOTING PROTEIN USING LENGTH-ALTERING MUTATIONS	69
2.1 Abstract	69
2.2 Introduction	70
2.3 Results	72
2.4 Discussion	82
2.5 Materials, Methods, and Acknowledgements	86
2.6 References	92
2.7 Figures and Tables	95

CHAPTER 3: MUTAGENIC ANALYSIS OF A DNA TRANSLOCATING TUBE'S INTERIOR SURFACE	109
3.1 Abstract	109
3.2 Introduction	110
3.3 Results.....	113
3.4 Discussion	121
3.5 Materials, Methods, and Acknowledgements	127
3.6 References	135
3.7 Figures and Tables	140
CHAPTER 4: RECESSIVE HOST RANGE MUTANTS AND UNSUSCEPTIBLE CELLS THAT INACTIVATE VIRIONS WITHOUT GENOME PENETRATION: ECOLOGICAL AND TECHNICAL IMPLICATIONS.....	152
4.1 Abstract	152
4.2 Introduction	153
4.3 Results.....	156
4.4 Discussion	167
4.5 Materials, Methods, and Acknowledgements	172
4.6 References	178
4.7 Figures and Tables	184
CHAPTER 5: FUTURE DIRECTIONS.....	195
5.1 Is the unique vertex induced or preordained?.....	195
5.2 How does H stimulate synthesis of viral coat protein?	200
5.3 The genome ejection model needs further testing and refinement	202
5.4 Does our model apply to other viral systems?	206
5.5: Φ X174 host range and attachment	208
5.6 References	211
5.7 Figure Legends.....	216
Full Dissertation References.....	230

LIST OF FIGURES

FIGURE 1.1 Bacteriophage virion morphotypes.....	58
FIGURE 1.2 Cystovirus $\phi 6$ penetration steps.....	59
FIGURE 1.3 Corticovirus PM2 penetration steps.....	60
FIGURE 1.4 Levivirus penetration steps.....	61
FIGURE 1.5 Inovirus Ff penetration steps	62
FIGURE 1.6 Tectivirus PRD1 penetration steps.....	63
FIGURE 1.7 Myovirus penetration steps.....	64
FIGURE 1.8 Siphovirus HK97 penetration steps.....	65
FIGURE 1.9 Podovirus penetration steps.....	66
FIGURE 1.10 Microvirus $\phi X174$ penetration steps.....	67
FIGURE 1.11 The $\phi X714$ DNA piloting protein x-ray structure.....	68
FIGURE 2.1 H protein structure and sequence.....	103
FIGURE 2.2 Assembled particles produced in wild-type, $H+14$, and $H+14 R12L$, and wild-type $\times H+14 R12L$ infected cells.....	104
FIGURE 2.3 Characterization of the $H+14$ mutant.....	105
FIGURE 2.4 Characterization of the $\Delta 7$ and $\Delta 14$ proteins in $am(H)$ or wild-type infected cells.	106
FIGURE 2.5 Characterization of $\Delta 11$ proteins in $am(H)$ or wild-type infected cells....	107
FIGURE 2.6 Viral protein levels in $am(H)$ infected cells with and without ΔH gene expression.....	108
FIGURE 3.1 Structure of the $\phi X174$ H-tube.....	146
FIGURE 3.2 Assembled particles produced in infected cells expressing mutant H constructs.....	147

FIGURE 3.3 Attachment (A) and eclipse (B) kinetics of virions containing either the wild-type or mutant H proteins.....	148
FIGURE 3.4 Viral coat protein levels in infected cells	149
FIGURE 3.5 Potassium efflux curves and genome quantification.....	150
FIGURE 3.6 Titers of progeny produced in lysis-resistant cells infected with wild-type ϕ X174, <i>su(H)-F T204I</i> , or <i>su(H)-F M330I</i>	151
FIGURE 4.1 Early microvirus infection.....	190
FIGURE 4.2 Attachment, eclipse and penetration as a function of host range.....	191
FIGURE 4.3 Amino acids sequences of the α 3 and ST-1 coat proteins.....	192
FIGURE 4.4 The location of PA substitutions within the α 3 x-ray structure.....	193
FIGURE 4.5 Structurally and genetically defined residues governing host range and extracellular virus-host interactions in ϕ X174 and α 3.....	194
FIGURE 5.1 Cryo-EM reconstructions of eclipsing ϕ X174.....	219
FIGURE 5.2 Φ X174 Morphogenetic pathway.....	220
FIGURE 5.3 Simulation of cryo-electron micrographs.....	221
FIGURE 5.4 ST-1 Bubblegram analysis.....	222
FIGURE 5.5 Viral protein and RF levels in wild-type and <i>am(H)</i> infected cells.....	223
FIGURE 5.6 Linear depiction of the ϕ X174 genetic map.....	224
FIGURE 5.7 SDS-PAGE analysis of particles produced in <i>am(H)</i> mutant-infected cells expressing cloned H genes.....	225
FIGURE 5.8 Potassium efflux curves from cells infected with Q195X mutants.....	226
FIGURE 5.9 Ribbon depiction of the calicivirus VP2 structure.....	227
FIGURE 5.10 Comparison of the ϕ X174 H-tube and the P22 portal structure.....	228
FIGURE 5.11 Ribbon depiction of the phage T4 gp19 structure.....	229

LIST OF TABLES

TABLE 2.1 Plating efficiency of H+14 and revertant mutants.....	95
TABLE 2.2 Wild-type and <i>am(H)</i> plating efficiencies on cells expressing $\Delta 7$, $\Delta 11$, or $\Delta 14$ H genes at 33°C.....	96
TABLE 2.3 Specific Infectivity (pfu/A280) of 110S-114S particles produced in <i>am(H)G7</i> and wild-type infections in cells expressing $\Delta 7$, $\Delta 11$, and $\Delta 14$ genes.....	97
TABLE 2.4 Plating efficiency and recombination rescue of $\Delta 7$, $\Delta 11$, and $\Delta 14$ mutant phage.....	99
TABLE 3.1 <i>am(H)</i> plating efficiencies on cells expressing gene H clones.....	140
TABLE 3.2 Specific infectivity of 114S particles at 37°C.....	141
TABLE 3.3 Suppressing Mutations of T244Q, M251Q, and T244Q+M251Q.....	142
TABLE 3.4 Comparison of gene F suppressing mutation activity in T244Q, M251Q, and T244Q+M251Q genetic backgrounds.....	143
TABLE 4.1: Host range of coat protein chimeric virions	184
TABLE 4.2: Expanded host range is recessive.....	185
TABLE 4.3. Plating efficiencies of PA mutants.....	186

ABSTRACT

In order to initiate an infection, bacteriophages must deliver their large, hydrophilic genomes across their host's hydrophobic cell wall. Bacteriophage ϕ X174 accomplishes this task with a set of identical DNA piloting proteins. The structure of the piloting protein's central domain was solved to 2.4 Å resolution. In it, ten proteins are oligomerized into an α -helical barrel, or tube, that is long enough to span the host's cell wall and wide enough for the circular, ssDNA to pass through. This structure was used as a guide to explore the mechanics of ϕ X174 genome delivery. In the first study, the H-tube's highly repetitive primary and quaternary structure made it amenable to a genetic analysis using in-frame insertions and deletions. Length-altered proteins were characterized for the ability to perform the protein's three known functions: participation in particle assembly, genome translocation, and stimulation of viral protein synthesis.

The tube's inner surface was altered in the second study. The surface is primarily lined with amide and guanidinium containing amino acid side chains with the exception of four sites near the tube's C-terminal end. The four sites are conserved across microvirus clades, suggesting that they may play an important role during genome delivery. To test this hypothesis and explore the general role of the amide and guanidinium containing side chains, the amino acids at these sites were changed to glutamine. The resulting mutants had a cold-sensitive phenotype at 22°C. Viral lifecycle steps were assayed in order to determine which step was disrupted by the mutant glutamine residues. The results support a model in which a balance of forces governs genome delivery: potential energy provided by the densely packaged viral genome and/or an osmotic gradient push the genome into

the cell, while the tube's inward facing residues exert a frictional force on the genome as it passes.

Bacteriophage must first identify a susceptible host prior to genome delivery. In the final study, biochemical and genetic analyses were conducted with two closely related bacteriophages, $\alpha 3$ and ST-1. Despite ~90% amino acid identity, the natural host of $\alpha 3$ is *Escherichia coli* C, whereas ST-1 is a K-12-specific phage. To determine which structural proteins conferred host range specificity, chimeric virions were generated by individually interchanging the coat, spike, or DNA pilot proteins. Interchanging the coat protein switched host range. However, host range expansion could be conferred by single point mutations in the coat protein. The expansion phenotype was recessive: mutant progeny from co-infected cells did not display the phenotype. Novel virus propagation and selection protocols were developed to isolate host range expansion mutants. The resulting genetic and structural data were consistent enough that host range expansion could be predicted, broadening the classical definition of antireceptors to include interfaces between protein complexes within the capsid.

INTRODUCTION

1.1 Problem Definition

Viral capsids have been honed by selective pressure into machines with two primary functions. They need to protect the viral genome until a suitable host cell has been found, and once located, they must efficiently penetrate the host's protective boundaries to initiate an infection. These boundaries define cellular life. Without them, a cell is incapable of accumulating biologically relevant molecules and it cannot harness electrochemical gradients. At a minimum, they consist of semi-permeable lipid membranes that provide protection from toxic molecules and foreign genetic elements, such as viruses. However, viruses have been evolving alongside their host's barriers since their inception.

Host penetration may be the most critical, yet least understood, step of the viral life cycle. In general, a virion must first locate and attach to a permissive host cell. Once bound, the virion undergoes irreversible structural changes to initiate the penetration process. The penetration event often occurs rapidly and fluidly. There are few, if any, trappable intermediate states, which often makes the process an all or nothing event from an experimental standpoint. Many of the viral penetration proteins are dynamic and must function in multiple environments, including host membranes, the cytoplasm, and the viral capsid's interior. Thus, they typically contain flexible and poorly soluble domains, making purification and/or structural determination difficult. Furthermore, mutations

intended to study a single aspect of a protein often disrupt its other functions, complicating genetic analyses.

The challenges have not blocked progress. Although questions still remain, several penetration mechanisms have been well defined. For example, the basic penetration mechanism of myoviruses, bacteriophages utilizing contractile tails, is well understood. The tail structure attaches to and penetrates the host's cell wall. Attachment triggers a series of conformational changes that propagate through the tail structure, causing its contraction. This drives a rigid tube through the cell wall, creating a conduit to the cytoplasm for genome transfer. However, several questions remain unanswered, the most enigmatic of which is what energy source drives the phage genome into the host's cytoplasm. A deeper understanding of genome delivery mechanisms may elucidate the systems' underlying biophysics. This may allow for its manipulation, which may be useful when managing or protecting prokaryotic populations used in industry or those in the environment. A more complete understanding of genome delivery could also assist drug delivery efforts, which also involve the transfer of large hydrophilic molecules across a cell's hydrophobic barrier.

The genome delivery mechanism of bacteriophage ϕ X174 has been explored in the following manuscript. Φ X174 has been used to explore DNA replication, macromolecular assembly, and protein structural relationships for approximately 50 years. Thus, it has been developed into a genetically tractable system that is easy to propagate and manipulate. The phage delivers its genome into an *Escherichia coli* host

with its DNA piloting protein. The basic delivery mechanism was not understood until a high-resolution X-ray structure of the piloting protein's central domain was solved. The proteins oligomerize into a tube structure that connects the infecting phage capsid to the host's cytoplasm. This structure was used to formulate and test several structural-functional hypotheses in an effort to understand the ϕ X174 delivery process and also the forces governing genome delivery.

1.2 Literature Review

Bacteriophages are found nearly everywhere bacteria reside and are likely the most abundant biological entities on earth, with some estimates having them outnumber their bacterial hosts 10 to 1 (1–5). Phages have been grouped into nine taxonomic families based on virion morphology and the nature of their genetic material. Each family has a distinct capsid morphology with helical, binary, or icosahedral symmetry constructed from multiple copies of one, or a few, distinct proteins. Lipid bilayers are also a component of some phage capsids, and can line the inner surface of the capsid's protein shell or envelope the capsid within a vesicle.

In order to replicate, phages must identify a susceptible, permissive host, i.e. one containing molecular machinery that is compatible with the phage system. For example, some phages rely on host chaperones to properly fold their capsid proteins (6, 7).

Infecting a host lacking the required proteins would be unproductive, therefore phage virions have evolved to bind unique molecular markers that are only present on their host's surface. The molecules recognized by virions, termed receptors, vary widely

between phage families and species. Surface receptors can include, but are not limited to, lipopolysaccharides, membrane proteins, and superstructures such as bacterial pili or flagellum (8–11). Once a host has been located, the virion must then penetrate the host's protective barriers and deliver its genetic material to the cytoplasm.

Viruses have been co-evolving with their hosts for billions of years, thus the characteristics of a host cell's external barrier have shaped viral entry mechanisms.

Animal viruses, for example, can usually interact directly with a host cell's cytoplasmic membrane. This gives them access to the cell's receptor proteins, allowing them to hijack endocytosis machinery to move across the cytoplasmic membrane (12). Plant viruses, by contrast, must infect cells encased within an impermeable cell wall. They overcome this with the help of an insect vector, whose mouthparts puncture the cell wall and inject the virus (13). Bacteriophages must also contend with cell walls of a different type. Bacterial cytoplasmic membranes are protected by a complex cell wall composed of multiple peptidoglycan and membrane layers. Cell walls come in one of two flavors, termed gram-positive or gram-negative. Gram-positive walls typically consist of a thick peptidoglycan layer facing the extracellular milieu. This is anchored to the cytoplasmic membrane by lipid-linked teichoic acids embedded in the peptidoglycan matrix. Gram-negative walls, by contrast, are composed of three layers. The outermost component is a lipid bilayer. Its external leaflet is composed of phospholipids and lipopolysaccharides (LPS), which are polysaccharide chains linked to a lipid anchor. Sandwiched between the outer and cytoplasmic membranes is the periplasm, which is an aqueous space containing a

relatively thin peptidoglycan layer and high concentrations of metabolites and proteins, including nonspecific nucleases.

The complexity of bacterial cell walls requires equally complex entry mechanisms. The mechanisms may be the most critical, yet least understood, aspect of the phage life cycle. It is a difficult process to study due to the event's short duration, lack of intermediate steps, and the involved viral proteins are difficult to experimentally characterize. They are often poorly soluble and/or are structurally dynamic. Few high-resolution structures have been determined, which impedes genetic structure-function analyses. However, studies have elucidated the basic genome delivery mechanisms used by many phage families, all of which are unique. However, there appear to be three general entry methods. In the first, membrane-containing phage virions fuse with or melt into the host's membranes. Families utilizing this method include the membrane containing *Corticoviridae* and the enveloped *Cystoviridae*. In the second method, the virion interacts closely with host cell proteins to penetrate the host. The filamentous *Inoviridae* and icosahedral *Leviviridae* appear to use this method, hijacking host pilus machinery and inner membrane proteins to gain entry. In the third method, the virion carries machinery that creates a cell wall spanning channel. This category includes the tailed *myo- siphoviridae* and *podoviridae*, the membrane containing *Tectiviridae*, and the tail-less *Microviridae*.

1.2.1 The *Cystoviridae*

Although most phage virions are composed solely of protein and nucleic acid, lipid membranes are a component of some virions. The membranes play a major role in host

penetration, and can line the capsid's inner surface or envelope the capsid within a vesicle. Members of the *Cysto*-, *Cortico*-, and *Tectiviridae* families penetrate their hosts in significantly different ways. The *Cystoviridae* will be described first. Phage in this family enclose a segmented, dsRNA genome within an enveloped icosahedral capsid (Figure 1.1a). Cystovirus $\phi 6$ was isolated from bean straw in the early 1970s and until recently was the only known cystovirus (14–16). An icosahedral image reconstruction of its virion has been determined with cryo-electron microscopy (17–19). It has three distinct layers. The genome is enclosed within a T=1 polymerase complex found at the virion's center. This complex is responsible for replication and packaging of the RNA genome and, unlike other phages, must be delivered to the host's cytoplasm intact. The polymerase complex is encased within a second, T=13, protein shell which is enveloped within a lipid bilayer containing the integral membrane proteins P6, P9, and P10. Only P6 is surface exposed. The host attachment protein, P3, binds to P6's exposed surface and protrudes away from the virion.

Cystoviruses can productively infect members of the pseudomonads and *Salmonella typhimurium* mutants with truncated LPS chains lacking heptose moieties. The virions attach to host LPS or the shafts of type IV pili (14, 15, 20). In the $\phi 6$ system, protein P3 initially binds to a host pilus (Figure 1.2a). When the pilus retracts, it pulls the virion down through the LPS to make contact with the host's outer membrane (21). P6 then mediates membrane fusion with the outer membrane (Figure 1.2b). Membrane fusion was verified *in vivo* by infecting cells with virions containing a high concentration of pyrene-labeled lipids (22). At high concentrations, the labeled lipids form fluorescence

quenching excimers. The excimers break apart and fluoresce if their intra-membrane concentration is reduced, which occurs when a labeled membrane fuses with a larger membrane. Fluorescence increased after labeled, quenched, wild-type virus was incubated with unlabeled, permissive cells. Membrane fusion was further confirmed after isolating the outer membranes of infected cells. The viral integral membrane proteins P6, P9, and P10 co-purified with the host's outer membrane fraction. Lastly, an *in vitro* membrane fusion assay was developed to determine which viral proteins triggered fusion. Membranes containing fusion promoting proteins can fuse together when brought into contact. In this assay, purified $\phi 6$ particles were brought into contact via centrifugation. Wild-type virions did not fuse together. However, fusion was observed after the viral host attachment protein P3 was removed. Its removal exposes the surface of viral membrane protein P6. Thus, the results suggest that protein P3 is removed from the virion after pilus retraction. The newly exposed portion of P6 can then initiate fusion with the host's outer membrane.

The nucleocapsid must traverse the periplasm after membrane fusion. However, the nucleocapsid is approximately 50 nm in diameter (14), which is too large to move through the periplasm's peptidoglycan network. A crosslinking analysis of the nucleocapsid showed that a lytic enzyme, protein P5, is associated with the nucleocapsid's surface (23). The enzyme was purified and characterized, and was found to have endopeptidase activity (24). However, the enzyme is thermolabile, and loses activity if incubated at high temperatures (24, 25). This property was exploited to further dissect the penetration process. Heat treated virions were capable of fusing with the outer

membrane, but became trapped in the periplasm as they could not cross the peptidoglycan network (22). Thus, it appears that P5 must create a local lesion in the peptidoglycan through which the nucleocapsid passes (24, 25). Once through the peptidoglycan, the nucleocapsid contacts the cytoplasmic membrane where a final protein, P8, interacts with the membrane (Figure 1.2c).

200 copies of protein P8 form a pseudo-T=13 lattice around the polymerase complex with P4 occupying the five-fold vertices (18, 23). P8 forms a trimer and, when released from virions at low pH, can self-assemble into shell-like structures (26). Cvirkaite-Krupovic and colleagues investigated the interaction between P8 and the cytoplasmic membrane (26). They performed membrane flotation assays to determine if a cytoplasmic membrane protein was interacting with P8. In these assays, the nucleocapsid was mixed with vesicles derived from the host's cytoplasmic membrane or mock cytoplasmic membrane vesicles produced with commercially sourced lipids. The nucleocapsid co-migrated with both host derived and mock vesicles. Unlike the host derived vesicles, the mock vesicles did not contain protein, suggesting that a nucleocapsid component was interacting directly with the lipids. The purified nucleocapsid proteins were tested in a similar manner. Proteins P2 and P8 floated with the lipid vesicles. However, P2 is buried within the nucleocapsid core, while P8 is exposed, indicating that P8 was facilitating the interaction. The protein appears to be mainly α -helical and does not contain any transmembrane helices based on sequence analysis. Thus P8 is most likely binding the lipid head groups, as it likely cannot insert itself into the cytoplasmic membrane.

Once protein P8 interacts with the head groups, the final phase of the viral entry process is initiated. The nucleocapsid proceeds into the cytoplasm in an endocytic-like manner similar to that utilized by animal viruses (Figure 1.2c and d). In the presence of an active proton motive force, nucleocapsid-bound P8 proteins create an invagination in the cytoplasmic membrane. This closes around the nucleocapsid and buds into the cytoplasm, leaving the nucleocapsid within a vesicle (27). The membrane vesicle then breaks down, releasing the polymerase complex into the cytoplasm (Figure 1.2e). This process is not fully understood. However, approximately 85% of P8 protein appears to be degraded during the entry process (27). This may disrupt the membrane vesicle, allowing viral genome replication.

1.2.2 The *Corticoviridae*

Members of the *Corticoviridae* infect species of *Pseudoalteromonas*, marine, gram-negative bacteria. Although corticoviral prophages appear to be common in marine bacterial genomes (28, 29), phage PM2 is the only characterized member. Corticoviruses package a circular, dsDNA genome into a membrane vesicle contained within a pseudo-T=21 icosahedral capsid (30–33). Thus, the envelope is an internal structure (Figure 1.1b). The capsid contains receptor binding protein P1 at each 5-fold axis of symmetry; however, the host receptor has not been identified. The presence of Ca²⁺ in the receptor binding protein and its similarity to bacterial carbohydrate binding proteins suggests that it binds host LPS (30). However, the receptor's presence on the cell surface is dependent on intracellular ATP concentration, suggesting that it may be a cell wall spanning complex (34). Utilizing an ATP-dependent receptor may be a particularly clever host

recognition mechanism, as the virion limits itself to metabolically healthy hosts that can support an infection.

The infection cycle of PM2 has not been thoroughly characterized. However, the virus does appear to utilize a unique entry mechanism. The proteinaceous capsid, composed of proteins P1 and 2, dissociates after receptor recognition (Figure 1.3b), exposing the membrane vesicle (35). Viral integral membrane protein PM10 then facilitates membrane fusion with the host's outer membrane (36). The protein's structure and mechanism of action are unknown. This event transfers the genome into the periplasm, where phage protein P7 and/or the cellular lytic factor locally degrade the peptidoglycan (34, 35). The genome must be protected from periplasmic nucleases at this time, but the mechanism is not known. Once through the peptidoglycan, a genome-associated protein creates or induces the opening of a cytoplasmic membrane pore (Figure 1.3c). This event is marked by the efflux of intracellular K^+ ions, which can only cross the cytoplasmic membrane through pores or disruptions. K^+ release is tightly correlated with genome entry in many other phage systems, particularly those that have been shown to open pores for genome delivery (37–39). It is assumed that K^+ is escaping through the channels used to transfer the phage genomes. Thus, a genome associated PM2 protein may create or induce the opening of a pore in the in the cytoplasmic membrane through which the genome moves.

1.2.3 The *Leviviridae*

Leviviruses package linear, ssRNA genomes into simple T=3 icosahedral capsids composed of two protein types (Figure 1.1d). 178 copies of the coat protein constitute the

capsid shell and a single copy of the maturation protein occupies one icosahedral vertex (40–42). Unlike most phages, levivirus genomes are not packaged into pre-formed procapsids. Instead, the genome is a participant in the capsid assembly reaction (43, 44). During assembly, the maturation protein binds specific sequences in the genome's 5' and 3' untranslated regions (45). Coat protein dimers then interact with nucleotide sequences known as packaging signals, and assemble into a capsid around the genome.

All known levivirus hosts express conjugative F pili, which are the viruses' receptor (10, 41, 46). The viral maturation protein, which can be seen protruding from the capsid in an asymmetric cryo-EM reconstruction, attaches to pili shafts (Figure 1.4a) (41, 42). Once attached, the virion undergoes its eclipse reaction: the maturation protein cleaves itself and the genome becomes RNase sensitive (47–50). The eclipse reaction may occur before the virion reaches the cell surface, as phage RNA can be removed from cells with pili after virion eclipse (51). The virion can also distinguish between host-bound and severed pili, as eclipse only occurs on the former, thus avoiding genome loss (10, 52). However, it is not known how the virion makes this distinction. After eclipse, both halves of the maturation protein remain attached to the RNA (48). This complex can be isolated and is infectious to the intact host (49, 53). After cleavage, the protein-genome complex become associated with the host cell, although the details of this step are not understood (Figure 1.4b) (47).

How the maturation protein-genome complex enters the cell is not known. There are two entry routes, directly through the host membrane or through the pilus/pilus pore complex.

The complex may remain attached to the pilus until it retracts, bringing the complex in contact with the host membrane. However, the X-ray structure of phage Q β 's maturation protein may argue against this (54). The structure is slightly similar to bacterial β -barrel containing membrane proteins, which are frequently found in bacterial outer membranes. However, it seems unlikely that the Q β maturation protein would become membrane associated. Although cleavage would alter its structure, the protein does not appear to have any transmembrane domains and hydrophobic, surface exposed residues are scant. Alternatively, the protein-genome complex may enter the inner lumen of the host's pilus. Virion attachment to the pilus appears to disrupt its structure, which may indicate that the phage is inserting its genome into the pilus's lumen (50). A cryo-EM structure of the F-pilus showed that there is a 30 Å wide channel running the length of the pilus, which is wide enough to accommodate ssDNA and ssRNA (55). Although controversial, there is some evidence suggesting ssDNA is transferred through the pilus during conjugation. DNA transfer can occur through filters that permit pili passage but prevent direct cell-cell contact. Transfer has also been observed between cells that did not appear to be in physical contact (56–58). However, the pilus lumen is not wide enough to accommodate passage of the intact Q β maturation protein. Maturation protein auto-cleavage may allow passage, but the precise timing of cleavage is not known.

1.2.4 The *Inoviridae*

Inoviruses are filamentous (Figure 1.1e) (59, 60). Numerous copies of their coat protein, p8, form a linear filament with helical symmetry around the circular, ssDNA genome (61). One end of the filament holds protein pIII, which is involved in host attachment.

Most inovirus pIII proteins attach to pili tips, although some attach to the pilus shaft (62). The most studied inoviruses, M13, fl, and fd, attach to the tips of conjugative F-pili (63, 64). Others, like CTX ϕ and IKE, attach to cholera toxin regulated pili or *E. coli* N-pili tips, respectively (65, 66). Pilus elongation is not required for infection, only the pilus tip needs to be exposed on the cell surface (67). Pilus retraction, however, is necessary to pull the virion head through the outer membrane to reach its secondary receptor, TolA, part of the TolQRA complex (68–70). This complex appears to play a role in cell envelope maintenance and cell division (71). Although phage binding may trigger pilus retraction, pili appear to randomly enter cycles of extension and retraction (72). Thus, virion bound to extended pili may simply wait until they retract.

Protein p3 plays a major role in host recognition, attachment, genome delivery and viral egress. The protein has three domains, N1, N2, and C, that are separated by glycine rich linkers (73). N2 and N1 recognize and bind the pilus tip and TolA, respectively, to initiate an infection. The x-ray structures of both N domains from phage M13 and fd have been solved (74). The two domains appear to be folded into a horseshoe-like confirmation in receptor-naive virions. N2 binds a pilus tip to initiate the infection process (Figure 1.5a). Pilus binding causes domain N1 to swing out, inducing a spontaneous prolyl cis-trans isomerization at a proline within the N1-N2 linker (75). This locks the N1 domain in its proper position for binding tolA (Figure 1.5b).

Domain C of p3 plays a role in viral egress and entry. During egress, virions are simultaneously assembled and extruded through the host's membranes without damaging

the host. Five copies of protein p3 are incorporated into the trailing end of the assembling virion. They terminate the assembly process and their C-termini release the “head” of the nascent virion from the host’s inner membrane (76). The process is run in reverse during entry. P3 domain N2 of the “head” binds the pilus and is pulled into the periplasm where domain N1 binds tolA. The subsequent entry steps were elucidated after a p3 complementation system was developed that separated the C-domain’s entry and egress functions (77). In this system, a null-p3 mutant is simultaneously complemented with two p3 constructs. One construct contains the wild-type N domains followed by a C domain fragment. The resulting protein cannot release phage from cells, but can be incorporated into filaments. The second construct contains only the full-length C domain, which allows incorporation and release. When expressed, both proteins become simultaneously incorporated into chimeric filaments. However, the filaments were not infectious unless they contained the wild-type p3 protein. The defect did not appear to affect pilus binding, suggesting that the C domain activated during entry only if it was covalently linked to the N domains. Subsequent experiments with p3 constructs containing wild-type N domains and various C domain fragments showed that an amphipathic α -helix within the C-domain is required for entry. The domain likely inserts itself into the cytoplasmic membrane during infection (Figure 1.5c) (78). Insertion may expose other hydrophobic α -helices within the protein, which also merge into the membrane, starting a chain reaction in which the trailing coat proteins also merge into the membrane (Figure 1.5d) (79, 80). It is unclear how this process is linked to genome delivery, as coat proteins become inner membrane associated in the absence of DNA penetration (79).

1.2.5 The *Tectiviridae*

The most studied tectivirus is PRD1, which packages a linear, dsDNA genome into a membrane vesicle contained within a pseudo-T=25 icosahedral capsid (Figure 1.1c) (81–84). PRD1 capsid walls are constructed with 240 trimers of protein P3 along with several accessory proteins. The vertices are occupied by pentamers of P31. Flexible host recognition proteins P2 and P5 attach to the P31 pentamers and extend outward from the capsid (85). Approximately half of the P3 proteins' amino-termini are anchored within the lipid membrane, securing the membrane to the capsid. The membrane is in a liquid crystalline phase and is approximately 50% protein by mass (86, 87). The genome is tightly packed within the membrane vesicle, and is estimated to exert ~50 atm of force on the capsid walls (88). The overall structure of tectivirus virions are similar to those of the *corticoviridae*. Both encapsidate genome containing membrane vesicles. However, their genome delivery mechanisms are quite divergent.

To initiate an infection, PRD1 protein P2 attaches to its receptor (89). Although the exact identity of the receptor is unknown, it is a component of conjugative plasmid type P, W, or N machinery (Figure 1.6a) (90). Receptor binding likely disrupts the underlying P31 pentamer, exposing the viral membrane. An extensive deletion analysis of PRD1 proteins elucidated the subsequent entry steps (91). Protein P11, which is loosely associated with the viral membrane, appears to puncture the host's outer membrane. Once a hole is opened, the viral membrane does not fuse with the host's membranes. Instead, it protrudes through and contacts the peptidoglycan. A membrane associated transglycosylase, P7, locally degrades the peptidoglycan. Virions lacking this

protein take significantly longer to enter their hosts, suggesting that the virus is not using a pre-existing opening through the peptidoglycan, like a pilus channel (92). After or while P7 opens a hole in the murein layer, the PRD1 membrane vesicle reorganizes into a tube structure connecting the virion to the cytoplasm (Figure 1.6b).

The tube structure has been visualized *in situ* (93). It emerges from a vertex at the 5-fold axis of symmetry, displacing the host interacting pentamer along with its neighboring P3 trimers. Viral membrane proteins P7, P14, P18, and P32 have been shown to play a role in tube formation (89, 91). However, their precise roles have not been defined. The density of the tube varies in the cryo-EM structure, suggesting that some of the mentioned proteins are acting as scaffolding during its formation.

Efflux of intracellular potassium is correlated with PRD1 genome delivery. The potassium is likely escaping through the same channel used to deliver the genome (94). This suggests that the membrane vesicle is ion permeable. Some of the vesicle's integral membrane proteins may be ion or water channels. If water permeability facilitates genome delivery, then the virus may harness the osmotic gradient between the cytoplasm and extracellular environment to drive the genome into the cell (95).

1.2.6 Order *Caudovirales*: The *Myo*-, *Podo*-, and *Siphoviridae*

The order *Caudovirales* contains the well-known tailed phages: the *Myo*-, *Podo*-, and *Siphoviridae*. All *Caudovirales* virions contain linear, dsDNA genomes of varying lengths. The genome is stored in an icosahedral head. A tubular, tail-like appendage is

connected to the head by a specialized portal structure occupying one of the icosahedral vertices. The distal end of the tail can be a relatively simple structure or a large multi-subunit baseplate to which multiple host-binding fibers or spikes are attached.

The *Caudovirales* families follow the same general infection pattern (96–98). The virion makes a random collision with its host and attaches via the tail's tip. The initial attachment event is a reversible reaction, as the virion can dissociate from the host without losing infectivity. *Caudovirales* reversible attachment is often mediated by tail fibers or spikes connected at or near the tip of their virion tail assemblies. These proteins usually bind to polysaccharides or membrane proteins. A series of reversible binding events may allow the virion to “walk” across the host surface to find a suitable infection site, which is often marked with a secondary receptor molecule. Once located, the virion then undergoes eclipse, or irreversible receptor binding. This commits the virion to the infection and the viral particle loses infectivity. Eclipse of *Caudovirales* virions is usually accompanied by conformational changes in the phage tail. The changes ultimately transform the tail into a cell wall spanning conduit. The genome then exits the eclipsed particle's head, flowing through the tail structure and into the cytoplasm.

1.2.6.1 The *Myoviridae*

Myoviruses utilize elaborate contractile tails to breach their host's cell wall (Figure 1.1f). Phage T4 is the most studied member, and a number of T4 tail structures have been published, including a high-resolution structure of its baseplate (99–101). The baseplate is attached to the distal end of the tail. T4 carries two sets of tail fibers, long and short,

which are both connected to the baseplate. The long tail fibers appear to make first contact with the host cell (Figure 1.7a) (100). Once attached, these fibers propagate their binding signal to the baseplate. The short tail fibers, normally folded on the baseplate's bottom, extend and bind irreversibly to the cell surface. This transition is part of a larger conformational change in the baseplate, which creates a star-shaped opening at its center. Once open, a second series of conformational changes occurs along the length of the tail.

The tail is composed of two concentric tubes, each composed of a repeating protein subunit. The outer tube is the tail sheath, whose subunits follow a six-start helical arrangement (102). The inner tube is known as the core, which consists of stacked, hexameric rings (99). Once the baseplate undergoes its conformational change, a second series of changes propagates up the tail sheath (103). The sheath proteins, originally in an imbricate arrangement, move as rigid bodies into a compressed, stacked structure (Figure 1.7b). The change reduces the length of the sheath by approximately 50%, pulling the particle's head towards the host. The tail's rigid inner core, which is connected to the head, is driven into the host. A spike complex at the tip of the tail tube, stabilized by an iron ion, is pushed through the outer membrane (104). The spike has glycosidic activity (105), and likely digests a local lesion in the peptidoglycan. Afterwards, the spike either interacts with the cytoplasmic membrane and/or dissociates, opening the distal end of the tail core. The tail tape measure proteins (TMP), stored within the tail tube, exit through this opening. The tape measure proteins run along the length of the tail, and are so named because they determine the tail's length during assembly. The T4 tape measure protein contains a predicted transmembrane domain within the middle of its sequence (100).

Thus, if the spike does not breach the inner membrane, then the tape measure protein may perform this function. The genome must then move through the tail tube and into the cytoplasm (Figure 1.7c); however, it is not known what triggers genome release.

1.2.6.2 The *Siphoviridae*

Siphoviruses utilize long, flexible tails to penetrate their host's cell wall. (Figure 1.1g).

The tails are similar to myovirus tail cores and are constructed with a stack of hexameric rings assembled around the phage's TMPs (106, 107). Siphovirus TMPs also determine the tail's length (108, 109). Each tail appears to be built around a core of six TMPs (97, 110); however, this has yet to be structurally demonstrated. The distal ends of siphovirus tails are capped with a tip complex, the structure of which varies between species. They can be relatively simple or can resemble myovirus baseplates, and both types may have attached tail fibers. Tail fibers and tip complexes contain host cell recognition proteins, which bind to host LPS, teichoic acids, or surface proteins (111–113).

After irreversibly attaching to the host, the phage must breach the outer layer of the host's cell wall. This has only been studied in gram-negative siphoviruses: λ , T5, and HK97. In each system, the TMPs are ejected from the tail after irreversible attachment (Figure 1.8b). This appears to be a necessary step in the DNA delivery process, as the TMPs prevent genome movement by occupying the tail's central channel. Some TMPs also contain predicted transmembrane domains and domains resembling those that digest peptidoglycan, both of which would assist cell wall breaching.

There is evidence that the TMPs interact with components of the cell wall and form channels during infection. A purified segment of the T5 TMP digested peptidoglycan and triggered fusion of unilamellar vesicles (114, 115). Phage HK97 has been shown to require a host periplasmic protein, FkpA, and an inner membrane protein PtsG, to breach the host's inner membrane. The requirements of both proteins are determined by HK97's TMP, suggesting that the TMP is interacting with the specified host proteins (116). The phage λ TMP may also be interacting with host envelope proteins (117, 118). Mutations in a host inner membrane protein, manY, prevented genome delivery. Phage mutants were isolated that could plaque on the unsusceptible cell line, and mutations conferred changes in either the TMP or tail tip proteins. Collectively, this suggests that the siphovirus TMPs are ejected from the tail and it creates a genome translocating channel across the host's cell wall (Figure 1.8c).

1.2.6.3 The *Podoviridae*

Podoviruses have short, stubby tails. Well studied podoviruses include P22, T7, and ϕ 29. The tail assembly contains host binding proteins projecting away from the virion's head, referred to as tailspikes, although some species utilize fibers like those seen on siphoviruses (119). Like the other tailed phages, these structures bind host LPS or surface proteins (120, 121). In some cases, the tail assembly carries two or more types of tailspike, each type capable of binding receptors of different hosts (122). The different spikes are arranged symmetrically around the tail's central axis in an alternating pattern. Spikes also can have enzymatic activity, allowing the virion to digest its way through bacterial capsules and dense, extended LPS arrays to the host's surface (123, 124). Once

through, the virion can engage the secondary receptor with the tail's central "knob" (9, 125). The knob likely undergoes a structural change and becomes membrane associated (126). This opens the tail's central channel and may form a pore through the host's outermost membrane (Figure 1.9a). Proteins stored within the virion, termed ejection proteins, are then released into the cell wall (Figure 1.9b) (127–130).

Genetic analyses of virion proteins with dynamic extracellular roles, such as ejection proteins, are more complex than analyses of intracellular viral proteins. In order to gain detailed functional insights, mutations cannot result in absolute lethal phenotypes, i.e. mutations can block incorporation during virion morphogenesis or, if incorporated, the mutant protein can be entirely non-functional. By contrast, mutations conferring conditional lethal phenotypes, such as temperature sensitivity, can reveal temporal and functional details that are obscured in absolute lethal phenotypes. One of the first ejection proteins to be analyzed was gp16 of phage P22. Ten to twenty copies of Gp16 are found within the virion (131). They become associated with phage proheads during virion assembly, yet they do not play a structural or scaffolding role, as null-gp16 infections produce normal, packaged phage particles. However, the particles are not infectious. Its function was not determined until a temperature sensitive gp16 (*gp16-ts*) mutant was isolated (128).

Gp16-ts was used in temperature shift assays to determine when gp16 was active during the infection (127, 128). The infection cycle's pre- and post-genome penetration phases were separated by a rapid temperature shift. For example, virions were added to cells at

the permissive temperature. After ten minutes, the cells were then quickly shifted to the restrictive temperature. This allows adsorption and genome penetration to occur permissively, while genome replication and assembly occur restrictively. Cells were monitored for infection products to assess when the temperature sensitive gp16 failed to function. Infection products accumulated when *gp16-ts* infections were initiated at the permissive temperature. A subsequent shift to the restrictive temperature did not affect intracellular steps of the viral life cycle. By contrast, infections initiated at the restrictive temperature were blocked. No phage products were observed, even after shifting to permissive conditions, suggesting that gp16 played a role during the early infection steps. Further experiments showed that *gp16-ts* particles could adsorb to cells at the restrictive temperature and a portion of the genome was released, however it was degraded by host enzymes.

Co-infections were performed with *gp16-ts* and phage containing wild-type gp16 to determine if the protein could be provided in *trans*. Cells were co-infected at the restrictive temperature with *gp16-ts* and a gp16 donor phage. The gp16 donor was incapable of genome synthesis, thus infection products are only produced if *gp16-ts* entered a cell. Infection products were observed when gp16 was provided in *trans*, suggesting it is ejected from the virion and plays a role in genome delivery. Later work showed that purified gp16 could become associated with membrane fractions. Purified gp16 could also trigger the release of dye from vesicles, suggesting it forms a pore for genome transport (130). Gp16 and two other proteins, gp7 and gp20, are also ejected prior to genome release (129). Neither protein becomes membrane associated,

suggesting that they may function in the gram-negative host's periplasm or possibly the cytoplasm. A low-resolution structure of phage Sf6's gp20 homolog showed that it forms 25 Å wide, 150 Å long, decameric channel (132). This may bridge the gap between the host's membranes, like that seen in the cryo-EM tomography structure of phage T7 infecting *E. coli* minicells (119). In this structure, it appears that proteins originally within the virions head are ejected and form a tubular structure under the virion spanning the minicell's membranes.

1.2.7 The *Microviridae*

The *Microviridae* family is composed of two subfamilies, the *Gokusho-* and *phixvirinae*. Both subfamilies package circular, ssDNA genomes within small, T=1 icosahedral capsids. Very little is known about *Gokushovirinae* life cycles, especially their mechanism of genome delivery. By contrast, the *phixvirinae* have been studied extensively. The subfamily is composed of three genera, named for their canonical members $\alpha 3$, G4, and $\phi X174$. They infect rough strains of *E. coli* and *Salmonella enterica*, strains expressing short LPS molecules consisting only of the lipid A moiety with its attached backbone and core saccharides. Host LPS molecules are the viruses' only known receptor (8, 133).

Phixvirinae capsids are composed of four structural proteins. Sixty copies of the coat (F protein), major spike (G protein), and DNA binding (J protein) proteins compose the capsid (134–136). The fourth protein, the DNA piloting protein (H protein), shares features with ejection proteins. Each virion contains ten to twelve copies of H protein and

they are ejected from the capsid during the infection event. Their location(s) within the virion have not been determined, as they cannot be seen in X-ray or cryo-EM virion structures, which were determined using averaging techniques (134, 136, 137). By contrast, the other capsid proteins are icosahedrally ordered and their structures have been determined. The capsid wall is composed of F protein. The highly basic J protein binds to a cleft on the inner surface of capsid wall, and is thought to neutralize the negatively charged genome. Five copies of G protein decorate the exterior surface of each five-fold axis of symmetry, creating a pentagonal frustum rising 32 Å above the coat proteins. The G pentamer makes few direct contacts with the underlying coat F pentamer, however several indirect contacts are made through coordinated water molecules.

Both F and G proteins play a role in host attachment. As with other phages, two distinct attachment steps are required to initiate the infection process, reversible and irreversible attachment. Reversible attachment may be mediated by protein F (Figure 1.10a). The exterior surface of F contains a Ca^{2+} dependent sugar binding site, which may bind to host LPS sugar moieties to initiate the infection process (138). Although this site is conserved in all *Phixvirinae* clades, there is no direct evidence this site is involved in host attachment. If this binding event is reversible, it may allow the virus to “roll” across the cell surface until a suitable infection site has been located or multiple sugar binding sites become occupied. Irreversible attachment may then occur after host LPS molecules interact with the F-G interface, as host range expanding mutations map to this region (Chapter 4) (139).

Irreversible attachment, also called the eclipse reaction, is the committed infection step. Two cryo-EM structures of eclipsing ϕ X174 particles bound to an LPS containing bilayer have been determined, one of a still-packaged particle and the other post-genome release (140). In the structures, one of the virion's 5-fold axes of symmetry is attached to the LPS-containing bilayer. The G-spike has been displaced from this vertex, thus the virion is attached via its coat proteins (Figure 1.10b). The location of the displaced G pentamer is unknown. Density from the ssDNA genome can be seen within the interior of the capsid, which is not uniformly distributed. There is a void above the attached vertex. This region may contain an oligomer of DNA piloting proteins, whose role in the infection will be discussed below. In the second structure, which lacks DNA density, the attached coat protein's structure is altered. This alteration opens a gate at the 5-fold axis. The DNA piloting proteins and genome presumably exit the capsid through this opening.

The DNA piloting protein (H protein) is responsible for "piloting" the phage genome through the host's treacherous cell wall and into the cytoplasm (141, 142). H accomplishes this task by creating a channel through the host's cell wall (Figure 1.10c). The structure of the ϕ X174's H protein channel has been determined (143). In it, residues 151 to 272 of 10 H proteins are oligomerized into an α -helical barrel (Figure 1.11, PDB ID: 4JPP). The barrel, or tube, is 170 Å long with an internal diameter of 22 Å. This is long enough to span the host's membranes and wide enough for two, intercalated strands of ssDNA to pass through (144). The barrel has two domains separated by a kink-like structure. In domain A, the α -helices contain an 11 residue semi-repeating unit that is three helical turns in length (11/3). This switches to a 7/2 semi-repeating unit in domain

B. The inner surface of the tube is lined with asparagine, glutamine, and arginine side chains. These side chains contain amide and guanidinium moieties, which are frequently seen interacting with nucleic acids in other protein structures (145–148). This arrangement may be a common feature of polynucleotide translocating tubes. The podovirus P22 portal, which is the opening through which the dsDNA genome enters and exits the capsid, also features an α -helical barrel with dimensions similar to the H-tube. This region of the protein contains semi-repeating hendecad and heptad motifs, demarcated by glutamine, asparagine, and arginine residues (143). However, it is not known if these residues line the tube's inner surface, as the portal structure was determined to 7.5 Å resolution. The H-tube arrangement is also seen in the portal structure of feline calicivirus, a ssRNA virus (149). In the structure, twelve α -helices emerge from the portal and form a tube with a minimum internal diameter of 17 Å. Several glutamine, asparagine, and arginine residues as well as acidic residues line the tube's inner surface. The tube is much shorter than that formed by H proteins, however the calicivirus only needs to penetrate an endosomal membrane and not a gram-negative cell wall.

1.2.8 Summary

Bacteriophage have been co-evolving with their hosts for billions of years, resulting in several unique host penetration mechanisms. The mechanisms can be roughly grouped into three categories. In the first, the penetration process is initiated when the virion's lipid membranes fuse with the host's outer membrane. Cystoviruses use this method to pass their entire nucleocapsid through the host's cell wall, while corticoviruses only

transport their genome. In the second category, the virion interacts with several host proteins to gain access to the cytoplasm. Although the data is sparse at this time, levivirus virions may interact extensively with the host's pilus machinery, while inoviruses rely on the host's TolQRA system to cross the cytoplasmic membrane. The tailed siphoviruses may also fall within this category, as their TMPs interact with both periplasmic and inner membrane proteins. Lastly, virions in the final category carry proteins capable of forming trans-cell wall channels. The channel construction mechanisms are also diverse.

Tectiviruses use an unusual mechanism in which their virion's internal lipid vesicle is extruded to form a trans-cell wall channel. Proteins associated with the tectivirus virion membrane assist in channel formation and prevent membrane fusion. By contrast, myo-, sipho-, and podovirus virions all carry tail structures that breach the host's membrane. The myovirus tail can span multiple membranes, while the podo- and siphovirus tails are used to eject channel forming proteins through the host's outer membrane. Finally, the tail-less ϕ X174-like viruses create a channel with their DNA-piloting protein.

Although the order of penetration events has been discerned for most bacteriophage families, one question still remains: what force or forces move the phage genomes through the cell wall? Several mechanisms have been proposed to explain ejection from icosahedral capsids (95). The most popularized mechanism points out that the genome strands are placed in close proximity. The strands repel each other, and this repulsive force pushes the genome out of the capsid once a channel opens. An alternative model downplays the role of repulsive forces. Instead, it proposes that osmotic forces power genome movement. The genome becomes partially dehydrated during packaging, which

creates an osmotic gradient across the capsid. Once a channel to the cytoplasm opens, water will flow down its osmotic gradient, i.e. through the capsid and into the cytoplasm. This rehydrates and drags the genome through the channel.

Addressing this final question is difficult, as a well-defined *in vivo* system has not been developed. However, the high-resolution structure of the ϕ X174 H-channel has provided new details of a DNA translocating channel. This system has been used to explore a possible balance of forces governing genome delivery in the ϕ X174 system.

1.3 Dissertation Format

Chapter 1, the introduction, has described the different host penetration processes used by nine phage families. Although the processes are diverse and some families use an entirely unique entry mechanism, there are common features, such as the use of peptidoglycan degrading enzymes, ejection proteins, and construction of cell-wall spanning channels. This information is meant to assist the reader in understanding how the following microvirus studies fit within a broader context.

Chapter 2 has been accepted with minor revisions to the Journal of Virology. The length of the ϕ X714 DNA piloting protein was altered in the first investigation. The repeating nature of the protein's hendecad and heptad motifs suggested that they could be deleted or duplicated without abolishing function. This approach was used to address whether there are restrictions on the piloting protein tube's length.

Chapter 3 is yet to be submitted to a journal. However, it is a full body of work that is fit for publication. The characteristics of the piloting protein tube's inner surface are conserved across *phixvirinae* clades. 18 of the 23 inward facing side chains belong to an arginine, glutamine, or asparagine residue, all of which contain amide or guanidinium groups. These groups can form hydrogen bonds with DNA nucleotides, suggesting that they may be regulating genome release. The remaining residues are clustered near the tube's C-terminal opening. These residues were replaced with glutamine and subjected to a genetic and biochemical analysis to discern the importance of this region and the inward facing side chains in general.

Chapter 4 has been accepted with minor revisions to The Journal of Virology. The viral proteins responsible for determining *phixvirinae* host range were identified. Two phixviruses, $\alpha 3$ and St-1, are over 90% identical on the nucleotide level. However, $\alpha 3$ exclusively infects *E. coli* C, while St-1 infects *E. coli* K12. Host range expansion mutants were isolated with novel selection protocols. The changes conferred by the mutations were analyzed and used to identify the protein regions dictating the viruses' host range.

Chapter 5, future directions, discusses the new questions raised by the current results and possible ways to address them.

1.4 References

1. Wommack KE, Colwell RR. 2000. Virioplankton: Viruses in Aquatic Ecosystems. *Microbiol Mol Biol Rev* 64:69–114.
2. Kimura M, Jia ZJ, Nakayama N, Asakawa S. 2008. Ecology of viruses in soils: Past, present and future perspectives. *Soil Sci Plant Nutr* 54:1–32.
3. Suttle CA. 2005. Viruses in the sea. *Nature* 437:356–361.
4. Breitbart M, Rohwer F. 2005. Here a virus, there a virus, everywhere the same virus? *Trends Microbiol* 13:278–284.
5. Breitbart M, Hewson I, Felts B, Mahaffy JM, Nulton J, Salamon P, Rohwer F. 2003. Metagenomic Analyses of an Uncultured Viral Community from Human Feces. *J Bacteriol* 185:6220–6223.
6. Georgopoulos CP, Hendrix RW, Kaiser AD, Wood WB. 1972. Role of the Host Cell in Bacteriophage Morphogenesis: Effects of a Bacterial Mutation on T4 Head Assembly. *Nat New Biol* 239:38–41.
7. Georgopoulos CP, Hendrix RW, Casjens SR, Kaiser AD. 1973. Host participation in bacteriophage lambda head assembly. *J Mol Biol* 76:45–60.
8. Jazwinski SM, Lindberg AA, Kornberg A. 1975. The lipopolysaccharide receptor for bacteriophages ϕ X174 and S13. *Virology* 66:268–282.
9. Parent KN, Erb ML, Cardone G, Nguyen K, Gilcrease EB, Porcek NB, Pogliano J, Baker TS, Casjens SR. 2014. OmpA and OmpC are critical host factors for bacteriophage Sf6 entry in *Shigella*. *Mol Microbiol* 92:47–60.
10. Valentine RC, Strand M. 1965. Complexes of F-Pili and RNA Bacteriophage. *Science* 148:511–513.
11. Lovett PS. 1972. PBP1: A flagella specific bacteriophage mediating transduction in *Bacillus pumilus*. *Virology* 47:743–752.
12. Nicola A V., Aguilar HC, Mercer J, Ryckman B, Wiethoff CM. 2013. Virus Entry by Endocytosis. *Adv Virol* 2013:1–2.
13. Dáder B, Then C, Berthelot E, Ducouso M, Ng JCK, Drucker M. 2017. Insect transmission of plant viruses: Multilayered interactions optimize viral propagation. *Insect Sci* 24:929–946.

14. Bamford DH, Palva ET, Lounatmaa K. 1976. Ultrastructure and Life Cycle of the Lipid-containing Bacteriophage $\Phi 6$. *J Gen Virol* 32:249–259.
15. Hoogstraten D, Qiao X, Sun Y, Hu A, Onodera S, Mindich L. 2000. Characterization of $\Phi 8$, a Bacteriophage Containing Three Double-Stranded RNA Genomic Segments and Distantly Related to $\Phi 6$. *Virology* 272:218–224.
16. Vidaver AK, Koski RK, Van Etten JL. 1973. Bacteriophage $\Phi 6$: a Lipid-Containing Virus of *Pseudomonas phaseolicola*. *J Virol* 11:799–805.
17. Jääliñoja HT, Huiskonen JT, Butcher SJ. 2007. Electron Cryomicroscopy Comparison of the Architectures of the Enveloped Bacteriophages $\Phi 6$ and $\Phi 8$. *Structure* 15:157–167.
18. Huiskonen JT, de Haas F, Bubeck D, Bamford DH, Fuller SD, Butcher SJ. 2006. Structure of the Bacteriophage $\Phi 6$ Nucleocapsid Suggests a Mechanism for Sequential RNA Packaging. *Structure* 14:1039–1048.
19. de Haas F, Paatero AO, Mindich L, Bamford DH, Fuller SD. 1999. A symmetry mismatch at the site of RNA packaging in the polymerase complex of dsRNA bacteriophage $\phi 6$. *J Mol Biol* 294:357–372.
20. Mäntynen S, Laanto E, Kohvakka A, Poranen MM, Bamford JKH, Ravantti JJ. 2015. New enveloped dsRNA phage from freshwater habitat. *J Gen Virol* 96:1180–1189.
21. Romantschuk M, Bamford DH. 1985. Function of Pili in Bacteriophage $\Phi 6$ Penetration. *J Gen Virol* 66:2461–2469.
22. Bamford DH, Romantschuk M, Somerharju PJ. 1987. Membrane fusion in prokaryotes: bacteriophage $\phi 6$ membrane fuses with the *Pseudomonas syringae* outer membrane. *EMBO J* 6:1467–1473.
23. Hantula J, Bamford DH. 1988. Chemical crosslinking of bacteriophage $\phi 6$ nucleocapsid proteins. *Virology* 165:482–488.
24. Caldentey J, Bamford DH. 1992. The lytic enzyme of the *Pseudomonas* phage $\phi 6$. Purification and biochemical characterization. *Biochim Biophys Acta - Protein Struct Mol Enzymol* 1159:44–50.
25. Mindich L, Lehman J. 1979. Cell Wall Lysin as a Component of the Bacteriophage $\Phi 6$ Virion. *J Virol* 30:489–496.
26. Cvirkaitė-Krupovic V, Poranen MM, Bamford DH. 2010. Phospholipids act as secondary receptor during the entry of the enveloped, double-stranded RNA bacteriophage $\Phi 6$. *J Gen Virol* 91:2116–2120.

27. Romantschuk M, Olkkonen VM, Bamford DH. 1988. The nucleocapsid of bacteriophage $\Phi 6$ penetrates the host cytoplasmic membrane. *EMBO J* 7:1821–1829.
28. Krupovič M, Bamford DH. 2007. Putative prophages related to lytic tailless marine dsDNA phage PM2 are widespread in the genomes of aquatic bacteria. *BMC Genomics* 8:236.
29. Leigh BA, Breitbart M, Oksanen HM, Bamford DH, Dishaw LJ. 2018. Genome Sequence of PM2-Like Phage Cr39582, Induced from a *Pseudoalteromonas* sp. Isolated from the Gut of *Ciona robusta*. *Genome Announc* 6.
30. Abrescia NGA, Grimes JM, Kivelä HM, Assenberg R, Sutton GC, Butcher SJ, Bamford JKH, Bamford DH, Stuart DI. 2008. Insights into Virus Evolution and Membrane Biogenesis from the Structure of the Marine Lipid-Containing Bacteriophage PM2. *Mol Cell* 31:749–761.
31. Camerini-Otero R., Franklin R. 1972. Structure and synthesis of a lipid-containing bacteriophage. *Virology* 49:385–393.
32. Espejo RT, Canelo ES. 1968. Origin of Phospholipid in Bacteriophage PM2. *J Virol* 2:1235–1240.
33. Kivelä HM, Männistö RH, Kalkkinen N, Bamford DH. 1999. Purification and Protein Composition of PM2, the First Lipid-Containing Bacterial Virus To Be Isolated. *Virology* 262:364–374.
34. Cvirkaitė-Krupovič V, Krupovič M, Daugelavičius R, Bamford DH. 2010. Calcium ion-dependent entry of the membrane-containing bacteriophage PM2 into its *Pseudoalteromonas* host. *Virology* 405:120–128.
35. Kivela HM, Daugelavicius R, Hankkio RH, Bamford JKH, Bamford DH. 2004. Penetration of Membrane-Containing Double-Stranded-DNA Bacteriophage PM2 into *Pseudoalteromonas* Hosts. *J Bacteriol* 186:5342–5354.
36. Kivela HM, Madonna S, Krupovic M, Tutino ML, Bamford JKH. 2008. Genetics for *Pseudoalteromonas* Provides Tools To Manipulate Marine Bacterial Virus PM2. *J Bacteriol* 190:1298–1307.
37. Berrier C, Bonhivers M, Letellier L, Ghazi A. 2000. High-conductance channel induced by the interaction of phage lambda with its receptor maltoporin. *FEBS Lett* 476:129–133.
38. Shapira A, Giberman E, Kohn A. 1974. Recoverable potassium fluxes variations following adsorption of T4 phage and their ghosts on *Escherichia coli* B. *J Gen*

Virology 23:159–171.

39. Boulanger P, Letellier L. 1992. Ion channels are likely to be involved in the two steps of phage T5 DNA penetration into *Escherichia coli* cells. *J Biol Chem* 267:3168–72.
40. Koning RI, Gomez-Blanco J, Akopjana I, Vargas J, Kazaks A, Tars K, Carazo JM, Koster AJ. 2016. Asymmetric cryo-EM reconstruction of phage MS2 reveals genome structure in situ. *Nat Commun* 7:12524.
41. Dent KC, Thompson R, Barker AM, Hiscox JA, Barr JN, Stockley PG, Ranson NA. 2013. The Asymmetric Structure of an Icosahedral Virus Bound to Its Receptor Suggests a Mechanism for Genome Release. *Structure* 21:1225–1234.
42. Toropova K, Stockley PG, Ranson NA. 2011. Visualising a Viral RNA Genome Poised for Release from Its Receptor Complex. *J Mol Biol* 408:408–419.
43. Rolfsson Ó, Middleton S, Manfield IW, White SJ, Fan B, Vaughan R, Ranson NA, Dykeman E, Twarock R, Ford J, Cheng Kao C, Stockley PG. 2016. Direct Evidence for Packaging Signal-Mediated Assembly of Bacteriophage MS2. *J Mol Biol* 428:431–448.
44. Stockley PG, White SJ, Dykeman E, Manfield I, Rolfsson O, Patel N, Bingham R, Barker A, Wroblewski E, Chandler-Bostock R, Weiß EU, Ranson NA, Tuma R, Twarock R. 2016. Bacteriophage MS2 genomic RNA encodes an assembly instruction manual for its capsid. *Bacteriophage* 6:e1157666.
45. Hung PP, Ling CM, Overby LR. 1969. Self-Assembly of Qbeta and MS2 Phage Particles: Possible Function of Initiation Complexes. *Science* (80-) 166:1638–1640.
46. Date T. 1979. Kinetic Studies of the Interaction between MS2 Phage and F Pilus of *Escherichia coli*. *Eur J Biochem* 96:167–175.
47. Krahn PM, O’Callaghan RJ, Paranchych W. 1972. Stages in phage R17 infection VI. Injection of A Protein and RNA into the Host Cell. *Virology* 47:628–637.
48. Shiba T, Suzuki Y. 1981. Localization of A protein in the RNA-A protein complex of RNA phage MS2. *Biochim Biophys Acta - Nucleic Acids Protein Synth* 654:249–255.
49. Leipold B, Hofschneider PH. 1975. Isolation of an infectious RNA-A-protein complex from the bacteriophage M12. *FEBS Lett* 55:50–52.
50. Paranchych W, Krahn PM, Bradley RD. 1970. Stages in phage R17 infection V. Phage Eclipse and the Role of F Pili. *Virology* 41:465–473.

51. Silverman PM, Valentine RC. 1969. The RNA Injection Step of Bacteriophage f2 Infection. *J Gen Virol* 4:111–124.
52. Danziger RE, Paranchych W. 1970. Stages in phage R17 infection III. Energy Requirements for the F-pili Mediated Eclipse of Viral Infectivity. *Virology* 40:554–564.
53. Shiba T, Miyake T. 1975. New type of infectious complex of E. coli RNA phage. *Nature* 254:157–158.
54. Rumnieks J, Tars K. 2017. Crystal Structure of the Maturation Protein from Bacteriophage Q β . *J Mol Biol* 429:688–696.
55. Wang YA, Yu X, Silverman PM, Harris RL, Egelman EH. 2009. The Structure of F-Pili. *J Mol Biol* 385:22–29.
56. Harrington LC, Rogerson AC. 1990. The F pilus of Escherichia coli appears to support stable DNA transfer in the absence of wall-to-wall contact between cells. *J Bacteriol* 172:7263–7264.
57. Ou JT, Anderson TF. 1970. Role of Pili in Bacterial Conjugation. *J Bacteriol* 102:648–654.
58. Babic A, Lindner AB, Vulic M, Stewart EJ, Radman M. 2008. Direct Visualization of Horizontal Gene Transfer. *Science* (80-) 319:1533–1536.
59. Goldbourn A, Gross BJ, Day LA, McDermott AE. 2007. Filamentous Phage Studied by Magic-Angle Spinning NMR: Resonance Assignment and Secondary Structure of the Coat Protein in Pf1. *J Am Chem Soc* 129:2338–2344.
60. Marvin DA, Welsh LC, Symmons MF, Scott WRP, Straus SK. 2006. Molecular Structure of fd (f1, M13) Filamentous Bacteriophage Refined with Respect to X-ray Fibre Diffraction and Solid-state NMR Data Supports Specific Models of Phage Assembly at the Bacterial Membrane. *J Mol Biol* 355:294–309.
61. Marvin DA, Symmons MF, Straus SK. 2014. Structure and assembly of filamentous bacteriophages. *Prog Biophys Mol Biol* 114:80–122.
62. Bradley DE, Whelan J. 1989. Escherichia coli tolQ Mutants Are Resistant to Filamentous Bacteriophages That Adsorb to the Tips, not the Shafts, of Conjugative Pili. *Microbiology* 135:1857–1863.
63. Webster RE. 1996. Biology of the Filamentous Bacteriophage, p. 1–20. *In Phage Display of Peptides and Proteins: A Laboratory Manual*. Elsevier.

64. Lorenz SH, Jakob RP, Weininger U, Balbach J, Dobbek H, Schmid FX. 2011. The Filamentous Phages fd and IF1 Use Different Mechanisms to Infect *Escherichia coli*. *J Mol Biol* 405:989–1003.
65. Heilpern AJ, Waldor MK. 2003. PIII CTX, a Predicted CTXphi; Minor Coat Protein, Can Expand the Host Range of Coliphage fd To Include *Vibrio cholerae*. *J Bacteriol* 185:1037.
66. Endemann H, Bross P, Rasched I. 1992. The adsorption protein of phage IKe. Localization by deletion mutagenesis of domains involved in infectivity. *Mol Microbiol* 6:471–478.
67. Novotny CP, Fives Taylor P. 1974. Retraction of F pili. *J Bacteriol* 117:1306–1311.
68. Sun TP, Webster RE. 1986. fii, a bacterial locus required for filamentous phage infection and its relation to colicin-tolerant tolA and tolB. *J Bacteriol* 165:107–115.
69. Sun TP, Webster RE. 1987. Nucleotide sequence of a gene cluster involved in entry of E colicins and single-stranded DNA of infecting filamentous bacteriophages into *Escherichia coli*. *J Bacteriol* 169:2667–2674.
70. Heilpern AJ, Waldor MK. 2000. CTXphi Infection of *Vibrio cholerae* Requires the tolQRA Gene Products. *J Bacteriol* 182:1739–1747.
71. Cascales E, Buchanan SK, Duche D, Kleanthous C, Lloubes R, Postle K, Riley M, Slatin S, Cavard D. 2007. Colicin Biology. *Microbiol Mol Biol Rev* 71:158–229.
72. Clarke M, Maddera L, Harris RL, Silverman PM. 2008. F-pili dynamics by live-cell imaging. *Proc Natl Acad Sci* 105:17978–17981.
73. Lee S-W, Mao C, Flynn CE, Belcher AM. 2002. Ordering of Quantum Dots Using Genetically Engineered Viruses. *Science* (80-) 296:892–895.
74. Holliger P, Riechmann L, Williams RL. 1999. Crystal structure of the two N-terminal domains of g3p from filamentous phage fd at 1.9 Å: evidence for conformational lability 1 Edited by J. M. Thornton. *J Mol Biol* 288:649–657.
75. Eckert B, Martin A, Balbach J, Schmid FX. 2005. Prolyl isomerization as a molecular timer in phage infection. *Nat Struct Mol Biol* 12:619–623.
76. Rakonjac J, Feng J, Model P. 1999. Filamentous phage are released from the bacterial membrane by a two-step mechanism involving a short C-terminal fragment of pIII 1 Edited by M. Gottesman. *J Mol Biol* 289:1253–1265.

77. Bennett NJ, Rakonjac J. 2006. Unlocking of the Filamentous Bacteriophage Virion During Infection is Mediated by the C Domain of pIII. *J Mol Biol* 356:266–273.
78. Bennett NJ, Gagic D, Sutherland-Smith AJ, Rakonjac J. 2011. Characterization of a Dual-Function Domain That Mediates Membrane Insertion and Excision of Ff Filamentous Bacteriophage. *J Mol Biol* 411:972–985.
79. Smilowitz H. 1974. Bacteriophage f1 infection: fate of the parental major coat protein. *J Virol* 13:94.
80. Trenkner E, Bonhoeffer F, Gierer A. 1967. The fate of the protein component of bacteriophage fd during infection. *Biochem Biophys Res Commun* 28:932–939.
81. Abrescia NGA, Cockburn JJB, Grimes JM, Sutton GC, Diprose JM, Butcher SJ, Fuller SD, San Martín C, Burnett RM, Stuart DI, Bamford DH, Bamford JKH. 2004. Insights into assembly from structural analysis of bacteriophage PRD1. *Nature* 432:68–74.
82. Bamford D, McGraw T, MacKenzie G, Mindich L. 1983. Identification of a protein bound to the termini of bacteriophage PRD1 DNA. *J Virol* 47:311–6.
83. Bamford DH, Caldentey J, Bamford JKH. 1995. Bacteriophage Prd1: A Broad Host Range Dsdna Tectivirus With an Internal Membrane, p. 281–319. *In* *Advances in Virus Research*.
84. Cockburn JJB, Abrescia NGA, Grimes JM, Sutton GC, Diprose JM, Benevides JM, Thomas GJ, Bamford JKH, Bamford DH, Stuart DI. 2004. Membrane structure and interactions with protein and DNA in bacteriophage PRD1. *Nature* 432:122–125.
85. Rydman PS, Caldentey J, Butcher SJ, Fuller SD, Rutten T, Bamford DH. 1999. Bacteriophage PRD1 contains a labile receptor-binding structure at each vertex. *J Mol Biol* 291:575–587.
86. Davis TN, Muller ED, Cronan JE. 1982. The virion of the lipid-containing bacteriophage PR4. *Virology* 120:287–306.
87. Tuma R, Bamford JKH, Bamford DH, Thomas GJ. 1996. Structure, interactions and dynamics of PRD1 virus II. Organization of the viral membrane and DNA. *J Mol Biol* 257:102–115.
88. Santos-Pérez I, Oksanen HM, Bamford DH, Goñi FM, Reguera D, Abrescia NGA. 2017. Membrane-assisted viral DNA ejection. *Biochim Biophys Acta - Gen Subj* 1861:664–672.
89. Mindich L, Bamford D, McGraw T, Mackenzie G. 1982. Assembly of

- bacteriophage PRD1: particle formation with wild-type and mutant viruses. *J Virol* 44:1021–30.
90. Kotilainen MM, Grahn AM, Bamford JK, Bamford DH. 1993. Binding of an *Escherichia coli* double-stranded DNA virus PRD1 to a receptor coded by an IncP-type plasmid. *J Bacteriol* 175:3089–3095.
 91. Grahn AM, Daugelavičius R, Bamford DH. 2002. Sequential model of phage PRD1 DNA delivery: Active involvement of the viral membrane. *Mol Microbiol* 46:1199–1209.
 92. Rydman PS, Bamford DH. 2000. Bacteriophage PRD1 DNA entry uses a viral membrane-associated transglycosylase activity. *Mol Microbiol* 37:356–363.
 93. Peralta B, Gil-Carton D, Castaño-Díez D, Bertin A, Boulogne C, Oksanen HM, Bamford DH, Abrescia NGA. 2013. Mechanism of Membranous Tunnelling Nanotube Formation in Viral Genome Delivery. *PLoS Biol* 11:e1001667.
 94. Daugelavicius R, Bamford JK, Bamford DH. 1997. Changes in host cell energetics in response to bacteriophage PRD1 DNA entry. *J Bacteriol* 179:5203–5210.
 95. Molineux IJ, Panja D. 2013. Popping the cork: mechanisms of phage genome ejection. *Nat Rev Microbiol* 11:194–204.
 96. Casjens SR, Molineux IJ. 2012. Short Noncontractile Tail Machines: Adsorption and DNA Delivery by Podoviruses, p. 143–179. *In* Rossmann, MG, Rao, VB (eds.), *Viral Molecular Machines*. Springer US, Boston, MA.
 97. Davidson AR, Cardarelli L, Pell LG, Radford DR, Maxwell KL. 2012. Long Noncontractile Tail Machines of Bacteriophages, p. 115–142. *In* Rossmann, MG, Rao, VB (eds.), *Viral Molecular Machines*. Springer US, Boston, MA.
 98. Leiman PG, Schneider MM. 2012. Contractile Tail Machines of Bacteriophages, p. 93–114. *In* Rossmann, MG, Rao, VB (eds.), *Viral Molecular Machines*. Springer US, Boston, MA.
 99. Taylor NMI, Prokhorov NS, Guerrero-Ferreira RC, Shneider MM, Browning C, Goldie KN, Stahlberg H, Leiman PG. 2016. Structure of the T4 baseplate and its function in triggering sheath contraction. *Nature* 533:346–352.
 100. Hu B, Margolin W, Molineux IJ, Liu J. 2015. Structural remodeling of bacteriophage T4 and host membranes during infection initiation. *Proc Natl Acad Sci* 112:E4919–E4928.
 101. Aksyuk AA, Leiman PG, Kurochkina LP, Shneider MM, Kostyuchenko VA, Mesyanzhinov V V., Rossmann MG. 2009. The tail sheath structure of

- bacteriophage T4: A molecular machine for infecting bacteria. *EMBO J* 28:821–829.
102. Leiman PG, Chipman PR, Kostyuchenko VA, Mesyanzhinov V V., Rossmann MG. 2004. Three-Dimensional Rearrangement of Proteins in the Tail of Bacteriophage T4 on Infection of Its Host. *Cell* 118:419–429.
 103. Guerrero-Ferreira RC, Hupfeld M, Nazarov S, Taylor NM, Shneider MM, Obbineni JM, Loessner MJ, Ishikawa T, Klumpp J, Leiman PG. 2019. Structure and transformation of bacteriophage A511 baseplate and tail upon infection of *Listeria* cells. *EMBO J* e99455.
 104. Browning C, Shneider MM, Bowman VD, Schwarzer D, Leiman PG. 2012. Phage Pierces the Host Cell Membrane with the Iron-Loaded Spike. *Structure* 20:326–339.
 105. Moak M, Molineux IJ. 2004. Peptidoglycan hydrolytic activities associated with bacteriophage virions. *Mol Microbiol* 51:1169–1183.
 106. Katsura I. 1976. Morphogenesis of bacteriophage lambda tail. Polymorphism in the assembly of the major tail protein. *J Mol Biol* 107:307–326.
 107. Vegge CS, Brondsted L, Neve H, Mc Grath S, van Sinderen D, Vogensen FK. 2005. Structural Characterization and Assembly of the Distal Tail Structure of the Temperate Lactococcal Bacteriophage TP901-1. *J Bacteriol* 187:4187–4197.
 108. Katsura I, Hendrix RW. 1984. Length determination in bacteriophage lambda tails. *Cell* 39:691–698.
 109. Katsura I. 1987. Determination of bacteriophage λ tail length by a protein ruler. *Nature* 327:73–75.
 110. Casjens SR, Hendrix RW. 1974. Locations and amounts of the major structural proteins in bacteriophage lambda. *J Mol Biol* 88:535–545.
 111. Schwartz M. 1975. Reversible interaction between coliphage lambda and its receptor protein. *J Mol Biol* 99:185–201.
 112. Heller K, Braun V. 1982. Polymannose O-antigens of *Escherichia coli*, the binding sites for the reversible adsorption of bacteriophage T5⁺ via the L-shaped tail fibers. *J Virol* 41:222–7.
 113. Baptista C, Santos MA, Sao-Jose C. 2008. Phage SPP1 Reversible Adsorption to *Bacillus subtilis* Cell Wall Teichoic Acids Accelerates Virus Recognition of Membrane Receptor YueB. *J Bacteriol* 190:4989–4996.

114. Boulanger P, Jacquot P, Plançon L, Chami M, Engel A, Parquet C, Herbeuval C, Letellier L. 2008. Phage T5 Straight Tail Fiber Is a Multifunctional Protein Acting as a Tape Measure and Carrying Fusogenic and Muralytic Activities. *J Biol Chem* 283:13556–13564.
115. Feucht A, Schmid A, Benz R, Schwarz H, Heller KJ. 1990. Pore formation associated with the tail-tip protein pb2 of bacteriophage T5. *J Biol Chem* 265:18561–18567.
116. Cumby N, Reimer K, Mengin-Lecreulx D, Davidson AR, Maxwell KL. 2015. The phage tail tape measure protein, an inner membrane protein and a periplasmic chaperone play connected roles in the genome injection process of *E. coli* phage HK97. *Mol Microbiol* 96:437–447.
117. Scandella D, Arber W. 1974. An *Escherichia coli* mutant which inhibits the injection of phage λ DNA. *Virology* 58:504–513.
118. Scandella D, Arber W. 1976. Phage λ DNA injection into *Escherichia coli* pel⁻ mutants is restored by mutations in phage genes V or H. *Virology* 69:206–215.
119. Hu B, Margolin W, Molineux IJ, Liu J. 2013. The bacteriophage T7 virion undergoes extensive structural remodeling during infection. *Science* (80-) 339:576–579.
120. Lindberg AA, Sarvas M, Makela PH. 1970. The Tail Sheath of Bacteriophage N4 Interacts with the *Escherichia coli* Receptor. *Infect Immun* 1:88–97.
121. McPartland J, Rothman-Denes LB. 2009. The Tail Sheath of Bacteriophage N4 Interacts with the *Escherichia coli* Receptor. *J Bacteriol* 191:525–532.
122. Leiman PG, Battisti AJ, Bowman VD, Stummeyer K, Mühlenhoff M, Gerardy-Schahn R, Scholl D, Molineux IJ. 2007. The Structures of Bacteriophages K1E and K1-5 Explain Processive Degradation of Polysaccharide Capsules and Evolution of New Host Specificities. *J Mol Biol* 371:836–849.
123. Bayer ME, Takeda K, Uetake H. 1980. Effects of receptor destruction by *Salmonella* bacteriophages ϵ 15 and c341. *Virology* 105:328–337.
124. Schulz EC, Schwarzer D, Frank M, Stummeyer K, Mühlenhoff M, Dickmanns A, Gerardy-Schahn R, Ficner R. 2010. Structural Basis for the Recognition and Cleavage of Polysialic Acid by the Bacteriophage K1F Tailspike Protein EndoNF. *J Mol Biol* 397:341–351.
125. Porcek NB, Parent KN. 2015. Key residues of *S. flexneri* OmpA mediate infection by bacteriophage Sf6. *J Mol Biol* 427:1964–1976.

126. Xu J, Gui M, Wang D, Xiang Y. 2016. The bacteriophage ϕ 29 tail possesses a pore-forming loop for cell membrane penetration. *Nature* 534:544–547.
127. Hoffman B, Levine M. 1975. Bacteriophage P22 virion protein which performs an essential early function. II. Characterization of the Gene 16 Function. *J Virol* 16:1547–1559.
128. Hoffman B, Levine M. 1975. Bacteriophage P22 virion protein which performs an essential early function. I. Analysis of 16-ts mutants. *J Virol* 16:1536–46.
129. Jin Y, Sdao SM, Dover JA, Porcek NB, Knobler CM, Gelbart WM, Parent KN. 2015. Bacteriophage P22 ejects all of its internal proteins before its genome. *Virology* 485:128–134.
130. Perez GL, Huynh B, Slater M, Maloy S. 2009. Transport of phage P22 DNA across the cytoplasmic membrane. *J Bacteriol* 91:135–140.
131. Israel V. 1977. E Proteins of Bacteriophage P22. I. Identification and Ejection from Wild-Type and Defective Particles. *J Virol* 23:91–97.
132. Zhao H, Speir JA, Matsui T, Lin Z, Liang L, Lynn AY, Varnado B, Weiss TM, Tang L. 2016. Structure of a bacterial virus DNA-injection protein complex reveals a decameric assembly with a constricted molecular channel. *PLoS One* 11:1–16.
133. Inagaki M, Kawaura T, Wakashima H, Kato M, Nishikawa S, Kashimura N. 2003. Different contributions of the outer and inner R-core residues of lipopolysaccharide to the recognition by spike H and G proteins of bacteriophage ϕ X174. *FEMS Microbiol Lett* 226:221–227.
134. McKenna R, Xia D, Willingmann P, Ilag LL, Krishnaswamy S, Rossmann MG, Olson NH, Baker TS, Incardona NL. 1992. Atomic structure of single-stranded DNA bacteriophage phi X174 and its functional implications. *Nature* 355:137–43.
135. McKenna R, Ilag L, Rossmann M. 1994. Analysis of the Single-stranded DNA Bacteriophage PhiX174 Refined at a Resolution of 3.0Å. *J Mol Biol*.
136. Bernal RA, Hafenstein S, Esmeralda R, Fane BA, Rossmann MG. 2004. The ϕ X174 protein J mediates DNA packaging and viral attachment to host cells. *J Mol Biol* 337:1109–1122.
137. Ilag LL, Olson NH, Dokland T, Music CL, Cheng RH, Bowen Z, McKenna R, Rossmann MG, Baker TS, Incardona NL. 1995. DNA packaging intermediates of bacteriophage ϕ X174. *Structure* 3:353–363.
138. Ilag LL, McKenna R, Yadav MP, BeMiller JN, Incardona NL, Rossmann MG.

1994. Calcium Ion-induced Structural Changes in Bacteriophage ϕ X174. *J Mol Biol* 244:291–300.
139. Roznowski AP, Young RJ, Love SD, Andromita AA, Guzman VA, Wilch MH, Block A, McGill A, Lavelle M, Romanova A, Sekiguchi A, Wang M, Burch AD, Fane BA. 2018. Recessive Host Range Mutants and Unsusceptible Cells That Inactivate Virions without Genome Penetration: Ecological and Technical Implications. *J Virol* 93:1–16.
140. Sun Y, Roznowski AP, Tokuda JM, Klose T, Mauney A, Pollack L, Fane BA, Rossmann MG. 2017. Structural changes of tailless bacteriophage Φ X174 during penetration of bacterial cell walls. *Proc Natl Acad Sci* 114:13708–13713.
141. Jazwinski SM, Lindberg AA, Kornberg A. 1975. The gene H spike protein of bacteriophages ϕ X174 and S13. I. Functions in phage-receptor recognition and in transfection. *Virology* 66:283–293.
142. Jazwinski SM, Marco R, Kornberg A. 1975. The gene H spike protein of bacteriophages ϕ X174 and S13. II. Relation to synthesis of the parental replicative form. *Virology* 66:294–305.
143. Sun L, Young LN, Zhang X, Boudko SP, Fokine A, Zbornik E, Roznowski AP, Molineux IJ, Rossmann MG, Fane BA. 2014. Icosahedral bacteriophage Φ X174 forms a tail for DNA transport during infection. *Nature* 505:432–435.
144. Shepard W, Cruse WBT, Fourme R, De La Fortelle E, Prangé T. 1998. A zipper-like duplex in DNA: The crystal structure of d(GCGAAAGCT) at 2.1 Å resolution. *Structure* 6:849–861.
145. Mandel-Gutfreund Y, Schueler O, Margalit H. 1995. Comprehensive Analysis of Hydrogen Bonds in Regulatory Protein DNA-Complexes: In Search of Common Principles. *J Mol Biol* 253:370–382.
146. Luscombe NM. 2001. Amino acid-base interactions: a three-dimensional analysis of protein-DNA interactions at an atomic level. *Nucleic Acids Res* 29:2860–2874.
147. Luscombe NM, Thornton JM. 2002. Protein–DNA Interactions: Amino Acid Conservation and the Effects of Mutations on Binding Specificity. *J Mol Biol* 320:991–1009.
148. Suzuki M. 1994. A framework for the DNA–protein recognition code of the probe helix in transcription factors: the chemical and stereochemical rules. *Structure* 2:317–326.

149. Conley MJ, McElwee M, Azmi L, Gabrielsen M, Byron O, Goodfellow IG, Bhella D. 2019. Calicivirus VP2 forms a portal-like assembly following receptor engagement. *Nature* 565:377–381.

1.5 Figure Legends

FIGURE LEGENDS

FIG 1.1 Bacteriophage virion morphotypes. a) Cystovirus, b) Corticovirus, c) Tectivirus, d) Levivirus, e) Inovirus, f) Myovirus, g) Siphovirus, h) Podovirus, i) Microvirus. Virions are not drawn to scale. Black lines represent or outline structural proteins. Dark red, edge-less lines represent lipid bilayers. RNA is depicted as brown and orange lines, while DNA is depicted as green and blue lines. Pairs of colored lines represent double-stranded nucleic acids.

FIG 1.2 Cystovirus $\phi 6$ penetration steps. a) Host attachment protein P3 binds to a pilus. The pilus retracts and triggers P3 dissociation. b) Viral membrane protein P6 initiates fusion with the host's outer membrane (maroon). Nucleocapsid protein P5 locally degrades peptidoglycan (purple). c) Protein P8 creates an invagination in the cytoplasmic membrane (green). d) The nucleocapsid buds into the cytoplasm. e) Protein P8 degrades and disrupts the vesicle, releasing the polymerase complex into the cytoplasm.

FIG 1.3 Corticovirus PM2 penetration steps. a) Receptor binding protein P1 its host receptor. b) The capsid dissociates, and viral membrane protein P10 initiates fusion with the host's outer membrane (maroon). Once through, P7 or the cellular lytic factor locally degrade the peptidoglycan (purple). c) The genome traverses the cytoplasmic membrane (green), possibly by opening a membrane spanning pore.

FIG 1.4 Levivirus penetration steps. Few details are known. a) The maturation protein binds the host's conjugative F pili. The maturation protein cleaves itself and the genome becomes sensitive to RNases. b) The genome and maturation proteins enter the cytoplasm.

FIG 1.5 Inovirus Ff penetration steps. a) Receptor binding protein PIII domain N2 binds to a host's conjugative F pilus tip. The pilus retracts, pulling the virion into the periplasm. b) PIII domain N1 binds toIa. c) PIII domain C1 merges into the cytoplasmic membrane (green). d) The genome passes into the cytoplasm while the coat proteins dissociate into the cytoplasmic membrane.

FIG 1.6 Tectivirus PRD1 penetration steps. a) Receptor binding protein P2 binds a component of the conjugative plasmid type P, W, or N machinery. Viral membrane protein P11 creates a hole in the outer membrane. The viral membrane protrudes through this opening and viral membrane protein P7 locally degrades the peptidoglycan (purple). b) Viral membrane proteins P7, P14, P18, and P32 rearrange the viral membrane into a tube spanning the cytoplasmic membrane (green). c) The genome passes into the cytoplasm.

FIG 1.7 Myovirus penetration steps. a) Tail fibers attach to the host outer membrane (maroon), inducing a conformational change within the baseplate. b) The tail sheath contracts, driving the rigid tail core through peptidoglycan (purple) to the cytoplasmic

membrane (green). c) The tail tip or tape measure proteins penetrate the membrane and allow genome release.

FIG 1.8 Siphovirus HK97 penetration steps. a) Tail fibers contact the outer membrane (maroon) and the tail tip contacts a secondary protein receptor. b) The tail tape measure proteins enter the periplasm, locally degrade the peptidoglycan (purple), and interacts with host periplasmic and cytoplasmic membrane proteins (yellow). c) The tape measure proteins breach the cytoplasmic membrane (green) and the genome is transferred.

FIG 1.9 Podovirus penetration steps. a) Tail fibers make contact with receptors and the tail knob forms a pore through the host's outer membrane (maroon). b) The ejection proteins exit the virion and form a cell wall spanning channel. c) Genome release.

FIG 1.10 Microvirus ϕ X174 penetration steps. a) The virion attaches to host LPS molecules (periwinkle). b) A spike pentamer is displaced and the underlying coat proteins bind to the outer membrane (maroon). An oligomer of DNA piloting proteins is above the attached vertex (red). c) The vertex opens and the DNA piloting proteins are ejected into the cell wall where they form a membrane spanning conduit. A portion of the ssDNA genome is exposed to host DNA replication machinery. d) The genome is internalized while the complementary strand is synthesized. The DNA piloting proteins become associated with the cytoplasmic membrane (green) and the dsDNA genome.

FIG 1.11 The ϕ X714 DNA piloting protein x-ray structure. Residues 151 to 272 are present. Inward facing residues are modeled as sticks. A) View of the structure's longitudinal axis. Four monomers have been removed to display the inner surface. B) View from the carboxy terminal opening. PDB ID: 4JPP

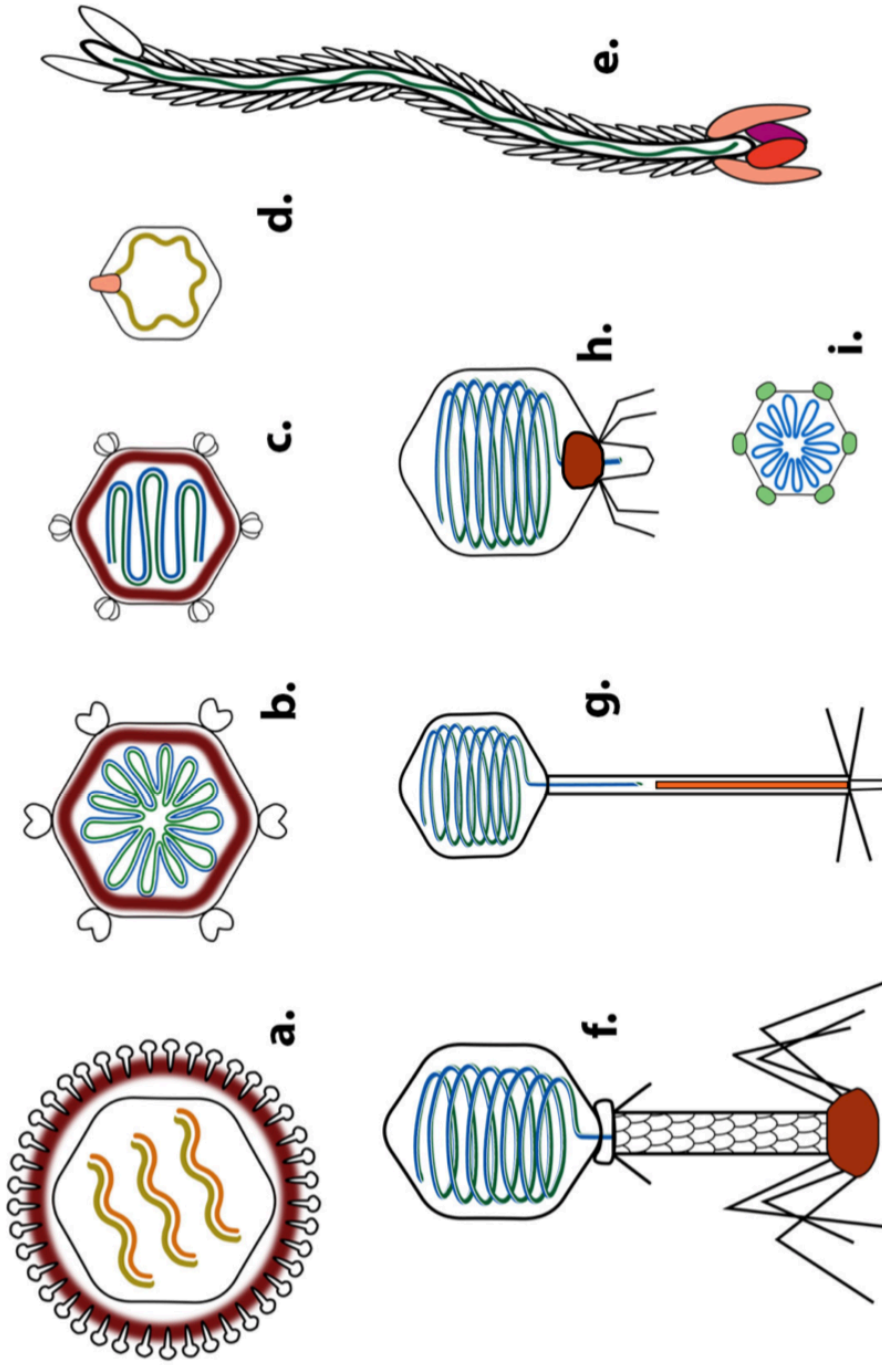


FIG 1.1 Bacteriophage virion morphotypes.

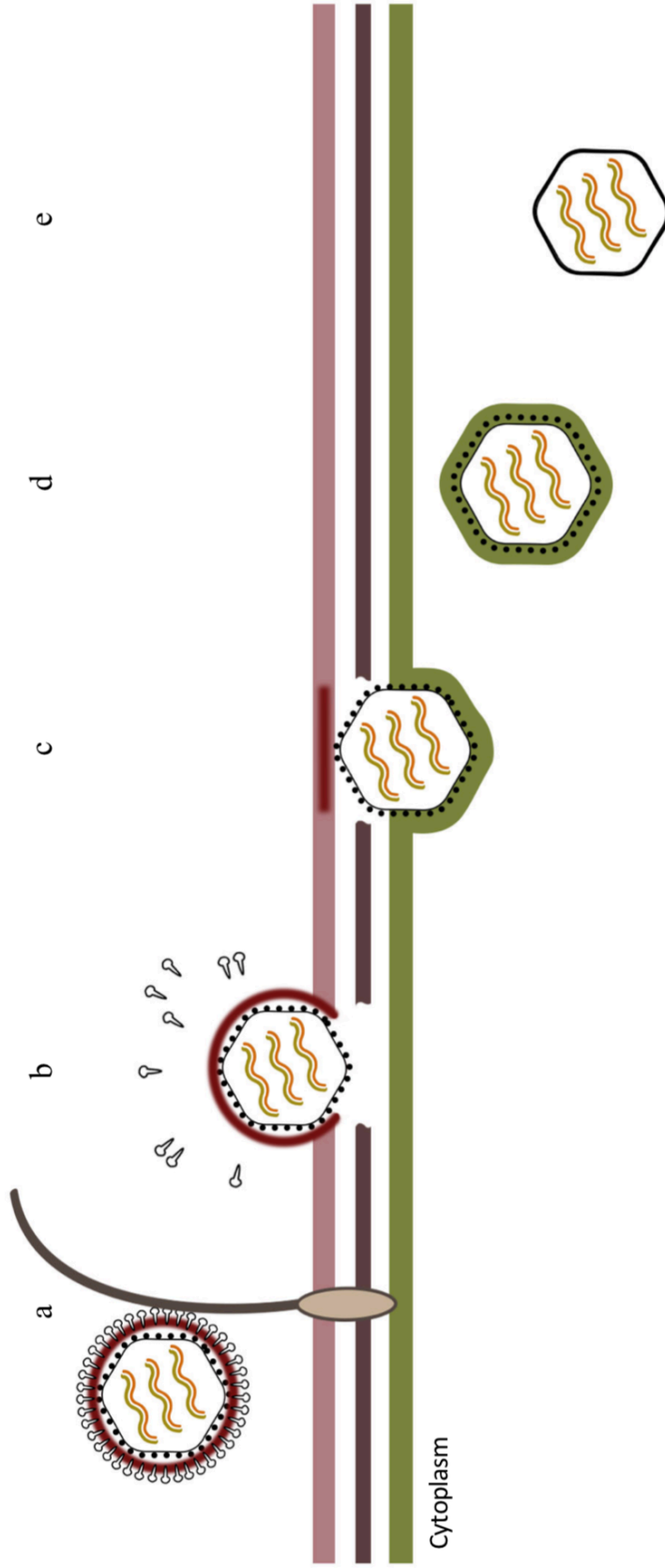


FIG 1.2 Cystovirus ϕ 6 penetration steps

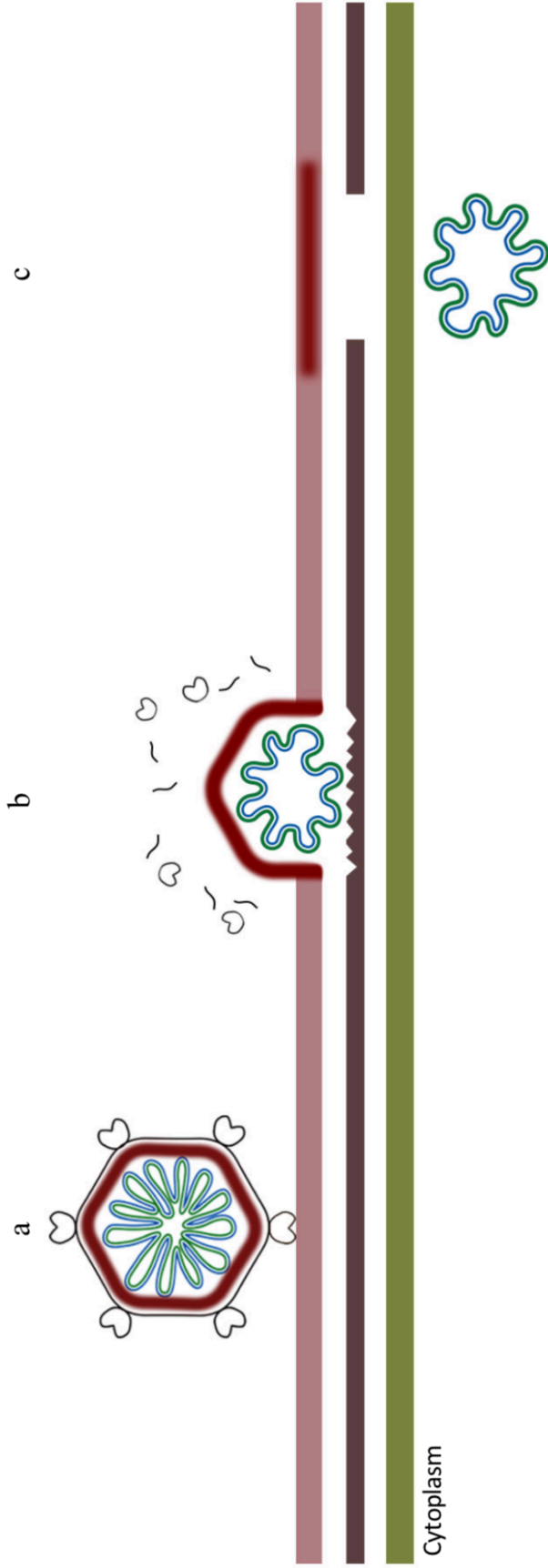


FIG 1.3 Corticovirus PM2 penetration steps

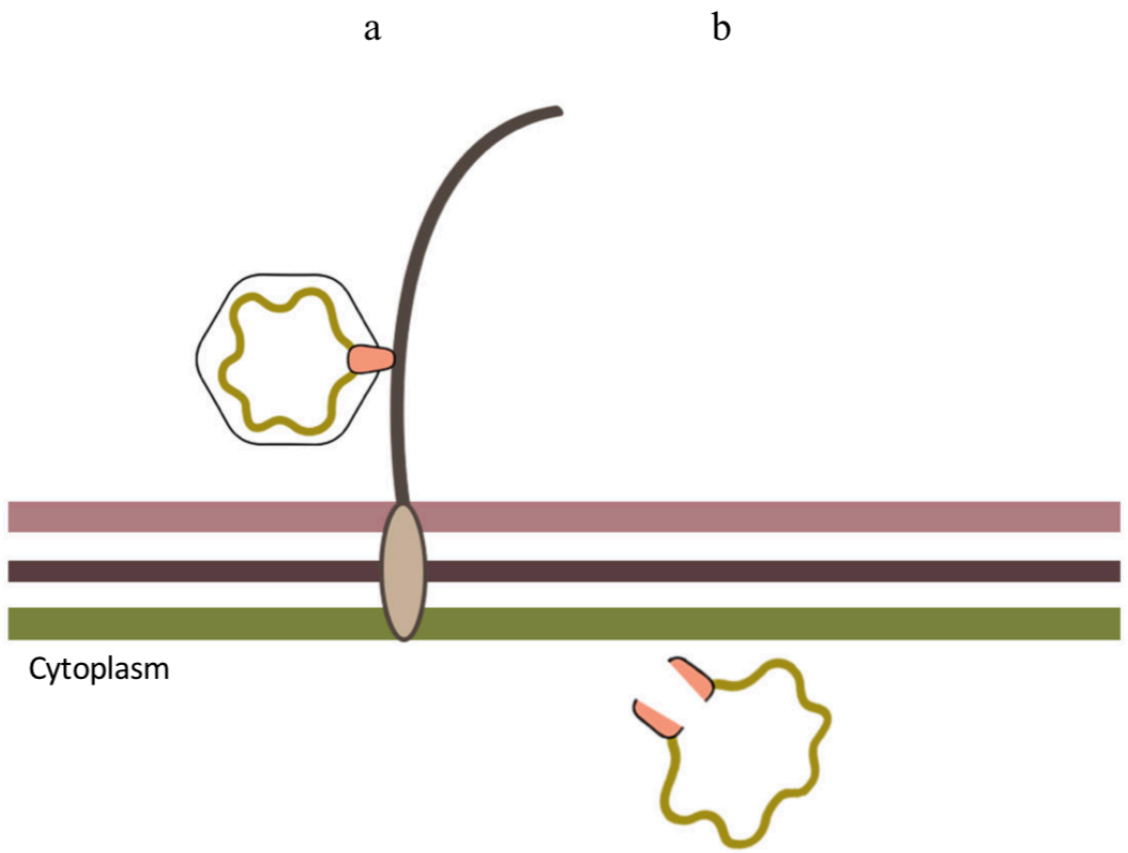


FIG 1.4 Levivirus penetration steps

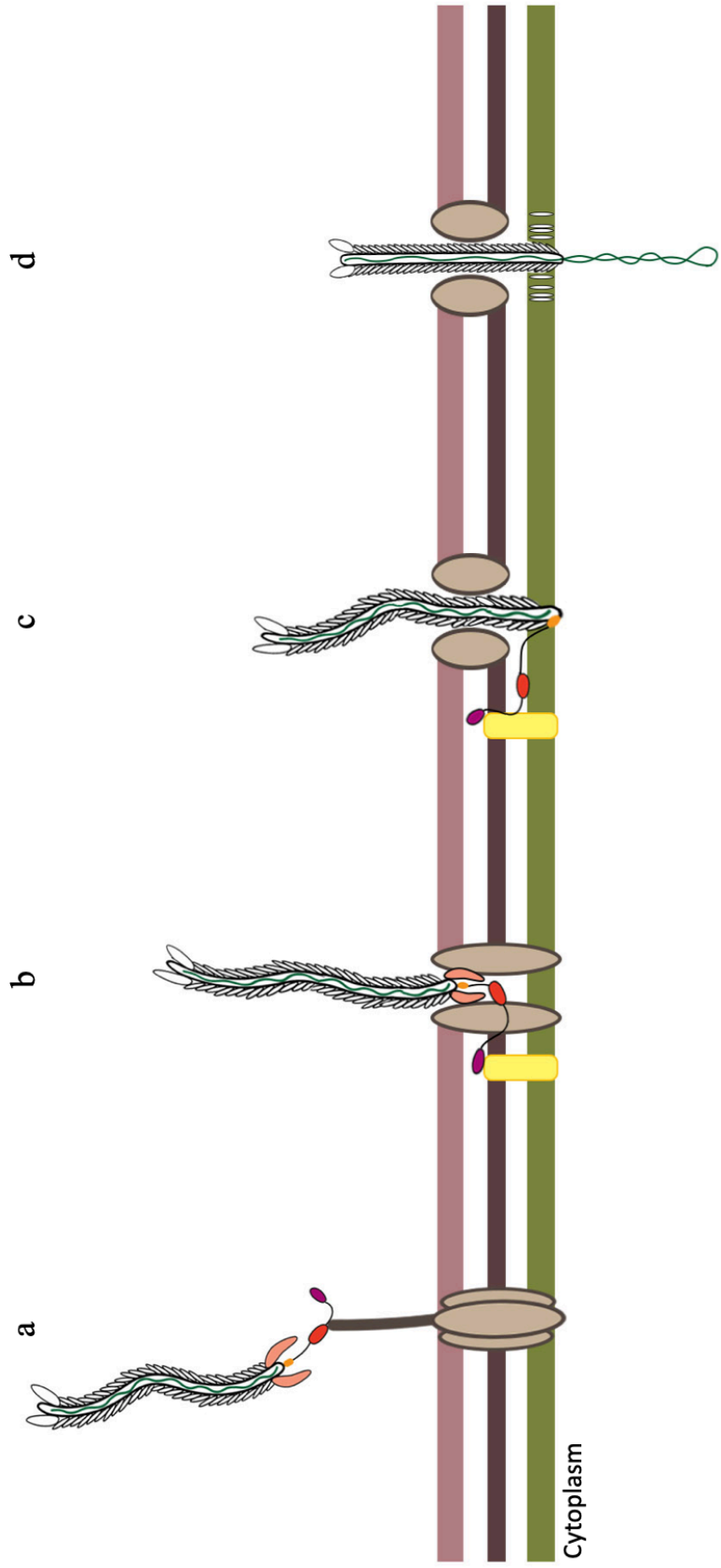


FIG 1.5 Inovirus Ff penetration steps

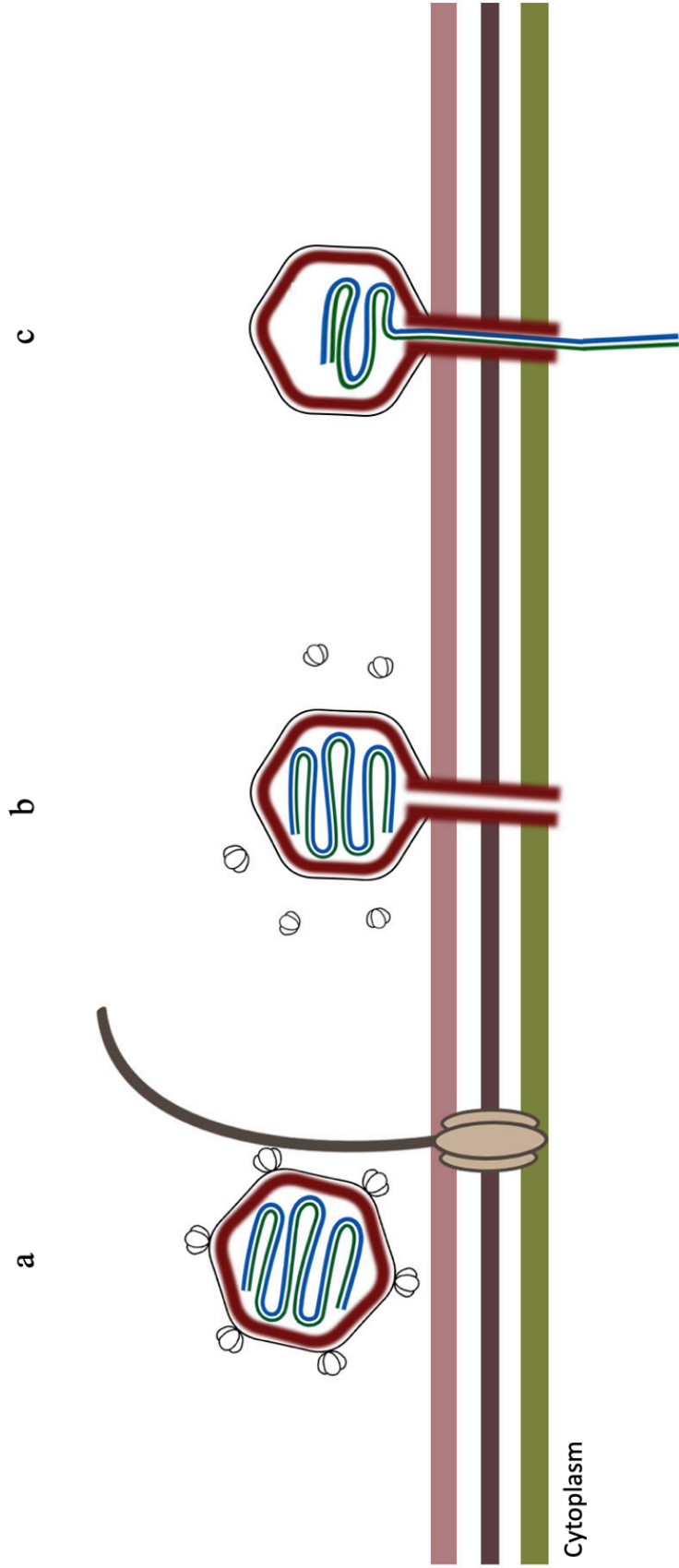


FIG 1.6 Tectivirus PRD1 penetration steps

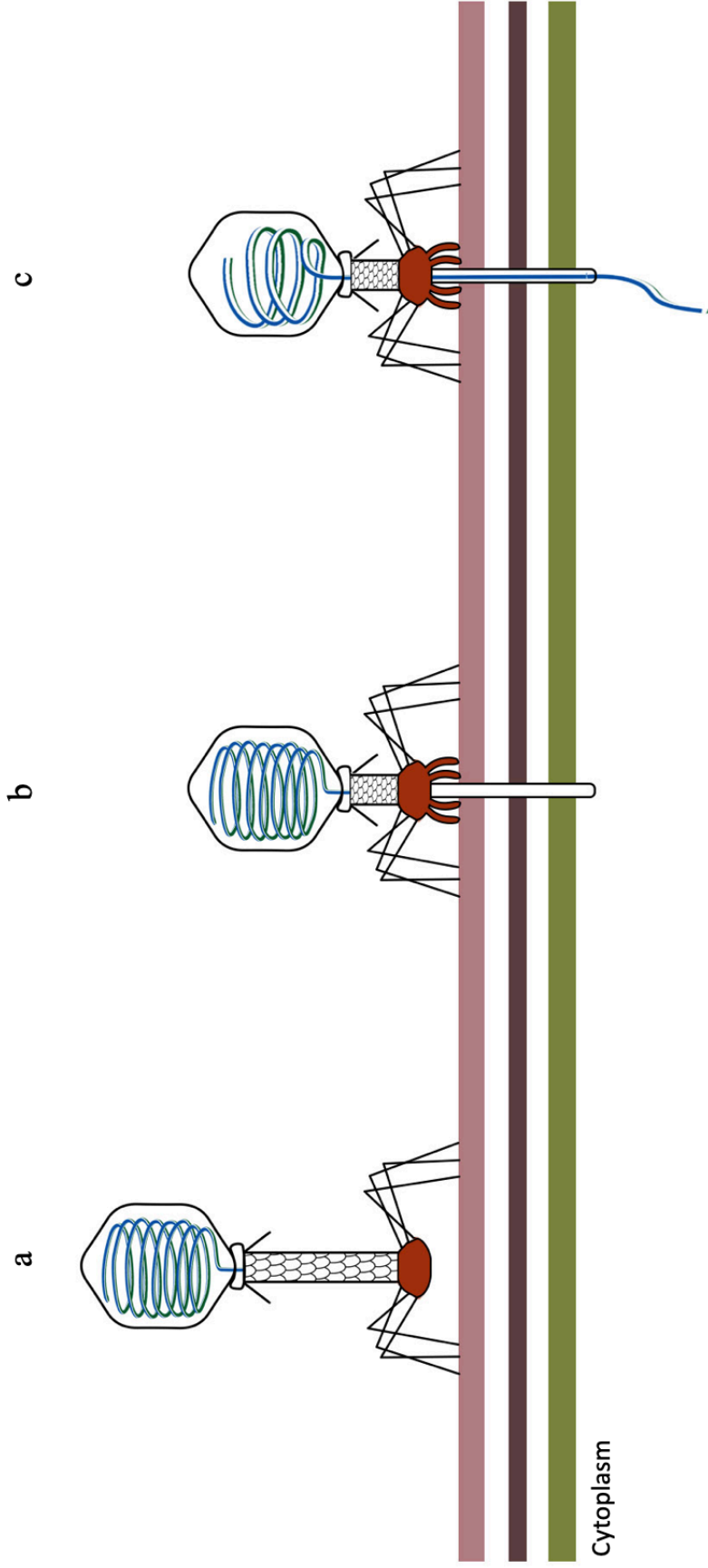


FIG 1.7 Myovirus penetration steps

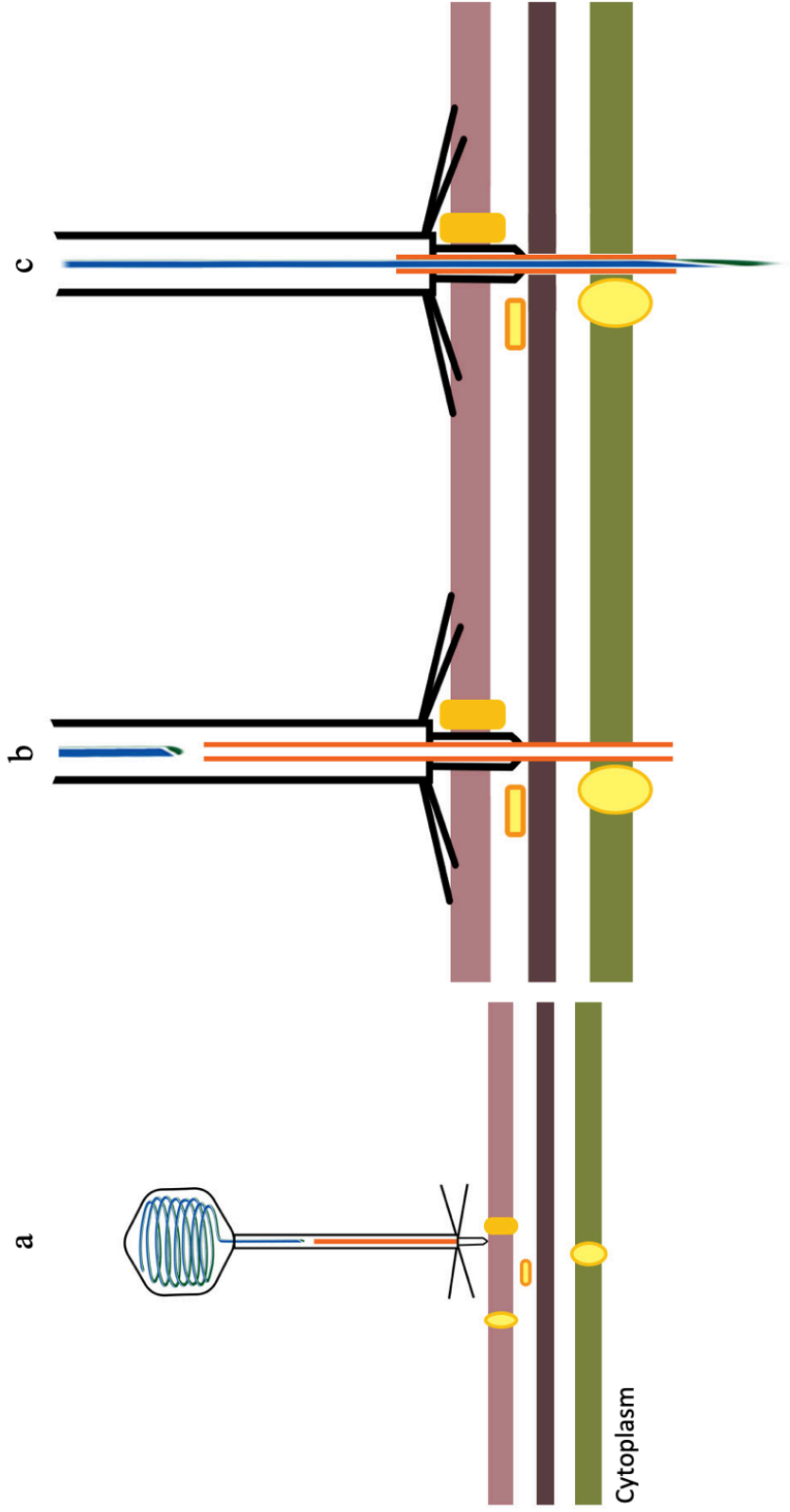


FIG 1.8 Siphovirus penetration steps

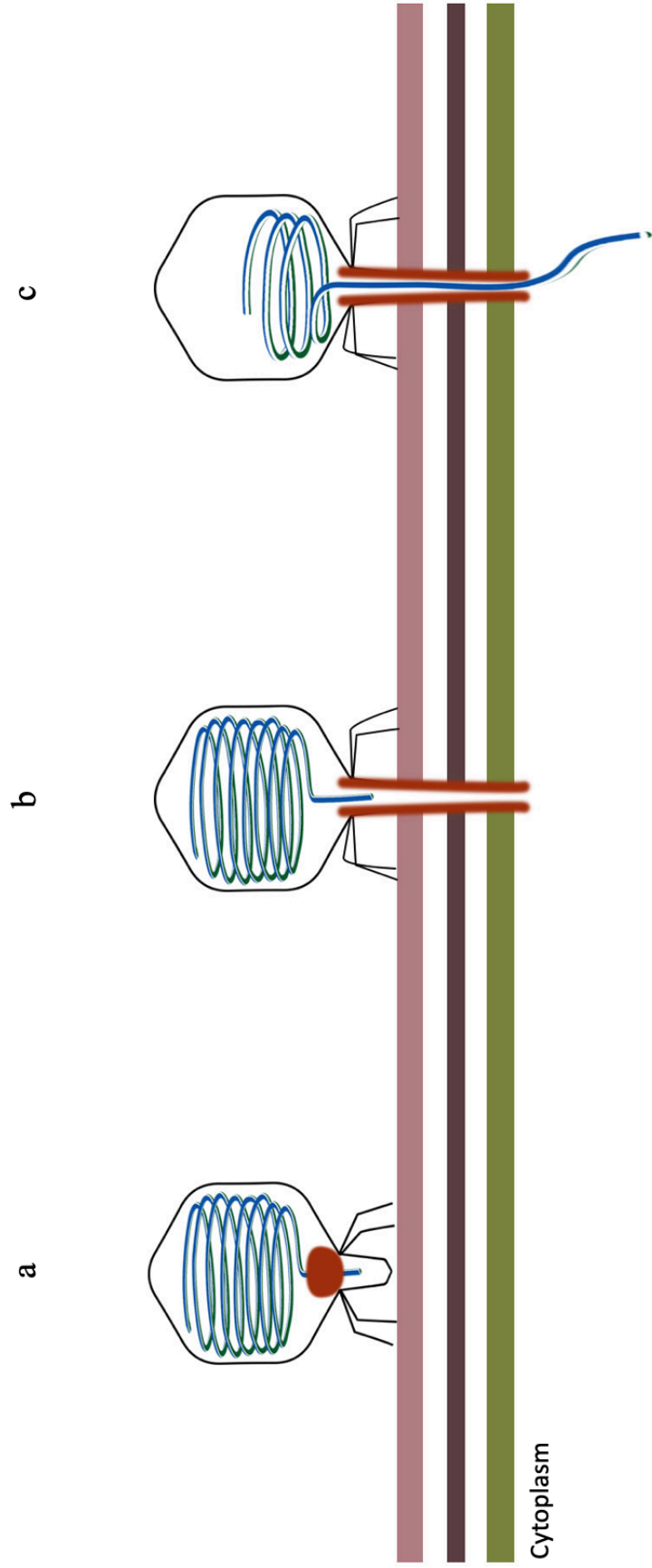


FIG 1.9 Podovirus penetration steps

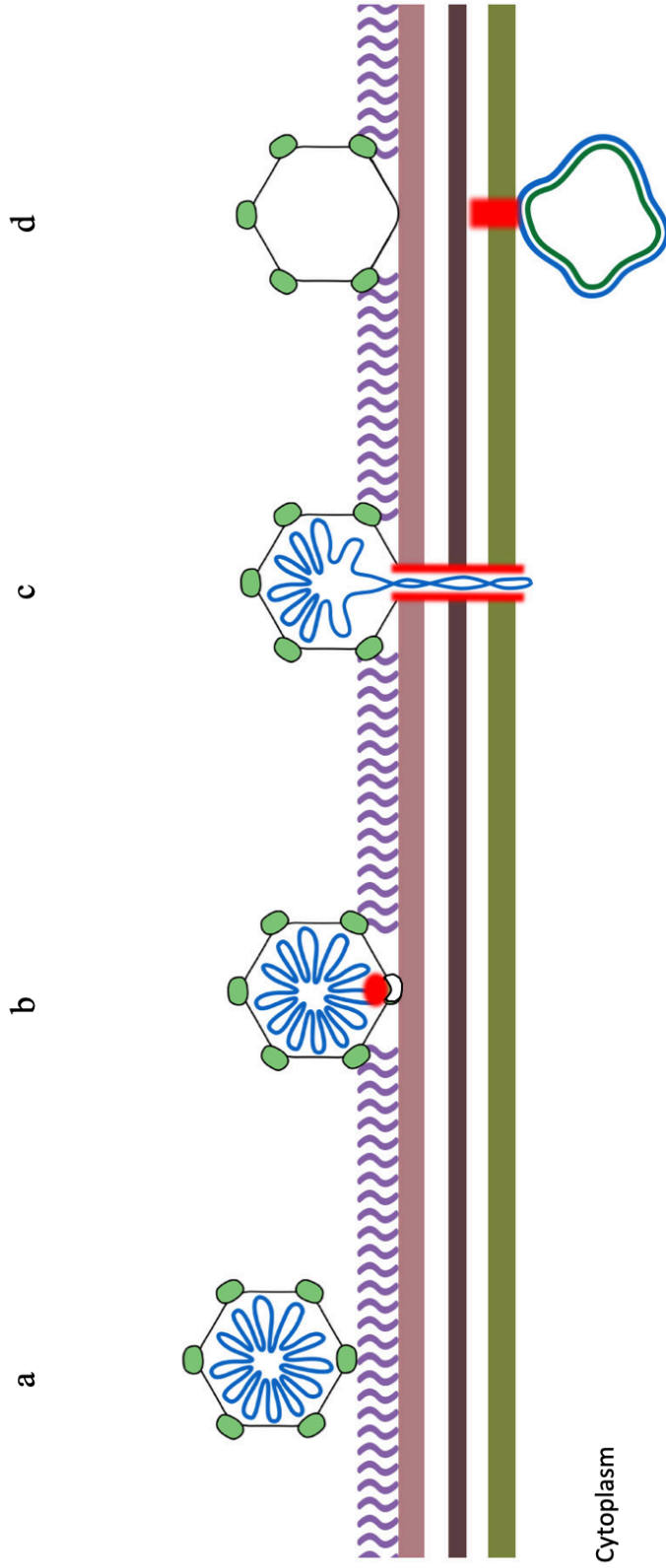


FIG 1.10 Microvirus ϕ X174 penetration steps

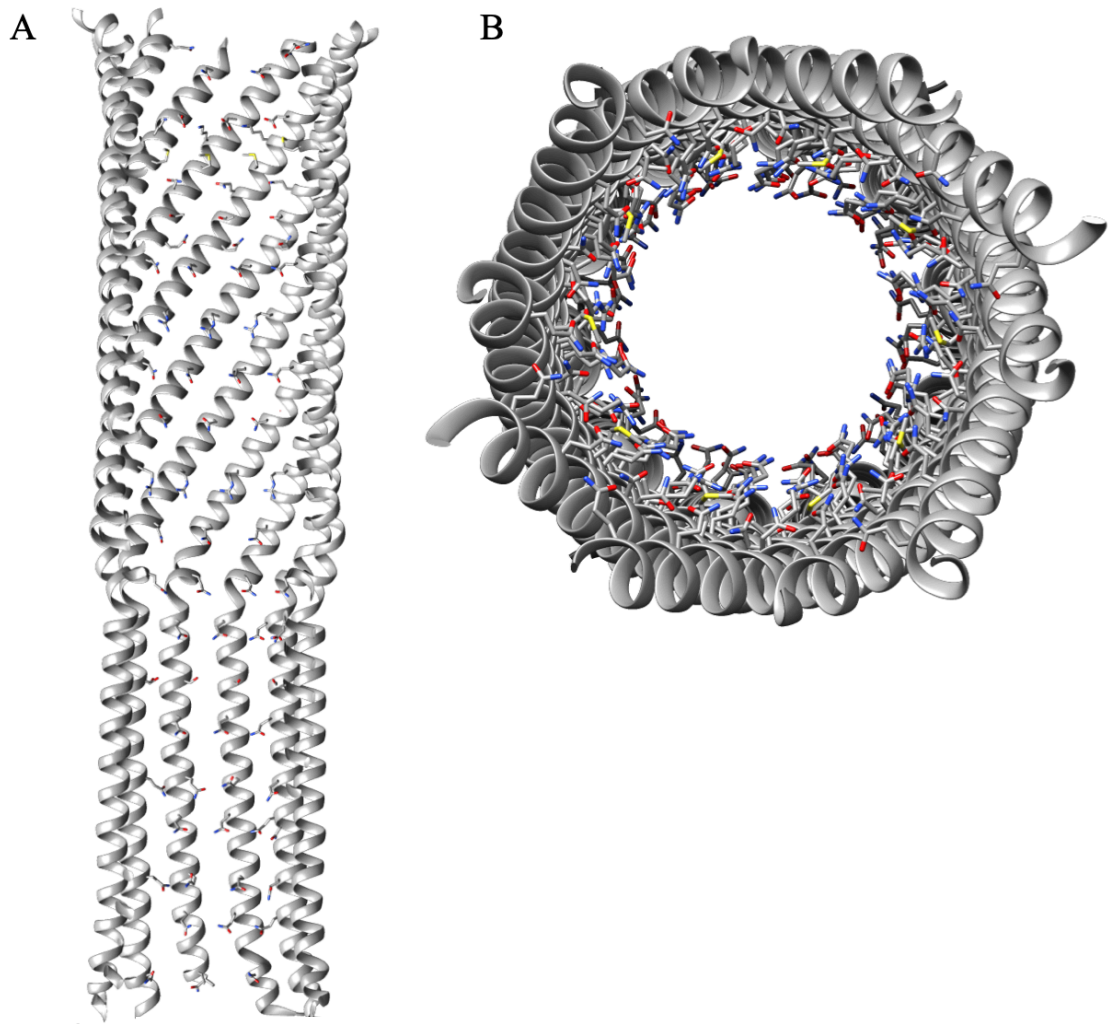


FIG 1.11 The ϕ X174 DNA piloting protein X-ray structure

CHAPTER 2

STRUCTURE-FUNCTION ANALYSIS OF THE Φ X174 DNA PILOTING PROTEIN USING LENGTH-ALTERING MUTATIONS

2.1 Abstract

Although the ϕ X174 H protein is monomeric during procapsid morphogenesis, 10 proteins oligomerize to form a DNA translocating conduit (H-tube) for penetration. However, the timing and location of H-tube formation are unknown. The H-tube's highly repetitive primary and quaternary structures made it amenable to a genetic analysis using in-frame insertions and deletions. Length-altered proteins were characterized for the ability to perform the protein's three known functions: participation in particle assembly, genome translocation, and stimulation of viral protein synthesis. Insertion mutants were viable. Theoretically, these proteins would produce an assembled tube exceeding the capsid's internal diameter, suggesting that virions do not contain a fully assembled tube. Lengthened proteins were also used to test the biological significance of the crystal structure. Particles containing H proteins of two different lengths were significantly less infectious than both parents, indicating an inability to pilot DNA. Shortened H proteins were not fully functional. Although they could still stimulate viral protein synthesis, they either were not incorporated into virions or, if incorporated, failed to pilot the genome. Mutant proteins that failed to incorporate contained deletions within an 85-amino-acid segment, suggesting the existence of an incorporation domain. The revertants of shortened H protein mutants fell into two classes. The first class duplicated sequences neighboring the deletion, restoring wild-type length but not wild-type sequence. The

second class suppressed an incorporation defect, allowing the use of the shortened protein.

2.2 Introduction

Bacteriophages have evolved several mechanisms to transport hydrophilic genomes through cell walls containing hydrophobic membranes and peptidoglycan. Myoviruses and podoviruses carry tails that, respectively, utilize contractile sheaths (1) and form extensions within the membrane (2). In contrast, siphoviruses, filamentous phage, and other tail-less viruses co-opt host cell membrane channels for penetration (3–5).

However, the tail-less microvirus ϕ X174 does not require a host-provided conduit for genome transport. Instead, genome translocation is mediated by 10 to 12 copies of the DNA-piloting protein H found inside the virion (6–8).

The X-ray structure of H protein's coiled-coil domain (8, 9) shows 10 parallel proteins oligomerized into a tube (Fig. 2.1) The tube is wide enough for passage of the single-stranded DNA (ssDNA) genome and has been visualized spanning the cell wall. It represents the first high-resolution structure of a virally encoded DNA-translocating conduit, sharing structural similarities with other viral proteins involved in DNA transport. For example, the H structure is entirely α -helical, similar to the α -helical barrel domain seen in the P22 portal protein (10, 11). Furthermore, it shares sequence similarities with T7 DNA-piloting proteins that form tail tube extensions during infection (2, 8). Thus, H protein serves as a paradigm for the assembly and function of long α -helical supramolecular structures and nanotubes (12, 13).

Protein H likely assumes multiple conformations during the ϕ X174 life cycle. For DNA translocation, 10 proteins form a 170- Å-long α -helical tube that is separated into two domains. The N-terminal domain is composed of 3 11-amino-acid repeating units (hendecads), whereas the C-terminal domain is composed of 11 7-amino-acid units (heptads). Each repeating unit is directly aligned with the equivalent units of neighboring H proteins. Although an oligomer is required for DNA translocation, H proteins are monomeric in early assembly intermediates (14, 15). Tubes have not been visualized in procapsids or virions, but structure determination assumed icosahedral symmetry. Therefore, the timing and location of H-tube assembly have yet to be determined. The H-tube could exist as a fully assembled tube within the capsid or a partially assembled core, or it may only assemble externally at the infection site. Lastly, H protein likely assumes a third conformation, one required to stimulate viral protein synthesis (16).

Taking advantage of the tube's repetitive structure, we conducted a genetic analysis: altering the protein's length by the addition or deletion of heptad and hendecad motifs. These mutations were used to determine whether larger H proteins could be accommodated within the volumetrically constrained capsid or if smaller H proteins could span the cell wall for DNA delivery. Length-altered proteins were also assayed for function during the intracellular stages of the ϕ X174 life cycle: incorporation during assembly and the ability to stimulate the synthesis of other viral proteins.

2.3 Results

Tube length can be increased beyond the internal diameter of the capsid. Although the ϕ X174 H-tube structure is a 170-Å-long decamer, H proteins are incorporated as monomers during assembly (14, 15). Thus, it is unknown whether they exist within the capsid as a fully formed tube, as a partially constructed core, or as monomers ready to complete assembly at the infection site. The related bacteriophage G4 encodes two extra heptad motifs within its coiled-coil domain, yet the G4 capsid has the same internal capsid diameter as ϕ X174, 172 Å. The additional G4 heptads are predicted to assume a helical structure (26) If the prediction is correct, the additional heptads would lengthen the tube by ~18 Å. While this suggests that the tube is not fully assembled within the mature virion, the internal diameter of the G4 capsid was derived from a degraded procapsid, not a mature virion (26). To rigorously test whether a fully assembled tube exists in the capsid, DNA encoding the two additional G4 heptads was placed within the ϕ X174 H gene (H+14). If a fully assembled tube is not encapsidated, motif insertions should not inhibit tube assembly or genome piloting. In the structure, neighboring H proteins are bound together via specific interhelical contacts between identical heptad and hendecad motifs (Fig. 2.1A). If motif alignment is maintained, additional units should not dramatically disrupt contacts or reduce tube integrity. Alternatively, if viability requires the internal assembly of a complete tube, lengthened H proteins will result in noninfectious particles.

The resulting H+14 mutant was viable but exhibited a cold-sensitive (cs) phenotype at 24°C. This defect was rescued by a variety of point mutations within the inserted codons

(Table 2.1; Fig. 1C). To determine if the mutant virions were as infectious as wild-type virions, permissively synthesized H+14 particles as well as a cs revertant (H+14 R12L) were purified by rate zonal sedimentation and their specific infectivity (PFU/A280) was determined. As can be seen in Fig. 2A, both mutant viruses sediment like the wild type: the A280 peak coincides with the specific infectivity peak at 114S. The protein composition was analyzed by SDS-PAGE (Fig. 2.2C). Elongated proteins were observed in mutant particles at wild-type levels as determined by densitometry (data not shown). The specific infectivity of the H+14 mutant was reduced compared to that of the wild type (Fig. 2.2B). However, reversion of the cs phenotype (H+14 R12L) restored specific infectivity to wild-type levels. The H+14 R12L mutant's wild-type phenotype suggests that elongated proteins can be fully tolerated. Thus, it is unlikely that virions contain a fully assembled H-tube. Similar results were obtained with the H+11 mutant, which contains a duplication of a ϕ X174 hendecad (Fig. 2.1D; see also below). Unlike the aforementioned G4-derived heptads, this hendecad is known to form a straight helix in the X-ray structure (8).

The ϕ X174 H+14 cs phenotype reflects a kinetic assembly defect. H protein is involved in multiple aspects of the viral life cycle, from host attachment to intracellular assembly. Previously characterized mutants exhibited both attachment and assembly defects (27, 28). Therefore, all aspects of the ϕ X174 H+14 life cycle were analyzed. In both attachment and eclipse assays conducted at 24°C, the mutant performed like the wild type (data not shown). Thus, the kinetics of attachment and the initiation of DNA transport (eclipse) did not appear to be affected.

Eclipse assays detect the loss of infectivity, which occurs at the initiation of DNA piloting. However, they do not determine whether DNA was transported into the cytoplasm. Mutations could prevent tube assembly, stall DNA mid-transit, or lower tube integrity but not affect eclipse kinetics. In a wild-type infection, a portion of the (+) ssDNA genome enters the cytoplasm. Host polymerases then complete genome translocation by synthesizing the complementary (-) strand (29), a prerequisite to viral transcription and translation. Thus, the kinetics of coat protein synthesis can serve as a surrogate marker for genome piloting. Lysis-resistant cells were infected at 24°C with wild-type ϕ X174 or the H+14 or H+14 R12L mutant. At designated time points, aliquots were removed and whole-cell lysates analyzed by SDS-PAGE (Fig. 2.3A). Coat protein band intensity was quantified relative to a host protein band (Fig. 2.3B). The appearance and accumulation of coat protein in H+14 mutant-infected cells closely matched those in cells infected with the wild type, suggesting that genome piloting is not dramatically affected at the restrictive temperature.

During the same experiment, the kinetics of virion production were also monitored; at each time point, samples of infected cells were chemically lysed, and titers of infectious particles were determined. The kinetics of H+14 progeny production were significantly reduced (Fig. 2.3C). Wild-type titers exceeded the input value at 100 min post-infection, whereas H+14 mutant titers did not reach that level until 150 min post-infection. Slow assembly likely prevents H \leq 14 mutant plaque formation on lysis-sensitive cells. Lysis is programmed to occur during host division (30). Progeny must be produced prior to this

event, which occurred at approximately 110 min during these experiments. The R12 L substitution in the H+14 R12L cs revertant partially alleviated this kinetic defect.

However, kinetics were not restored to wild-type levels (see Discussion).

The reduced infectivity of virions containing two species of piloting protein further

validate the X-ray structure. In the H-tube, monomers are bound together through a set of specific interhelical contacts. As seen in other coiled-coil structures (31), these contacts keep monomers parallel and in register, aligning equivalent heptad and hendecad motifs. This arrangement likely confers stability during tube assembly and/or DNA piloting. A virion containing H proteins of differing lengths could not achieve this arrangement and may not assemble into a functional tube. Since H proteins are incorporated as monomers during assembly, it is possible to assemble particles containing a heterogeneous complement of H proteins. However, these particles should exhibit reduced infectivity. To test this hypothesis, lysis-resistant cells were coinfecting with the wild type and the equally infectious H+14 R12L mutant at 37°C. Particles were purified and assayed for protein content and specific infectivity. As shown in Fig. 2C, the wild-type and H+14 R12LH proteins were found in particles at approximately equal levels. The specific infectivity of the heterogeneous particles was reduced compared to those of homogeneous wild-type and H+14 R12L populations (Fig. 2.2B). Similar results were obtained for wild-type-infected cells expressing the cloned H+14 R12L gene (data not shown).

Proteins with deleted hendecad and heptad motifs fail to transport DNA or are not incorporated into virions. During genome piloting, the coiled-coil domain spans the periplasmic space or a membrane adhesion zone (8, 32). A minimal length is likely required to bridge this gap. Although characterizing the phenotypes associated with length-shortened tubes could directly address this question, internal deletions could also affect H protein incorporation or oligomerization. To explore these possibilities, nine cloned H genes with internal deletions were constructed. The mutant genes lacked DNA encoding a single hendecad ($\Delta 11$), a single heptad ($\Delta 7$), or two sequential heptads ($\Delta 14$). Cloned-gene expression was assayed for the ability to complement an *am(H)* mutant or inhibit wild-type plaque formation. Unlike the cloned wild-type gene, the mutant genes were unable to complement (Table 2.2). Although wild-type plating efficiency was not significantly lowered, the expression of the $\Delta 11$ -1 and $\Delta 11$ -2 genes reduced wild-type plaque size. Expression of the remaining genes, the $\Delta 11$ -3, $\Delta 7$ -3, $\Delta 7$ -10, $\Delta 14$ -2&3, $\Delta 14$ -3&4, $\Delta 14$ -9&10, and $\Delta 14$ -10&11 genes, did not affect wild-type plating efficiency or plaque size.

To determine whether the ΔH proteins failed to function in DNA transport or were not incorporated during assembly, lysis-resistant cells expressing the deletion constructs were infected with an *am(H)* mutant. The resulting particles were purified (Fig. 2.4A and B), and their protein composition (Fig. 2.4D and E) and specific infectivity (Table 2.3) were determined. In this assay, specific infectivity is strictly defined as PFU/ A_{280} , regardless of the genotype of the plaque-forming particle. For particles generated in cells expressing

the mutant H genes, plaques were formed by am^+ revertants. Thus, the actual specific infectivity of the mutant particles is lower than the assay suggested.

The sedimentation profiles of the *am(H)* infections are depicted in Fig. 4A and B. Particles containing mutant H proteins or lacking H protein are known to sediment at 110S and/or 70S (33). Therefore, naturally occurring am^+ revertants were used to estimate particle S values. When the *am(H)* mutant was complemented by the cloned wild-type gene, particle infectivity and absorbance peaks aligned. In contrast, particles from infections with uncomplemented mutants or from cells expressing the $\Delta 7$ and $\Delta 14$ H genes migrated in two distinct peaks. The material in the faster peak migrated slightly slower than 114S. As previously documented for particles that sediment at 110S (33), these particles exhibited a reduced specific infectivity (Table 2.3) and lacked scaffolding proteins (Fig. 2.4D and E). The A_{260}/A_{280} ratios, used to estimate DNA content, did not significantly differ from that of the wild type (data not shown). The rightmost peak is likely composed of 70S particles. Noninfectious, they arise from aborted genome packaging attempts or premature eclipse (33).

Although all infections of $\Delta 7$ - and $\Delta 14$ gene-expressing cells produced assembled particles (Fig. 2.4A and B), H protein content varied depending on which heptad(s) was deleted (Fig. 2.4D). Only the proteins lacking just the 10th or both the 10th and 11th heptads appeared to be incorporated efficiently. However, the expression of these cloned genes did not affect wild-type plating efficiency or plaque size, as would be expected if virions contained H proteins of two different lengths. This suggests that the shortened

proteins cannot compete with the wild-type protein for incorporation. To test this hypothesis, cells expressing the cloned $\Delta 7-10$ or $\Delta 14-10\&11$ genes were infected with either wild-type or *am(H)* $\phi X174$. Cells expressing the cloned $\Delta 14-9\&10$ gene were used as a control for an unincorporated protein. Expression of the cloned genes did not appear to affect wild-type progeny sedimentation (Fig. 2.4D): infectivity and A_{280} peaks coincided, and specific infectivity was not significantly reduced (Table 2.3). Particles were analyzed by SDS-PAGE (Fig. 2.4E). For each exogenously expressed ΔH gene, the particles synthesized in cells infected with either the wild type or the *am(H)* mutant were analyzed adjacent to each other. The wild-type H protein migrates more slowly than the ΔH proteins. While the $\Delta 7-10$ or $\Delta 14-10\&11$ proteins are present in the particles produced in the *am(H)* mutant infections, only the larger wild-type protein is present in the particles isolated from wild-type-infected cells.

A similar analysis was conducted with $\Delta 11$ proteins. *am(H)* progeny produced in cells expressing $\Delta 11$ H genes were characterized as described above. The resulting particles were not infectious and migrated slower than 114S (Fig. 2.5A and Table 2.3). H protein content varied depending on which hendecad motif was deleted. As can be seen in Fig. 5C, $\Delta 11-1$ and $\Delta 11-2$ proteins were incorporated into particles, whereas $\Delta 11-3$ proteins were not. As previously described, $\Delta 11-1$ and $\Delta 11-2$ gene expression reduced wild-type plaque size. To investigate this dominant negative effect, cells expressing $\Delta 11$ constructs were infected with the wild-type virus (Fig. 2.5B). Particles synthesized in $\Delta 11-1$ and $\Delta 11-2$ gene-expressing cells exhibited a reduced infectivity compared to those assembled in $\Delta 11-3$ gene-expressing or nonexpressing cells (Table 2.3). The $\Delta 11-1$ and

$\Delta 11-2$ proteins were incorporated at approximately equal levels alongside the wild-type protein (Fig. 2.5C). Incorporation of the $\Delta 11-1$ and $\Delta 11-2$ proteins likely reduced both infectivity and plaque size.

Irrespective of functional piloting and incorporation, all mutant proteins retain some level of function. In addition to the aforementioned functions, *de novo* H protein synthesis is required for the efficient production of other viral proteins (16). To determine if the $\Delta 7$, $\Delta 11$, and $\Delta 14$ H proteins retained the last function, lysis-resistant cells expressing the ΔH gene constructs were infected with an *am(H)* mutant. The resulting whole-cell lysates were examined by SDS-PAGE 3 h post infection. Without complementation, the amount of viral coat protein seen in lysates of cells infected with the *am(H)* mutant is greatly diminished (Fig. 2.6, top, rightmost lane). Complementation with the wild type or any of the ΔH genes restored coat protein levels to that observed in infections with the wild type. This result demonstrates that once in the cell, this additional function occurs independently of the protein's ability to be incorporated into particles.

Reversion analysis of ΔH mutants. To determine if the virus could adapt and utilize the ΔH proteins, a reversion analysis was conducted. For this analysis, the ΔH genes were constructed directly within the $\phi X174$ genome instead of being expressed from a plasmid. This allows selective pressure to be applied to all viral genes. The resulting strains displayed a complementation-dependent phenotype, growing only in cells expressing a cloned wild-type gene (Table 2.4). A cloned H gene from the related $\alpha 3$ bacteriophage also complemented. Based on sequence similarities, the overall

architecture and length of the $\alpha 3$ and $\phi X174$ coiled-coil domains are identical. To avoid recovering wild-type recombinants when selecting for second-site revertants, ΔH mutants were propagated in cells expressing the $\alpha 3$ H gene before the selection. Although the $\Delta 7-10$, $\Delta 11-1$, $\Delta 11-2$, and $\Delta 14-10\&11$ mutants were recovered, they could not be propagated in cells synthesizing the $\alpha 3$ H protein, likely because the proteins could outcompete $\alpha 3$ H for incorporation. To alleviate this problem, an amber mutation was placed at a glutamine codon immediately upstream of the deleted hendecad or heptad(s), resulting in the $\Delta 7-10am$, $\Delta 11-1am$, $\Delta 11-2am$, and $\Delta 14-10\&11am$ mutants. Although this prevented the synthesis of the ΔH proteins during viral propagation, ΔH -utilizing mutants could still be isolated on *supE* cells. The *supE* informational suppressor inserts glutamine at amber codons during translation.

Revertants were selected for the loss of the complementation- dependent phenotype. Only two types of revertants were isolated, one each from the $\Delta 11-1am$ and $\Delta 7-3$ mutants. In the $\Delta 11-1am$ revertant, the hendecad immediately following the deletion was duplicated. Thus, the revertant ($\Delta 11-1am+11$) possessed a wild- type number of hendecads but not a wild-type sequence. This mutant was independently isolated from two stocks; in each instance, it appeared at a frequency of 10^{-9} . Amber reversion resulted in the $\Delta 11-1+11$ strain (Fig. 2.1E), which displayed a wild-type plating phenotype and specific infectivity (data not shown). In addition, a more complex reversion event occurred during strain construction. The resulting $H+11$ mutant contained four hendecads (Fig. 2.1D). Its phenotype and specific infectivity were similar to those of the wild type. In coinfections, both the wild- type and H+11 proteins were incorporated into particles. These particles

also exhibited a reduced specific infectivity, 4.7×10^{11} PFU/A₂₈₀, compared to 1.7×10^{12} PFU/A₂₈₀ and 9.7×10^{11} PFU/A₂₈₀ for the wild-type and H+11 parents, respectively.

The $\Delta 7-3$ revertant contained a true deletion utilizer. It was isolated from two independently grown stocks at a frequency of 10^{-8} (Table 2.4). A single point mutation in gene H, causing a G→V substitution at amino acid 80, restored plaque formation. Although utilizers of the other ΔH proteins were not found above a frequency of 10^{-9} , recombination rescue experiments were performed to determine if the G80V mutation was active in other backgrounds. Two plasmids containing only a portion of the H gene were used in these experiments. One plasmid contained the G80V mutation, while the other contained only wild-type sequence. As these plasmids contain only the first 149 codons of the complete 328 codon gene, ΔH or *am(H)* mutant plaque formation requires recombination with the plasmid. These results are presented in Table 2.4. A mutant with an amber mutation at codon 26, the *am(H)Q26* mutant, served as a positive control. In the absence of a complementing clone, it exhibited a reversion frequency of 4×10^{-6} . However, in the presence of the wild-type or G80V H gene fragments, plating efficiency rose to 10^{-3} and 9.0×10^{-4} , respectively. The higher plating efficiency on non-complementing cells resulted from recombination rescue. The $\Delta 7-3$ revertant produced viable recombinants in cells containing the G80V gene H fragment at a frequency of 3×10^{-4} . No viable recombinants were obtained in cells containing the wild-type gene H fragment (frequency $< 5.0 \times 10^{-7}$). The plating efficiencies of the remaining mutants—the *$\Delta 7-10am$* , *$\Delta 11-1am$* , *$\Delta 11-2am$* , *$\Delta 11-3$* , *$\Delta 14-2\&3$* , *$\Delta 14-3\&4$* , *$\Delta 14-9\&10$* , and *$\Delta 14-$*

I0&I1am mutants—were several orders of magnitude lower than the positive control, indicating that the G80V mutation is not active in these backgrounds.

2.4 Discussion

Fully assembled tubes are unlikely to exist in the capsid. The inner diameter of the ϕ X174 capsid is 172 Å, whereas the H-tube is 170 Å in length. The similar dimensions suggest that the assembled tube is not stored in the capsid. To test this hypothesis, tubes were theoretically lengthened by inserting either one hendecad or two heptad motifs, increasing the tube length by 16 or 18 Å, respectively. However, the X-ray structures of the length-altered proteins were not determined.

The H+14 mutant displayed a *cs* phenotype and a reduced specific infectivity, approximately one-half the wild-type value. At the restrictive temperature, attachment, eclipse, and DNA piloting appeared to be unaffected; however, mutant particles assembled more slowly than the wild-type control. The underlying molecular defect remains to be determined. The mutant H protein could be incorporated into pentameric assembly intermediates more slowly than the wild-type protein, or the resulting intermediates may be less efficiently organized into procapsids. Nonetheless, a single substitution within the inserted sequence (*H+14 R12L*) suppressed the assembly defect and restored specific infectivity to the wild-type level. The nearly wild-type phenotype of the *H+14 R12L*, as well as the wild-type phenotype of the *H+11* mutant, demonstrates that the virus can tolerate these insertions. This result, along with the absence of an external tail-like structure, strongly suggests that the H-tube is not fully assembled in the

capsid. The proteins may remain monomeric or could associate into a semiassembled, core-like structure. A core could be located in the virion's center or situated under a single 5-fold axis of symmetry, creating a unique vertex. Further structural studies are necessary to investigate these possibilities. Previous X-ray structures or electron microscopy (EM) reconstructions could not determine the location of H proteins due to the imposition of icosahedral averaging and/or noise created by the packaged DNA (8, 34, 35).

Defective particles containing functional H proteins of differing lengths support the biological significance of the X-ray structure. In the H-tube structure, equivalent heptad and hendecad motifs are aligned via specific interhelical contacts. This arrangement likely keeps the parallel α -helices in register, possibly guiding tube assembly and ensuring stability during genome piloting. If functional H proteins of differing lengths were packaged into the same particle, the length mismatch would place α -helices out of register and likely prevent proper tube assembly. To test the biological significance of this arrangement, cells were coinfecting with wild-type and the equally infectious *H+14 R12L* or *H+11* mutants. The two H proteins were found at equal levels in the resulting 114S particle population, but a significant portion of the population was defective. The incorporation of both H protein species likely explains the loss of specific infectivity. This reduction was not complete; approximately 10% of particles were still infectious. Virions can carry 12 H proteins. However, only 10 compose an H-tube. Although some virions may contain 10 identical H proteins, the probability of this randomly occurring is far lower than 10% if each species of H protein is incorporated

with equal efficiency. Indeed, the elongated and wild-type H proteins appear to be present in the progeny population at roughly equal levels. This suggests that a functional tube can be constructed with some heterogeneous protein combinations or that there is a cis-acting mechanism that partially governs assembly: i.e., virions are preferentially assembled from proteins translated from the same message. Similar results were obtained with the $\Delta 11-1$ and $\Delta 11-2$ deletion proteins that could effectively compete with the wild-type protein.

Deletions of hendecad and heptad motifs result in H protein incorporation defects and/or infectivity loss. The ΔH proteins can be divided into two groups: those that were incorporated into virions and those that were not. H proteins containing deletions within an 85-amino-acid segment, spanning the third hendecad to the ninth heptad, were not efficiently incorporated into particles (Fig. 2.4D). This region either contains an incorporation domain or is essential for its proper folding. However, a single amino acid substitution, G80V, in *cis* with the $\Delta 7-3$ mutation resulted in viable virions. This suppressor is allele specific, rescuing only the $\Delta 7-3$ mutant. This mutation resides 128 residues away from the deletion, possibly indicating that multiple regions affect incorporation. Alternatively, the G80V substitution may suppress competing off-pathway reactions favored by the $\Delta 7-3$ H protein. The other deletions may more efficiently promote these competing reactions, requiring multiple or stronger suppressors. Alternatively, the G80V substitution could rescue the incorporation of these proteins, but unlike $\Delta 7-3$ protein, they may be unable to form functional tubes. Our assays were

based on the formation of viable progeny; thus, they do not distinguish between these models.

Proteins with deletions of the first two hendecads or the last two heptads were incorporated. However, these particles were un- infectious, indicating a defect in tube formation or genome piloting. These proteins differed in the ability to compete with the wild-type H protein. When the wild type was allowed to assemble in the presence of $\Delta 11-1$ and $\Delta 11-2$ proteins, the two species were incorporated at approximately equal levels. As before, the resulting hybrid particles exhibited reduced infectivity. In contrast, only the wild-type H protein was found in particles synthesized in the presence of the $\Delta 7-10$ and $\Delta 14-10\&11$ proteins.

Tube length requirements and its evolution. A minimum tube length is likely required to span the cell wall. Compared to the wild-type structure, deletions of two heptads, one hendecad, or a single heptad would, respectively, shorten the 170-Å tube by approximately 18 Å, 16 Å, or 9 Å. The G80V mutation permitted $\Delta 7-3$ mutant protein incorporation into viable progeny, which reduces the minimum tube length to 161 Å. The assays used in these studies measure viability: ΔH proteins that fail to properly oligomerize cannot be distinguished from those too short to span the cell wall. Thus, the minimal tube length imposed by the host has not been precisely determined. The tube length required for infectivity could change throughout the course of evolution. If the cell wall became thicker, the virus would need to adapt by duplicating DNA encoding

repeating motifs. Indeed, duplication events occurred during our studies: the $\Delta 11-1$ mutant duplicated a neighboring hendecad, restoring the protein to wild-type length.

Multiple functions likely require multiple structures. H protein must adopt at least two conformations during the viral life cycle. It is incorporated as a monomer during procapsid assembly and then oligomerizes into a tube during infection. As discussed above, both conformations can be perturbed by deleting a hendecad or heptad. It was previously demonstrated that efficient viral coat protein production requires *de novo* H protein synthesis (16), indicating that H plays another intracellular role in the viral life cycle independent of assembly. Thus, it is likely that H has a third conformation.

Regardless of the incorporation and tube assembly defects, exogenous expression of each ΔH construct restored *am(H)* coat protein synthesis to wild-type levels, indicating that its ability to perform this third function has remained intact. The region(s) of the protein associated with this function has yet to be determined.

2.5 Materials, Methods, and Acknowledgements

Phage plating, media, buffers, and stock preparation. Plating, media, buffers, and stock preparation have been previously described (17).

Bacterial strains, phage strains, and plasmids. The *Escherichia coli* C strains C122 (Su-), BAF5 (*supE*), and BAF30 (*recA*) have been previously described (17, 18). RY7211 contains a mutation in the *mraY* gene, conferring resistance to viral E protein-mediated lysis (19).

The ϕ X174 H gene was cloned by PCR amplification. DNA between nucleotides 2931 and 3917 in the published sequence (20) was amplified with primers that introduced an XbaI site upstream of the gene's start codon and a downstream XhoI site. The PCR product was digested with XbaI and XhoI and ligated into pSE420 DNA (Invitrogen) digested with the same enzymes.

Cloned Δ 11 H genes were constructed by first PCR amplifying the gene's 5' region up to the hendecad to be deleted. The upstream primer introduced an XbaI site as described above. The introduced downstream restriction sites were SacII for the Δ 11-1 gene, NaeI for the Δ 11-2 gene, and SpeI for the Δ 11-3 gene. The PCR product and pSE420 were digested with the desired enzymes and ligated. The remaining 3' H gene codons were then PCR amplified with primers introducing restriction sites at each end of the product. The downstream primer introduced an XhoI site, while the upstream primers introduced the matching restriction site downstream of the 5' cloned fragment. The PCR products and the respective cloned 5' genes were digested and ligated.

Clones of all Δ 7 and Δ 14 H genes were constructed by directly mutagenizing the cloned ϕ X174 H gene. Primers were designed to flank the heptad(s) to be deleted. The entire plasmid was then PCR amplified using Q5 DNA polymerase (New England BioLabs [NEB]) and the requisite primers. The PCR product's 5' hydroxyl termini were phosphorylated and ends ligated using T4 polynucleotide kinase and ligase

(New England BioLabs), respectively. The nucleotide sequence of all clones was verified by a direct DNA sequencing analysis.

The H+14 clone was generated by first PCR amplifying nucleotides 2931 to 3719 of the ϕ X174 sequence, which includes the 5' region of gene H up to the insertion site for the additional 14 codons. The upstream primer introduced an XbaI site as described above. The downstream primer introduced seven codons of the inserted sequence and a BmgBI restriction site. The PCR product was digested with XbaI and BmgBI and ligated into pSE420 digested with the same enzymes. ϕ X174 nucleotides 3720 to 3917 were then PCR amplified. The upstream primer introduced a BmgBI restriction site along with the remaining seven codons of the inserted sequence. The downstream primer introduced an XhoI site. The PCR product and the previously constructed clone were digested with BmgBI and XhoI. The digestion products were ligated, resulting in the cloned H+14 gene.

ϕ X174 H+14 was generated via recombination-rescue with a non-expressing H+14 clone. A mutant containing an amber mutation at codon E265 in gene H, the *am(H)E265* mutant, was plated on cells containing the plasmid at 37°C. Plaques that developed at a frequency higher than the am^+ reversion frequency were isolated. The H genes were sequenced to confirm the presence of the inserted codons.

To generate the ϕ X174 $\Delta I1-1am$ and $\Delta I1-2am$ amber mutants, ssDNA

was first mutated by site-directed mutagenesis as previously described (21). For the $\Delta 11-1am$ mutant, Eco53KI and EcoRV restriction sites were, respectively, introduced into gene H codons 154 and 165 and 166 along with an amber mutation in codon 151. For the $\Delta 11-2am$ mutant, Eco53KI and EcoRV restriction sites were, respectively, introduced in codons 164 and 165 and 175 and 176 with an amber mutation in codon 158. The mutated DNA was transfected into cells expressing the wild-type H gene. The resulting amber mutants were isolated and their replicative-form (RF) DNA was purified as previously described (22), digested with the requisite enzymes, and re-ligated. The ligation product was transfected into cells expressing the H gene of phage $\alpha 3$, and the resulting $\Delta 11-1am$ and $\Delta 11-2am$ mutants were isolated and sequenced to verify the genotype.

The $\phi X174 \Delta 7-3$, $\Delta 7-10am$, $\Delta 11-3$, $\Delta 14-2\&3$, $\Delta 14-3\&4$, $\Delta 14-9\&10$, and $\Delta 14-10\&11am$ mutants were generated using the same method as used to generate $\Delta 7$ and $\Delta 14$ H gene clones. Primers flanked the hendecad or heptad(s) to be deleted and, if necessary, introduced amber codons. The entire genome was then PCR amplified with Q5 DNA polymerase (NEB) and the described primers. The product's 5' hydroxyl termini were phosphorylated and ends ligated using T4 polynucleotide kinase and ligase (NEB), respectively. The resulting viral genomes were transfected into cells expressing the H gene of phage $\alpha 3$. Mutants were isolated as described above and sequenced to verify their genotypes.

Generation of ssDNA and double-stranded RF DNA, rate zonal sedimentation, and protein electrophoresis. The protocols for ssDNA and double-stranded RF DNA

isolation and purification, rate zonal sedimentation, and protein electrophoresis protocols have been previously described (21–23).

Attachment, eclipse, and coat protein quantification. Attachment and eclipse assays have been previously described (24, 25). Coat protein quantification as a surrogate marker for genome piloting was performed as follows. Phage were pre-attached to RY7211 cells infected at a multiplicity of infection (MOI) of 1.0 in HFB buffer (17) at 15°C and incubated for 30 min. The infected cells were pelleted at 4°C and the supernatant was removed. Infected cells were suspended in 1.0 ml of iced TKY medium (1.0% tryptone, 0.5% KCl, 0.5% yeast extract) with 10mM MgCl₂ and 5.0 mM CaCl₂. The infected cells were added to 9.0 ml of TKY broth with 10 mM MgCl₂ and 5 mM CaCl₂ warmed to the experimental temperatures. At the desired time points, 1.0-ml aliquots were pelleted and resuspended in 0.1 ml of HFB buffer. Ten microliters of the concentrated sample was diluted into 90 µl of BE buffer (17) containing 10 mg/ml of lysozyme. Infected cells were allowed to lyse overnight at 4°C, and the titers of released virions were determined. The remainder of the concentrated sample was placed at -20°C immediately after collection. Thirty-microliter volumes of the concentrated samples were run on SDS-PAGE gels as previously described (23). SDS-PAGE gels were stained with Coomassie brilliant blue and digitized with a LICOR scanner. Relative coat protein levels were determined by densitometry analysis using ImageJ software (NIH). Coat protein intensity was normalized to the intensity of a host protein band indicated in Fig. 3.

Acknowledgements

We would like to acknowledge S. M. Doore for productive discussions. This research was supported by National Science Foundation grants MCB-1408217 (B.A.F.), U.S. Department of Agriculture Hatch funds to the University of Arizona, and the BIO5 Institute.

2.6 References

1. Leiman PG, Schneider MM. 2012. Contractile Tail Machines of Bacteriophages, p. 93–114. *In* Rossmann, MG, Rao, VB (eds.), *Viral Molecular Machines*. Springer US, Boston, MA.
2. Hu B, Margolin W, Molineux IJ, Liu J. 2013. The bacteriophage T7 virion undergoes extensive structural remodeling during infection. *Science* (80-) 339:576–579.
3. Esquinas-rychen M, Erni B. 2001. Facilitation of Bacteriophage Lambda DNA Injection by Inner Membrane Proteins of the Bacterial Phosphoenolpyruvate:Carbohydrate Phosphotransferase System (PTS). *J Mol Microbiol Biotechnol* 3:361–370.
4. Russel M, Model P. 2006. Filamentous phage, p 146–160. *In* Calendar R (ed), *The bacteriophages*, 2nd ed. Oxford Press, London, United Kingdom.
5. Van Duin J, Tsareva N. 2006. Single-stranded RNA phages, p 175–196. *In* Calendar R (ed), *The bacteriophages*, 2nd ed. Oxford Press, London, United Kingdom
6. Jazwinski SM, Lindberg AA, Kornberg A. 1975. The gene H spike protein of bacteriophages Φ X174 and S13. I. Functions in phage-receptor recognition and in transfection. *Virology* 66:283–293.
7. Jazwinski SM, Marco R, Kornberg A. 1975. The gene H spike protein of bacteriophages Φ X174 and S13. II. Relation to synthesis of the parental replicative form. *Virology* 66:294–305.
8. Sun L, Young LN, Zhang X, Boudko SP, Fokine A, Zbornik E, Roznowski AP, Molineux IJ, Rossmann MG, Fane BA. 2014. Icosahedral bacteriophage Φ X174 forms a tail for DNA transport during infection. *Nature* 505:432–435.
9. Sun L, Rossmann MG, Fane BA. 2014. High-Resolution Structure of a Virally Encoded DNA-Translocating Conduit and the Mechanism of DNA Penetration. *J Virol* 88:10276–10279.
10. Tang J, Lander GC, Olia A, Li R, Casjens S, Prevelige P, Cingolani G, Baker TS, Johnson JE. 2011. Article Peering Down the Barrel of a Bacteriophage Portal : The Genome Packaging and Release Valve in P22. *Struct Des* 19:496–502.
11. Olia AS, Prevelige PE, Johnson JE, Cingolani G. 2011. Three-dimensional structure of a viral genome-delivery portal vertex. *Nat Struct Mol Biol* 18:597–

603.

12. Egelman EH, Xu C, DiMaio F, Magnotti E, Modlin C, Yu X, Wright E, Baker D, Conticello VP. 2015. Structural Plasticity of Helical Nanotubes Based on Coiled-Coil Assemblies. *Structure* 23:280–289.
13. Pieters BJGE, van Eldijk MB, Nolte RJM, Mecinović J. 2016. Natural supramolecular protein assemblies. *Chem Soc Rev* 45:24–39.
14. Cherwa JE, Organtini LJ, Ashley RE, Hafenstein SL, Fane BA. 2011. In vitro assembly of the ϕ X174 procapsid from external scaffolding protein oligomers and early pentameric assembly intermediates. *J Mol Biol* 412:387–396.
15. Cherwa JE, Uchiyama A, Fane BA. 2008. Scaffolding Proteins Altered in the Ability To Perform a Conformational Switch Confer Dominant Lethal Assembly Defects. *J Virol* 82:5774–5780.
16. Ruboyianes M V, Chen M, Dubrava MS, Cherwa JE, Fane BA. 2009. The Expression of N-Terminal Deletion DNA Pilot Proteins Inhibits the Early Stages of Φ X174 Replication. *J Virol* 83:9952–9956.
17. Fane BA, Hayashi M. 1991. Second-site suppressors of a cold-sensitive prohead accessory protein of bacteriophage ϕ X174. *Genetics* 128:663–71.
18. Fane BA, Head S, Hayashi M. 1992. Functional relationship between the J proteins of bacteriophages ϕ X174 and G4 during phage morphogenesis. *J Bacteriol* 174:2717–2719.
19. Bernhardt TG, Struck DK, Young R. 2001. The Lysis Protein E of ϕ X174 Is a Specific Inhibitor of the *MraY*-catalyzed Step in Peptidoglycan Synthesis. *J Biol Chem* 276:6093–6097.
20. Sanger F, Coulson AR, Friedmann T, Air GM, Barrell BG, Brown NL, Fiddes JC, Hutchison CA, Slocombe PM, Smith M. 1978. The nucleotide sequence of bacteriophage ϕ X174. *J Mol Biol* 125:225–246.
21. Fane BA, Shien S, Hayashi M. 1993. Second-site suppressors of a cold-sensitive external scaffolding protein of bacteriophage ϕ X174. *Genetics* 134:1003–11.
22. Burch AD, Ta J, Fane BA. 1999. Cross-functional analysis of the Microviridae internal scaffolding protein. *J Mol Biol* 286:95–104.
23. Uchiyama A, Fane BA. 2005. Identification of an Interacting Coat-External Scaffolding Protein Domain Required for both the Initiation of Φ X174 Procapsid Morphogenesis and the Completion of DNA Packaging. *J Virol* 79:6751–6756.

24. Cherwa JE, Sanchez-Soria P, Wichman HA, Fane BA. 2009. Viral Adaptation to an Antiviral Protein Enhances the Fitness Level to Above That of the Uninhibited Wild Type. *J Virol* 83:11746–11750.
25. Hafenstein SL, Chen M, Fane BA. 2004. Genetic and functional analyses of the ϕ X174 DNA binding protein: the effects of substitutions for amino acid residues that spatially organize the two DNA binding domains. *Virology* 318:204–213.
26. McKenna R, Bowman BR, Ilag LL, Rossmann MG, Fane BA. 1996. Atomic structure of the degraded procapsid particle of the bacteriophage G4: Induced structural changes in the presence of calcium ions and functional implications. *J Mol Biol* 256:736–750.
27. Cherwa JE, Young LN, Fane BA. 2011. Uncoupling the functions of a multifunctional protein: The isolation of a DNA pilot protein mutant that affects particle morphogenesis. *Virology* 411:9–14.
28. Young LN, Hockenberry AM, Fane BA. 2014. Mutations in the N Terminus of the Φ X174 DNA Pilot Protein H Confer Defects in both Assembly and Host Cell Attachment. *J Virol* 88:1787–1794.
29. Mano Y, Sakai H, Komano T. 1979. Growth and DNA synthesis of bacteriophage ϕ X174 in a dnaP mutant of *Escherichia coli*. *J Virol* 30:650–6.
30. Harbury P, Zhang T, Kim P, Alber T. 1993. A switch between two-, three-, and four-stranded coiled coils in GCN4 leucine zipper mutants. *Science* (80-) 262:1401–1407.
32. Bayer ME, Starkey TW. 1972. The adsorption of bacteriophage Φ X174 and its interaction with *Escherichia coli*; a kinetic and morphological study. *Virology* 49:236–256.
33. Spindler KR, Hayashi M. 1979. DNA synthesis in *Escherichia coli* cells infected with gene H mutants of bacteriophage ϕ X174. *J Virol* 29:973–82.
34. Dokland T, McKenna R, Llag LL, Bowman BR, Incardona NL, Fane BA, Rossmann MG. 1997. Structure of a viral procapsid with molecular scaffolding. *Nature* 389:308–313.
35. McKenna R, Xia D, Willingmann P, Ilag LL, Krishnaswamy S, Rossmann MG, Olson NH, Baker TS, Incardona NL. 1992. Atomic structure of single-stranded DNA bacteriophage phi X174 and its functional implications. *Nature* 355:137–43.

2.7 Figures and Tables

TABLE 2.1 Plating efficiency^a of H+14 and revertant mutants

Mutant	Temperature		
	24°C	33°C	42°C
Wild-Type	0.6	1.0	0.9
H+14	1×10^{-4}	1.0	0.9
H+14 T3I ^b	4×10^{-2}	1.0	1.5
H+14 R5H	0.3	1.0	0.6
H+14 H7Y	0.2	1.0	0.5
H+14 R12L	0.1	1.0	0.5

^a Plating efficiency is defined as assay titer/titer at 33°C.

^b Revertant names reflect the amino substitution found in within the inserted two heptads. Thus, T3I indicates a T→I substitution for amino acid 3 in the inserted sequence (Figure 2.1C).

TABLE 2.2 Wild-type and *am(H)* plating efficiencies^a on cells expressing $\Delta 7$, $\Delta 11$, or $\Delta 14$ H genes at 33°C.

Expressed gene	Virus		WT ^c plaque size reduction >50%
	<i>am(H)</i> ^b	wild-type	
None	6.0×10^{-5}	1.0	No
Wild-type H	1.0	1.1	No
$\Delta 7$ -3	1.5×10^{-4}	1.1	No
$\Delta 7$ -10	1.6×10^{-4}	1.0	No
$\Delta 14$ -2&3	1.6×10^{-4}	1.1	No
$\Delta 14$ -3&4	1.8×10^{-4}	1.1	No
$\Delta 14$ -9&10	1.7×10^{-4}	0.8	No
$\Delta 14$ -10&11	1.9×10^{-4}	0.9	No
$\Delta 11$ -1	$<4.0 \times 10^{-6}$	0.5	No
$\Delta 11$ -2	2.0×10^{-4}	1.2	Yes
$\Delta 11$ -3	2.0×10^{-4}	1.5	Yes

^a For *am(H)*, plating efficiency is defined as assay titer/titer on cells expressing the wild-type H gene. For wild-type, it is defined as assay titer/titer on cells with no cloned gene.

^b *am(H)G7* was used in the experiments with $\Delta 7$ and $\Delta 14$ H genes, whereas *am(H)Q158* was used in experiments with $\Delta 11$ genes. Both amber mutants exhibited the same reversion *am*⁺ frequency.

^c Plaques were compared to those formed on cells expressing the wild-type H gene.

TABLE 2.3 Specific Infectivity (pfu/A280) of 110S-114S particles produced in am(H)G7 and wild-type infections in cells expressing $\Delta 7$, $\Delta 11$, and $\Delta 14$ genes

Virus	Expressed Gene	Specific infectivity ^a		H Proteins Incorporated ^d	Corresponding Figure
		Raw ^b	Normalized ^c		
<i>am(H)G7</i>	None	2.0×10^{10}	2.0×10^{-2}	None	Fig. 4A, B, & D
	WT H	9.0×10^{11}	1.0	Yes	Fig. 4A, B, & D
	$\Delta 7$ -3	9.0×10^9	1.0×10^{-2}	None	Fig. 4A & D
	$\Delta 7$ -10	4.0×10^9	5.0×10^{-3}	Yes	Fig. 4B, D & E
	$\Delta 14$ -2&3	7.0×10^9	8.0×10^{-3}	Trace	Fig. 4A & D
	$\Delta 14$ -3&4	2.0×10^{10}	2.0×10^{-2}	Trace	Fig. 4A & D
	$\Delta 14$ -9&10	2.0×10^8	2.0×10^{-4}	No	Fig. 4B, D & E
	$\Delta 14$ -10&11	2.0×10^8	2.0×10^{-4}	Yes	Fig. 4B, D & E
Wild-Type	None	2.0×10^{12}	1.0	WT	Fig. 4C & E
	$\Delta 7$ -3	9.0×10^{11}	0.5	only WT	Data not shown
	$\Delta 7$ -10	2.0×10^{12}	0.8	only WT	Fig. 4C & E
	$\Delta 14$ -2&3	1.0×10^{12}	0.6	only WT	Data not shown
	$\Delta 14$ -3&4	2.0×10^{12}	1.1	only WT	Data not shown
	$\Delta 14$ -9&10	2.0×10^{12}	1.2	only WT	Fig. 4C & E
	$\Delta 14$ -10&11	1.0×10^{12}	0.8	only WT	Fig. 4C & E

Continued on following page

TABLE 2.3 Continued

Virus	Expressed Gene	Specific infectivity ^a		H Proteins Incorporated ^d	Corresponding Figure ^e
		Raw ^b	Normalized ^c		
<i>am(H)G7</i>	WT H	4.0×10^{11}	1.0	Yes	Fig 5A & C
	$\Delta 11-1$	2.0×10^8	5.0×10^{-4}	Yes	Fig 5A & C
	$\Delta 11-2$	2.0×10^8	5.0×10^{-4}	Yes	Fig 5A & C
	$\Delta 11-3$	4.0×10^7	9.0×10^{-5}	No	Fig 5A & C
Wild-type	none	4.0×10^{11}	1.0	WT	Fig 5B & C
	$\Delta 11-1$	2.0×10^{10}	7.0×10^{-2}	Both proteins	Fig 5B & C
	$\Delta 11-2$	2.0×10^{10}	4.0×10^{-2}	Both proteins	Fig 5B & C
	$\Delta 11-3$	4.0×10^{11}	1.1	Only WT	Fig 5B & C

^a In these assays specific infectivity is strictly defined as pfu's/A₂₈₀, regardless of the genotype of the plaque-forming particle (see text for details).

^b Raw data is pfu's/A₂₈₀.

^c For experiments conducted with *am(H)G7*, data is normalized to the specific infectivity of particles generated in cells expressing the wild-type H gene. For experiments conducted with wild-type ϕ X174, data is normalized to the specific infectivity of particles generated in cells without mutant cloned gene expression.

^d For experiments conducted with *am(H)G7*, “Yes” indicates that mutant H protein was found at levels comparable to the particles generated in cells expressing the wild-type H gene; “No:” H protein levels were below the sensitivity required for detection; “Trace:” a faint amount of protein could be detected by SDS-PAGE.

TABLE 2.4 Plating efficiency^a and recombination rescue of $\Delta 7$, $\Delta 11$, and $\Delta 14$ mutant phage.

Virus	Expressed cloned gene		Unexpressed clone of codons 1-149	
	None	Wild-type H	without G80V	with G80V
<i>am(H)Q26</i>	4.0×10^{-6}	1.0	1.0×10^{-3c}	9.0×10^{-4}
$\Delta 11$ -1am ^b	1.0×10^{-9}	1.0	$<3 \times 10^{-6}$	$<3 \times 10^{-6}$
$\Delta 11$ -2am	$<3 \times 10^{-9}$	1.0	$<5 \times 10^{-7}$	$<5 \times 10^{-7}$
$\Delta 11$ -3	$<2.0 \times 10^{-9}$	1.0	$<1.0 \times 10^{-6}$	$<1.0 \times 10^{-6}$
$\Delta 7$ -3	1.0×10^{-8}	1.0	$<5.0 \times 10^{-7}$	3.0×10^{-4}
$\Delta 7$ -10am	$<8.0 \times 10^{-9}$	1.0	$<1.0 \times 10^{-6}$	$<1.0 \times 10^{-6}$
$\Delta 14$ -2&3	$<8.0 \times 10^{-10}$	1.0	$<8.0 \times 10^{-6}$	$<8.0 \times 10^{-6}$
$\Delta 14$ -3&4	$<3.0 \times 10^{-10}$	1.0	$<2.0 \times 10^{-7}$	$<2.0 \times 10^{-7}$
$\Delta 14$ -9&10	$<6.0 \times 10^{-10}$	1.0	$<3.0 \times 10^{-7}$	$<3.0 \times 10^{-7}$
$\Delta 14$ -10&11am	$<1 \times 10^{-9}$	1.0	$<1 \times 10^{-6}$	$<1 \times 10^{-6}$

^a Plating efficiency is defined as assay titer/titer on cells expressing the wild-type H gene.

^b Plating efficiencies calculated with titers obtained on sup⁺ cells containing the specified clone.

^c bold text indicates recombination rescue.

FIGURE LEGENDS

FIG. 2.1 H protein structure and sequence. (A) The crystal structure of the H protein coiled-coil domain (PDB ID: 4JPP). A single monomer is shown in cyan. (B) The sequence of the H protein's structured region. Hendecad and heptad start positions, sequences, and numerical designations are listed in the figure. (C) The sequence and position of the 14 inserted amino acids found in the *H+14* mutant. Mutant residues are underlined. Arrows indicate mutated residues found in *cs* revertants. (D) The sequence and position of the inserted hendecad found in the *H+11* mutant. (E) The sequence and position of the hendecad duplication found in the *Δ11-1* revertant.

FIG. 2.2 Assembled particles produced in wild-type (black circles), *H+14* (white circles), and *H+14 R12L* (white squares), and wild-type × *H+14 R12L* infected cells (black squares). (A) 280nm absorbance profiles of infected cell extracts analyzed by rate zonal sedimentation. Fraction 1 represents the gradient bottom. Profiles were aligned by the most infectious fraction, marked 114S. (B) Specific infectivity (pfu/A₂₈₀ × 10¹²) of fractions. (C) SDS-PAGE analysis of 114S peaks.

FIG. 2.3 Characterization of the *H+14* mutant. (A) SDS-PAGE analysis of cells infected with either wild-type, *H+14*, or *H+14 R12L*. (B) Quantification of coat to host protein ratios seen in panel A; wild-type (black circles), *H+14* (white circles), *H+14 R12L* (white squares). The host protein used in this analysis is indicated in the figure. (C) Titers of

progeny produced in wild-type (black circles), *H+14* (white circles), or *H+14 R12L* (white squares) infected cells.

FIG 2.4 Characterization of the $\Delta 7$ and $\Delta 14$ proteins in *am(H)* or wild-type infected cells. 280nm absorbance profiles of either *am(H)* (A and B) or wild-type (C) infected cell extracts analyzed by rate zonal sedimentation. Particles were assembled in cells expressing cloned wild-type H (black), $\Delta 7-3$ (green), $\Delta 7-10$ (yellow), $\Delta 14-2\&3$ (red), $\Delta 14-3\&4$ (blue), $\Delta 14-9\&10$ (purple), $\Delta 14-10\&11$ (maroon) genes, and in non-expressing cells (white). Fraction 1 represents the gradient bottom. Profiles were aligned by the most infectious fraction, marked 114S. (D) SDS-PAGE analysis of particles produced in *am(H)* infected cells expressing cloned wild-type H (WT H), $\Delta 7-3$ ($\Delta 3$), $\Delta 7-10$ ($\Delta 10$), $\Delta 14-2\&3$ ($\Delta 2\&3$), $\Delta 14-3\&4$ ($\Delta 3\&4$), $\Delta 14-9\&10$ ($\Delta 9\&10$), and $\Delta 14-10\&11$ ($\Delta 10\&11$) genes, or non-expressing cells (NE). (E) SDS-PAGE analysis comparing wild-type and *am(H)* particles synthesized in cells expressing $\Delta 7-10$, $\Delta 14-9\&10$, or $\Delta 14-10\&11$ genes.

FIG. 2.5 Characterization of the $\Delta 11$ proteins in *am(H)* or wild-type infected cells. 280nm absorbance profiles of either *am(H)* (A) or wild-type (B) infected cell extracts analyzed by rate zonal sedimentation. Particles were assembled in cells expressing cloned wild-type (black), $\Delta 11-1$ (blue), $\Delta 11-2$ (green), $\Delta 11-3$ (purple) H genes, and in the absence of cloned gene expression (white). (C) SDS-PAGE analysis comparing wild-type (WT) and *am(H)* particles synthesized in cells expressing $\Delta 11-1$, $\Delta 11-2$, or $\Delta 11-3$ H genes.

FIG 2.6 Viral protein levels in *am(H)* infected cells with and without ΔH gene expression. Viral coat protein levels in uninfected (UI), wild-type (WT), and *am(H)* infected cells expressing the ΔH gene constructs.

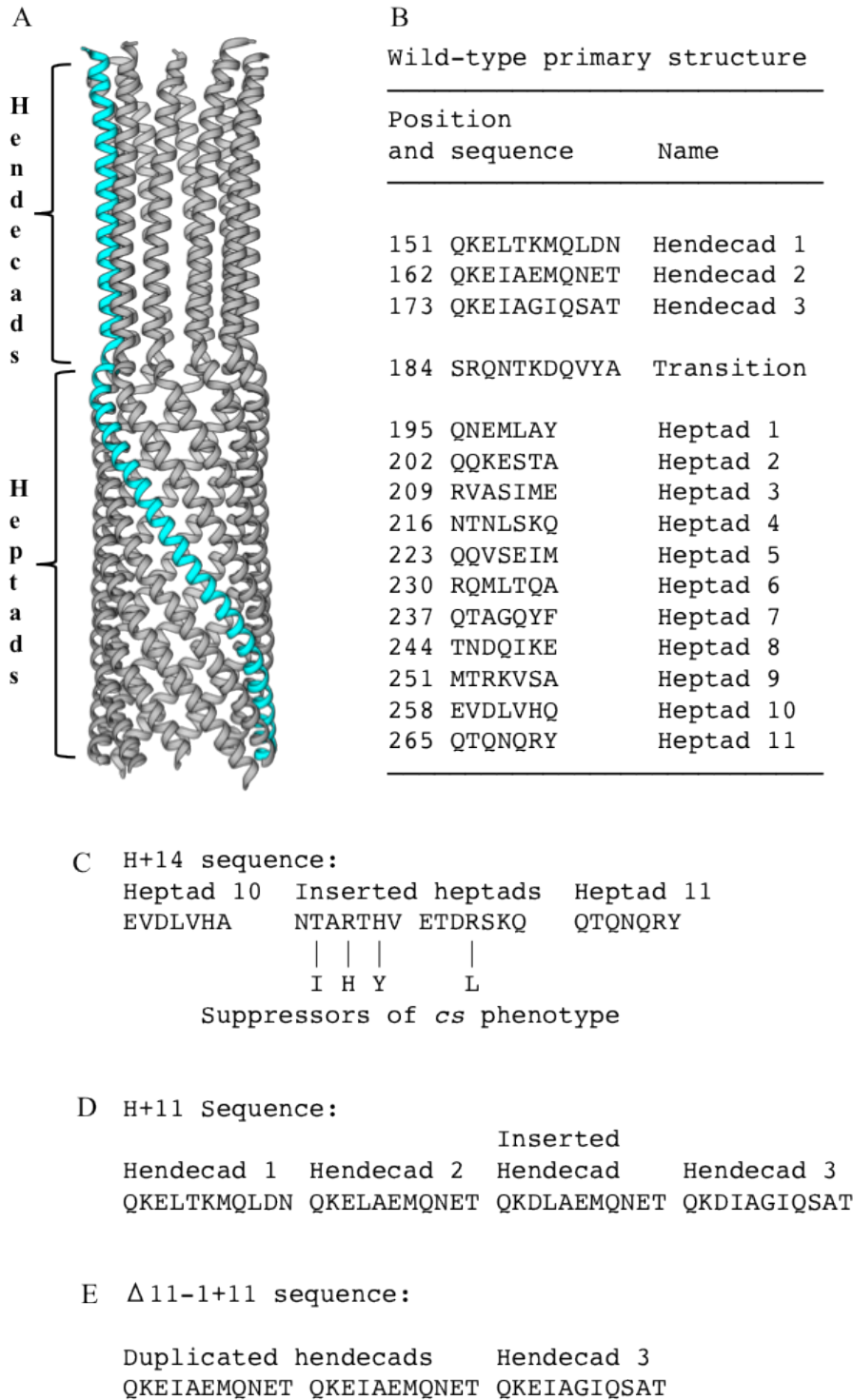


FIG 2.1 H protein structure and sequence

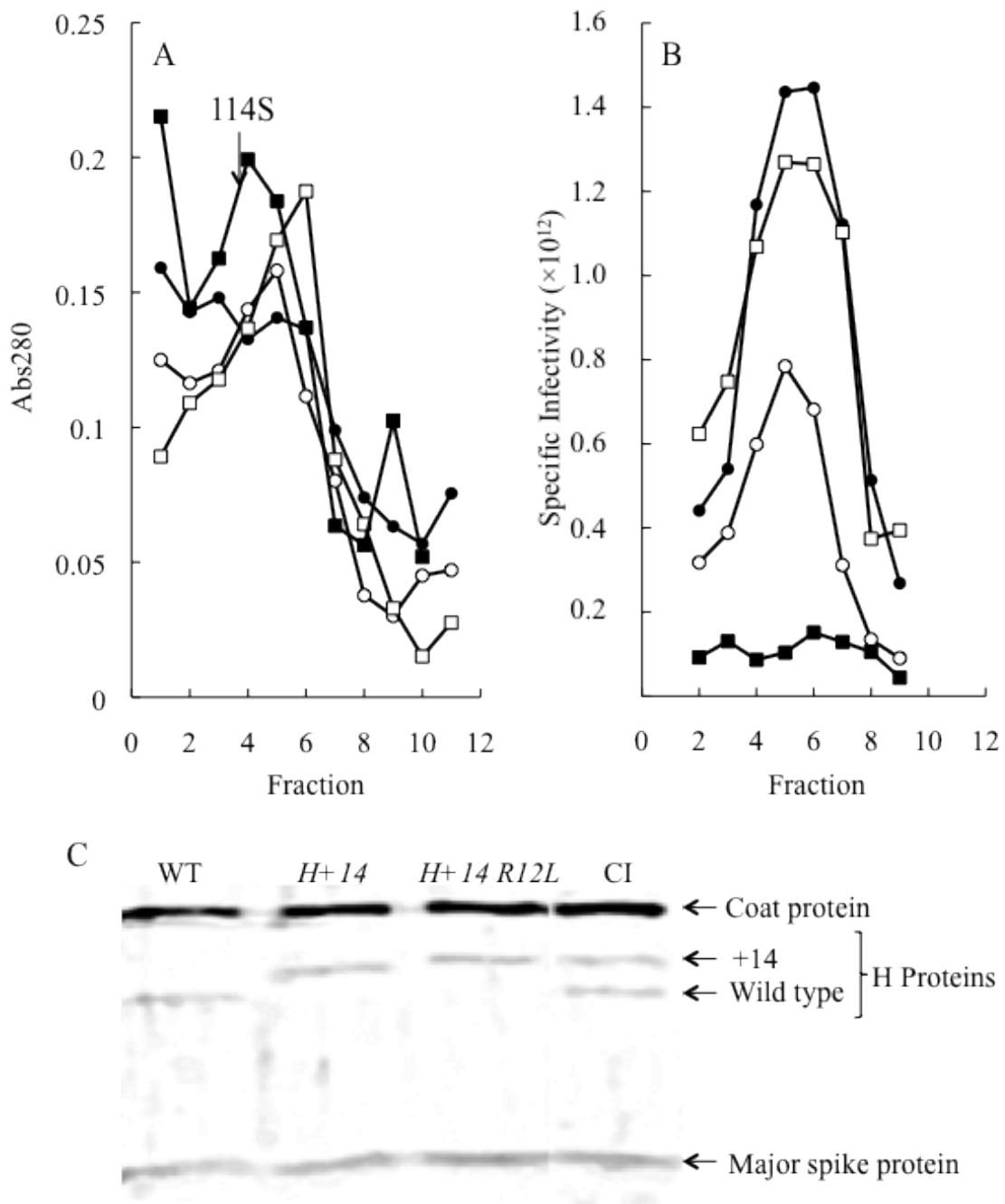


FIG 2.2 Assembled particles produced in wild-type, *H+14*, *H+14 R12L*, and wild-type \times *H+14 R12L* infected cells

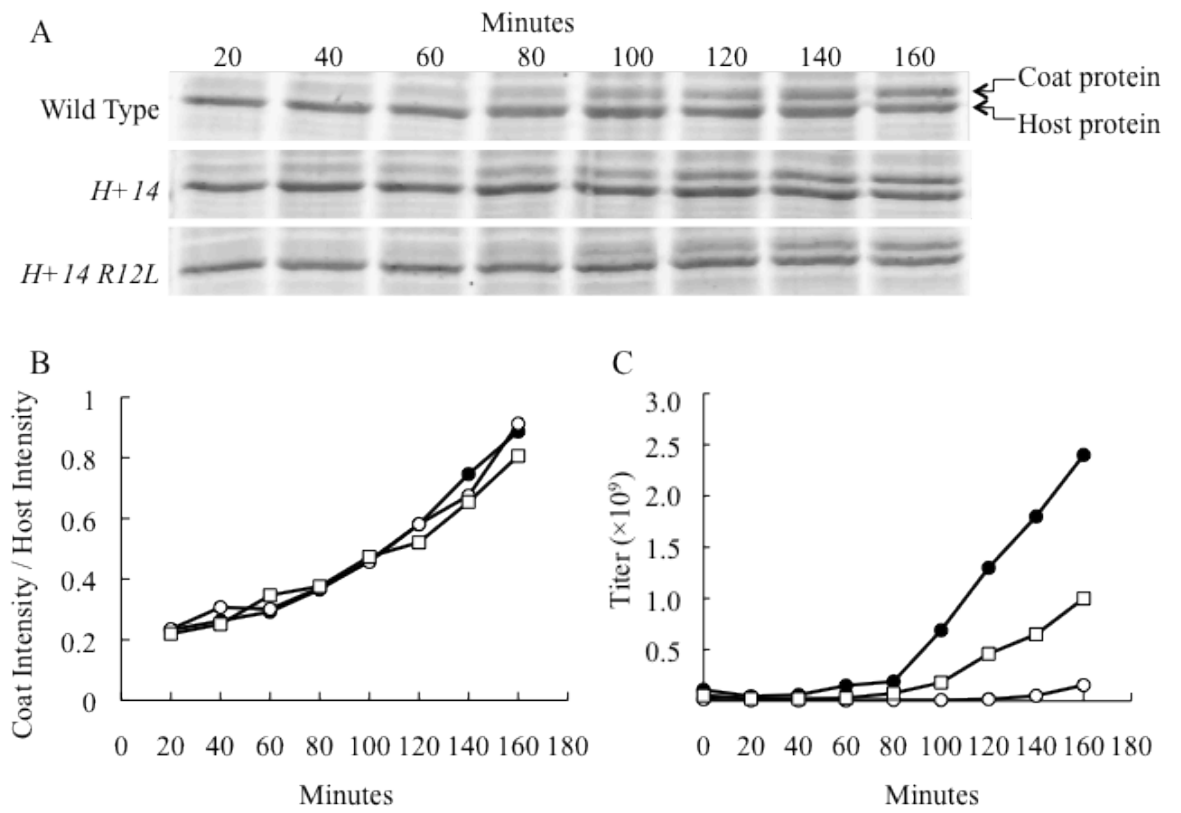


FIG 2.3 Characterization of the *H + 14* mutant

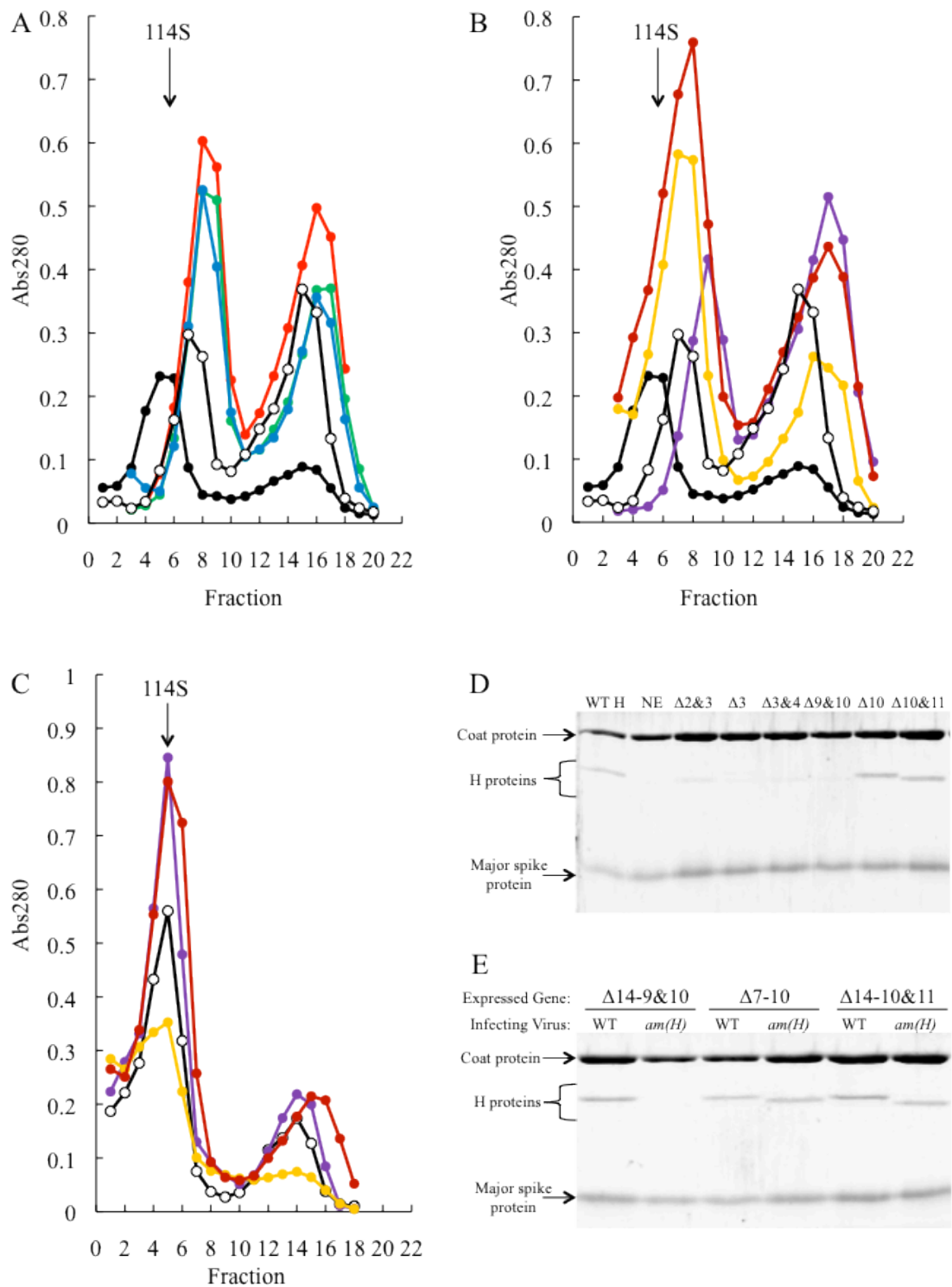


FIG 2.4 Characterization of the $\Delta 7$ and $\Delta 14$ proteins in *am(H)* or wild-type infected cells

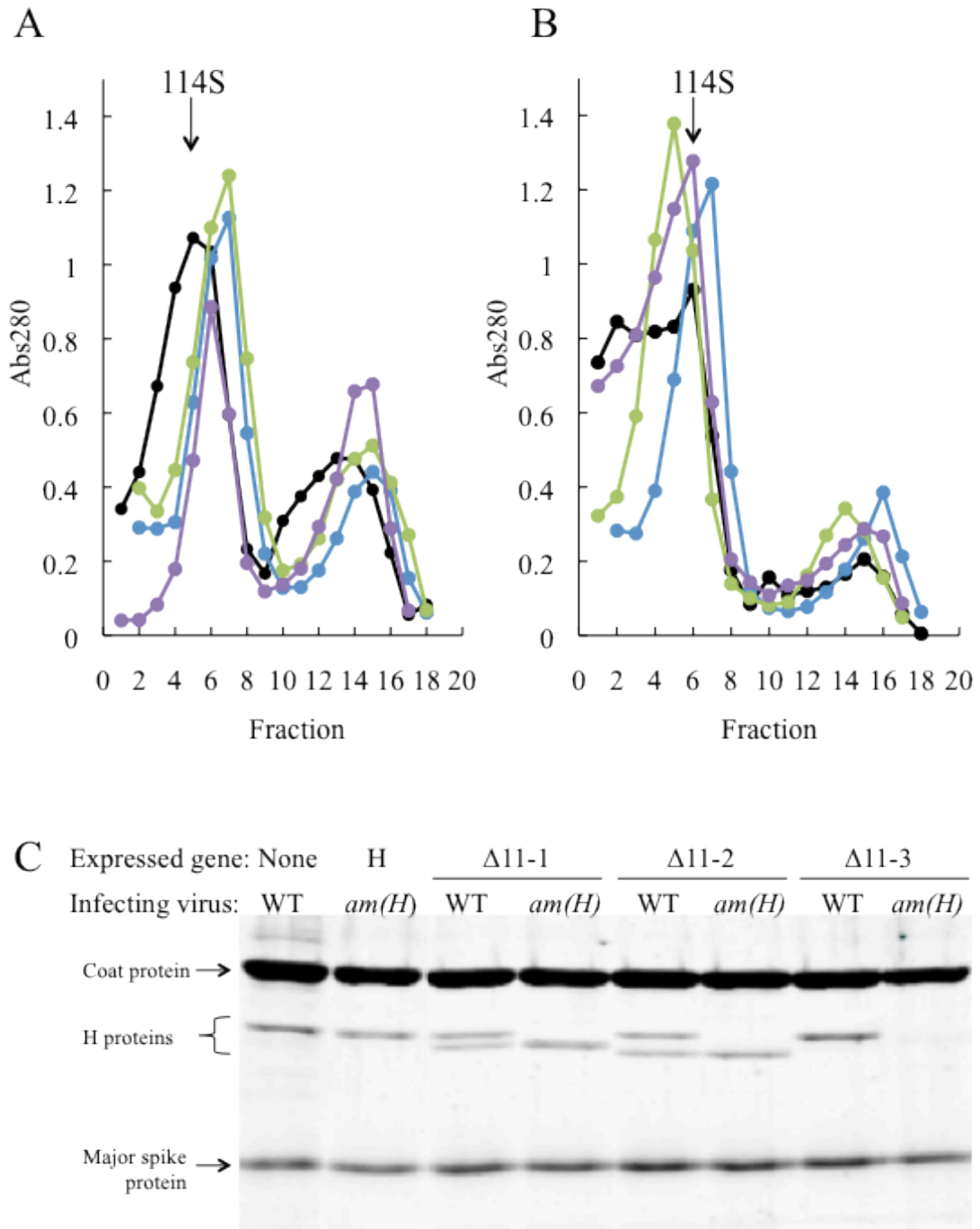


FIG 2.5 Characterization of the $\Delta 11$ proteins in *am(H)* or wild-type infected cells

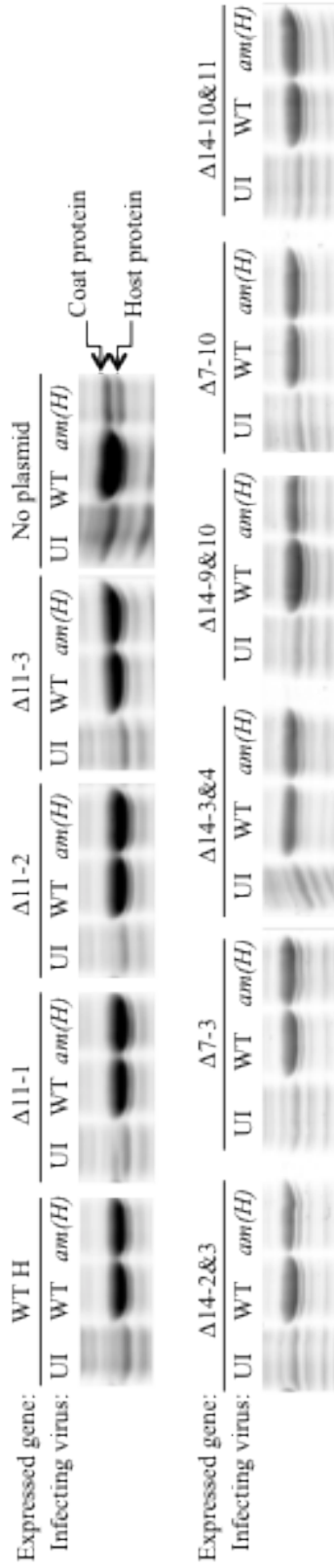


FIG 2.6 Viral protein levels in *am(H)* infected cells with and without ΔH gene expression

CHAPTER 3

MUTAGENIC ANALYSIS OF A DNA TRANSLOCATING TUBE'S INTERIOR SURFACE

3.1 Abstract

To initiate an infection, bacteriophage Φ X174 uses a collection of identical DNA piloting proteins to move its genome into a host *Escherichia coli*. To accomplish this, the piloting proteins oligomerize into a cell wall spanning, decameric tube that is wide enough for the genome to pass through. The inner surface of the tube is primarily lined with amide and guanidinium containing amino acid side chains with the exception of four sites near the tube's C-terminal end. The four sites are conserved across microvirus clades, suggesting that they may play an important role during genome delivery. To test this hypothesis and explore the general role of the amide and guanidinium containing side chains, the amino acids at these sites were changed to glutamine. The resulting mutants had a cold-sensitive phenotype at 22°C. Viral lifecycle steps were assayed in order to determine which step was disrupted by the mutant glutamine residues. Virion assembly, host adsorption, and virion eclipse were not affected. Genome delivery, however, appeared to be inhibited. The genome delivery event was dissected into two parts: 1) channel formation was observed by monitoring cytoplasmic K⁺ efflux, and 2) the location of the infecting genomes within fractionated host membranes was tracked with qPCR. The results support a model in which a balance of forces governs genome delivery: potential energy provided by the densely packaged viral genome and/or an osmotic gradient push the genome into

the cell, while the tube's inward facing residues exert a frictional force on the genome as it passes.

3.2 Introduction

To establish an infection, bacteriophages (phages) must move their hydrophilic genomes through hydrophobic host cell membranes. In general, phage virions undergo irreversible conformational changes after binding their requisite host surface receptor. The changes allow specialized cell wall breaching proteins to create an opening in the host's cytoplasmic membrane through which the genome passes. Genome transfer is powered by potential energy that may be stored within the highly condensed, packaged genome or by the osmotic gradient existing across the cytoplasmic membrane (1, 2).

The mechanism by which phage breach the gram-negative cell wall varies between phage families. Myovirus contractile tails push a rigid tube through the outer membrane and periplasm, allowing the tail's tip to puncture the cytoplasmic membrane. The linear, dsDNA genome then moves through this tube into the cytoplasm (3–5). Like myoviruses, podo- and siphoviruses use tail structures to breach outer membranes. However, their tails are not contractile; instead, proteins are ejected from the virion that form an inner membrane traversing conduit (6, 7). By contrast, the tail-less, icosahedral leviviruses use an attachment protein that binds to host pili (8). Pilus retraction pulls the virion to the cell surface where the attachment protein with its bound RNA genome enter the cell (9, 10). Similarly, filamentous inoviruses initially attach to host pili(11). Again, retraction brings the virion within reach of cytoplasmic membrane. Interactions between the virion and a

host periplasmic protein allow the viral coat proteins to melt into the cytoplasmic membrane, simultaneously delivering the ssDNA genome to the cytoplasm (12, 13).

The mechanism employed by the icosahedral, tail-less, ssDNA containing microviruses combines many features observed in the aforementioned phages. Microviruses first attach to host lipopolysaccharides, triggering the removal of a spike protein G complex at the membrane-interacting vertex (14). Whether the spike complex melds into the membrane, as is seen with inovirus coat proteins, is not known. A portion of the newly exposed coat protein pentamer interacts with the host's outer membrane. The coat proteins undergo a conformational change to form a pore at the virion's 5-fold axis of symmetry that is reminiscent of myovirus base plates transforming from closed to star configurations. Then, like the siphon and podovirus ejection proteins, 10 copies of the DNA pilot protein H emerge from the capsid. They form a genome translocating channel which has been visualized traversing the cell wall (15).

Protein H is monomeric during early assembly and within the procapsid (16–20); however, 10 encapsidated monomers must oligomerize for genome delivery(15). Although an H oligomer appears to exist in unopened, membrane-bound virions (14), it is unknown whether the monomers oligomerize into a core structure prior to host contact like that seen inside the T7 virion (5). After the virion opens, the H proteins form a channel to the cytoplasm through which Φ X174's circular, ssDNA genome moves. Afterwards, both H and the genome become associated with the host's cytoplasmic

membrane in a process that appears to be coupled to synthesis of the complementary genomic strand (21–23).

An X-ray structure of the ϕ X174 H protein's central domain was solved to 2.4 Å resolution (15). In the structure (Figure 3.1A), H protein residues 151-271 form a decameric α -helical tube that is 170 Å long and 22-25 Å wide. Although tube-like oligomers are typically associated with phages, a similar structure has recently been reported in caliciviruses (24). H protein likely adopts this structure during genome delivery, as the tube is long enough to span the host's cell wall and wide enough to permit passage of the circular genome's two antiparallel ssDNA strands (25). The tube's inner surface is primarily lined with amino acid side chains containing amide and guanidinium moieties. 18 of the 23 inward facing positions are occupied by asparagine, glutamine, and arginine side chains, with glutamine being the most abundant (Figure 3.1C). As these amino acids are frequently observed interacting with DNA nucleotides in other protein structures (26–29), they may be facilitating the release and transit of the phage genome.

Four of the five inward facing sites lacking amide and guanidinium groups cluster near the H-tube's C-terminus: T244, M251, K254, and E258 (Figure 3.1C and D). The location and chemical characteristics of this region are conserved across the three microvirus clades, indicating that this region may be important for optimal DNA transport. To test this hypothesis and explore the general role of the amide and guanidinium groups, the amino acids at these sites were changed to glutamine. The

results of the subsequent genetic and biochemical analyses suggest a general model in which the H-tube's inner surface exerts a frictional force on the passing viral genome. This may balance the force provided by capsid pressure and/or the osmotic gradient that drives the genome into the cytoplasm, thereby regulating genome delivery.

3.3 Results

Mutating inward facing residues to glutamine results in a cold sensitive phenotype.

Amino acid side chains with amide and guanidinium groups; like those found in asparagine, glutamine, and arginine; can interact with nitrogenous bases (26–29). Eighteen of the 23 side chains lining the H tube's inner surface belongs to N, Q, or R residue (15). The remaining inward facing side chains lacking amide or guanidinium groups cluster between amino acids 244 and 258 (Figure 3.1B). This arrangement is highly conserved. Forty-two H protein sequences from all three microvirus clades (30) were aligned using the PRALINE multiple sequence alignment program (31, 32). Of the four inward facing residues, T244 and K254 are completely conserved, whereas the respective hydrophobic and acidic characteristics of M251 and E258 are maintained. This suggests that this region of the H-tube may regulate ssDNA transport. To test this hypothesis, codons T244, M251, K254 and E258 were individually mutated to glutamine codons in a cloned wild-type H gene, resulting in four mutant genes: T244Q, M251Q, K254Q, E258Q. A double mutant gene, T244Q/M251Q, was also constructed. For all subsequent biochemical experiments, virions were generated by complementing a *null-H* mutant, *am(H)M251*, with cloned wild-type or mutant H genes. This complementation-dependent approach circumvents genetic differences arising from compensatory

mutations. Thus, any phenotype or defect can be directly associated with the mutant H proteins.

The mutant and wild-type genes were assayed for the ability to complement a *null-H* mutant, *am(H)M251*, at 22, 37, and 42°C (Table 3.1). The cloned K254Q and E258Q genes complemented the *null-H* mutant at all temperatures. By contrast, the T244Q, M251Q, and T244Q/M251Q genes complemented poorly at 22°C. The severity of the cold-sensitive (*cs*) phenotype varied. Plating efficiencies on M251Q and T244Q/M251Q expressing cells was several orders of magnitude below those obtained at higher temperatures. Only a slight plating efficiency reduction was seen on T244Q expressing cells, however plaque size was greatly reduced (Table 3.1).

Infectious particles containing T244Q, M251Q, and T244Q/M251Q H proteins are produced at 22°C. Mutations in the H gene can prevent H protein incorporation during morphogenesis or result in H-containing, uninformative particles (33, 34). To determine whether the *cs* H proteins were incorporated at 22°C, lysis resistant cells expressing the mutant H genes were infected with *am(H)M251*. As stated above, this approach circumvented the possible effects of fitness-enhancing secondary mutations. Thus, all other viral structural protein sequences should be identical. The infected cultures were split and concentrated after a 5-minute incubation at 37°C to ensure rapid infection initiation. The resulting infected cell pellets were resuspended in media pre-heated to 22 or 37°C and respectively incubated for 6 or 3 hours. Infected cell extracts were applied to linear sucrose gradients and centrifuged. Each infection produced particles that

sedimented at 114S, the S value of ϕ X174 virions (Figure 3.2A). The 114S peak fraction was run on an SDS-PAGE gel to determine protein content. The mutant H proteins appeared to be incorporated at levels comparable to the wild-type H protein (Figure 3.2B). Particle specific infectivity (Plaque forming units/Abs₂₈₀) was determined by titrating the 114S particles at 37°C. Infectious particles were produced at both temperatures. However, the specific infectivity of mutant H protein particles was reduced compared to those containing the wild-type H protein (Table 3.2). The reduction was independent of synthesis temperature: populations synthesized at 22 and 37°C had nearly identical infectivity values. The greatest reduction was seen for the T244Q/M251Q H protein particles, which was only 10% the wild-type value. These data suggest that the primary defect involved mutant H protein function, and not H protein incorporation.

Mutant H proteins did not alter attachment or eclipse kinetics at the restrictive temperature. After virions are assembled, they must attach to and eclipse on host cells. Eclipse, also called irreversible attachment, is the committed early infection step during which virions undergo conformational changes and lose infectivity (14). Defects affecting either event could produce the *cs* phenotype. Therefore, the kinetics of both extracellular steps were determined. For both assays, virions were produced in *am(H)M251* infected cells expressing the mutant and wild-type H genes. In this, and all other experiments, the multiplicity of infection (MOI) was based on plaque forming units (PFUs) to control for the observed differences in specific infectivity.

To assay attachment kinetics, viruses and cells were mixed in liquid media containing Ca^{2+} (5.0 mM) which is required for efficient attachment (35). At selected times post infection, samples were centrifuged to separate attached and unattached particles. The latter remain in the supernatant. Thus, supernatant titers reflect the titer of unattached virions. No significant differences were observed between mutant and wild-type H-protein containing particles at 22°C (Figure 3.3A). Eclipse kinetics were measured by pre-attaching virions at 4°C, a temperature that inhibits eclipse. Subsequently, cells and attached phage were diluted into 22°C media. At selected time points, attached particles were removed by diluting samples into an EDTA solution. EDTA chelates the Ca^{2+} ions required for attachment; thus, releasing attached but uneclipsed virions. The proportion of uneclipsed, infectious particles was then determined. Mutant eclipse kinetics did not significantly differ from those of the wild-type control at 22°C (Figure 3.3B).

Particles containing mutant H proteins did not efficiently infect cells at 22°C. After eclipse, H protein delivers the viral genome to the host. This process can be indirectly monitored by observing the kinetics of viral coat protein accumulation within infected cells. To perform these experiments, *am(H)M251* virions carrying mutant H proteins were pre-attached to lysis resistant cells containing an inducible wild-type H gene. Thus, differences in genome delivery can be attributed to the mutant H proteins. However, after genome delivery, only wild-type H protein will be synthesized. This strategy eliminates any differences that could arise from *de novo* H protein synthesis, which is required for optimal viral protein synthesis (36). After pre-attachment, the infected cell culture was split. Each aliquot was diluted into pre-heated 22 or 37°C media containing IPTG to

induce the wild-type H gene. At each time point, a sample was collected, the cells pelleted, and the whole cell lysates run on an SDS-PAGE gel. The resulting gels were coomassie stained and digitized. The intensity of the viral coat protein band was compared to the indicated host protein band to determine the relative amount of coat protein in each sample (Figure 3.4A). The results of three biological replicates are plotted in Figures 3.4B and C. Virions carrying the wild-type H protein appeared to efficiently deliver their genomes at both 37 and 22°C: viral coat protein levels started to respectively rise after 50 and 320 minutes (Figures 3.4B and C). At 37°C, no significant differences were observed between cells infected with T244Q, M251Q, and wild-type H protein containing virions. However, protein levels within the T244Q/M251Q infected cells appeared to be mildly reduced (Figure 3.4B). By contrast, viral coat protein accumulation at 22°C was greatly reduced or entirely blocked in cells infected with mutant H protein containing particles (Figure 3.4C). These data indicate that the *cs* H proteins cannot perform a function occurring between eclipse and viral gene expression at 22°C.

Mutant H proteins opened cytoplasmic channels at 22°C, but viral DNA delivery to the cytoplasmic membrane was inhibited. After attachment and eclipse, the virus must open a channel to the cytoplasm through which the infecting genome traverses. As with other phage systems, cytoplasmic K⁺ diffuses through the genome delivery channel (6, 37–39). Thus, channel formation can be assayed by monitoring the release of intracellular K⁺ ions. To this end, *am(H)M251* virions containing mutant or wild-type H proteins were pre-attached to lysis resistant cells on ice. The infected cultures were split and diluted into K⁺ free starvation media pre-warmed to 22 or 37°C. A K⁺ selective electrode was

used to monitor the extracellular K^+ concentration. Representative plots are shown in Figure 3.5A and 5B. K^+ efflux was observed regardless of assay temperature or H protein within the virus. The virions carrying mutant H proteins produced as much or more efflux as virions carrying the wild-type protein. This suggests that the mutant H proteins can open a channel, but the 10 α -helices that constitute the channel are dysfunctional.

At 22°C, cells infected with T244Q and M251Q mutant particles consistently exhibited more efflux than wild-type. The experiment depicted in Figure 3.5A and B was conducted five times and the relative efflux was the same in each iteration. The five biological replicates were analyzed with a linear mixed effects model (Material and Methods and Supplemental Material). The results of this analysis suggest that the differences were statistically significant. Although the amount of input phage was determined by plaque forming units, mutant particles exhibit a lower specific infectivity than wild-type particles. Thus, elevated efflux may reflect this, at least for the single mutants.

It is possible to follow infecting genomes as they traverse the cell wall from the inner to the outer membrane (21, 40). Some of the energy needed to fully transport the genome is provided by DNA replication machinery (22, 23). If the mutant H proteins cause a significant portion of the infecting genomes to stall mid-transit, then a higher proportion of them may remain associated with the outer membrane, which can be detected using qPCR after separating the cell wall into inner and outer membrane fractions.

To locate the infecting genomes, cells were infected at 22 or 37°C. Cells were extensively washed in a starvation buffer (Materials and Methods) to inhibit post-eclipse viral DNA

replication. After eclipse, infected cells were collected, washed twice to remove unattached and uneclipsed particles, converted to spheroplasts, and sonicated in the presence of EDTA. The resulting cytoplasmic and outer membrane vesicles were collected and separated in percoll gradients. Separation efficiency was determined by analyzing gradient fractions for succinate dehydrogenase activity and keto-deoxy-d-manno-8-octanoic acid (KDO) content, respective inner and outer membrane markers (41). Fractions with the most KDO had a density of 1.03 g/mL. Those with the highest succinate dehydrogenase activity had a density of 1.01 g/mL. Both values are consistent with those previously reported when using this membrane separation protocol (41).

The fractions were analyzed by qPCR to produce an inner/outer membrane, genome copy-number ratio (I:O ratio). As depicted in Figure 3.5C, there was approximately 22-fold more wild-type genomic DNA associated with the inner membrane than the outer membrane at both temperatures (I:O ratio \approx 22). Infecting cells with M251Q H containing particles resulted in lower I:O ratios, approximately 68 and 50% of the respective wild-type values at 37°C and 22°C. T244Q/M251Q H containing particles appeared to be even less efficient, producing ratios approximately 33% and 12% of the respective 37°C and 22°C wild-type values. As can be seen in Figure 3.5C, DNA transport was not entirely blocked for mutant H-tubes, especially at 22°C. Several technical, structural, and biological factors may account for this (See Discussion). Nonetheless, these data indicate that DNA is less efficiently transported by the mutant H-tubes.

Second-site genetic analysis of *cs* H mutants. Second-site suppressing mutations often elucidate mechanisms by which the phage can overcome a defective process, providing mechanistic insights that are often difficult to obtain solely with biochemical data. To conduct the second-site reversion analysis, the T244Q, M251Q, and T244Q/M251Q mutations were moved into the phage genome by recombination rescue. As expected, all three resulting mutants exhibited a cold-sensitive phenotype (Table 3.3). The mutants were plated at 22°C to select for suppressors of the *cs* phenotype. To ensure the recovery of a broad suppressor array, 26 independent sources of *cs(H)T244Q* and *cs(H)M251Q* and 19 independent sources of *cs(H)T244Q/M251Q* were used in the analysis (42). The recovered suppressors are listed in Table 3.3. Eight unique suppressing mutations were found in the coat protein F gene and five in the piloting protein H gene. The suppressors in gene H confer substitutions near the narrowest region of the H-tube X-ray structure (Figure 3.1B), and likely suppress by altering H protein structure (see Discussion).

The coat protein substitutions occurred near, adjacent to, or at sites previously isolated when selecting for suppressors of *cs* assembly defects. Two of the identified coat protein substitutions, T204I and M330I, were identical to previously isolated suppressors (43–46). Although particle assembly and DNA transport are seemingly unrelated phenomena, second-site suppressor isolation is based on plaque formation, which can be affected by modest burst size increases. Thus, broad allele specificity can reflect general suppressing mechanisms (47, 48). To test this hypothesis, the F-T204I and F-M330I were moved into the wild-type background and the kinetics of phage production was monitored at 22°C

(Figure 3.6). The burst size of both *su(H) F-T204I* and *su(H) F-M330I* were significantly higher than the wild-type control.

The ability to rescue via a general mechanism may be related to the severity of the parental defect. The *cs* phenotype of the double mutant is significantly tighter than both single mutants. Suppressing mutations in gene F were only recovered for the single mutants. This could reflect a limited sample pool, as it is unlikely that the selections went to saturation, or it could be directly related to the defect severity conferred by the parental mutations. To distinguish between these two possibilities, the suppressors in gene F were moved into the *cs(H)T244Q/M251Q* background. As can be seen in Table 3.4, the suppressing mutations in gene F were unable to rescue the double mutant.

3.4 Discussion

Mutant phenotype and H-tube structure: As seen in the X-ray structure, the inner surface of the H tube is lined with amide and guanidinium containing glutamine, asparagine, and arginine side chains. However, there are four exceptions near the tube's C-terminal end: T244, M251, K254, and E258 (Figure 3.1). This arrangement is conserved across the three microvirus clades, which suggests that the residues play an important role during DNA transport. The four residues were mutated to glutamine to investigate the arrangement and function of the H-tube lumen. The K254Q and E258Q mutations did not result in a discernable phenotype, whereas the T244Q and M251Q mutants conferred *cs* phenotypes when expressed from plasmids in complementation studies and when placed directly within the phage genome. A third mutant,

T244Q/M251Q, also conferred a particularly pronounced *cs* phenotype. The H-tube atomic structure may explain the phenotypic differences associated with these four sites. Unlike T244 and M251, K254 and E258 form an inter-helical salt bridge (15). Thus, their side chains may not be entirely free to interact with the DNA as it passes through the tube. Moreover, glutamine can also act as both a hydrogen bond donor and acceptor. Replacing K254 or E258 with glutamine may replace the inter-helical salt bridge with an inter-helical hydrogen bond.

Mutant phenotype and defective function: The viral life cycle was investigated to determine which step was disrupted by the *cs* H proteins. At 22°C, the mutant H proteins were incorporated into virions as efficiently as wild-type. The resulting particles also displayed wild-type attachment and eclipse kinetics at the restrictive temperature. Lastly, the results of K⁺ efflux experiments indicate that they can form channels through host cell walls. However, the results of two experiments suggest that the infecting viral DNA was not efficiently reaching the cytoplasmic membrane at 22°C, the site of stage I viral DNA replication. 1) Viral coat protein did not accumulate within cells infected with mutant H containing virions. 2) After cell wall fractionation, less genomic DNA was associated with the inner membrane than observed in wild-type samples.

To the best of our knowledge, tracking infecting genomes in separated cell wall components via qPCR has not been previously attempted in other phage systems. Thus, the extent that results can be directly related to the severity of mutant phenotypes is not entirely known. The M251Q and T244Q/M251Q mutants have strong cold-sensitive

phenotypes and temperature affected the results of the pPCR assay. Unlike the assay conducted with the wild-type H protein, in which the same amount of genomic DNA became associated with the cytoplasmic membrane regardless of temperature, samples generated with mutant H proteins exhibited a marked decrease of inner membrane associated viral DNA at 22°C, which is consistent with a *cs* phenotype. However, inner membrane genome association was not entirely eliminated. Indeed, more DNA was consistently detected in the inner membrane fraction. For example, the I:O ratio for the T244Q/M251Q mutant at 22°C was approximately 2, indicating that twice as much genomic DNA was detected in the inner membrane fraction. By comparison, the I:O ratio for wild-type was an order of magnitude higher.

Several factors may affect I:O ratios. Firstly, cell wall fractionation is a messy affair; definitely not for the faint hearted or those traumatized by impurities. The molecular markers used to distinguish between inner and outer membrane fractions typically differ by only 5-10 fold regardless of protocol (41), indicating a significant amount of cross contamination. Secondly, it is unknown into which fraction the genome will segregate if it is within the H-tube, which spans the cell wall. Thirdly, the requisite experimental conditions under which the assay had to be performed differ from those occurring during a typical infection. However, all of these phenomena would equally affect wild-type and mutant samples. Thus, the results likely reflect the nature of the defective phenotype.

The function of the amide and guanidium group surface: This data can be interpreted within a model in which a balance of opposing forces governs genome movement. One

force propels the genome inward. It is likely driven by capsid pressure created by the densely packaged viral genome, the osmotic gradient existing between the host's cytoplasm and environment, or a combination of the two (1, 2). The opposing force may be friction created by the H tube's inward facing, amide and guanidinium groups, which form hydrogen bonds with DNA nucleotides (26–29).

While invoking a force that opposes genome delivery may seem counter-intuitive, systems more effectively perform work when potential energy is released in small, manageable increments. Nuclear power plants, internal combustion engines, and oxidative phosphorylation, in which electrons are transferred from NADH to O₂ via several intermediate reactions, all demonstrate this concept: releasing too much potential energy at one time can destructively overwhelm the systems. Our results are consistent with this model and the observed *cs* phenotypes. The additional amide groups, via interactions with DNA, may be increasing the frictional force. Hydrostatic and osmotic pressures are directly proportional to. Thus, the force driving the genome into the cell would be decreased at lower temperature. This, combined with the increased drag introduced by the additional amide group, could perturb the optimal balance between the two forces, either kinetically trapping the genome or greatly slowing its delivery. Alternatively, the added amide groups could have unanticipated effects on the H-tube's structure, which could produce the same phenotype. Regardless of the molecular mechanism, the defect occurs after the cell wall is breached.

The results of the K^+ efflux studies indicate that the *cs* H proteins breached the inner membrane. The relative magnitude of phage-induced efflux at 22°C was dependent on the H protein type. This observation was found to be significant after constructing a linear mixed effects model built from five replicate data sets. To the best of our knowledge, a similar statistical analysis has not been conducted on K^+ efflux data. Thus, the biological significance of this statistically significant observation cannot be rigorously adjudicated. Nonetheless, some speculation may be warranted. Single mutants effluxed more K^+ than wild-type at 22°C, whereas double mutant efflux resembled wild-type. For the single mutants, this may be due to reduced specific infectivity. MOI was based on PFUs. Thus, if a population of virions had a reduced specific infectivity, as was observed for the mutants, more non-plaque forming, virus-like particles were added. These particles may still be capable of forming effluxing channels. However, the double mutant, which effluxed K^+ like wild-type, exhibited the lowest specific infectivity. It also exhibited the strongest *cs* phenotype and accordingly, transported less DNA to the cytoplasmic membrane. Thus, an additional variable may be influencing this phenomenon, one directly related to the efflux through any one H-tube. The two extra glutamine residues within double mutant tubes may grip the DNA so tightly that the tube becomes more clogged or obstructed. Alternatively, as mentioned above, the added amide groups could have unanticipated effects on the H-tube's structure, which may cause a percentage of double-mutant H-tubes to collapse.

Regardless of the molecular defect, the results of the second-site genetic analysis further underscore the synergistic effects conferred by the two mutations. The *cs* phenotype of

the single mutants *cs(H)T244Q* and *cs(H)M251Q* could be suppressed by intergenic and intragenic mechanisms, i.e. alterations to the viral coat or DNA pilot proteins, respectively. By contrast, only the intragenic mechanism appears to operate in the *cs(H)T244Q/M251Q* double mutant background. The suppressors in gene H confer changes at the H-tube's narrowest point. In general, these mutations decrease side chain size but did not radically alter chemical characteristics. The changes could be increasing the tube's diameter or the tube's elasticity or flexibility. Regardless of the precise suppression mechanism, the mutations are likely alleviating inhibited genome delivery by directly modifying the H-tube structure. By contrast, the coat protein suppressors appear to be compensating for inhibited genome delivery instead of correcting it. These suppressors were similar or identical to previously isolated suppressors of *cs* assembly defects. When moved into the wild-type background, they increased the viral burst size at 22°C. Thus, increasing the burst size may be compensating for inhibited genome delivery, which can be explained by the mechanics of plaque formation. As evinced by the leaky phenotypes of the single mutants (plating efficiencies $\sim 10^{-2}$ at 22°C), DNA delivery is not entirely inhibited. However, to form a plaque, enough first-round progeny must successfully infect neighboring cells: a situation made more probable by a larger burst size. As can be seen in the piloting assay results, the double mutant phenotype is quite tight when compared to the single mutants. Its ability to associate DNA with the inner membrane is pronouncedly less efficient. Thus, its DNA delivery success rate may be too low and can only be rescued by an unobtainable burst size. Accordingly, when the suppressors found in the coat protein were placed directly within the double mutant background, they did not rescue on the level of plaque formation.

Relationship to other phage systems: Evoking a force that naturally counters the one propelling the genome into the cell may seem counterintuitive. However, slow, regulated penetration may be common in other phage systems in which large amounts of potential energy, in the form of capsid pressure and/or osmotic imbalance, must be controlled. For example, the complete transit of the phage λ genome requires approximately five minutes (49). Moreover, in some phage systems, potential energy may not need to drive the entire genome into the cell. The efficient transfer of ϕ X174 ssDNA appears to be coupled to synthesis of the complementary genomic strand (21–23). Thus, the H-tube may not be intended to deliver the entire genome to the host. The friction produced by the amide and guanidinium groups may prevent complete transfer, so that only a small portion is presented to host DNA synthesis machinery. If hosts are not actively synthesizing DNA, penetration is often incomplete. The energy released by the hydrolysis of the dNTP's during DNA synthesis is greater than the potential energy stored within the newly formed bonds of DNA's phosphate backbone. Thus, microvirus genome penetration may have evolved to exploit the unharnessed energy released in nucleic acid biosynthesis. Phages T5 and T7 may be other examples of phages that exploit the unharnessed energy released in cellular processes to perform work. They release their genomes in discrete steps (50, 51) and internalization of the entire T7 or T5 genome may be facilitated by host transcription or translation machinery, respectively (52, 53).

3.5 Materials, Methods, and Acknowledgements

Bacterial strains, phage strains, and plasmids. The *Escherichia coli* C strains C122 (Su-), BAF8 (*supF*), and BAF30 (*recA*) have been previously described (43, 54). RY7211 contains a mutation in the *mraY* gene, which confers resistance to viral E protein mediated lysis (55).

The T244Q, M251Q, K254Q, E258Q, and T244Q/M251Q H genes were constructed by mutagenizing the previously described cloned ϕ X174 H gene (33). Abutting primers introducing the desired mutation were used to PCR amplify the entire plasmid with Q5 DNA polymerase (New England Biolabs). The PCR product's 5' hydroxyl termini were phosphorylated with T4 polynucleotide kinase (New England Biolabs) and the resulting product was circularized with T4 DNA ligase (New England Biolabs). Cloned nucleotide sequences were verified with direct DNA sequencing.

Mutant phage strains *cs(H)T244Q*, *cs(H)M251Q*, and *cs(H)T244Q/M251Q* were generated via recombination-rescue with the T244Q, M251Q, and T244Q/M251Q H clones using *am(H)M251*, a mutant containing an amber mutation at codon M251 in gene H. Cells carrying mutant H constructs were infected with *am(H)M251*. Recombinants were then selected by plating the resulting progeny on C122 (Su-) and confirmed by sequencing the H genes. Strains *su(H)-F T204I*, *su(H)-F M330I*, *su(H)-F R386H*, *su(H)-F T204I/cs(H)T244Q/M251Q*, *su(H)-F M330I/cs(H)T244Q/M251Q*, and *su(H)-F R386H/cs(H)T244Q/M251Q* were generated via site-directed mutagenesis using purified phage ssDNA in the same manner used to create the mutant H constructs.

Second-site genetic analysis. Second-site suppressing mutations of the cold-sensitive (*cs*) phenotype were isolated in direct selections. *cs(H)T244Q*, *cs(H)M251Q*, and *cs(H)T244Q/M251Q* were plated with C122 at 37°C. Plaques were allowed to develop and were collected. *cs(H)T244Q* plaque samples were suspended in 0.1 mL of water. This solution was plated with C122 at 22°C. *cs(H)M251Q* and *cs(H)T244Q/M251Q* plaque samples were added directly to 2 mL of molten top agar, slewing agar bombs, and plated with C122 at 22°C. Plaques that appeared larger or more transparent than background plaques, if any, were selected and re-plated at 22°C to confirm the loss of the *cs* phenotype. *Cs* revertant genomes were sequenced to identify the second-site suppressing mutation.

Media, buffers, phage plating assays, and mutant H containing particle preparation.

Media, buffers, phage plating assays, and phage stock preparation have been previously described (43). For the majority of assays, mutant H containing particles were generated by infecting RY7211 at $OD_{660}=0.08$ with *am(H)M251* at a MOI of 1. Infections were performed at 37°C and the cells were expressing either wild-type or mutant H constructs. Expression of the constructs was induced at the time of infection by adding IPTG to a final concentration of 40 μ M. The cells were pelletized three hours after infection and resuspended in BE at 1/100 the original culture volume. Lysozyme was added to a final concentration of 1.0 mg/mL and the infections were lysed at 4°C overnight. Afterwards, 150 μ l chloroform was added and the lysates were vigorously vortexed. Cell debris was pelletized and the phage containing supernatant was collected.

Protein electrophoresis, rate zonal sedimentation, and generation of ssDNA. The protocols for protein electrophoresis, rate zonal sedimentation, and ssDNA purification have been previously described (46, 56, 57).

Attachment, eclipse, coat protein quantification, and burst size assays. Attachment and eclipse assays have been previously described (58, 59). Coat protein quantification as a surrogate for genome DNA delivery was performed as follows. RY7211 cells were grown to $OD_{660}=0.08$, pelletized, and suspended in one tenth the original volume of HFB buffer [0.06M NH₄Cl / 0.09M NaCl / 0.1M KCl / 0.1M Tris-HCl (pH 7.4) / 1.0 mM MgSO₄ / 1.0 mM CaCl₂] containing 10 mM MgCl₂ and 5.0 mM CaCl₂ at 4°C. Phages were pre-attached to cells for 30 minutes at 4°C. The cells and attached phage were pelletized and resuspended in 4°C TKY media [1% tryptone, 0.5% KCl, 0.5% yeast extract] containing 10 mM MgCl₂ and 5.0 mM CaCl₂. The samples were then diluted into TKY containing 10 mM MgCl₂ and 5.0 mM CaCl₂ at 22 or 37°C. At time points, 1.0 mL samples were collected, pelletized, and the pellets frozen. After freezing, the pellets were suspended in 100 µL HFB. 30 µL of the concentrated samples were run on SDS-PAGE gels as previously described (57). SDS-PAGE gels were then stained with Coomassie brilliant blue and digitized with a LICOR scanner. Relative coat protein levels were determined by densitometry analysis using ImageJ software (NIH). Coat protein intensity was normalized to the intensity of the host protein band indicated in Figure 3.4.

Burst size assays followed the same protocol as the coat protein quantification assay with the following changes. At time points, 1.0 mL samples were collected, pelletized, and

suspended in 100 μ L HFB. 10 μ L of the concentrated sample was diluted into 1.0 mL of BE buffer containing 1.0 mg/ml of lysozyme. The concentrated samples were frozen and the diluted samples allowed to lyse overnight at 4°C. Lysates were titered the following day and bursts were calculated by dividing the time point's total phage by the total input phage.

Potassium efflux assays. K⁺ efflux experiments are based on those described by Cumby *et al.* (6) and assays were performed by first producing mutant H containing virions as described above. The virions were dialyzed thrice against 1.0 L of SM buffer (100 mM NaCl, 10 mM MgSO₄, 50 mM Tris pH=7.5) at 4°C to remove potassium. C122 was grown to OD₆₆₀=0.08 in TKY at 37°C. Cells were pelletized and washed in an equal volume of SM buffer, washed again in 1/10th the volume SM buffer, and suspended in 1/100th the volume iced SM+ buffer: SM buffer containing 10 mM MgCl₂ and 5 mM CaCl₂. The cell culture was divided into 1.0 mL aliquots, kept on ice, and chilled virus was added to a MOI of 75. Iced SM+ buffer was added to equalize aliquot volumes. Infections were incubated for 15 minutes on ice to allow virus pre-attachment. A single infection was diluted into 9.0 mL 37°C SM+ buffer every minute. Immediately after the first dilution, an Orion Ionplus potassium electrode (Thermo Scientific) connected to a Sartorius PB-11 pH meter was inserted into an infection and a reading was taken after 1 minute. This electrode was then rinsed with DI H₂O, blotted dry, and placed into the dilution of the subsequent infection. The electrode was rotated between infections at one-minute intervals once all infections were diluted.

Statistical analysis of the K⁺ efflux data: Raw K⁺ efflux data was modeled with a linear mixed effects model. Fixed effects were included for virus condition (levels: uninfected, wild-type, T244Q, M251Q, K254Q, and T244Q+M251Q), temperature (levels: 22 and 37°), and time. Because plots of the data showed a clear non-linear (half-parabolic) change in the extracellular K⁺ level over time, both linear and quadratic effects of time were incorporated into the model. Additionally, because different K⁺ efflux trajectories for each virus/temperature condition were desired, all fixed effect interactions were included. Finally, in order to capture some of the correlation structure likely present in the data due to the experimental design, two random intercepts were included: one for experiment day and another for the final test tube from which measurements were collected. Planned contrasts of the four mutant virus conditions versus both wild-type and uninfected were conducted at 25 and 150 minutes in the 37 and 22° conditions, respectively.

It is worth noting that the correlation and variance structure of the data is likely more complex than that described above. Firstly, there are actually four potential sources of random variation and consequent correlation in the data: virus batch, experiment day, original test tube (before splitting into separate tubes for the two temperature conditions), and final test tube. Second, sequentially close measurements from the same final test tube are likely correlated. Third, evidence of temporal heteroscedasticity was revealed after modeling explorations. In order to determine whether incorporating this more complex variance and correlation structure into the model affected the contrast inferences, another model was fit to the K⁺ efflux data. It included an exponentially

decreasing correlation and variance structures over time and also random intercepts for virus batch, experiment day, original test tube, and final test tube. The fixed effects structure was identical to that of the simpler model, and the same planned contrasts were conducted. Because the two models' inferential results were identical, the simpler model conclusions were presented. The complete details of the statistical analysis are posted in the supplemental material.

Infected membrane separations and qPCR. The membrane separation protocol was based on that described by Morein *et al.* (41). C122 was grown to $OD_{660}=0.1$ in TKY at 37°C. The cells were pelletized and washed in an equal volume of SM buffer, then concentrated 10-fold in SM buffer, and again concentrated 10 fold in iced SM+ buffer. The concentrated culture was divided into 2.0 mL aliquots and kept on ice. Chilled virus was added to a MOI of 1.0 and additional iced SM+ buffer was added to equalize infection volumes. The virus was allowed to pre-attach for 30 minutes at 4°C. The infections were split and each half was diluted 10-fold in 37 or 22°C SM+ buffer and incubated for 10 or 30 minutes, respectively. The infections were then diluted 10-fold in iced SM+ buffer, pelletized, and washed in 40 mL iced BE buffer. Pellets were suspended in 15 mL iced 10 mM Tris (pH = 7.5) containing 0.5 M sucrose. Lysozyme was added to a final concentration of 0.1 mg/mL. The infections were incubated for 30 minutes at 4°C and were then slowly diluted (~3 mL/minute) with 15 mL iced 10 mM Tris (pH = 7.5). EDTA was added to a final concentration of 1.0 mM and samples were sonicated in an ice bath with a Branson Sonifier 450. Samples were sonicated 15 seconds at a time with a 45 second cool down between pulses. This cycle was repeated until the

OD₆₀₀ of the infection stopped decreasing. This took four to five cycles and an infection's final OD₆₀₀ was usually between 10 and 30% its original value. Samples were then spun at 1500×g for 10 minutes to pelletize any remaining intact cells. The supernatants were then centrifuged for 90 minutes at 257,000×g in a Beckman Type 70Ti rotor to pellet membrane vesicles. The resulting supernatant was removed and the moist pellets were stored at 4°C overnight in sealed containers. Membrane pellets were then suspended in 15 mL gradient buffer [10 mM Tris, 1 mM EDTA, 16.2% Percoll (v/v), pH = 7.5] with an 18-gauge syringe and vigorous vortexing. The mixtures were transferred to 15 mL glass corex tubes and spun for 50 minutes at 14,500×g in a Sorvall SA600 rotor. The resulting gradients were fractionated into 250 µL fractions from the bottom with the peristaltic pump of a BioRad BioLogic LP connected to a model 2110 fraction collector. Fraction succinate dehydrogenase activity was tested with a Biovision succinate dehydrogenase activity colorimetric assay kit and KDO content was determined by the thiobarbituric acid method (60).

qPCR analysis of fractions was performed on an Applied Biosystems 7300 Real-Time PCR System using Applied Biosystems SYBR Green PCR Master Mix. The thermal cycling program started with 2 minutes at 50°C followed by 3 minutes at 95°C to activate the DNA polymerase. This was followed by 40 cycles of 95°C for 15 seconds and 58°C for 1 minute. Absolute quantification was performed by generating a standard curve with purified φX174 ssDNA. Dissociation curves were performed to confirm primer fidelity.

Acknowledgements

This research was supported by National Science Foundation grant MCB-1408217 (B.A.F.), the BIO5 Institute at the University of Arizona, and US Department of Agriculture Hatch funds to the University of Arizona.

3.6 References

1. Bauer DW, Huffman JB, Homa FL, Evilevitch A. 2013. Herpes Virus Genome, The Pressure Is On. *J Am Chem Soc* 135:11216–11221.
2. Molineux IJ, Panja D. 2013. Popping the cork: mechanisms of phage genome ejection. *Nat Rev Microbiol* 11:194–204.
3. Aksyuk AA, Leiman PG, Kurochkina LP, Shneider MM, Kostyuchenko VA, Mesyanzhinov V V., Rossmann MG. 2009. The tail sheath structure of bacteriophage T4: A molecular machine for infecting bacteria. *EMBO J* 28:821–829.
4. Fokine A, Rossmann MG. 2014. Molecular architecture of tailed double-stranded DNA phages. *Bacteriophage* 4:e28281.
5. Hu B, Margolin W, Molineux IJ, Liu J. 2013. The bacteriophage T7 virion undergoes extensive structural remodeling during infection. *Science* (80-) 339:576–579.
6. Cumby N, Reimer K, Mengin-Lecreulx D, Davidson AR, Maxwell KL. 2015. The phage tail tape measure protein, an inner membrane protein and a periplasmic chaperone play connected roles in the genome injection process of *E. coli* phage HK97. *Mol Microbiol* 96:437–447.
7. Jin Y, Sdao SM, Dover JA, Porcek NB, Knobler CM, Gelbart WM, Parent KN. 2015. Bacteriophage P22 ejects all of its internal proteins before its genome. *Virology* 485:128–134.
8. Dent KC, Thompson R, Barker AM, Hiscox JA, Barr JN, Stockley PG, Ranson NA. 2013. The Asymmetric Structure of an Icosahedral Virus Bound to Its Receptor Suggests a Mechanism for Genome Release. *Structure* 21:1225–1234.
9. Krahn PM, O’Callaghan RJ, Paranchych W. 1972. Stages in phage R17 infection VI. Injection of A Protein and RNA into the Host Cell. *Virology* 47:628–637.

10. Toropova K, Stockley PG, Ranson NA. 2011. Visualising a Viral RNA Genome Poised for Release from Its Receptor Complex. *J Mol Biol* 408:408–419.
11. Webster RE. 1996. Biology of the Filamentous Bacteriophage, p. 1–20. *In Phage Display of Peptides and Proteins: A Laboratory Manual*. Elsevier.
12. Bennett NJ, Rakonjac J. 2006. Unlocking of the Filamentous Bacteriophage Virion During Infection is Mediated by the C Domain of pIII. *J Mol Biol* 356:266–273.
13. Bennett NJ, Gagic D, Sutherland-Smith AJ, Rakonjac J. 2011. Characterization of a Dual-Function Domain That Mediates Membrane Insertion and Excision of Ff Filamentous Bacteriophage. *J Mol Biol* 411:972–985.
14. Sun Y, Roznowski AP, Tokuda JM, Klose T, Mauney A, Pollack L, Fane BA, Rossmann MG. 2017. Structural changes of tailless bacteriophage Φ X174 during penetration of bacterial cell walls. *Proc Natl Acad Sci* 114:13708–13713.
15. Sun L, Young LN, Zhang X, Boudko SP, Fokine A, Zbornik E, Roznowski AP, Molineux IJ, Rossmann MG, Fane BA. 2014. Icosahedral bacteriophage Φ X174 forms a tail for DNA transport during infection. *Nature* 505:432–435.
16. Cherwa JE, Young LN, Fane BA. 2011. Uncoupling the functions of a multifunctional protein: The isolation of a DNA pilot protein mutant that affects particle morphogenesis. *Virology* 411:9–14.
17. Dokland T, Bernal RA, Burch A, Pletnev S, Fane BA, Rossmann MG. 1999. The role of scaffolding proteins in the assembly of the small, single-stranded DNA virus ϕ X174. *J Mol Biol* 288:595–608.
18. Dokland T, McKenna R, Llag LL, Bowman BR, Incardona NL, Fane BA, Rossmann MG. 1997. Structure of a viral procapsid with molecular scaffolding. *Nature* 389:308–313.
19. Ilag LL, Olson NH, Dokland T, Music CL, Cheng RH, Bowen Z, McKenna R, Rossmann MG, Baker TS, Incardona NL. 1995. DNA packaging intermediates of bacteriophage ϕ X174. *Structure* 3:353–363.
20. Novak CR, Fane BA. 2004. The functions of the N terminus of the ϕ X174 internal scaffolding protein, a protein encoded in an overlapping reading frame in a two scaffolding protein system. *J Mol Biol* 335:383–390.
21. Azuma J, Morita J, Komano T. 1980. Process of Attachment of Φ X174 Parental DNA to the Host Cell Membrane. *J Biochem* 88:525–532.
22. Mano Y, Sakai H, Komano T. 1979. Growth and DNA synthesis of bacteriophage ϕ X174 in a dnaP mutant of *Escherichia coli*. *J Virol* 30:650–6.

23. Murakami Y, Nagata T, Schwarz W, Wada C, Yura T. 1985. Novel dnaG mutation in a dnaP mutant of *Escherichia coli*. *J Bacteriol* 162:830–2.
24. Conley MJ, McElwee M, Azmi L, Gabrielsen M, Byron O, Goodfellow IG, Bhella D. 2019. Calicivirus VP2 forms a portal-like assembly following receptor engagement. *Nature* 565:377–381.
25. Shepard W, Cruse WBT, Fourme R, De La Fortelle E, Prangé T. 1998. A zipper-like duplex in DNA: The crystal structure of d(GCGAAAGCT) at 2.1 Å resolution. *Structure* 6:849–861.
26. Luscombe NM. 2001. Amino acid-base interactions: a three-dimensional analysis of protein-DNA interactions at an atomic level. *Nucleic Acids Res* 29:2860–2874.
27. Luscombe NM, Thornton JM. 2002. Protein–DNA Interactions: Amino Acid Conservation and the Effects of Mutations on Binding Specificity. *J Mol Biol* 320:991–1009.
28. Mandel-Gutfreund Y, Schueler O, Margalit H. 1995. Comprehensive Analysis of Hydrogen Bonds in Regulatory Protein DNA-Complexes: In Search of Common Principles. *J Mol Biol* 253:370–382.
29. Suzuki M. 1994. A framework for the DNA–protein recognition code of the probe helix in transcription factors: the chemical and stereochemical rules. *Structure* 2:317–326.
30. Rokyta DR, Burch CL, Caudle SB, Wichman H a. 2006. Horizontal Gene Transfer and the Evolution of Microvirid Coliphage Genomes. *J Bacteriol* 188:1134–1142.
31. Simossis VA, Heringa J. 2005. PRALINE: a multiple sequence alignment toolbox that integrates homology-extended and secondary structure information. *Nucleic Acids Res* 33:W289–W294.
32. Simossis VA. 2005. Homology-extended sequence alignment. *Nucleic Acids Res* 33:816–824.
33. Roznowski AP, Fane BA. 2016. Structure-Function Analysis of the ΦX174 DNA-Piloting Protein Using Length-Altering Mutations. *J Virol* 90:7956–7966.
34. Young LN, Hockenberry AM, Fane BA. 2014. Mutations in the N Terminus of the ΦX174 DNA Pilot Protein H Confer Defects in both Assembly and Host Cell Attachment. *J Virol* 88:1787–1794.
35. Ilag LL, McKenna R, Yadav MP, BeMiller JN, Incardona NL, Rossmann MG. 1994. Calcium Ion-induced Structural Changes in Bacteriophage φX174. *J Mol*

Biol 244:291–300.

36. Ruboyianes M V, Chen M, Dubrava MS, Cherwa JE, Fane BA. 2009. The Expression of N-Terminal Deletion DNA Pilot Proteins Inhibits the Early Stages of Φ X174 Replication. *J Virol* 83:9952–9956.
37. Boulanger P, Letellier L. 1992. Ion channels are likely to be involved in the two steps of phage T5 DNA penetration into *Escherichia coli* cells. *J Biol Chem* 267:3168–72.
38. Keweloh H, Bakker EP. 1984. Permeability changes in the cytoplasmic membrane of *Escherichia coli* K-12 early after infection with bacteriophage T1. *J Bacteriol* 160:347–353.
39. Roznowski AP, Young RJ, Love SD, Andromita AA, Guzman VA, Wilch MH, Block A, McGill A, Lavelle M, Romanova A, Sekiguchi A, Wang M, Burch AD, Fane BA. 2018. Recessive Host Range Mutants and Unsusceptible Cells That Inactivate Virions without Genome Penetration: Ecological and Technical Implications. *J Virol* 93:1–16.
40. Jazwinski SM, Marco R, Kornberg A. 1975. The gene H spike protein of bacteriophages Φ X174 and S13. II. Relation to synthesis of the parental replicative form. *Virology* 66:294–305.
41. Morein S, Henricson D, Rilfors L. 1994. Separation of Inner and Outer Membrane Vesicles from *Escherichia coli* in Self-Generating Percoll Gradients. *Anal Biochem* 216:47–51.
42. Luria S, Delbrück M. 1943. Mutations of Bacteria from Virus Sensitivity to Virus Resistance. *Genetics* 28:491–511.
43. Fane BA, Hayashi M. 1991. Second-site suppressors of a cold-sensitive prohead accessory protein of bacteriophage ϕ X174. *Genetics* 128:663–71.
44. Fane BA, Shien S, Hayashi M. 1993. Second-site suppressors of a cold-sensitive external scaffolding protein of bacteriophage ϕ X174. *Genetics* 134:1003–11.
45. Gordon EB, Fane BA. 2013. Effects of an Early Conformational Switch Defect during Φ X174 Morphogenesis Are Belatedly Manifested Late in the Assembly Pathway. *J Virol* 87:2518–2525.
46. Gordon EB, Knuff CJ, Fane BA. 2012. Conformational Switch-Defective ϕ X174 Internal Scaffolding Proteins Kinetically Trap Assembly Intermediates before Procapsid Formation. *J Virol* 86:9911–9918.
47. Floor E. 1970. Interaction of morphogenetic genes of bacteriophage T4. *J Mol Biol*

47:293–306.

48. Sternberg N. 1976. A genetic analysis of bacteriophage λ head assembly. *Virology* 71:568–582.
49. Van Valen D, Wu D, Chen Y-J, Tuson H, Wiggins P, Phillips R. 2012. A Single-Molecule Hershey-Chase Experiment. *Curr Biol* 22:1339–1343.
50. García LR, Molineux IJ. 1995. Incomplete entry of bacteriophage T7 DNA into F plasmid-containing *Escherichia coli*. *J Bacteriol* 177:4077–4083.
51. Lanni YT. 1968. First-step-transfer deoxyribonucleic acid of bacteriophage T5. *Bacteriol Rev* 32:227–42.
52. Lanni YT. 1965. DNA transfer from phage T5 to host cells: dependence on intercurrent protein synthesis. *Proc Natl Acad Sci* 53:969–973.
53. Moffatt BA, Studier FW. 1988. Entry of bacteriophage T7 DNA into the cell and escape from host restriction. *J Bacteriol* 170:2095–2105.
54. Fane BA, Head S, Hayashi M. 1992. Functional relationship between the J proteins of bacteriophages ϕ X174 and G4 during phage morphogenesis. *J Bacteriol* 174:2717–2719.
55. Bernhardt TG, Struck DK, Young R. 2001. The Lysis Protein E of ϕ X174 Is a Specific Inhibitor of the *MraY*-catalyzed Step in Peptidoglycan Synthesis. *J Biol Chem* 276:6093–6097.
56. Burch AD, Ta J, Fane BA. 1999. Cross-functional analysis of the Microviridae internal scaffolding protein. *J Mol Biol* 286:95–104.
57. Uchiyama A, Fane BA. 2005. Identification of an Interacting Coat-External Scaffolding Protein Domain Required for both the Initiation of Φ X174 Procapsid Morphogenesis and the Completion of DNA Packaging. *J Virol* 79:6751–6756.
58. Cherwa JE, Sanchez-Soria P, Wichman HA, Fane BA. 2009. Viral Adaptation to an Antiviral Protein Enhances the Fitness Level to Above That of the Uninhibited Wild Type. *J Virol* 83:11746–11750.
59. Hafenstein SL, Chen M, Fane BA. 2004. Genetic and functional analyses of the ϕ X174 DNA binding protein: the effects of substitutions for amino acid residues that spatially organize the two DNA binding domains. *Virology* 318:204–213.
60. Karkhanis YD, Zeltner JY, Jackson JJ, Carlo DJ. 1978. A new and improved microassay to determine 2-keto-3-deoxyoctonate in lipopolysaccharide of gram-negative bacteria. *Anal Biochem* 85:595–601.

3.7 Figures and Tables

TABLE 3.1. am(H) plating efficiencies on cells expressing gene H clones

Expressed H Gene	E.O.P. ^a at:		
	22°C	37°C	42°C
Wild-Type	1.0	1.0	1.0
None	$<1.3 \times 10^{-4}$	$<9.0 \times 10^{-5}$	$<4 \times 10^{-5}$
T244Q	0.3 ^b	1.0	0.5
M251Q	$<1.3 \times 10^{-4}$	1.9	0.7
K254Q	0.7	1.0	0.5
E258Q	0.8	2.8	0.6
T244Q+M251Q	$<1.3 \times 10^{-4}$	0.7	0.8

a Efficiency of plating. Values are normalized to those obtained from cells expressing the wild-type H gene at the same temperature.

b Plaque size reduced by >50% of wild type.

TABLE 3.2. Specific infectivity^a of 114S particles at 37°C

Synthesis Temperature	Expressed Gene	Specific Infectivity	
		Raw S.I. ^b	Wild-type Normalized ^c
37°C	Wild-Type	8.0×10^{11}	1.0
	None	3.9×10^8	3.9×10^{-4}
	T244Q	1.9×10^{11}	0.4±0.1
	M251Q	2.3×10^{11}	0.4±0.1
	T244Q/M251Q	5.4×10^{10}	0.1±0.02
22°C	Wild-Type	3.3×10^{12}	1.0
	None	4.9×10^8	1.5×10^{-4}
	T244Q	9.7×10^{11}	0.4±0.2
	M251Q	9.4×10^{11}	0.4±0.1
	T244Q/M251Q	2.3×10^{11}	0.1±0.1

a Specific infectivity is defined as pfu's/A₂₈₀, regardless of the plaque forming particle's genotype.

b Raw S.I. reported in units of pfu's/A₂₈₀.

c Data is normalized to the specific infectivity of particles generated in cells at the same temperature expressing the wild-type H gene. ± values represent the standard deviation obtained from three biological replicates.

TABLE 3.3. Suppressing Mutations of T244Q, M251Q, and T244Q+M251Q

Strain ^b	Independent Isolations ^c	E.O.P. ^a		
		22°C	37°C	42°C
Wild Type	N/A ^d	0.2	1.0	0.7
<i>cs(H)T244Q</i>	N/A	4.8×10 ⁻²	1.0	1.0
<i>su(H)-F H73Y/cs(H)T244Q</i>	Two	0.3	1.0	1.2
<i>su(H)-F Y158H/cs(H)T244Q</i>	Three	0.2	1.0	0.7
<i>su(H)-F T204I/cs(H)T244Q</i>	One	0.2	1.0	1.3
<i>su(H)-F M330I/cs(H)T244Q</i>	One	0.3	1.0	0.9
<i>su(H)-F R386H/cs(H)T244Q</i>	One	0.3	1.0	0.9
<i>su(H)-H R185H/cs(H)T244Q</i> ₅	One	1.0	<6.4×10 ⁻⁵	<6.4×10 ⁻⁵
<i>su(H)-H A194S/cs(H)T244Q</i>	One	0.2	1.0	1.0
<i>cs(H)M251Q</i>	N/A	2.6×10 ⁻²	1.0	1.0
<i>su(H)-F T100A/cs(H)M251Q</i>	One	0.1	1.0	1.6
<i>su(H)-F Y158H/cs(H)M251Q</i>	One	0.3	1.0	1.2
<i>su(H)-F T204I/cs(H)M251Q</i>	One	0.2	1.0	1.1
<i>su(H)-F L319F/cs(H)M251Q</i>	One	0.1	1.0	0.6
<i>su(H)-F M330I/cs(H)M251Q</i>	Two	0.3	1.0	0.8
<i>su(H)-F V333F/cs(H)M251Q</i>	One	0.1	1.0	1.2
<i>su(H)-F R386H/cs(H)M251Q</i>	One	0.1	1.0	0.7
<i>su(H)-H E197D/cs(H)M251Q</i>	One	0.4	1.0	1.1
<i>su(H)-H M198V/cs(H)M251Q</i>	One	0.5	1.0	0.9
<i>cs(H)T244Q/M251Q</i>	N/A	<9.5×10 ⁻⁶	1.0	1.2
<i>su(H)-H M198I/cs(H)T244Q/M251Q</i>	One	0.1	1.0	1.2
<i>su(H)-H M198V/cs(H)T244Q/M251Q</i>	Two	0.2	1.0	0.9

a Efficiency of plating. Values are normalized to those obtained from plates incubated at 37°

b Strains with mutations suppressing the T244Q, M251Q, or T244Q/M251Q mutations are labeled with the gene in which the suppressing mutation was found, the corresponding amino acid change, and the genetic background in which it resides. For example, *su(H)-F H73Y/cs(H)T244Q* indicates that the strain has H73Y in gene F within the *cs(H)T244Q* background.

c Plaques were picked from plates incubated at 22°C

d Not applicable. Strains were either pre-existing or constructed.

TABLE 3.4. Comparison of gene F suppressing mutation activity in T244Q, M251Q, and T244Q+M251Q genetic backgrounds

Background ^b	E.O.P. ^a at:		
	22°C	37°C	42°C
Wild-Type	0.4	1.0	0.8
<i>su(H)-F T204I</i>	1.2	1.0	0.7
<i>su(H)-F M330I</i>	0.4	1.0	0.6
<i>su(H)-F R386H</i>	0.7	1.0	0.8
<i>cs(H)T244Q</i>	2.8×10^{-2}	1.0	0.8
<i>su(H)-F T204I/cs(H)T244Q</i>	0.4	1.0	0.8
<i>su(H)-F M330I/cs(H)T244Q</i>	0.5	1.0	1.0
<i>su(H)-F R386H/cs(H)T244Q</i>	0.2	1.0	1.0
<i>cs(H)M251Q</i>	2.6×10^{-2}	1.0	1.1
<i>su(H)-F T204I/cs(H)M251Q</i>	0.1	1.0	0.6
<i>su(H)-F M330I/cs(H)M251Q</i>	0.2	1.0	0.5
<i>su(H)-F R386H/cs(H)M251Q</i>	0.1	1.0	0.7
<i>cs(H)T244Q/M251Q</i>	$<1.1 \times 10^{-5}$	1.0	0.7
<i>su(H)-F T204I/cs(H)T244Q/M251Q</i>	$<1.9 \times 10^{-3}$	1.0	$<1.9 \times 10^{-3}$
<i>su(H)-F M330I/cs(H)T244Q/M251Q</i>	$<6.9 \times 10^{-6}$	1.0	0.5
<i>su(H)-F R386H/cs(H)T244Q/M251Q</i>	$<6.0 \times 10^{-6}$	1.0	1.0

a Efficiency of plating. Values are normalized to those obtained from plates incubated at 37°

b Strains with mutations suppressing the T244Q, M251Q, or T244Q/M251Q mutations are labeled with gene in which the suppressing mutation was found, the corresponding amino acid change, and the suppressed mutation, if any. For example, *su(H)-F T204I/cs(H)T244Q* indicates that the strain has T204I in gene F and T244Q in gene H while *su(H)-F T204I* indicates that the strain has T204I in gene F and a wild-type H gene.

FIGURE LEGENDS

FIG 3.1: Structure of the ϕ X174 H-tube. A) The ϕ X174 H protein's coiled-coil domain when oligomerized as a decameric tube. The amino terminal end is facing up and two opposing monomers are colored in cyan (PDB file: 4JPP). B) The H-tube as seen from its C-terminal opening. Inward facing residues are modeled as sticks. C) Primary sequence of the coiled-coil domain. Inward facing residues are colored. Blue residues were mutated in this study. D) The inner surface of three α -helices between Q241 and Q265. Inward facing side chains are modeled as sticks. Inward facing side chain labels appear to the right of the helices.

FIG 3.2: Assembled particles produced in infected cells expressing mutant H constructs. (A) 280nm absorbance profiles of infected cell extracts analyzed by rate zonal sedimentation. Fraction 1 represents the gradient bottom. The specific infectivity peak is indicated with an arrow and a color legend resides in the upper right graph quadrant. (B) SDS-PAGE analysis of specific infectivity peaks. The white space between lanes indicates the removal of irrelevant lanes from the gel.

FIG 3.3: Attachment (A) and eclipse (B) kinetics of virions containing either the wild-type or mutant H proteins. A color legend is provided in the lower right quadrant of each panel. Error bars represent the standard error of the mean calculated from either six biological replicates (attachment) or three biological replicates (eclipse).

FIG 3.4: Viral coat protein levels in infected cells expressing the wild-type H protein. SDS-PAGE analysis of infected cells incubated at 37 (A left) or 22°C (A right).

Quantification of coat to host protein ratios of infected cells seen in panel A. The host protein band used in this analysis is indicated with an arrow in panel A. 37°C results are shown in panel B, 22°C results are in panel C. A color legend is provided in the upper left quadrant of panel B. Error bars represent the standard error of the mean calculated from three biological replicates.

FIG 3.5: Potassium efflux curves and genome quantification. Efflux values are reported as the increase in millivolts after the initial millivolt reading. More positive values indicate more extracellular K⁺ is present. (A) Representative potassium efflux curves in ϕ X174 infected cells at 37°C and (B) 22°C. A color legend is provided in the upper left quadrant of panel B. (C) Infecting genome copy number ratios. Data is presented as I:O ratios, which is the genome copy number of the inner membrane over that of the outer membrane. I:O ratios of particles carrying wild-type H (black), M251Q H (blue), and T244Q+M251Q H (purple) are shown. Error bars represent the standard deviation obtained from three technical replicates.

FIG 3.6: Titers of progeny produced in lysis-resistant cells infected with wild-type ϕ X174 (circles), *su(H)-F T204I* (triangles), or *su(H)-F M330I* (squares). Data is displayed as the viral burst size, which is calculated by dividing the total progeny by the total input phage. Error bars depict the standard deviation obtained from three biological replicates.

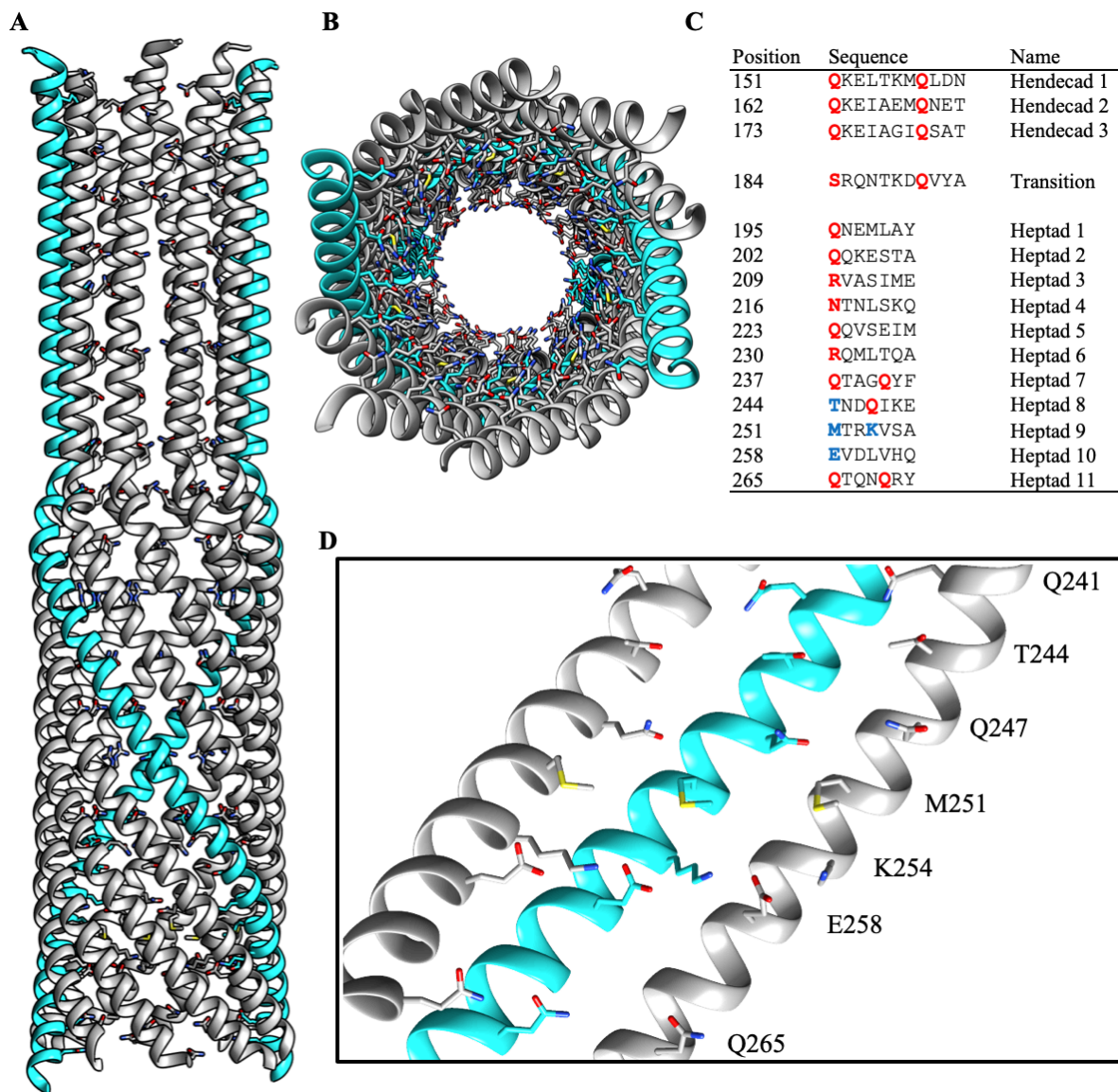


FIG 3.1 Structure of the ϕ X174 H-tube

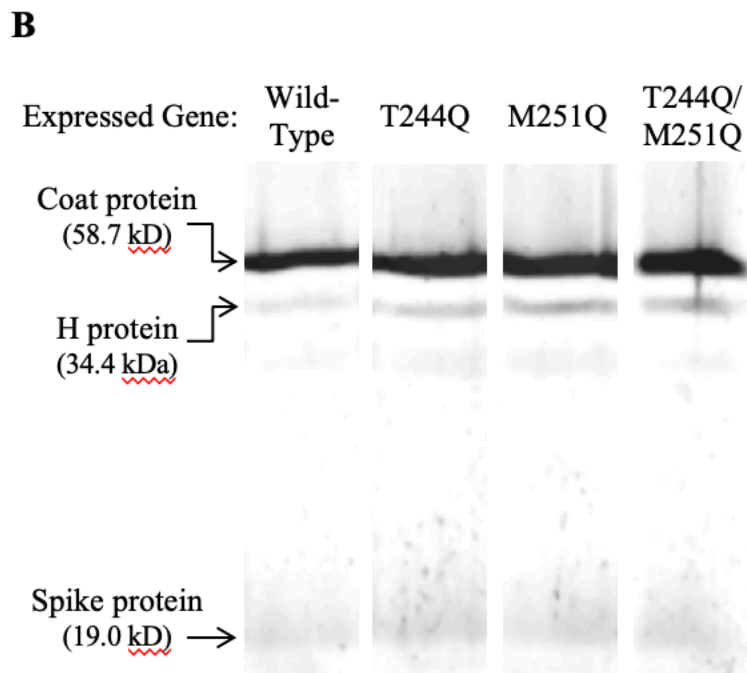
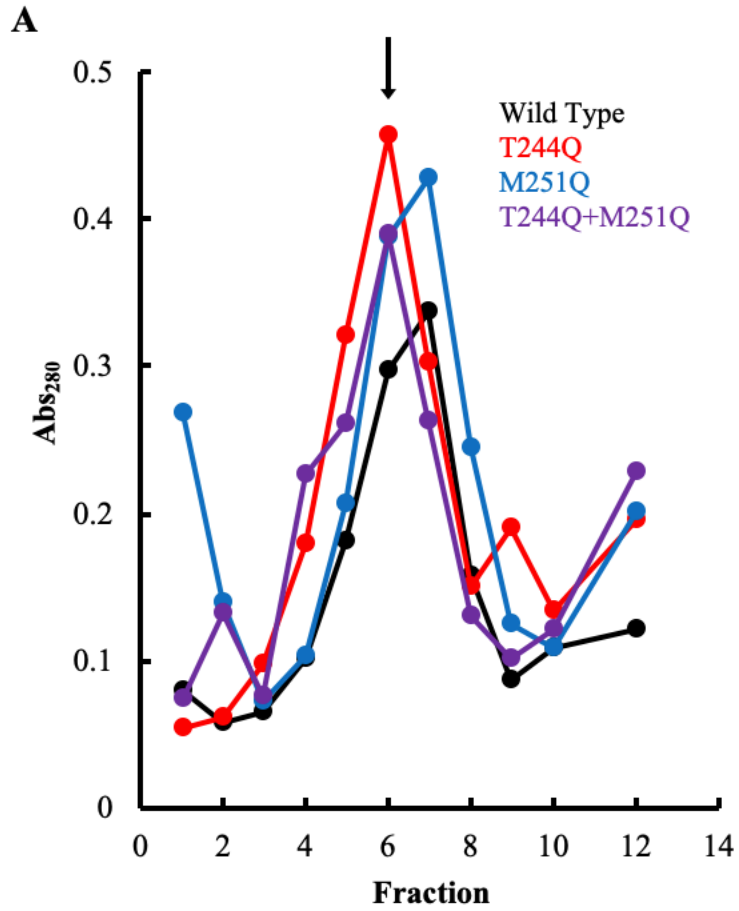


FIG 3.2 Assembled particles produced in infected cells expressing mutant H constructs

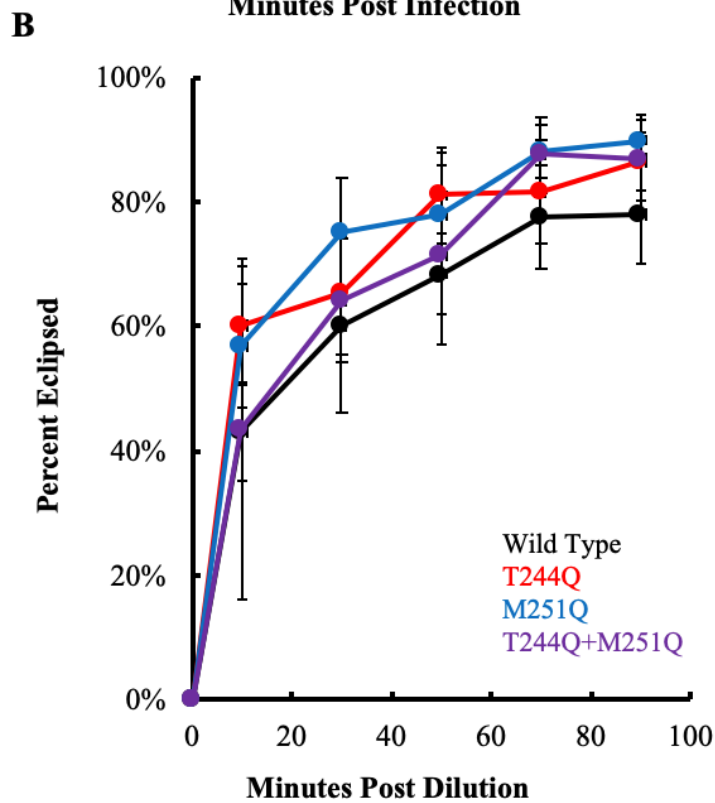
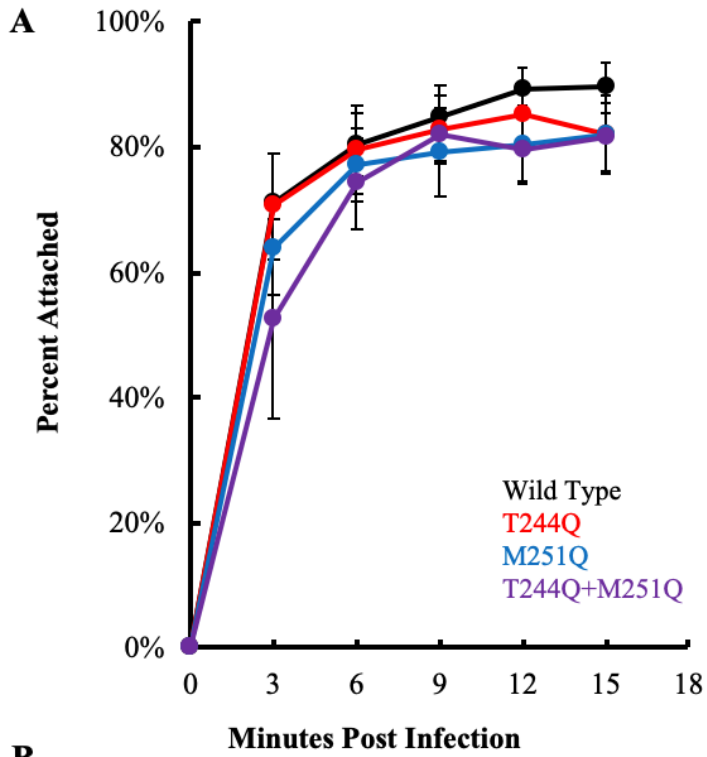


FIG 3.3 Attachment (A) and eclipse (B) kinetics of virions containing either the wild-type or mutant H proteins

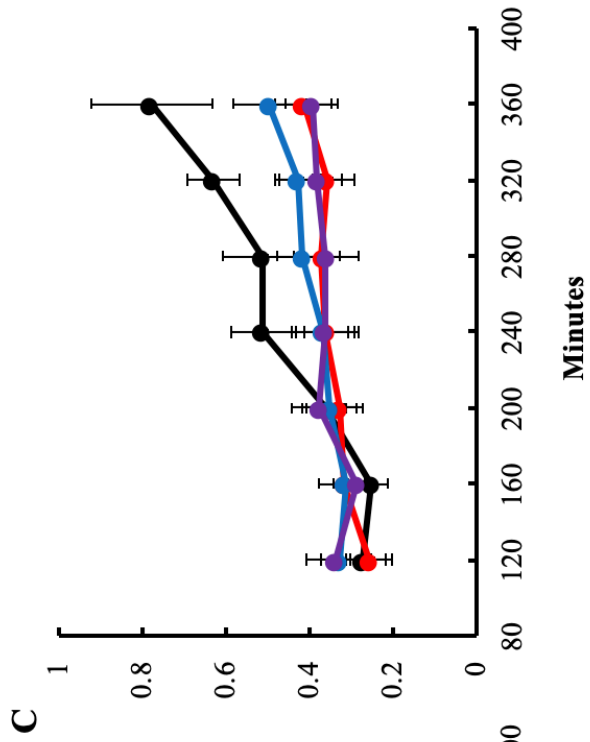
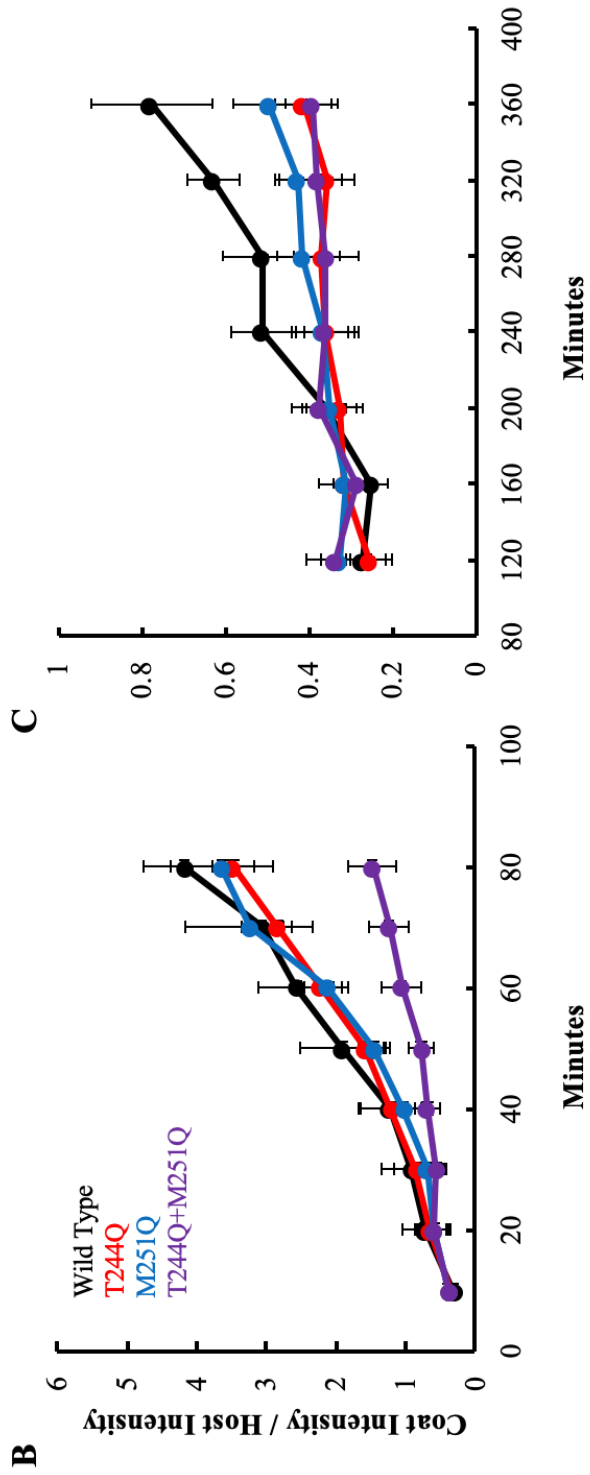
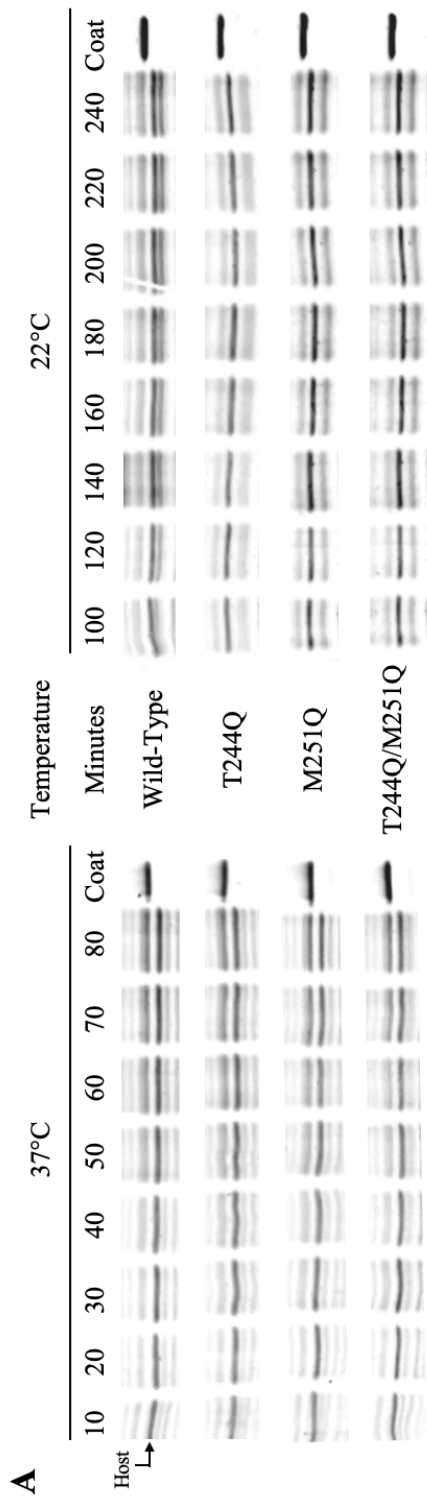


FIG 3.4 Viral coat protein levels in infected cells

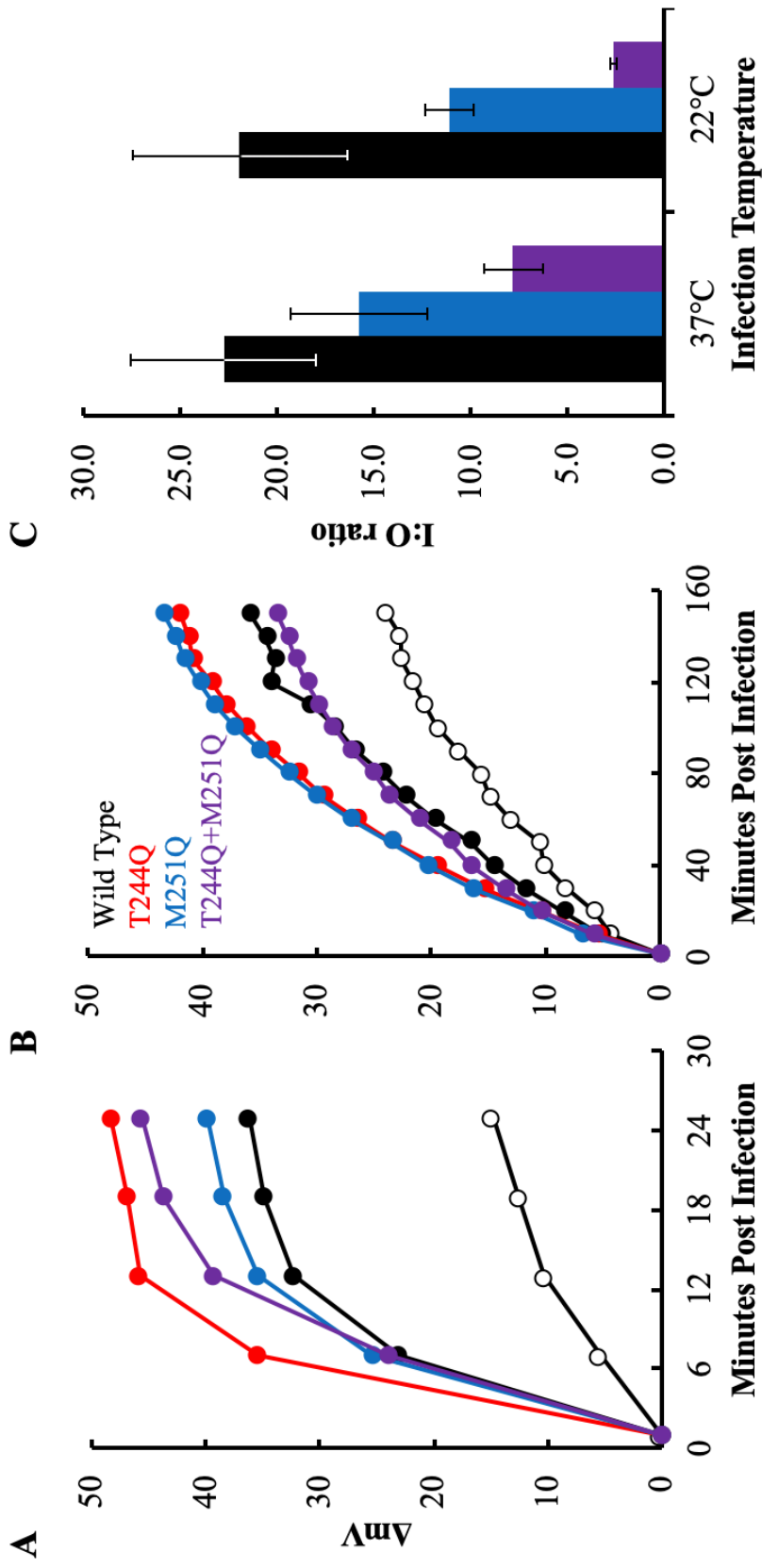


FIG 3.5 Potassium efflux curves and genome quantification

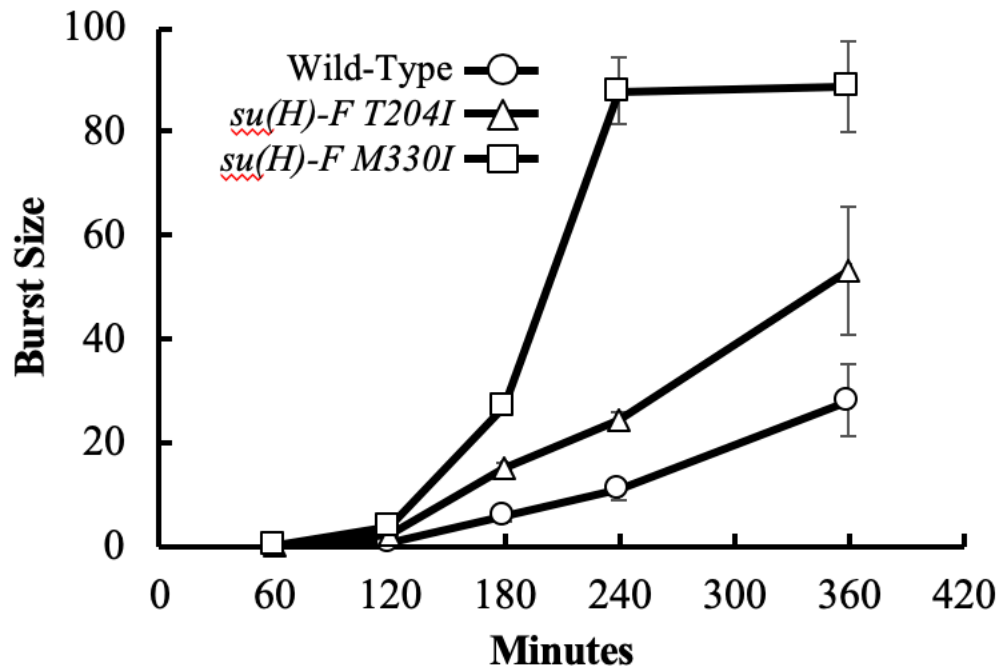


FIG 3.6 Titers of progeny produced in lysis-resistant cells infected with wild-type ϕ X174, *su(H)-F T204I*, or *su(H)-F M330I*

CHAPTER 4

RECESSIVE HOST RANGE MUTANTS AND UNSUSCEPTIBLE CELLS THAT INACTIVATE VIRIONS WITHOUT GENOME PENETRATION: ECOLOGICAL AND TECHNICAL IMPLICATIONS

4.1 Abstract

Although microviruses do not possess a visible tail structure, one vertex rearranges after interacting with host lipopolysaccharides. Most examinations of host range, eclipse, and penetration were conducted before this “host-induced” unique vertex was discovered and before DNA sequencing became routine. Consequently, structure-function relationships dictating host range remain undefined. Biochemical and genetic analyses were conducted with two closely related microviruses, $\alpha 3$ and ST-1. Despite ~90% amino acid identity, the natural host of $\alpha 3$ is *E. coli* C; whereas ST-1 is a K12-specific phage. Virions attached and eclipsed to both native and unsusceptible hosts; however, they breached only the native host’s cell wall. This suggests that unsusceptible host-phage interactions promote off-pathway reactions that can inactivate viruses without penetration. This phenomenon may have broader ecological implications. To determine which structural proteins conferred host range specificity, chimeric virions were generated by individually interchanging the coat, spike, or DNA pilot proteins. Interchanging the coat protein switched host range. However, host range expansion could be conferred by single point mutations in the coat protein. The expansion phenotype was recessive: genetically mutant progeny from co-infected cells did not display the phenotype. Thus, mutant isolation required populations generated in low MOI environments: a phenomenon that may have

impacted past host range studies in both prokaryotic and eukaryotic systems. The resulting genetic and structural data were consistent enough that host range expansion could be predicted, broadening the classical definition of antireceptors to include interfaces between protein complexes within the capsid.

4.2 Introduction

The molecular events mediating early infection have been defined for many bacterial and animal viruses (1-6). This process begins with receptor recognition, perhaps the most critical extracellular factor governing host range. Accordingly, mutations in viral antireceptors are often necessary and sufficient to gain access to new hosts (7-11).

Bacteriophage tail components recognize a diverse range of host cell receptors: monomeric proteins, multimeric complexes, lipopolysaccharides (LPS), peptidoglycan, and teichoic acids (12). For most non-tailed and filamentous phages, unique vertices, spike complexes, or terminal proteins perform this function (13-16). Some phages require two receptors: one located on the cell wall's outermost surface, and a second one embedded within a membrane (17-19). In general, interactions with the initial receptor govern reversible attachment, whereas interactions with the secondary receptor are irreversible, inducing the conformational changes leading to penetration.

Considering the genetic tractability of most model phages, host range mutants have been isolated in relatively few systems. When isolated, mutations overwhelmingly alter the protein mediating irreversible attachment (8-10, 20). As is typical of most *enfants*

terribles, ϕ X174-like phages behave badly. The ϕ X174-like phages fall into three evolutionary clades, each represented by ϕ X174, G4, and α 3 (34). To date, all characterized microviruses use host LPS as a receptor (35) (21) and, with the exception of a few phages within the α 3 clade (see below), all known phages share a common host, *E. coli* C. Φ X174 host range mutations alter one of three structural proteins: the capsid, the spike, and the DNA pilot proteins (22-27). Indeed, conformational changes involving all three structural proteins have been documented during early infection (28-30).

LPS outer core structure is the most critical, and perhaps the only, extracellular host range determinant of the ϕ X174-like phages (21). Reversible attachment may be mediated by conserved coat protein residues that form a 6-carbon sugar binding site (Figure 4.1). Although this has yet to be experimentally addressed, x-ray structures of the ϕ X174 capsid contain ordered sugars bound to these residues (31, 32). Moreover, Ca^{++} ions, which facilitate attachment, structurally change this site from a nonbinding to a binding conformation (33).

Two lipid bilayer-attached structures derived from cryo-EM studies, pre- and post-DNA release, elucidate the conformational switches associated with irreversible attachment, or eclipse. In both structures, the G protein spike at the lipid-interacting vertex has been removed (30). An annulus of coat protein residues merges with the lipid bilayer, anchoring the infecting virion to the membrane. In the post DNA-release structure, there is a pore at the attached vertex, presumably through which the DNA translocating conduit, or H-tube, emerges and penetrates the cell wall (28, 29).

While the cryo-EM and x-ray structures demonstrate how three proteins can mediate attachment and penetration, without supporting genetic and biochemical data, the relationship to host range remains obscure. The results of past studies are limited. Firstly, most were conducted before DNA sequencing was commonplace. Thus, the identity of the host range altering substitution remains unknown. Secondly, host strains were often poorly defined, many being *E. coli* C-K12 hybrids. Thus, selections were unilateral: expanding host range to an alternative host. More detailed comparisons would be facilitated if a naturally occurring microvirus of the alternate host was concurrently examined.

Bacteriophage ST-1 is one of two known *E. coli* K12 specific microvirus (36). The three structural proteins that may govern host range: the viral coat, major spike, and DNA pilot proteins; respectively display 91.4, 89.8, and 85.7% identity with those of bacteriophage α 3, an *E. coli* C specific phage. The three early infection stages: attachment, eclipse and penetration; were biochemically characterized in both native and unsusceptible hosts. To compliment these biochemical assays, host range switching and expansion was genetically analyzed. During the course of this study, it became apparent that standard laboratory protocols, often deemed trivial, can greatly influence experimental results. Due to recessive phenotypes, standard protocols had to be altered. This phenomenon may have broader implications, influencing the results of other prokaryotic and eukaryotic virus host range research. Moreover, unsusceptible host interactions inactivated viruses; in essence culling the population from which an expanded host range mutant could

emerge. This may reflect a novel facet of the virus-host arms race. Lastly, the genetic and biochemical data were easily interpreted within a structural context, allowing phenotype prediction, which may expand the classic antireceptor definition to include interfaces between capsid complexes.

4.3 Results

Virions reversibly and irreversibly attach to unsusceptible hosts, but breach only

native host cell walls: Reversible attachment, eclipse, and K^+ efflux assays were used to analyze phage-cell interactions with both permissive and unsusceptible hosts. To assay attachment, phage and cells were co-incubated in a $CaCl_2$ containing starvation buffer at $16^\circ C$. Calcium ions promote reversible attachment (33), whereas low temperature and starvation prevent eclipse (49). Cells and attached phage were removed by centrifugation. Thus, supernatant titers directly reflect the unattached phage population. To analyze the next entry step, eclipse or irreversible attachment, the pellets were resuspended in a $CaCl_2$ -containing nutrient broth pre-heated to $37^\circ C$. Uneclipsed particles were removed by the addition of EDTA, which chelates the Ca^{++} ions. For $\alpha 3$, no significant differences in attachment or eclipse efficiencies were observed as a function of host range (Figure 4.2A). By contrast, some statistical differences were observed for ST-1.

However, they are likely too small to account for the $<10^{-10}$ titer on the *E. coli C* host.

During penetration, many phages create a conduit connecting the phage particle with the host's cytoplasm. Potassium ions, the cells' primary osmolyte, diffuse through this channel (46, 48, 50). Thus, K^+ efflux assays detect viral-mediated cell wall breaches.

Phages were pre-attached to cells at 4° to inhibit eclipse. Afterwards, infected cultures were diluted into K⁺-free buffer at 37° and extracellular K⁺ levels were monitored as described in Materials in Methods. In contrast to the previous experiments, biologically significant differences were observed. Efflux only occurred when the phages were incubated with their respective permissive hosts (Figure 4.2B and C). Negative ΔmV readings were observed when phages were added to unsusceptible hosts, suggesting K⁺ uptake. However, the initial cell and phage preparations are lacking significant K⁺ levels. This effect may be caused by an influx of trace NH₄⁺ ions present in the phage preparations. NH₄⁺, when above 2.7 ppm, can interfere with K⁺ selective electrodes when K⁺ concentrations are at or below 1 ppm. All efflux experiments were conducted using the same cell and phage preparations. Thus, trace ions effects should be the same in all experiments, but are masked when K⁺ efflux occurs.

Host range correlates with the viral coat protein found in $\alpha 3$ – ST-1 chimeric

particles: To determine whether interchanging individual structural proteins altered host range, chimeric particles were generated by separately interchanging the viral coat F, major spike G, and DNA pilot H proteins. To interchange the G and H proteins, the corresponding genes were cloned and used to complement $\alpha 3$ and ST-1 nonsense mutants. Chimeric phages were generated in their permissive hosts and subsequently assayed for plaque formation on their unsusceptible hosts, both expressing the appropriate cloned gene. For example, $\alpha 3$ *am(G)* phage was initially grown in *E. coli C* expressing the ST-1 G gene, which complemented as well as the $\alpha 3$ gene. The resulting progeny were then plated on *E. coli K12* expressing the ST-1 G gene. Plating efficiency

was less than 10^{-6} . Similar results were obtained for the other three chimeric particles. Thus, the G and H proteins were interchangeable but did not alter host range.

Cloned coat F gene induction was too toxic to conduct complementation assays as described above. Therefore, chimeric particles were generated via recombination as described in Material and Methods. Briefly, *E. coli* C cells harboring the cloned ST-1 F gene were infected with wild-type $\alpha 3$. For ST-1, K12 cells contained the cloned $\alpha 3$ gene. Putative recombinants were identified by plaque formation on the parental phage's unsusceptible host. They were recovered for both phages (frequency $\sim 10^{-5}$). Subsequent plating assays were used to determine whether host range had expanded or switched entirely. Both phenotypes were observed. Members of each phenotypic class had their coat protein genes sequenced (Table 4.1 and Figure 4.3).

Figure 3 contains the amino acid sequences of both phages, which are $\sim 90\%$ identical. Although differences were observed throughout the entire sequence, they tended to cluster in small groups. Due to highly similar viral genome sequences, it was not possible to determine precise recombination junctions. Therefore, recombinant names reflect the position of the first amino acid categorically encoded by the donor gene. Thus, the name $\alpha 3$ -R184 describes an $\alpha 3$ parent in which all gene F codons after and including 184 were donated by the ST-1 gene (Figure 4.3). As can be seen in Table 4.1, host range correlates with the coat protein. $\alpha 3$ -R1, which now synthesizes the ST-1 coat protein, only forms plaques on *E. coli* K12. ST-1-R26, which produces the $\alpha 3$ protein with the exception of

one amino acid, is an *E. coli* C specific phage. By contrast, chimeric coat proteins ($\alpha 3$ -R184 and ST-1-R184) expand host range to both cell types.

Expanded host range mutations are recessive: In most genetic selections using microviruses, single gain of function mutations typically appear at frequencies between 10^{-4} – 10^{-6} . (43, 51-57) However, unsusceptible host plating efficiencies were less than 10^{-10} (Table 4.1) when using standard phage stocks, which are incubated until total cell lysis. Moreover, unsusceptible host cell growth was unaffected despite draconian multiplicity of infection (MOI) values between 100-1000. This tight restrictive phenotype may indicate that altering host range requires multiple mutational events. However, one $\alpha 3$ expanded host range mutant was isolated. Despite the 10^{-11} isolation frequency associated with the $\alpha 3$ PA (polyamorous) mutant, only a single G→A transition was found within the entire genome. It conferred a D→N substitution in the viral coat protein. The structural consequences of this substitution, as well as other PA mutations, are discussed below. The exceptionally low isolation frequency of a single transition suggested an additional level of genetic complexity was affecting the selections.

Both hosts lack restriction modification systems. *E. coli* C is naturally restriction minus (41), whereas the K12 strain (IJ1133) has been genetically modified (40). However, the presence of an unknown or uncharacterized restriction modification system could explain the low mutant isolation frequency. To test this hypothesis, the $\alpha 3$ PA mutant was propagated in each host. Afterwards progeny titers were determined on both *E. coli*

strains. They did not significantly differ (data not shown); thus, the existence of an unknown restriction system seemed unlikely.

Alternatively, the PA phenotype may be recessive. Unlike functions governing intracellular growth, host range can operate on the extracellular level. Consequently, the MOI of the previously infected cell can influence phenotype penetrance and mutant isolation frequency. In this model, a PA genome packaged within a capsid containing both WT and PA coat proteins may not infect the new host. Viral stock preparations are designed to produce the highest possible titers. To allow for multiple propagation cycles, the culture's initial MOI is very low. However, cultures incubate until all cells have been infected and slaughtered. Consequently, the last growth cycles occur at MOIs favoring co-infections. To test this hypothesis, a dominance assay was performed. Lysis-resistant cells were co-infected with a PA and non-PA parent at varying ratios (Table 4.2). The non-PA parent contained an amber mutation in gene H, which was complemented by a cloned $\alpha 3$ H gene. The resulting progeny could be distinguished by three differential plating assays.

- 1) Total progeny: titer on *E. coli* C expressing the cloned $\alpha 3$ H gene.
- 2) Genetically PA progeny, regardless of PA phenotype: titer on *E. coli* C without the cloned $\alpha 3$ H gene. This selects against the non-PA *am(H)* parent.
- 3) Genetically and phenotypically PA progeny: titer on *E. coli* K12.

PA phenotype penetrance is classically defined as the percentage of genetically PA individuals displaying the associated phenotype. It can be determined with the following formula:

$$\text{Phenotype Penetrance Value (PPV)} = \frac{\text{titer on } E. coli \text{ K12}}{\text{titer on } E. coli \text{ C without the cloned } \alpha 3 \text{ H gene}}$$

In these experiments, the MOI of the PA parent was kept constant at 0.5, whereas the non-PA parental MOI varied from 0.5 to 10. At the higher MOIs (>5), nearly all PA infected cells will be co-infected with the non-PA parent. Thus, PA genomes will likely be packaged into heterogeneous capsids as described above. If the PA phenotype is recessive, the Phenotype Penetrance Value (PPV) will decrease as the non-PA parent MOI increases. As can be seen in Table 4.2, the PPV dropped nearly three orders of magnitude.

Population life-history influences mutant isolation frequencies: If the PA phenotype is recessive, as the data suggest, the population's "life-history" could significantly influence mutant isolation. If the population was derived from co-infected cells, frequencies could be misleadingly low. To test this hypothesis, genetic selections were performed with populations generated without co-infections. Several techniques were employed: overlay plates, plating permissive host infectious centers with unsusceptible hosts, terminating stock preparation before culture lysis, and low MOI infections with lysis inhibition. Of all four techniques, the lysis inhibition protocol was the most efficient, least problematic, and easily incorporated into high school curriculums. The

technical advantages and drawbacks of each method and how they can be integrated into high school curricula are detailed in the Material and Methods section.

Regardless of protocol, $\alpha 3$ PA mutants were isolated at a frequency of $\sim 10^{-5}$, which is consistent with the generation of single point mutations. Although these mutants form plaques on both hosts, plaque morphology was noticeably smaller on *E. coli* K12. By contrast, no altered host range ST-1 mutants were isolated by these techniques. In this instance, the low isolation frequency may truly indicate that multiple mutational events are required.

The $\alpha 3$ PA substitutions localize to a protein-protein interface: The PA mutations identified by direct selections are listed in Table 4.3 (first five entries). Five genetically distinct substitutions altered three coat protein residues. The mutant genomes were sequenced and no other substitutions were found, suggesting the identified mutations were both necessary and sufficient to confer the PA phenotype. Although more than 10 independent sources were used, it is unlikely that the selections went to saturation. Two mutations, D395N and Q401K, were independently isolated once, whereas the Q401 and Q402 \rightarrow R mutations were isolated from almost every independently prepared population. The positions of these amino acids, as well as other substitutions conferring the PA phenotype (see below), are indicated with asterisks in Figure 4.3 and are marked within the $\alpha 3$ x-ray structure (Figure 4.4). Only the D395N mutation is located directly at a diverged residue between $\alpha 3$ and ST-1. The amino acid in the ST-1 sequence is asparagine.

To identify other mutations, the existing PA mutants were experimentally evolved on both hosts. Wild-type $\alpha 3$ was similarly treated on *E. coli* C to identify mutations that may arise from the passaging technique (Material and Methods). 19 genomes were selected for whole genome sequence analysis. Numerous substitutions were identified in each genome. However, many of them may not directly affect host range. Therefore, only mutations exclusively found in *E. coli* K12-evolved genomes were selected for further analysis: coat protein substitutions K361R and Q384K. To determine whether these mutations affected host range, they were placed in a wild-type background and assayed for plaque formation on *E. coli* K12. As can be seen in Table 4.3, both mutations conferred the PA phenotype.

All of the PA mutations substitute a more basic amino acid for the wild-type residue: K \rightarrow R (361), Q \rightarrow R (401 and 402), Q \rightarrow K (384, 401 and 402) or D \rightarrow N (395). Unlike the other mutations, the Q384K conferred a very weak PA phenotype (Table 4.3). Moreover, in the $\alpha 3$ crystal structure (58), it is not located near the other substitutions, which reside within the outer circumference of the coat-spike protein interface (Figure 4.4, panels A B, and C).

Mutations conferring the PA phenotype can be predicted, albeit in a limited

manner: The location of the four sites conferring the strongest PA phenotypes: D395, Q401, Q402, and K361; cluster with their side chains oriented toward a descending loop of the major spike protein G (Figure 4.4, panel C). Chemically, the PA substitutions are

more basic than the wild-type residues. These observations suggest that PA phenotypes may be predictable, a hypothesis tested by site-directed mutagenesis.

Mutations in both genes F and G were designed to replace the wild-type residues with more basic ones. Based on location and side chain orientation, G protein substitutions at T75 and D76 were predicted to confer the PA phenotype, whereas substitutions at I177, H178, and Q181 were not expected to alter host range. With the exception of the D76 mutagenesis, primers contained ARA at the target site, encoding either lysine (AAA) or arginine (AGA). Codon D76 was changed to AAC (asparagine). Mutagenized DNA was transfected into both *E. coli* C and K12. The T75 and D76 reactions produced plaques on both hosts. Two mutants were recovered, T75R and D76N, and both displayed the PA phenotype (Table 4.3). The other G gene reactions: I177, H178, and H181; only produced plaques on *E. coli* C. I177R, I177K, H178K, Q181K, and Q181R mutants were recovered on that host but did not alter host range: *E. coli* K12 plating efficiencies were four orders of magnitude lower than those obtained on *E. coli* C.

In the capsid protein, PA phenotypes were predicted for substitutions at S400, but not at Q399 and L404. However, the results were more complex. Transfection plates were incubated at both 30° and 37°C. With one exception (see below), plaques only developed on *E. coli* C. The coat F genes were sequenced (N>12) and all were wild-type. Typically, in our laboratory, viable mutants represent 25-50% of recovered progeny. Thus, these negative results may indicate lethal phenotypes. Alternatively, mutating these codons may be technically problematic. However, an unintended mutation was recovered. It

contained a methionine codon at Q399, likely arising from a spontaneous event after site-directed mutagenesis: CAG (Q) → AAG (K) → ATG (M); or a contaminating primer.

While the recovery of the Q399M mutant argues against technically problematic site-directed mutagenesis; it falls short of compelling. To more rigorously determine whether substitutions were lethal, recombination rescue experiments were performed with cloned genes containing the S400K, S400R, L404K, or L404R mutations. On the *sup*^o host without a plasmid, the plating efficiency of *am(F)Q399* was five orders of magnitude below the permissive titer. Thus, 10⁻⁵ represents the background *am*⁺ reversion frequency. Plating efficiency rose to ~10⁻³ in the presence of the uninduced, cloned wild-type gene, reflecting a recombination frequency two logs above background. By contrast, plating efficiency with the mutant plasmids was equal to the *am*⁺ reversion frequency. Thus, the inability to recover these mutant phages suggests that the substitutions confer a lethal phenotype. However, the underlying molecular basis of the lethal phenotype cannot be determined with this genetic assay.

Exceptions to rules governing phenotype prediction: The unintended Q399M mutant was isolated on *E. coli* K12. Thus, it was subjected to selective pressure beyond viability, expanded host range. The mutation introduces a more hydrophobic amino acid that conferred a very weak PA phenotype (Table 4.3). Unlike the side chains at the neighboring PA sites, which are oriented toward the G protein spike, the Q399 side chain descends into the capsid. A more hydrophobic descending side chain, one oriented into the capsid, may affect the F-G interface like a more basic, ascending side chain. The

general rule also suggests that a D395→R substitution, like D395N, would similarly alter host range. However, it did not: the *E. coli* K12 plating frequency was less than 10⁻⁵. Lastly, residue Q384 is not in the F-G interface, yet Q384K conferred a weak PA phenotype. As visualized in the Cryo-EM structure of an infecting virion (30), this residue may affect a nearby lipid interacting ring.

Reversion of the PA phenotype and structural data may identify another coat region governing host range: As described above, PA mutants were experimentally evolved on both *E. coli* C and K12. Afterwards, approximately 50 plaques were assayed for host range phenotypes differing from their respective parents. All assayed plaques arising from passages through *E. coli* K12 retained the ability to form plaques on *E. coli* C. By contrast, Q402R and Q402K lineages evolved on *E. coli* C gave rise to strains that lost the PA phenotype. A common coat protein substitution was found in both lineages: I112V. To determine whether this mutation was both necessary and sufficient to nullify the PA phenotype, it was placed directly into the Q401K, Q402R, Q402K, Q402R, and D395N genetic backgrounds. In all instances, the K12 plating efficiency fell more than five orders of magnitude. Thus, the I112V mutation nullified the PA phenotype. Residue I112V is not in the F-G interface. Instead, it resides within the aforementioned lipid interacting ring (30).

4.4 Discussion

Host-mediated virus inactivation and its evolutionary significance: Despite structural proteins displaying ~90% identity, bacteriophages $\alpha 3$ and ST-1 infect different *E. coli* strains. Extracellular tropism can be divided into three stages: 1) attachment; 2) eclipse, defined as host-mediated inactivation; and 3) penetration, which involves breaching the cell wall and subsequent genome transport. Regardless of the permissive/unsusceptible nature of the host, attachment and eclipse did not appear to be affected. However, phages could breach only their permissive host's cell wall. In the unsusceptible host, eclipse leads to an off-pathway reaction that inactivates the infecting particle. Thus, sampling unsusceptible host surfaces can have negative consequences that could influence evolutionary trajectories in natural environments. While detrimental to the virus, at least in the laboratory setting, this could be evolutionarily advantageous to potential hosts, perhaps representing a prophylactic strategy in the virus-host arms race. The potential host culls the population from which an expanded host range mutant can emerge. Alternatively, this may be a consequence of lab adaptation: a virus, removed from its natural multi-host environment, is continually propagated in one cell type. In a homogeneous host environment, selective pressure to avoid harmful non-host cell interactions, if they existed, would be greatly relaxed.

The genetics of host range expansion and switching: The host range of bacteriophage $\alpha 3$ and ST-1 were switched by interchanging their viral coat proteins. Thus, by strict definition, the viral coat protein is both necessary and sufficient to change host range.

However, genetic data suggest that there is a distinction between host switching and expansion, which is conferred by recessive, single point mutations.

Unlike dominant and recessive phenotypes associated with intracellular processes, readily discerned by co-infection burst sizes, phenotypes governing extracellular phenomena affect the next generation. When genetically PA genomes were packaged into heterogeneous particles composed of wild-type and PA coat proteins, the phenotypic penetrance was greatly reduced (Table 4.2). Consequently, $\alpha 3$ PA mutants were only efficiently isolated from populations generated in low MOI environments. Single mutants arose at a $10^{-4} - 10^{-5}$ frequency from those samples. By contrast, when selections were conducted with standard, high-titer stocks, the frequency was $\sim 10^{-11}$. To generate the high titers favored by most researchers, cultures incubate until all cells produce progeny. Therefore, most cells will be co-infected in the final stages of stock growth. If the proteins governing host-range operate within complexes; e. g. trimeric tailspikes, baseplates, multimeric spikes or an entire capsid; the population's co-infection "life-history" will affect selections. Dominant alleles will be favored, whereas recessive ones will be under-isolated or undetected (8-10, 25). A similar phenomenon has been documented for antibody escape mutants (59), which are significantly underestimated in populations containing heterogeneous particles.

The relative effect of the population's life history may vary depending on whether the phage encodes a super-infection exclusion mechanism and/or has the ability to lysogenize. Two super-infection exclusion mechanisms have been documented in $\phi X174$

(60, 61), which is lytic phage. However, there is a temporal aspect to super-infection exclusion: the excluding phage must first establish an infection. Indeed, super-infection exclusion was experimentally defined using delayed secondary infection protocols (60, 61). Thus, simultaneous or near simultaneous coinfections could occur during a standard stock preparation, especially if the rounds of infections are somewhat synchronized. The penultimate burst would rapidly change the culture from a low to a high MOI environment.

ST-1 host range could be switched by interchanging its coat protein with $\alpha 3$. However, no PA mutants could be isolated regardless of the population's "life-history." When $\alpha 3$ PA mutants were experimentally evolved in *E. coli* C, a second-site, PA-nullifying, mutation emerged. If the ST-1 coat protein naturally contains a "nullifying" amino acid, host range expansion may require two mutations: the acquisition of a PA mutation and the loss of the "nullifier." The "nullifying" moniker is entirely semantic, reflecting its isolation after the PA mutations. Nonetheless, its existence demonstrates that small, often ignored, conservative differences between independently lab adapted wild-type strains can have experimental consequences. Kumbaya, seemingly different yet rigorously generated and analyzed data sets may all be correct.

The structural basis of host range, receptor interactions, and phenotype prediction:

When visualized within the $\alpha 3$ virion structure, most of the coat protein PA mutations clustered to the outer circumference of the coat-spike interface. The substitutions were more positively charged than the wild-type amino acid residues. Moreover, side chains

were oriented toward a descending G protein insertion loop. This suggested that PA phenotypes could be predicted, at least within the limited context of the hosts and phages used in this study. To test this simple hypothesis, charges were introduced into the descending G protein insertion loop (Figure 4.4), which resulted in the PA phenotype (Table 4.3). By contrast, alterations in side chains oriented away from this region did not expand host range. However, two observations suggest that the initial hypothesis requires refinement: 1) Some substitutions conferred lethal phenotypes, which precluded host range examination, and 2) the introduction of a more hydrophobic amino acid (Q→M) with a descending side chain also conferred a PA phenotype, albeit a weak one.

The viral antireceptor may be an interface between protein complexes: Crill and colleagues examined evolutionary reversals when ϕ X174 was adapted by repetitively switching between two permissive deep rough LPS hosts (62). Similar to our results, they identified three fitness-elevating, coat protein residues located on the outer circumference of the coat-spike interface (Figure 4.5). Although the experimental approaches differed, the collective results are very consistent with the cryo-EM reconstruction of infecting particles, further indicating that G spike removal is critical to early infection (30). This may broaden the classical concept of viral antireceptors to structural interfaces between protein subassemblies. The contrasting phenotypes of G protein PA substitutions and the G protein chimeric virions further support the importance of the interface. The chimeras, generated by exchanging the entire G protein between α 3 and ST-1, did not exhibit altered host ranges. However, the F-G interface would not be identical in these strains. The limited differences between the α 3 and ST-1 G protein primary structure are

confined to the protein's apical regions. By contrast, G protein PA substitutions affect the interface located on the basal surface.

Multiple interactions with a single receptor most likely govern early infection:

Many bacterial viruses require primary and secondary receptors. Primary receptors are usually located on the host's exterior surface (e.g. LPS, teichoic acid, and pili), and typically mediate reversible attachment. The second receptor, which induces penetration, is often a membrane protein (17-19). Although LPS appears to be the only receptor used by ϕ X174-like viruses (21), distinct LPS-virion interactions may mimic a multiple-receptor system. Both structural and genetic data support this model.

Figure 5 illustrates the amino acids genetically identified to affect ϕ X174 and α 3 host range. It also depicts residues identified in x-ray and cryo-EM studies that may play a role in early infection. A 6-carbon sugar binding site, located near the three-fold axis of symmetry (Figure 4.5, purple residues), may govern reversible attachment. Although its direct role has yet to be experimentally addressed, x-ray structures show bound sugar molecules (31, 32). Moreover, Ca^{++} ions, which facilitate attachment, change this site from a nonbinding to sugar binding conformation (33). This interaction is followed by at least two additional LPS-mediated reactions: 1) spike removal, and 2) capsid protein melding with the lipid bilayer. Although the exact residues merging with the cell membrane are not known, they all reside in the EF insertion loop that extends from the coat protein's jelly roll fold. Some residues within this loop form a bulge surrounding the

five-fold axis of symmetry (Fig. 4.5 dark grey). Like the nullifying mutation described in this study, other host range affecting-mutations map to this region (26, 62).

Standard laboratory techniques: less can be more: During the course of this study, it became apparent that standard laboratory techniques and protocols, often deemed trivial, can greatly influence experimental results. The PA mutants isolated in this study had a recessive phenotype. If not for the first author's tenacity or dumb luck isolating the initial mutant (frequency = 10^{-11}), the study would have been terminated. Either no conclusion or incorrect ones would have been drawn. In this instance, standard virus stock preparation; a + 50-year practice, never questioned and falsely deemed adequate for any experiment; could have greatly influenced outcomes. During viral penetration and genome trafficking, proteins often operate in complexes, which were assembled in the previously infected cell. As demonstrated here, the recovery of recessive gain of function mutants can be highly influenced by the "life history" of the population subjected to selective pressure.

4.5 Materials, Methods, and Acknowledgements

Phage plating, media, buffers, and stock preparation. Plating, media, buffers, and standard stock preparation have been previously described (37).

Bacterial strains. The wild-type *Escherichia coli* C strain C122 and derivatives BAF5 (*supE*) and BAF8 (*supF*) have been previously described (37, 38). RY7211 contains a mutation in the *mraY* gene, conferring resistance to viral E protein-mediated lysis (39). The *E. coli* K12 strain IJ1133 was genetically modified to eliminate restriction modification systems (40). *E. coli* C is naturally devoid of restriction modification systems (41). IJ1198 and IJ1220 are respective *supF* and *supE* derivatives of IJ1133 (40).

Cloning of α 3 and ST-1 genes. To clone the α 3 and ST-1 coat F genes, nucleotides 3067-4362 (42) were PCR-amplified with primers with introducing upstream NcoI and downstream HindIII sites. To clone the ST-1 spike G gene, nucleotides 4348-4985 were PCR amplified with primers introducing upstream NcoI and downstream EcoRI sites. To clone the α 3 spike G gene nucleotides 4366 to 4961 were amplified primers introducing upstream NcoI and downstream AclI sites. To clone the ST-1 DNA pilot H gene nucleotides 5063-42 were amplified with primers introducing upstream SacII and downstream XhoI sites. And lastly, to clone the α 3 pilot H gene nucleotides 5083-6089 were amplified with primers introducing upstream BglII and downstream XhoI sites. The PCR products were digested with the specified enzymes and ligated into pSE420 DNA (Invitrogen) digested with the same enzymes.

Mutations were introduced into the cloned α 3 F gene by amplifying the entire plasmid with Q5 DNA polymerase (NEB) with abutting primers, one of which introduced the desired mutation. The PCR product's 5' hydroxyl termini were phosphorylated and ends

ligated together using T4 polynucleotide kinase and ligase (NEB), respectively. The nucleotide sequences of all clones were verified by a direct DNA sequencing analysis.

Construction of $\alpha 3$ and ST-1 chimera via recombination. *E. coli* C cells harboring the cloned ST-1 F gene was infected with wild-type $\alpha 3$. For ST-1, K12 cells contained the cloned $\alpha 3$ F gene. 30 ml cell cultures were grown to a concentration of $\sim 10^8$ cells/ml, infected at an MOI of $\sim 10^{-5}$ and incubated for 2 hr. Cultures did not incubate until lysis. After the addition of lysozyme, cultures were titered on both permissive and unsusceptible hosts. Putative recombinants were identified as described in the Results.

Site directed phage mutants of $\alpha 3$. Single-stranded (ss) viral DNA was isolated by the OLT (Our Little Trick) protocol, which has been previously described (43). Mutations were introduced by amplifying the entire genome with abutting primers, one of which introduced the desired mutation. The PCR products were treated as described above. The resulting ligation products were transfected into C122. If the ligation product contained an amber mutation, BAF5(*supE*) was transfected.

Attachment, eclipse, and K^+ assays. Attachment and eclipse assays have been previously described (44, 45). K^+ efflux assays, modeled after a previously published protocol (46), were performed by first growing cells to an OD_{660} of 0.08 in TKY media (1.0 % tryptone, 0.5% KCl, 0.5% yeast extract) at 37°C. Cells were pelleted and washed in an equal volume of SM buffer (100 mM NaCl, 10 mM $MgSO_4$, 50 mM Tris pH=7.5), washed again in 1/10th the volume of SM buffer, and resuspended in 1/100th the

volume of iced SM buffer containing 10 mM MgCl₂ and 5.0 mM CaCl₂. The cell culture was divided into 1.0 mL aliquots, kept on ice, and chilled phage was added at an MOI of 75. Presumably, high MOIs are required to detect the efflux signal (46-48). Iced SM buffer containing MgCl₂ and CaCl₂ was added to equalize aliquot volumes. Cultures were incubated for 15 minutes on ice to allow phage pre-attachment. At 1.0-minute intervals, cultures were diluted 10-fold into SM buffer containing MgCl₂ and CaCl₂ preheated to 37°C. Immediately after dilution, an Orion Ionplus potassium electrode (Thermo Scientific) connected to a Sartorius PB-11 pH meter was inserted into an infection and a reading was taken after 1.0 minute. This electrode was then rinsed with DI H₂O, blotted dry, and placed into the dilution of the subsequent infection. The electrode was rotated between infections at one-minute intervals once all infections were diluted.

Genetic selections with populations generated in low MOI environments. Four different techniques were used to obtain populations generated in low MOI environments. 1) Overlay protocol: $\sim 10^7$ infectious particles and $\sim 10^8$ permissive host cells were mixed in 2.0 ml soft agar (37) and plated. After a 30 min incubation at 33°C, $\sim 10^8$ unsusceptible host cells in soft agar were poured atop the plates, which were then incubated at 37°C for 5 hrs. 2) Pre-attachment protocol: approximately $\sim 10^6$ infectious particles and $\sim 10^7$ permissive host cells were mixed and incubated at 37°C for five minutes. Afterwards, $\sim 5.0 \times 10^8$ unsusceptible host cells in 2.0 ml soft agar was added to the reaction mixtures, plated and incubated at 37°C. 3) Low titer stock protocol: This was identical to a standard stock preparation (37) but the culture was not allowed to incubate until lysis. 4) Lysis inhibition protocol: for $\alpha 3$, a single plaque ($\sim 10^6 - 10^7$ phage) and 0.1 ml of lysis

resistant cells ($\sim 10^8$ cells) were placed into 1.0 ml TKY media (1.0% tryptone, 0.5 KCl, 0.5 yeast extract) supplemented with 10.0 mM $MgCl_2$ and 5.0 mM $CaCl_2$. Infections were incubated for 5 hr at 37°C and then placed on ice. Egg white lysozyme was added to a final concentration of 2.0 mg/ml and incubated overnight at 4°C. For mutant isolation, progeny were plated on the unsusceptible host. For ST-1, a phage with an amber mutation in the gene E, which encodes the viral lysis protein, was used. The protocol was identical to that used for $\alpha 3$ except *E. coli* K12 IJ1133 cells (*sup*^o) were infected. The unsusceptible host for mutant isolation was *E. coli* C BAF8 (*supF*).

Of all four techniques, the lysis inhibition protocol was the most efficient. Each single plaque infection represents an independent population source. Unlike generating low titer stocks, infections did not need to be continuously monitored for lysis. For the overlay and pre-attachment techniques, permissive rounds of infections occurred on the same plate from which host range mutants were picked. Consequently, mutant plaques often contained a high level of wild-type phage, which obscured sequencing results without prior plaque purification. The lysis inhibition protocol was also the easiest to integrate into off-campus, high school schedules as a “fully hands on” endeavor. Infections were started before the school day began and incubated while the students attended their other classes. Lysozyme was added during their scheduled laboratory class and incubated overnight. The next morning, selection plates were prepared before the start of classes and incubated during the day. Students picked plaques during their scheduled science hour. PCR reactions and product purification were also performed during scheduled science hours.

Experimental evolution: Starting with single plaques of each PA mutant, virions were stabbed into plates freshly seeded with bacteria and incubated for five hours at 37°C. Virions from the same starting plaque were initially stabbed into both *E. coli* C and K12 containing plates. Afterwards, the subsequent populations were kept separate. A portion of the phage from each clearing were then transferred to a freshly prepared plate. Wild-type $\alpha 3$ was similarly passaged on *E. coli* C to identify mutations that may arise from the passaging technique. After the 10th passage, at which time clearings had become substantially larger, 24 individual plaques were isolated from each population and plated on both *E. coli* C and K12 to determine whether passaging on one host lead to any alterations in host range. For the reasons discussed above, this protocol was also easy to integrate into off-campus, high school schedules as a “fully hands on” endeavor.

Acknowledgements

The authors thank Dr. I. J. Molineux for providing ST-1 and the *E. coli* K12 strains used in this study. This research was supported by National Science Foundation grant MCB-1408217 (B.A.F.), the BIO5 Institute at the University of Arizona, and US Department of Agriculture Hatch funds to the University of Arizona. The authors also acknowledge the support of programs in which undergraduate and high school students participated: The Steps 2 STEM Program (University of Arizona) and The Advanced Math/Science Research Programs at Berkshire School and Tucson Magnet High School.

4.6 References

1. Leiman PG, Chipman PR, Kostyuchenko VA, Mesyanzhinov VV, Rossmann MG. 2004. Three-dimensional rearrangement of proteins in the tail of bacteriophage T4 on infection of its host. *Cell* 118:419-29.
2. Belnap DM, Filman DJ, Trus BL, Cheng N, Booy FP, Conway JF, Curry S, Hiremath CN, Tsang SK, Steven AC, Hogle JM. 2000. Molecular tectonic model of virus structural transitions: the putative cell entry states of poliovirus. *J Virol* 74:1342-54.
3. Bubeck D, Filman DJ, Cheng N, Steven AC, Hogle JM, Belnap DM. 2005. The structure of the poliovirus 135S cell entry intermediate at 10-angstrom resolution reveals the location of an externalized polypeptide that binds to membranes. *J Virol* 79:7745-55.
4. Hu B, Margolin W, Molineux IJ, Liu J. 2013. The bacteriophage t7 virion undergoes extensive structural remodeling during infection. *Science* 339:576-9.
5. Cotmore SF, Tattersall P. 2007. Parvoviral host range and cell entry mechanisms. *Adv Virus Res* 70:183-232.
6. Lee H, Shingler KL, Organtini LJ, Ashley RE, Makhov AM, Conway JF, Hafenstein S. 2016. The novel asymmetric entry intermediate of a picornavirus captured with nanodiscs. *Sci Adv* 2:e1501929.
7. Hueffer K, Parker JS, Weichert WS, Geisel RE, Sgro JY, Parrish CR. 2003. The natural host range shift and subsequent evolution of canine parvovirus resulted from virus-specific binding to the canine transferrin receptor. *J Virol* 77:1718-26.
8. Duffy S, Turner PE, Burch CL. 2006. Pleiotropic costs of niche expansion in the RNA bacteriophage phi 6. *Genetics* 172:751-7.
9. Ford BE, Sun B, Carpino J, Chapler ES, Ching J, Choi Y, Jhun K, Kim JD, Lalloo GG, Morgenstern R, Singh S, Theja S, Dennehy JJ. 2014. Frequency and fitness consequences of bacteriophage phi6 host range mutations. *PLoS One* 9:e113078.
10. Tetart F, Repoila F, Monod C, Krisch HM. 1996. Bacteriophage T4 host range is expanded by duplications of a small domain of the tail fiber adhesin. *J Mol Biol* 258:726-31.
11. Yosef I, Goren MG, Globus R, Molshanski-Mor S, Qimron U. 2017. Extending the Host Range of Bacteriophage Particles for DNA Transduction. *Mol Cell* 66:721-728 e3.

12. Bertozzi Silva J, Storms Z, Sauvageau D. 2016. Host receptors for bacteriophage adsorption. *FEMS Microbiol Lett* 363.
13. Mindich L, Bamford D, McGraw T, Mackenzie G. 1982. Assembly of bacteriophage PRD1: particle formation with wild-type and mutant viruses. *J Virol* 44:1021-30.
14. Mindich L, Sinclair JF, Cohen J. 1976. The morphogenesis of bacteriophage phi6: particles formed by nonsense mutants. *Virology* 75:224-31.
15. Mindich L, Sinclair JF, Levine D, Cohen J. 1976. Genetic studies of temperature-sensitive and nonsense mutants of bacteriophage phi6. *Virology* 75:218-23.
16. Stengele I, Bross P, Garces X, Giray J, Rasched I. 1990. Dissection of functional domains in phage fd adsorption protein. Discrimination between attachment and penetration sites. *J Mol Biol* 212:143-9.
17. Baptista C, Santos MA, Sao-Jose C. 2008. Phage SPP1 reversible adsorption to *Bacillus subtilis* cell wall teichoic acids accelerates virus recognition of membrane receptor YueB. *J Bacteriol* 190:4989-96.
18. McPartland J, Rothman-Denes LB. 2009. The tail sheath of bacteriophage N4 interacts with the *Escherichia coli* receptor. *J Bacteriol* 191:525-32.
19. Parent KN, Erb ML, Cardone G, Nguyen K, Gilcrease EB, Porcek NB, Pogliano J, Baker TS, Casjens SR. 2014. OmpA and OmpC are critical host factors for bacteriophage Sf6 entry in *Shigella*. *Mol Microbiol* 92:47-60.
20. Meyer JR, Dobias DT, Weitz JS, Barrick JE, Quick RT, Lenski RE. 2012. Repeatability and contingency in the evolution of a key innovation in phage lambda. *Science* 335:428-32.
21. Michel A, Clermont O, Denamur E, Tenaillon O. 2010. Bacteriophage PhiX174's ecological niche and the flexibility of its *Escherichia coli* lipopolysaccharide receptor. *Appl Environ Microbiol* 76:7310-3.
22. Weisbeek PJ, van de Pol JH, van Arkel GA. 1973. Mapping of host range mutants of bacteriophage phiX174. *Virology* 52:408-16.
23. Sinsheimer RL. 1968. Bacteriophage phi-X174 and related viruses. *Prog Nucleic Acid Res Mol Biol* 8:115-69.
24. Tessman ES. 1965. Complementation Groups in Phage S13. *Virology* 25:303-21.

25. Bone DR, Dowell CE. 1973. A mutant of bacteriophage phiX174 which infects E. coli K12 strains. I. Isolation and partial characterization of phiXtB. *Virology* 52:319-29.
26. Cox J, Putonti C. 2010. Mechanisms responsible for a PhiX174 mutant's ability to infect Escherichia coli by phosphorylation. *J Virol* 84:4860-3.
27. Newbold JE, Sinsheimer RL. 1970. The process of infection with bacteriophage phiX174. XXXII. Early steps in the infection process: attachment, eclipse and DNA penetration. *J Mol Biol* 49:49-66.
28. Sun L, Rossmann MG, Fane BA. 2014. High-resolution structure of a virally encoded DNA-translocating conduit and the mechanism of DNA penetration. *J Virol* 88:10276-9.
29. Sun L, Young LN, Zhang X, Boudko SP, Fokine A, Zbornik E, Roznowski AP, Moulineux I, Rossmann MG, Fane BA. 2014. Icosahedral Φ X174 forms a tail for DNA transport. *Nature* 505:432-5.
30. Sun Y, Roznowski AP, Tokuda JM, Klose T, Mauney A, Pollack L, Fane BA, Rossmann MG. 2017. Structural changes of tailless bacteriophage PhiX174 during penetration of bacterial cell walls. *Proc Natl Acad Sci U S A* 114:13708-13713.
31. McKenna R, Ilag LL, Rossmann MG. 1994. Analysis of the single-stranded DNA bacteriophage phi X174, refined at a resolution of 3.0 Å. *J Mol Biol* 237:517-43.
32. McKenna R, Xia D, Willingmann P, Ilag LL, Krishnaswamy S, Rossmann MG, Olson NH, Baker TS, Incardona NL. 1992. Atomic structure of single-stranded DNA bacteriophage phi X174 and its functional implications. *Nature* 355:137-43.
33. Ilag LL, McKenna R, Yadav MP, BeMiller JN, Incardona NL, Rossmann MG. 1994. Calcium ion-induced structural changes in bacteriophage phi X174. *J Mol Biol* 244:291-300.
34. Rokyta DR, Burch CL, Caudle SB, Wichman HA. 2006. Horizontal gene transfer and the evolution of microvirid coliphage genomes. *J Bacteriol* 188:1134-42.
35. Sandulache R, Prehm P, Kamp D. 1984. Cell wall receptor for bacteriophage Mu G(+). *J Bacteriol* 160:299-303.
36. Bowes JM, Dowell CE. 1974. Purification and some properties of bacteriophage ST-1. *J Virol* 13:53-61.
37. Fane BA, Hayashi M. 1991. Second-site suppressors of a cold-sensitive prohead accessory protein of bacteriophage phi X174. *Genetics* 128:663-71.

38. Fane BA, Head S, Hayashi M. 1992. Functional relationship between the J proteins of bacteriophages phi X174 and G4 during phage morphogenesis. *J Bacteriol* 174:2717-9.
39. Bernhardt TG, Struck DK, Young R. 2001. The lysis protein E of phi X174 is a specific inhibitor of the MraY-catalyzed step in peptidoglycan synthesis. *J Biol Chem* 276:6093-7.
40. Moak M, Molineux IJ. 2000. Role of the Gp16 lytic transglycosylase motif in bacteriophage T7 virions at the initiation of infection. *Mol Microbiol* 37:345-55.
41. Daniel AS, Fuller-Pace FV, Legge DM, Murray NE. 1988. Distribution and diversity of hsd genes in *Escherichia coli* and other enteric bacteria. *J Bacteriol* 170:1775-82.
42. Kodaira K, Nakano K, Okada S, Taketo A. 1992. Nucleotide sequence of the genome of the bacteriophage alpha 3: interrelationship of the genome structure and the gene products with those of the phages, phi X174, G4 and phi K. *Biochim Biophys Acta* 1130:277-88.
43. Blackburn BJ, Li S, Roznowski AP, Perez AR, Villarreal RH, Johnson CJ, Hardy M, Tuckerman EC, Burch AD, Fane BA. 2017. Coat protein mutations that alter the flux of morphogenetic intermediates through the phiX174 early assembly pathway. *J Virol* doi:JVI.01384-17 [pii]
44. Cherwa JE, Jr., Sanchez-Soria P, Wichman HA, Fane BA. 2009. Viral adaptation to an antiviral protein enhances the fitness level to above that of the uninhibited wild type. *J Virol* 83:11746-50.
45. Hafenstein SL, Chen M, Fane BA. 2004. Genetic and functional analyses of the oX174 DNA binding protein: the effects of substitutions for amino acid residues that spatially organize the two DNA binding domains. *Virology* 318:204-13.
46. Cumby N, Reimer K, Mengin-Lecreulx D, Davidson AR, Maxwell KL. 2015. The phage tail tape measure protein, an inner membrane protein and a periplasmic chaperone play connected roles in the genome injection process of *E. coli* phage HK97. *Mol Microbiol* 96:437-47.
47. Boulanger P, Letellier L. 1992. Ion Channels Are Likely to Be Involved in the 2 Steps of Phage-T5 DNA Penetration into *Escherichia-Coli*-Cells. *Journal of Biological Chemistry* 267:3168-3172.
48. Letellier L, Plancon L, Bonhivers M, Boulanger P. 1999. Phage DNA transport across membranes. *Res Microbiol* 150:499-505.

49. Newbold JE, Sinsheimer RL. 1970. Process of infection with bacteriophage phi-X174. XXXIV. Kinetic of the attachment and eclipse steps of the infection. *J Virol* 5:427-31.
50. Boulanger P, Letellier L. 1992. Ion channels are likely to be involved in the two steps of phage T5 DNA penetration into *Escherichia coli* cells. *J Biol Chem* 267:3168-72.
51. A. ZA. 1972. Protein volume in solution. *Prog Biophys Mol Biol* 24:107-123.
52. Cherwa JE, Jr., Fane BA. 2009. Complete virion assembly with scaffolding proteins altered in the ability to perform a critical conformational switch. *J Virol* 83:7391-6.
53. Cherwa JE, Jr., Uchiyama A, Fane BA. 2008. Scaffolding proteins altered in the ability to perform a conformational switch confer dominant lethal assembly defects. *J Virol* 82:5774-80.
54. Doore SM, Baird CD, Roznowski AP, Fane BA. 2014. The evolution of genes within genes and the control of DNA replication in microviruses. *Mol Biol Evol* 31:1421-31.
55. Gordon EB, Knuff CJ, Fane BA. 2012. Conformational Switch-Defective ϕ X174 Internal Scaffolding Proteins Kinetically Trap Assembly Intermediates before Procapsid Formation. *J Virol* 86:9911-8.
56. Roznowski AP, Fane BA. 2016. Structure-Function Analysis of the varphiX174 DNA-Piloting Protein Using Length-Altering Mutations. *J Virol* 90:7956-66.
57. Uchiyama A, Chen M, Fane BA. 2007. Characterization and function of putative substrate specificity domain in microvirus external scaffolding proteins. *J Virol* 81:8587-92.
58. Bernal RA, Hafenstein S, Olson NH, Bowman VD, Chipman PR, Baker TS, Fane BA, Rossmann MG. 2003. Structural studies of bacteriophage alpha3 assembly. *J Mol Biol* 325:11-24.
59. Holland JJ, de la Torre JC, Steinhauer DA, Clarke D, Duarte E, Domingo E. 1989. Virus mutation frequencies can be greatly underestimated by monoclonal antibody neutralization of virions. *J Virol* 63:5030-6.
60. Hutchison CA, 3rd, Sinsheimer RL. 1971. Requirement of protein synthesis for bacteriophage phi X174 superinfection exclusion. *J Virol* 8:121-4.

61. van der Avoort HG, van Arkel GA, Weisbeek PJ. 1982. Cloned bacteriophage phi X174 DNA sequence interferes with synthesis of the complementary strand of infecting bacteriophage phi X174. *J Virol* 42:1-11.
62. Crill WD, Wichman HA, Bull JJ. 2000. Evolutionary reversals during viral adaptation to alternating hosts. *Genetics* 154:27-37.
63. Pettersen EF, Goddard TD, Huang CC, Couch GS, Greenblatt DM, Meng EC, Ferrin TE. 2004. UCSF Chimera--a visualization system for exploratory research and analysis. *J Comput Chem* 25:1605-12.

4.7 Figures and Tables

Table 4.1: Host range of coat protein chimeric virions

Phage ^a	Coat protein composition ^a		Plating efficiency ^b :	
	α 3	ST-1	C122	K12
Wild-type α 3	100%	0%	1.0	<10 ⁻¹⁰
α 3-R1	0%	100%	<10 ⁻⁶	1.0
α 3-R184	43%	57%	0.9	1.0
Wild-type ST-1	0%	100%	<10 ⁻¹⁰	1.0
ST-1-R26	6%	94%	1.0	<10 ⁻⁴
ST-1-R184	43%	57%	0.4	1.0

^a Coat protein composition and mutant phage nomenclature were derived from the coat protein sequence. They indicate the first amino acid that is identical to the foreign protein sequence within the recombinant strain. For example, the coat protein sequence found in strain α 3-R184 becomes identical to the ST-1 sequence at residue 184. With the exception of the coat protein gene, or a portion thereof, the remaining genome is derived entirely from α 3. Both coat proteins are 431 amino acids in length.

^b Plating efficiency is defined as assay titer/most permissive titer. Thus, if assay and most permissive titers were obtained on the same host, the plating efficiency was reported as 1.0.

Table 4.2: Expanded host range is recessive

Parental MOIs		Frequency of gene H complementation-independent progeny determined on ^a :		PPV: PA phenotype penetrance value ^b
<i>am(H)</i>	PA	A) <i>E. coli</i> K12	B) <i>E. coli</i> C	(A/B)
0.5	0	< 10 ⁻⁶	10 ^{-5c}	NA
0	0.5	0.7	1.0	0.7 ^d
0.5	0.5	0.08	0.5	0.16
5.0	0.5	1.5 × 10 ⁻³	0.15	1.0 × 10 ⁻²
10	0.5	5.0 × 10 ⁻⁴	0.1	5.0 × 10 ⁻³

^a The titer of gene H complementation-independent progeny was determined by plating on *sup*^o strains of *E. coli* C and K12, which selects against the non-PA *am(H)* parent.

^b PPV conveys the percentage of genetically PA individuals, inferred by the absence of the *am(H)* mutation, that display the PA phenotype, determined by the ability to form plaques on *E. coli* K12.

^c This value established experimental background: the loss of the *am(H)* phenotype via either reversion or recombination with the cloned α 3H gene. The total titer was determined with *E. coli* C cells expressing the cloned α 3 H gene.

^d This value established the background level arising from natural differences in plating efficiencies.

Table 4.3. Plating efficiencies of PA mutants

Mutant	Identification or isolation method ^a	Independent isolations	Plating efficiency on	
			<i>E. coli</i> C	<i>E. coli</i> K12
$\alpha 3$ <i>PA(F)D395N</i>	Direct selection	1	1.0	0.7
$\alpha 3$ <i>PA(F)Q401K</i>	Direct selection	1	0.9	1.0
$\alpha 3$ <i>PA(F)Q401R</i>	Direct selection	9	1.0	1.0
$\alpha 3$ <i>PA(F)Q402K</i>	Direct selection	2	0.5	1.0
$\alpha 3$ <i>PA(F)Q402R</i>	Direct selection	8	1.0	0.9
$\alpha 3$ <i>PA(F)K361R</i>	Exp. ^b Evolution	NA	1.0	1.0
$\alpha 3$ <i>PA(F)Q384K</i>	Exp. Evolution	NA	1.0	$\sim 10^{-1} - 10^{-2}$ ^c
$\alpha 3$ <i>PA(G)T75R</i>	SDM	NA	1.0	0.5
$\alpha 3$ <i>PA(G)D76N</i>	SDM	NA	1.0	$\sim 10^{-1} - 10^{-2}$ ^c
$\alpha 3$ <i>PA(F)Q399M</i>	SDM & reversion	NA	1.0	$\sim 10^{-1} - 10^{-2}$ ^c
Non-PA mutants G protein: I177R, I177K, H178K, Q181K, Q181R Protein F: D395R	SDM	NA	1.0	$< 10^{-5}$
Nullifier (F)I112V with Q401K, Q401R, Q402K, Q401R, D395N	SDM	NA	1.0	$< 10^{-5}$

^a Mutant nomenclature: mutant names reflect the protein, position, and substitutions conferring the PA phenotype. For example, *PA(F)D395N* reflects a D→N substitution at position 395 in the coat F protein.

^b Abbreviations: Exp. Evolution: experimental evolution. NA: not applicable. SDM: site-directed mutagenesis. SDM & reversion: site-directed mutagenesis followed by a reversion event, see text for details.

^c The PA phenotype was extremely weak, as reflected by low variable plating efficiencies and pathetic pinprick plaques.

FIGURE LEGENDS

FIG. 4.1 Early microvirus infection. Reversible attachment, likely mediated by a 6-carbon sugar binding site, is followed by the formation of a host-induced unique vertex. The infecting particle loses the G protein spike complex at the lipid-interacting vertex and the capsid protein merges with the membrane. Five coat proteins rearrange, forming a pore through which the H-tube, a DNA-translocating conduit, emerges from the particle.

FIG. 4.2 Attachment, eclipse and penetration as a function of host range. The permissive host for $\alpha 3$ is *E. coli* C, whereas ST-1 is a K12 specific phage. A) Attachment and eclipse experiments were performed in triplicate. The host cells and phages used in each experiment are given in the figure. Error bars convey standard deviation. B) $\alpha 3$ -induced K^+ efflux. Solid blue: *E. coli* C with $\alpha 3$; solid magenta: *E. coli* K12 with $\alpha 3$; open blue: *E. coli* C alone; open magenta, *E. coli* K12; alone. C) ST-1-induced K^+ efflux. Solid blue: *E. coli* C with ST-1; solid magenta: *E. coli* K12 with ST-1; open blue: *E. coli* C alone; open magenta, *E. coli* K12; alone.

FIG. 4.3 Amino acids sequences of the $\alpha 3$ and ST-1 coat proteins. Identical amino acids are depicted in black text on the central line, whereas diverged amino acids are indicated with blue ($\alpha 3$) and magenta (ST-1) text, above and below the central line, respectively. The junctions found in recombinants are given by the position of the colored boxes. Colors and arrows indicate which viruses donated the sequence. For example, the coat

protein sequence of $\alpha 3$ -R1 is 100% identical to ST-1. Thus, it is positioned at the beginning of the sequence and is shaded magenta. By contrast, the first 183 amino acids in the $\alpha 3$ -R184 coat protein are derived from $\alpha 3$, as indicated by the blue leftward arrow. The remaining amino acids are derived from ST-1. Asterisks indicate sites at which point mutations conferred PA phenotypes in $\alpha 3$.

FIG. 4.4 The location of PA substitutions within the $\alpha 3$ x-ray structure. A and B) Space filling renderings of the $\alpha 3$ x-ray structure. The coat F protein is depicted in white, the spike G protein in magenta. The PA substitutions are depicted in blue. One G protein spike has been removed (panel B) to illustrate the location of PA substitutions within the F–G protein interface. C) The F–G interface. The PA substitutions, coat and spike proteins are colored as described above. Numbers depict the amino acid's location within the primary structure. D) Phenotypes of site-directed mutations. Side chain colors: blue, substitutions conferring the PA phenotype; grey, substitutions that did not alter host range; black, substitutions likely conferring a lethal phenotype.

FIG. 4.5 Structurally and genetically defined residues governing host range and extracellular virus-host interactions in $\phi X174$ and $\alpha 3$. The image depicts the $\alpha 3$ structure. The root-mean-square deviations between equivalent C^α atoms of the $\phi X174$ and $\alpha 3$ coat proteins, which share 72% sequence identity, is only 0.8 Å (58). Thus, equivalent $\phi X174$ residues could be reasonably mapped onto the $\alpha 3$ virion. Mutations identified in this study are colored dark blue. Primarily residing within the coat F – spike G protein interface, they are more easily visualized when a spike complex is removed (right image).

Mutations identified in ϕ X174 studies (26, 62) are depicted in cyan. The residues of the conserved 6-carbon sugar binding site are highlighted in purple (31-33). The bulge-forming EF insertion loop, which contains the residues that merge with the lipid bilayer (30), is depicted in dark grey. The images was generated using Chimera (63) and Protein Data Bank accession code 1M06.

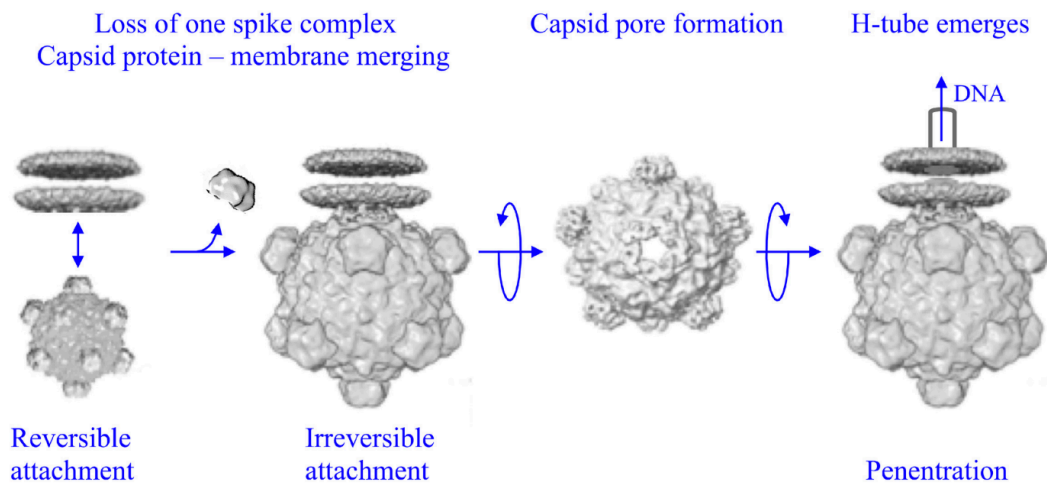


FIG 4.1 Early microvirus infection

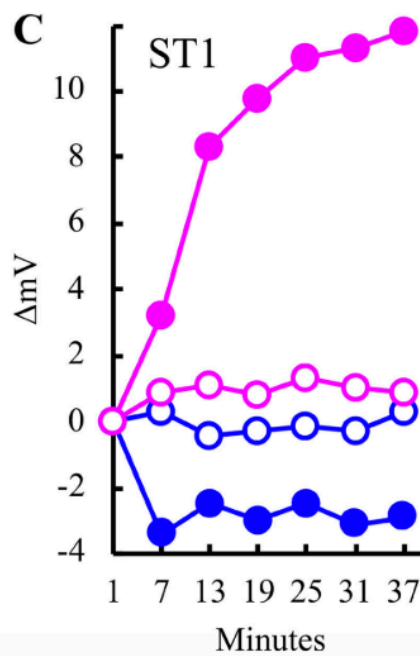
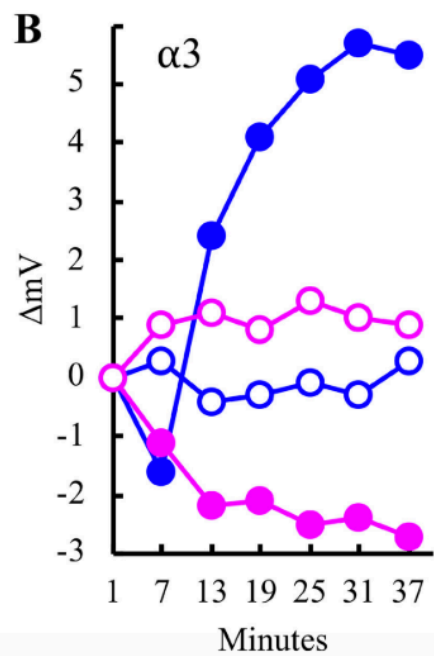
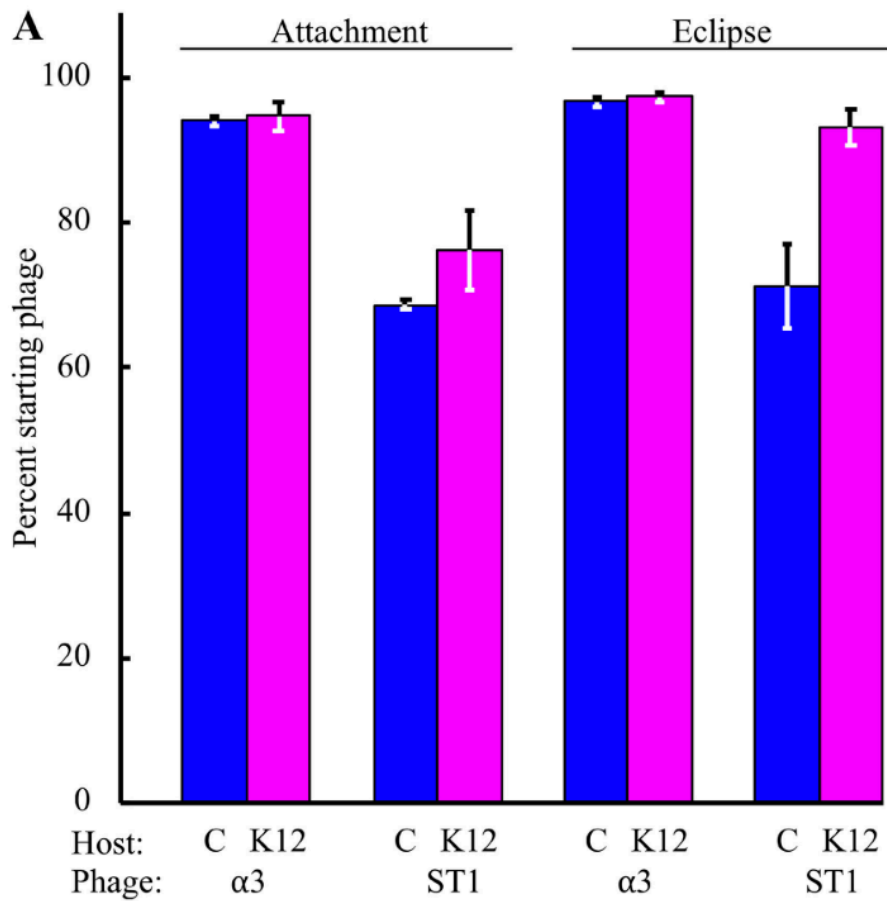


FIG 4.2 Attachment, eclipse and penetration as a function of host range

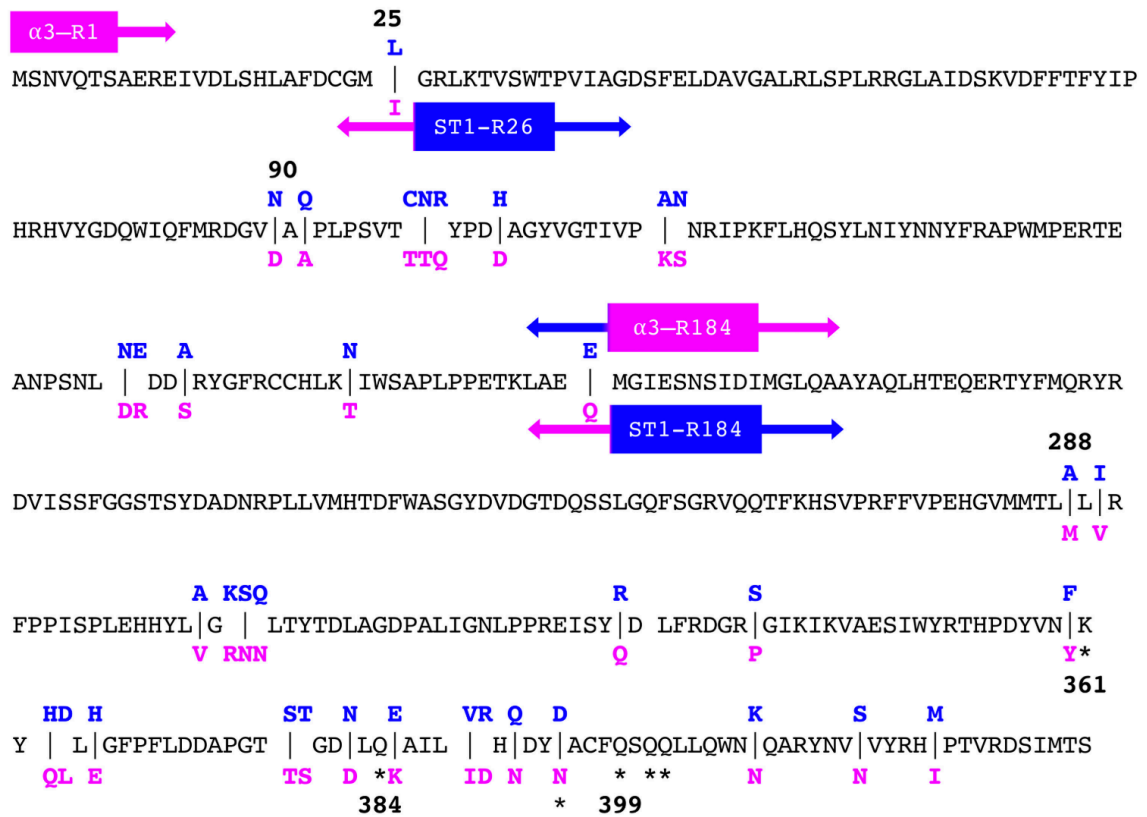


FIG 4.3 Amino acids sequences of the $\alpha 3$ and ST-1 coat proteins

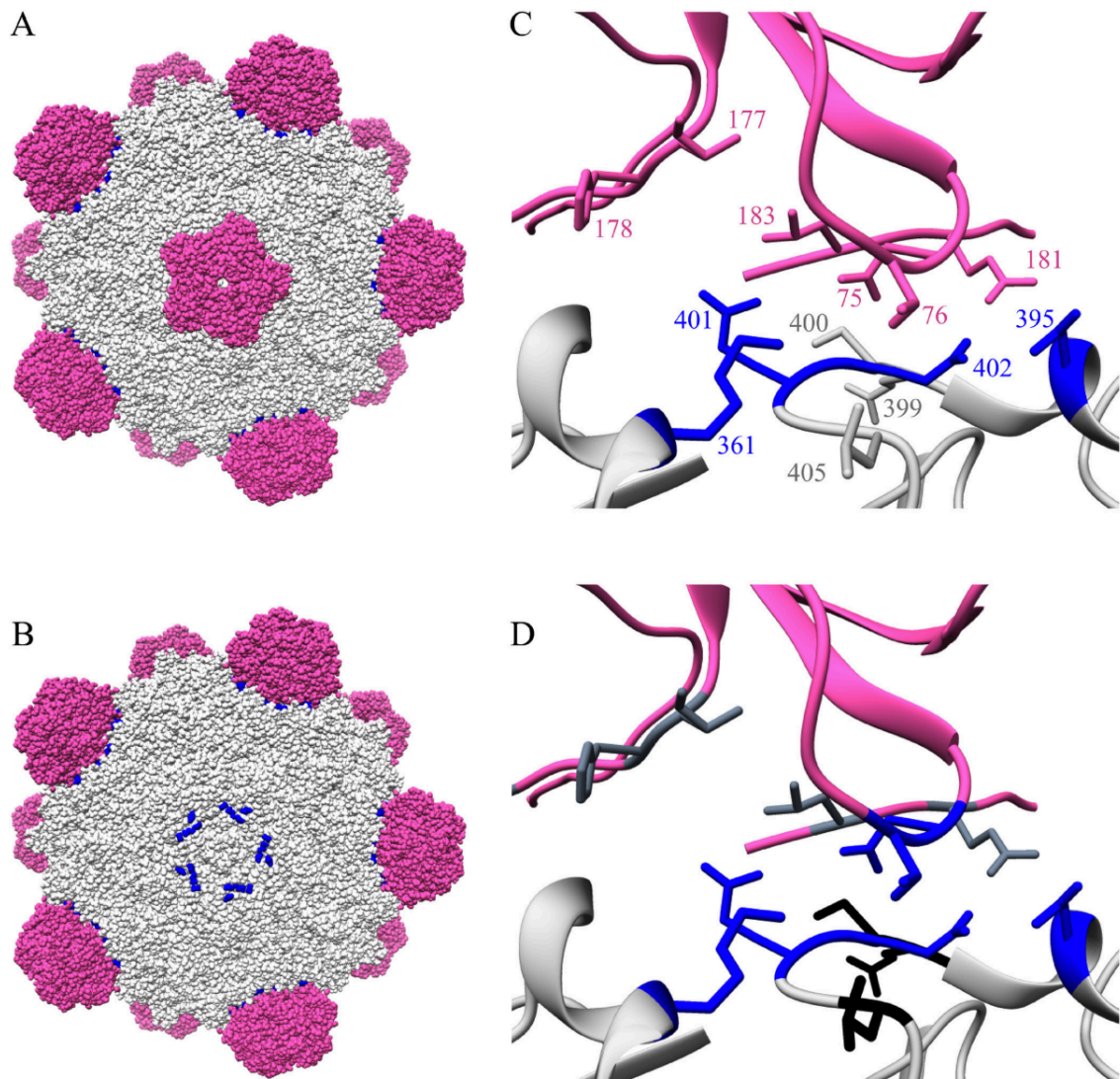


FIG 4.4 The location of PA substitutions within the $\alpha 3$ x-ray structure

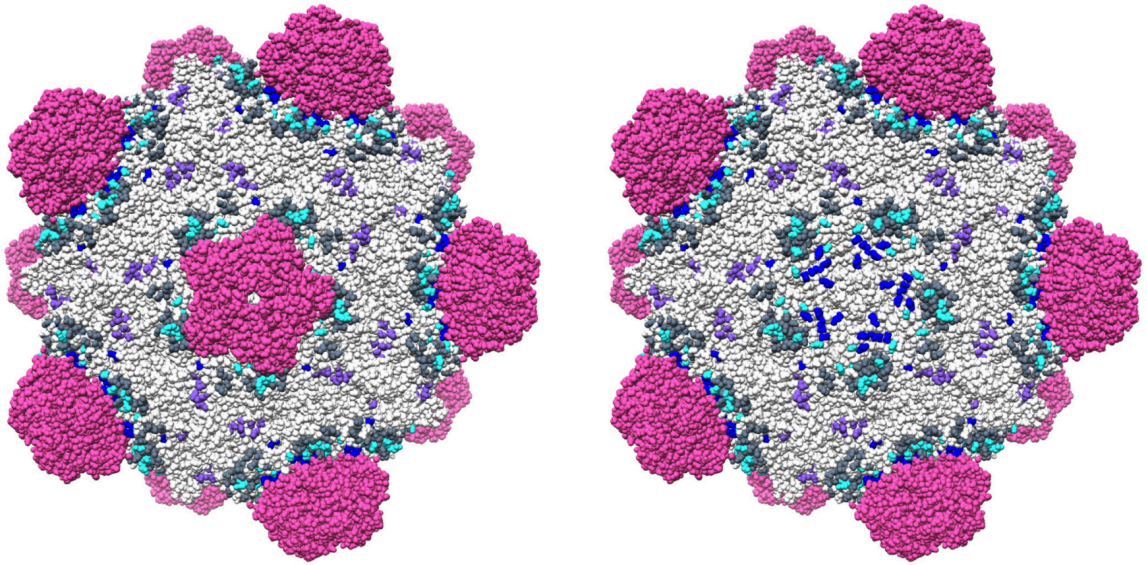


FIG 4.5 Structurally and genetically defined residues governing host range and extracellular virus-host interactions in ϕ X174 and α 3

CHAPTER 5

FUTURE DIRECTIONS

5.1 Is the unique vertex induced or preordained?

Many viruses eject their genetic material through a unique vertex. The vertex contains specialized proteins that participate in the ejection process. In tailed phages, a dodecameric portal structure occupies their procapsid's unique vertex (1, 2). The genome is packaged through the portal by the viral terminase, an enzymatic complex that couples ATP hydrolysis to genome packaging (3). The phage tail attaches to the portal once packaging is completed. Thus the genome is ejected through the portal structure to initiate an infection (4, 5).

Portals are not limited to phage systems. Herpesviruses, for example, also utilize these structures (6, 7). Their portals are structurally similar to those of phage, and they also package and eject their genomes through them (8, 9). During infection, the enveloped herpes virion fuses with the cytoplasmic or endocytic membrane, releasing the capsid into host cell's cytoplasm (10). The capsid is then trafficked to the nucleus. The portal docks with a nuclear pore and the viral genome is ejected into the nucleus (11–13). The unique vertex is preordained in all of the above systems. It is found in the procapsid and remains in place throughout the assembly process. However, some viruses appear to lack a preordained unique vertex.

Poliovirus, for example, appears to utilize a single vertex during genome delivery, yet all of the virion's vertices are identical. To initiate an infection, poliovirus first binds to a host cell's surface receptors, triggering its endocytic pathway (14, 15). The virus becomes internalized within an endosome where it undergoes structural changes, releasing its internal protein VP4 (16, 17). VP4, together with the VP1 capsid proteins at the open vertex, become membrane associated and form a channel, releasing the ssRNA genome into the host cell's cytoplasm (18–20). It appears that poliovirus does not need a unique vertex, as the viral proteins are contained within an endosome and its capsid contains 60 copies of both VP4 and VP1 (21). The proteins are icosahedrally ordered. They are present at every 5-fold symmetry axis; therefore, any vertex is capable of pore formation.

Φ X174, by contrast, carries twelve copies of its DNA piloting protein H. During an infection event, ten H proteins exit the capsid and form a cell wall spanning conduit. The cryo-electron microscopy (Cryo-EM) reconstructions of eclipsing ϕ X174 particles, both DNA-filled and empty, suggest that the H proteins appear to emerge from a single 5-fold axis of symmetry. (22). In the DNA-filled reconstruction, a single, unopened vertex is attached to the lipid bilayer (Figure 4.1A and D). There is a cylindrical region of lower density above the attached vertex. The region extends 110 Å into the virion and is 80 Å wide. This region likely contains the H protein oligomer as proteins are typically less dense than DNA. In the second structure, the contents of the virion have exited through a 30 Å wide opening at the attached vertex (Figure 4.1B and E). Thus, ϕ X174 also utilizes

a unique vertex. However, it is not known if the unique vertex is preordained during virion morphogenesis or induced at the infection site.

An H protein oligomer would likely be found at a preordained vertex, if one exists. However, the ϕ X174 procapsid is constructed from twelve identical, 12S*, assembly intermediates, each containing a monomeric H protein (Figure 4.2). The H proteins would need to congregate at a single vertex after procapsid assembly. Two procapsid structures were determined, a 26 Å resolution cryo-EM reconstruction and a 3.5 Å resolution X-ray crystal structure (23, 24). In both structures, under each 5-fold axis of symmetry, there is a region of protein-like density that has been attributed to H protein, but the density could not be confidently assigned. This region is surrounded by density belonging to the internal scaffolding protein. If this is correct, H appears to remain monomeric within the procapsid and the internal scaffolding protein may hold it in place.

H oligomerization could occur during genome packaging or at the subsequent infection site. During packaging, the internal scaffolding proteins are displaced by the DNA binding protein. H protein may be freed and allowed to congregate at a single vertex during this process. The structure of the ϕ X174 virion was determined to 3.5 Å resolution. Like the procapsid structures, electron density could not be unambiguously assigned to H proteins. Again, there is diffuse density under the 5-fold axes. It may be produced by H protein or the ssDNA genome, thus the status of a unique vertex is still ambiguous. Cryo-EM was also used to examine virions for any asymmetric features. Thousands of particles were examined and no asymmetry was detected. However,

simulated micrographs were produced of an H-tube containing ϕ X174 virion, i.e. the H-tube X-ray structure was placed inside the virion X-ray structure (Figure 5.3, row a). Increasing amounts of noise were added to the simulated micrographs. Nearly all structural details were washed out when this level of noise reached that of actual ϕ X174 virion micrographs.

A second approach was taken to detect asymmetry within ϕ X174 virions: bubblegram imaging. During electron microscopy, samples are bombarded with an electron beam. Repeated bombardment of biological samples causes radiolytic damage to the sample's proteins and nucleic acids, producing H_2 . Samples are embedded in vitreous ice in cryo-EM preparations. This traps the H_2 , producing a bubble that is visible in the resulting micrographs. For reasons that are not understood, the different biological components undergo radiolysis at different rates. The rate is also influenced by the component's local environment. For example, proteins embedded in DNA bubble faster than surface exposed proteins, while surface proteins bubble faster than DNA. Thus, this technique can be used to determine if a virion contains proteinaceous structures embedded within its packaged genome (25, 26). If the bubbles' locations are consistent, they can be used to generate an asymmetric reconstruction of the virion based on its inner features.

A bubblegram analysis was performed on the microvirus ST-1 to determine if an H protein core exists within the virion. Purified ST-1 virions were flash frozen on cryo-EM grids. The virions were repeatedly dosed with electrons and monitored for bubble formation. As can be seen in Figure 4, bubbles only formed within virions. Arrows

indicate unpackaged virus-like particles in panel 1 and 8. It appears that proteins, most likely protein H, are embedded within the ST-1 genome. However, the bubble locations were not consistent enough to guide image reconstruction. Thus, it is still unknown if the H proteins form a core within the virion and if so, where it is located.

A third approach could be designed; however, it relies on an unproven assumption. Many results suggest, but do not rigorously demonstrate, that a portion of H protrudes from the virion. Two studies have shown that H protein may participate in host attachment. In the first, his-tagged H was purified and tested for LPS binding specificity (27, 28). The protein only bound LPS purified from ϕ X174-susceptible host strains. This evidence falls short of compelling, as H protein evolved alongside its host's LPS. The protein may bind poorly to foreign LPS because it has been optimized to the host's LPS structure. In the second study, mutations conferring changes near H protein's N-terminus inhibited attachment (29). Again, this is not entirely compelling; mutant DNA binding proteins, which are completely internalized, can affect attachment kinetics (30). Thus, anything could possibly affect virion structure could affect attachment. Lastly, it was reported that monoclonal antibodies that bind to denatured H protein can cross-react with virions and procapsids. However, this data was only mentioned as a personal communication within another manuscript (23).

Each finding falls short of compelling when considered individually. Yet, the results tend to suggest that a portion of H protein may protrude from the virion. If this is true, then it may be possible to raise an antibody against or tag the exposed portion of H protein.

Once marked, cryo-EM could be used to visualize the location(s) of the exposed H-protein segment. If a single vertex is marked, then this would be a strong indication that a preordained unique vertex exists. The tag or Fab fragments could then be used to reveal unique vertex's structure after building an asymmetric or 5-fold averaged reconstruction of the virion. Alternatively, if all vertices were marked, efforts could be focused on understanding how ten H proteins relocate and oligomerize at a single vertex during the infection.

5.2 How does H stimulate synthesis of viral coat protein?

In chapter 2, infected cell lysates were run on SDS-PAGE gels and the viral coat protein band intensity was compared to a host protein band. In null-H infections lacking H complementation, the viral coat/host protein ratio was reduced when compared to wild-type or complemented null-H mutant infections (Figure 5.5A). This result suggests that *de novo* synthesis of H protein is required for efficient viral coat protein synthesis. It is not known if H protein affects synthesis of other viral proteins. Other viral protein bands cannot be sufficiently resolved when using SDS-PAGE. Western blotting with antibodies raised against viral proteins may answer this question.

The mechanism by which H stimulates protein synthesis is unknown. It could act on the level of genome replication, transcription, or translation. Previous work has investigated the effect of *de novo* H synthesis on double-stranded (ds) genome replication (31). In the study, cells resistant to viral induced lysis harboring an empty, non-expressing plasmid

were infected with wild-type ϕ X174 or a null-H mutant. The infections were chemically lysed after three hours and the plasmid and ds genome molecules purified. The purified molecules were run on an agarose gel and the genome/plasmid intensity ratio was determined. The null-H and wild-type infections had similar ratios, suggesting that de novo H synthesis has no effect on ds genome replication (Figure 5.5B). Thus, it appears that H is affecting a step downstream of DNA synthesis.

Φ X174 utilizes a relatively simple gene expression system. Unlike other phages with early and late gene expression programs, all of its genes are transcribed simultaneously. Transcription is controlled by three promoters and four inefficient terminators. The promoters are located upstream of genes A, B, and D, while the terminators are downstream of genes J, F, G, and H (Figure 5.6). The terminators are inefficient, and the polymerase has a 40 to 60% chance of continuing through the J, F, and G terminators and a 10% chance of continuing through the final terminator (32). This system appears to govern viral protein stoichiometry. For example, each procapsid contains 240 copies of the external scaffolding protein D. The gene encoding protein D is sandwiched between the promoters and terminators. Thus, every viral transcript contains the D message. By contrast, each procapsid contains twelve copies of protein H. An RNA polymerase must pass three terminators to produce an H containing message, thereby making it one of the rarest messages.

Viral transcription levels in the context of de novo H synthesis have not been thoroughly investigated. Protein H may be acting as a transcription factor or may be affecting

terminator efficiency. This hypothesis could be initially explored by determining transcript ratios. Lysis-resistant cells containing a plasmid encoding an inducible wild-type H gene and a constitutively expressed chloramphenicol acetyltransferase (CAT) gene will be infected with a null-H mutant. The infected culture will be split, pelletized, and each half resuspended in media containing a repressor or inducer. At timepoints, the infected cells will be collected, lysed, and their mRNA purified. cDNA will be produced from the RNA and used in qPCR reactions. Primers targeting viral gene B, viral gene F, viral gene H, or the CAT transcript will be used to determine the relative transcript amounts.

If protein H somehow modulates transcription, then there may be a difference in transcript ratios between the induced and repressed infections. For example, the ratio of viral B and F messages could be compared. Gene B is upstream of the terminators, while gene F lies downstream of a single terminator. If H is affecting terminator efficiency, then the F:B transcript ratio may be higher in induced infections. If a difference is found, the region of DNA interacting with protein H could possibly be identified with a bacterial one-hybrid system and/or an electrophoretic mobility shift assay. Alternatively, if H is acting as a transcriptional attenuator, the RNA target could be identified with RNA electrophoretic mobility shift assays or CLIP (crosslinking and immunoprecipitation of RNA–protein complexes). In the unlikely case that H has no effect on transcription and plays a role in translation, then a Co-IP analysis may identify its interaction partners.

5.3 The genome ejection model needs further testing and refinement

Chapter 3 focused on the H-tube's inner surface. The surface is lined primarily with glutamine side chains with the exception of one region near the tube's C-terminal opening. This region is conserved in other microvirus clades, suggesting it may play a role during genome delivery. The non-glutamine residues in this region were replaced with glutamine to explore the region's significance and the general role of glutamine residues. Three of the mutant H proteins conferred a cold-sensitive phenotype. The results of subsequent experiments suggested that the extra glutamine residues did not prevent channel formation, yet genome delivery was inhibited. The results were used to construct a model describing microvirus genome delivery mechanics. In this model, there are two primary forces acting on the genome while in transit: a force driving the genome into the cytoplasm and another opposing its movement.

The energy source driving genome transit is not definitively known. There are two competing models. The continuum mechanics model proposes that the required energy could be stored within the packaged genome. Most dsDNA phage genomes are packaged with an ATP hydrolyzing motor. Although each motor has slightly different characteristics, most appear to package the dsDNA genomes very tightly, usually to a density of approximately 500 mg/mL. DNA strands, which repel each other, are forced into close proximity within the capsid. This repulsive force is thought to drive the ejection process. Thus, a portion of the chemical energy used to power packaging becomes stored within the compressed genome. Although data collected from *in vitro* genome ejection experiments supports this model, there is debate as to whether this energy powers genome delivery *in vivo* (33, 34).

In the hydrodynamic model, by contrast, the energy source may exist at the infection site (35). During growth, bacteria must maintain turgor pressure, resulting in an osmotic pressure imbalance between the cell and its environment. Water will be pulled into the cytoplasm if the cell wall is punctured. This osmotic imbalance could provide the energy required to complete genome delivery. Like the continuum mechanics model, the process begins during genome packaging. The packaging motor performs reverse osmosis: water is stripped off the DNA and driven out of the water permeable capsid. However, instead of interhelical repulsion forces driving genome transport, osmosis drives genome transport. When a phage forms a channel across its host's cell wall, water will flow back into the capsid and through the channel, dragging the genome into the host.

Either energy source can be incorporated into our microvirus genome delivery model. However, in our model, there is a force opposing the genome's movement. This may counter the force driving the genome into the host, thereby slowing and regulating its transit. A regulated release may prevent genome tangling or tube failure. In our model, the opposing force is provided by the amide and guanidinium containing side chains lining the H-tube's inner surface. They can form hydrogen bonds with nucleotides; thus, H-bond formation and separation may create friction on the genome as it passes.

Multiple aspects of this model have not been fully tested. In the current work, additional glutamine side chains were added near the tube's C-terminal opening. The data suggests that these mutant side chains trap genomes within the tube at low temperatures. If the

model is correct, then the additional glutamine residues are increasing the frictional force acting on the genome during its passage. If the force driving the genome into the cell is reduced at lower temperatures, then the increased frictional force may completely counter it, trapping the genome mid-transit. Two other approaches can be taken to further test and refine the model: the number of inward facing glutamines can be reduced and/or the size of the genome can be altered.

The first approach is already underway. The glutamine residues near the tube's narrowest point have been targeted in a preliminary genetic analysis. Site directed mutagenesis was used to separately randomize the glutamine codons at sites Q191 and Q195 and elsewhere. The resulting mutants were screened for temperature dependent phenotypes and their H genes sequenced. Several mutants have been isolated at sites Q191 and Q195. Although some mutants have cold-sensitive phenotypes, the majority appear to struggle at high temperatures. Mutation of the other inward-facing glutamine sites yielded only wild-type phenotypes. Preliminary results show that particles carrying the mutant H trigger K^+ efflux at the restrictive temperature (Figure 5.9). Thus, it can be assumed that the virions are adsorbing to the host and forming channels. It is now a matter of determining if the mutant genomes reach the host's inner membrane.

The effects of genome size can be tested in the second approach. If the energy used during genome delivery is stored in the packaged genome, then changing the genome's size will alter the amount of stored energy. *In vitro* experiments have shown that the amount of packaged DNA has an effect on capsid pressure in dsDNA phage systems

(34). Bacteriophage λ mutants with reduced genome sizes were tested in an *in vitro* ejection assay. The phage was mixed with its purified receptor in solutions of varying osmotic pressure. Ejection is inhibited if the solution's osmotic pressure is high enough, allowing calculation of the ejection force. Wild-type λ ejected its DNA with a force of 13.8 pN, while reducing the genome size by 22% reduced the ejection force by 57%. An *in vivo* experiment could be designed using the ϕ X174 system. Genome size can be reduced by 18-26% or increased by 2-6% without abolishing particle infectivity (36, 37). If capsid pressure is playing a role in the ϕ X174 system then genome-length altered viruses may have more extreme temperature dependent phenotypes. Since pressure is dependent on temperature, virions carrying smaller genomes would be less pressurized at lower temperatures. This would reduce the force driving the genome into the cytoplasm, and if the microvirus genome ejection model is correct, the frictional force exerted by the glutamine residues may trap the genome while in transit. By contrast, increasing the genome size would increase the capsid pressure. This may overwhelm the frictional force at higher temperatures, which could disrupt the tube structure.

5.4 Does our model apply to other viral systems?

Perhaps the most striking feature of the ϕ X174 genome delivery system are the H-tube's inward facing amide and guanidinium containing side chains. These residues and their proposed function are the crux of the microvirus genome ejection model. Although the model needs further confirmation, refinement, and adjustment, there are two similar protein structures that suggest the findings may be applicable to other systems: the feline calicivirus and bacteriophage P22 portal proteins.

Feline calicivirus is a ssRNA virus. Cryo-EM was used to create a 3.5 Å reconstruction of a receptor bound feline calicivirus particle (38). Calicivirus enters host cells by hijacking their endocytic pathway. Once in an endosome, twelve copies of the minor capsid protein VP2 appear to emerge from a single 3-fold axis. The proteins form a dodecameric α -helical tube structure that presumably penetrates the endocytic membrane (Figure 5.10). Like the H-tube, the VP2-tube is also lined with D, E, K, N, Q, and R side chains and has a minimum internal diameter of 17 Å, wide enough for ssRNA passage. The structure is much shorter than the H-tube, however the tube must only penetrate an endocytic membrane and not a bacterial cell wall.

The structure of the dsDNA phage P22 portal protein was recently refined to 7.0 Å resolution (2, 39, 40). The portal also features a dodecameric α -helical tube that is approximately 34 Å wide and 140 Å long (Figure 5.11B). This tube is found within the P22 capsid, and the genome must move through this structure during packaging and during penetration. The resolution of the structure is not high enough to resolve the tube's inward facing side chains. However, the tube's primary sequences are 30% identical to that of protein H. Moreover, a sequence alignment shows that the H tube's inward facing K, N, Q, and R residues line up reasonably to those of the P22 portal tube (Figure 5.11A). If these residues are also inward facing, then they may be generating a frictional force on a dsDNA genome.

Although there are two similar structures, the characteristics of the H-tube do not appear to be universal. The dsDNA phage T4 uses a contractile tail to puncture the host cell wall. During contraction, a rigid, tube contained within the tail is driven through the host cell wall. The tube is composed of multiple copies of gp19, arranged into a stack of hexameric rings (Figure 5.12). A 3.4 Å cryo-EM reconstruction was generated (41). Unlike the tubes described above, the T4 tube is not α -helical. Gp19 is composed primarily of β -sheets. The tube's inner diameter is 35 Å and its inner surface is lined primarily with D and E side chains, making the surface electronegative. This may repel the negatively charged phosphate groups in the genome's backbone. If this mechanism is correct, then friction may not have a role in T4 genome delivery or it may be provided elsewhere.

5.5: Φ X174 host range and attachment

In chapter 4, the factors dictating microvirus host range were defined. Two viruses, α 3 and ST-1, respectively infect *E. coli* C and *E. coli* K12. Their structural proteins are 90% identical. Thus, it seemed possible to isolate mutants with altered host ranges, e.g. an α 3 mutant capable of infecting *E. coli* K12. After developing new viral stock preparation protocols, numerous α 3 mutants were isolated that could form plaques on both *E. coli* C and K12. The mutants all had single point mutations conferring changes in the coat protein at the coat-spike interface, suggesting that this interface may determine the virus's host range. ST-1 mutants capable of infecting K12 were also isolated, although

this only occurred after large portions of the ST-1 coat gene recombined with a cloned $\alpha 3$ coat gene.

$\Phi X174$ was also included in the study. It infects *E. coli* C and its coat protein is 72% identical to $\alpha 3$'s coat protein. The extracellular steps of the $\phi X174$ infection cycle were also analyzed to determine if the virus adsorbs to K12. Unlike ST-1 and $\alpha 3$, $\phi X174$ attached poorly to K12. Eclipse assays were also performed on the fraction that attached, but the results were highly variable. Unlike $\alpha 3$, no $\phi X174$ host range expansion mutants were isolated from populations generated in low MOI environments. This suggests that a number of mutational changes are likely required for $\phi X174$ to productively infect K12.

In order to establish a productive infection, the virion must first adsorb to the host, move its genome into the cytoplasm, and interact with host replication machinery. It may be possible to generate a $\phi X174$ mutant capable of efficient attachment, however there is no guarantee the virus is compatible with K12's DNA replication machinery. This question could be addressed by transfecting purified $\phi X174$ ssDNA into K12. Any produced progeny could be detected by lysing the transfected K12 culture and titering on C122.

If progeny $\phi X174$ can be produced in K12, then it may only be a matter of isolating a mutant capable of adsorption. It appears that a number of mutational steps are required before $\phi X174$ can efficiently attach to and eclipse on K12. This makes isolation of a mutant capable of infecting K12 from a low M.O.I. environment highly unlikely; thus, it may be necessary to first select for mutants capable of efficient K12 attachment. Isolation

of a mutant that attaches may reduce the number of mutational steps required to infect K12, which may make subsequent selections more productive.

If the temperature is below 16°C, φX174 can attach to cells, but cannot initiate the penetration process. This characteristic can be used to select for mutants capable of improved K12 attachment by incubating the virus with K12 cells at 15°C. The cells and any attached virions can be pelleted, leaving unattached particles in the supernatant. Since attachment is Ca²⁺ dependent, the pellet can be resuspended in an EDTA-containing solution to release attached phage. The collected virions can be passaged through *E. coli* C to increase their numbers and allow more mutations to accumulate. This process can be repeated until a mutant capable of efficient K12 attachment is isolated. If this reduces the number of mutational steps required to infect K12, then selections for a mutant capable of plaque formation may be successful.

5.6 References

1. Sun L, Zhang X, Gao S, Rao PA, Padilla-Sanchez V, Chen Z, Sun S, Xiang Y, Subramaniam S, Rao VB, Rossmann MG. 2015. Cryo-EM structure of the bacteriophage T4 portal protein assembly at near-atomic resolution. *Nat Commun* 6:1–11.
2. Olia AS, Prevelige PE, Johnson JE, Cingolani G. 2011. Three-dimensional structure of a viral genome-delivery portal vertex. *Nat Struct Mol Biol* 18:597–603.
3. Casjens SR. 2011. The DNA-packaging nanomotor of tailed bacteriophages. *Nat Rev Microbiol* 9:647–657.
4. Rajagopala S V, Casjens S, Uetz P. 2011. The protein interaction map of bacteriophage lambda. *BMC Microbiol* 11:213.
5. Kikuchi Y, King J. 1975. Assembly of the tail of bacteriophage T4. *J Supramol Struct* 3:24–38.
6. Rochat RH, Liu X, Murata K, Nagayama K, Rixon FJ, Chiu W. 2011. Seeing the Portal in Herpes Simplex Virus Type 1 B Capsids. *J Virol* 85:1871–1874.
7. Bauer DW, Li D, Huffman J, Homa FL, Wilson K, Leavitt JC, Casjens SR, Baines J, Evilevitch A. 2015. Exploring the Balance between DNA Pressure and Capsid Stability in Herpesviruses and Phages. *J Virol* 89:9288–9298.
8. Newcomb WW, Juhas RM, Thomsen DR, Homa FL, Burch AD, Weller SK, Brown JC. 2001. The UL6 Gene Product Forms the Portal for Entry of DNA into the Herpes Simplex Virus Capsid. *J Virol* 75:10923–10932.
9. Chang JT, Schmid MF, Rixon FJ, Chiu W. 2007. Electron Cryotomography

- Reveals the Portal in the Herpesvirus Capsid. *J Virol* 81:2065–2068.
10. Connolly SA, Jackson JO, Jardetzky TS, Longnecker R. 2011. Fusing structure and function: a structural view of the herpesvirus entry machinery. *Nat Rev Microbiol* 9:369–381.
 11. Ojala PM, Sodeik B, Ebersold MW, Kutay U, Helenius A. 2000. Herpes Simplex Virus Type 1 Entry into Host Cells: Reconstitution of Capsid Binding and Uncoating at the Nuclear Pore Complex In Vitro. *Mol Cell Biol* 20:4922–4931.
 12. Padeloup D, Blondel D, Isidro AL, Rixon FJ. 2009. Herpesvirus Capsid Association with the Nuclear Pore Complex and Viral DNA Release Involve the Nucleoporin CAN/Nup214 and the Capsid Protein pUL25. *J Virol* 83:6610–6623.
 13. Shahin V, Hafezi W, Oberleithner H, Ludwig Y, Windoffer B, Schillers H, Kuhn JE. 2006. The genome of HSV-1 translocates through the nuclear pore as a condensed rod-like structure. *J Cell Sci* 119:23–30.
 14. Belnap DM, McDermott BM, Filman DJ, Cheng N, Trus BL, Zuccola HJ, Racaniello VR, Hogle JM, Steven a C. 2000. Three-dimensional structure of poliovirus receptor bound to poliovirus. *Proc Natl Acad Sci* 97:73–78.
 15. Brandenburg B, Lee LY, Lakadamyali M, Rust MJ, Zhuang X, Hogle JM. 2007. Imaging Poliovirus Entry in Live Cells. *PLoS Biol* 5:e183.
 16. Belnap DM, Filman DJ, Trus BL, Cheng N, Booy FP, Conway JF, Curry S, Hiremath CN, Tsang SK, Steven AC, Hogle JM. 2000. Molecular Tectonic Model of Virus Structural Transitions: the Putative Cell Entry States of Poliovirus. *J Virol* 74:1342–1354.
 17. Strauss M, Schotte L, Karunatilaka KS, Filman DJ, Hogle JM. 2017. Cryo-electron

- Microscopy Structures of Expanded Poliovirus with VHHs Sample the Conformational Repertoire of the Expanded State. *J Virol* 91:1–22.
18. Gropelli E, Levy HC, Sun E, Strauss M, Nicol C, Gold S, Zhuang X, Tuthill TJ, Hogle JM, Rowlands DJ. 2017. Picornavirus RNA is protected from cleavage by ribonuclease during virion uncoating and transfer across cellular and model membranes. *PLOS Pathog* 13:e1006197.
 19. Danthi P, Tosteson M, Li Q -h., Chow M. 2003. Genome Delivery and Ion Channel Properties Are Altered in VP4 Mutants of Poliovirus. *J Virol* 77:5266–5274.
 20. Fricks CE, Hogle JM. 1990. Cell-induced conformational change in poliovirus: externalization of the amino terminus of VP1 is responsible for liposome binding. *J Virol* 64:1934–45.
 21. Hogle J, Chow M, Filman D. 1985. Three-dimensional structure of poliovirus at 2.9 Å resolution. *Science* (80-) 229:1358–1365.
 22. Sun Y, Roznowski AP, Tokuda JM, Klose T, Mauney A, Pollack L, Fane BA, Rossmann MG. 2017. Structural changes of tailless bacteriophage Φ X174 during penetration of bacterial cell walls. *Proc Natl Acad Sci* 114:13708–13713.
 23. Ilag LL, Olson NH, Dokland T, Music CL, Cheng RH, Bowen Z, McKenna R, Rossmann MG, Baker TS, Incardona NL. 1995. DNA packaging intermediates of bacteriophage ϕ X174. *Structure* 3:353–363.
 24. Dokland T, Bernal RA, Burch A, Pletnev S, Fane BA, Rossmann MG. 1999. The role of scaffolding proteins in the assembly of the small, single-stranded DNA virus ϕ X174. *J Mol Biol* 288:595–608.

25. Cheng N, Wu W, Watts NR, Steven AC. 2014. Exploiting radiation damage to map proteins in nucleoprotein complexes: The internal structure of bacteriophage T7. *J Struct Biol* 185:250–256.
26. Cheng N, Wu W, Steven AC, Thomas J, Black L. 2012. Bubblegrams reveal the inner body of bacteriophage phiKZ. *Microsc Microanal* 18:112–113.
27. Suzuki R, Inagaki M, Karita S, Kawaura T, Kato M, Nishikawa S, Kashimura N, Morita J. 1999. Specific interaction of fused H protein of bacteriophage ϕ X174 with receptor lipopolysaccharides. *Virus Res* 60:95–99.
28. Nishikawa S. 2000. Characterization of the Binding of spike H Protein of Bacteriophage phiX174 with Receptor Lipopolysaccharides 127:577–583.
29. Young LN, Hockenberry AM, Fane BA. 2014. Mutations in the N Terminus of the Φ X174 DNA Pilot Protein H Confer Defects in both Assembly and Host Cell Attachment. *J Virol* 88:1787–1794.
30. Bernal RA, Hafenstein S, Esmeralda R, Fane BA, Rossmann MG. 2004. The ϕ X174 protein J mediates DNA packaging and viral attachment to host cells. *J Mol Biol* 337:1109–1122.
31. Ruboyianes M V, Chen M, Dubrava MS, Cherwa JE, Fane BA. 2009. The Expression of N-Terminal Deletion DNA Pilot Proteins Inhibits the Early Stages of Φ X174 Replication. *J Virol* 83:9952–9956.
32. Hayashi M, Aoyama A, Richardson DL, Hayashi MN. 1988. Biology of the Bacteriophage ϕ X174, p. 1–71. *In* Calendar, R (ed.), *The Bacteriophages Volume 2*. Plenum Publishing Corporation, New York.
33. Molineux IJ, Panja D. 2013. Popping the cork: mechanisms of phage genome

- ejection. *Nat Rev Microbiol* 11:194–204.
34. Grayson P, Evilevitch A, Inamdar MM, Purohit PK, Gelbart WM, Knobler CM, Phillips R. 2006. The effect of genome length on ejection forces in bacteriophage lambda. *Virology* 348:430–436.
 35. Lemay SG, Panja D, Molineux IJ. 2013. Role of osmotic and hydrostatic pressures in bacteriophage genome ejection. *Phys Rev E* 87:022714.
 36. Aoyama A, Hayashi M. 1985. Effects of genome size on bacteriophage Φ X174 DNA packaging in vitro. *J Biol Chem* 260:11033–11038.
 37. Russell PW, Muller UR. 1984. Construction of Bacteriophage ϕ X174 Mutants with Maximum Genome Sizes. *J Virol* 52:822–827.
 38. Conley MJ, McElwee M, Azmi L, Gabrielsen M, Byron O, Goodfellow IG, Bhella D. 2019. Calicivirus VP2 forms a portal-like assembly following receptor engagement. *Nature* 565:377–381.
 39. Sun L, Young LN, Zhang X, Boudko SP, Fokine A, Zbornik E, Roznowski AP, Molineux IJ, Rossmann MG, Fane BA. 2014. Icosahedral bacteriophage Φ X174 forms a tail for DNA transport during infection. *Nature* 505:432–435.
 40. Lokareddy RK, Sankhala RS, Roy A, Afonine P V., Motwani T, Teschke CM, Parent KN, Cingolani G. 2017. Portal protein functions akin to a DNA-sensor that couples genome-packaging to icosahedral capsid maturation. *Nat Commun* 8:14310.
 41. Zheng W, Wang F, Taylor NMI, Guerrero-Ferreira RC, Leiman PG, Egelman EH. 2017. Refined Cryo-EM Structure of the T4 Tail Tube: Exploring the Lowest Dose Limit. *Structure* 25:1436–1441.e2.

5.7 Figure Legends

FIGURE LEGENDS

FIG 5.1 Cryo-EM reconstructions of eclipsing ϕ X174. A and D) Unopened particle. B and E) Opened, empty particle. C) Superposition of panels A and B. Panels A, B, and C are cross sections along the 2-fold symmetry axis. Panels D and E show the reconstructions from their attached 5-fold axis.

FIG 5.2 Φ X174 Morphogenetic pathway.

FIG 5.3 Simulation of cryo-electron micrographs of WX174 containing one H tube. (a-f) Each column (1–8) shows a different orientation of the virus. Each row shows progressively more noise. The top row has no noise and clearly shows the fivefold vertices of the virus and the buried H tube (sideways in column 1 and top view in column 5). (g) Micrographs of the actual virus. All evidence of the five-fold spikes has been lost in row f. Similarly, there is no evidence of the spikes in the actual micrographs shown in row g. Thus, the micrographs give no hint of whether there is an H tube or partly assembled H tube in the virus.

FIG 5.4 ST-1 Bubblegram analysis. Micrograph images are numbered with their exposure number. For example, the upper right micrograph depicts the sample's 14th exposure to the electron beam, thus it is labeled "14." Empty particles are marked with

white arrows in micrographs 1 and 22. A single particle has been circled to illustrate bubble development.

FIG 5.5 A) Viral protein levels in am(H) mutant-infected cells with and without Δ H gene expression. SDS-PAGE analysis of viral coat protein levels in uninfected (UI), wild-type-infected (WT), and null-H (am(H)) mutant-infected cells expressing the Δ H gene constructs. B) Agarose gel analysis showing relative recovery of plasmid and viral RF DNAs from cells. The white space between lanes indicates removal of irrelevant lanes from the image.

FIG 5.6 Linear depiction of the ϕ X174 genetic map. Promoters and terminators are depicted with “P’s” and “T’s,” respectively. The subscript letter demarks the location and name of the promoter or terminator. Grey lines represent transcripts. The width of the line reflects the gene transcript’s relative abundance in an infected cell. Transcripts from PA are unstable, which is indicated with a series of dots.

FIG 5.7 SDS-PAGE analysis of particles produced in am(H) mutant-infected cells expressing cloned wild-type H (WT H), Δ 7-3, Δ 7-10, Δ 14-2&3, Δ 14-3&4, Δ 14-9&10, and Δ 14-10&1 genes or non-expressing cells (NE).

FIG 5.8 Potassium efflux curves from cells infected with Q195X mutants at 42°C. Efflux values are reported as the increase in millivolts after the initial millivolt reading. More positive values indicate more extracellular K^+ is present.

FIG 5.9 Ribbon depiction of the calicivirus VP2 structure. Four VP2 monomers have been colored for clarity, the remaining are gray. Inward facing residues are shown as sticks. A) View from the tube's N-terminal opening, which is outside the virus particle. B) Cross-section of the tube. Six VP2 monomers have been removed to show the tube's interior. PDB ID: 6GSI

FIG 5.10 A) Alignment of the phiX174 H protein to the P22 portal protein (30% identical residues, 40% similar residues). Residues highlighted in green are both conserved and inward facing in the phiX174 structure.

FIG 5.11 Ribbon depiction of the phage T4 gp19 structure. A single gp19 monomer has been colored for clarity, the remaining are gray. Inward facing residues are shown as sticks. A) Cross-section of the tube. B) View down the tube's central axis. PDB ID: 5W5F

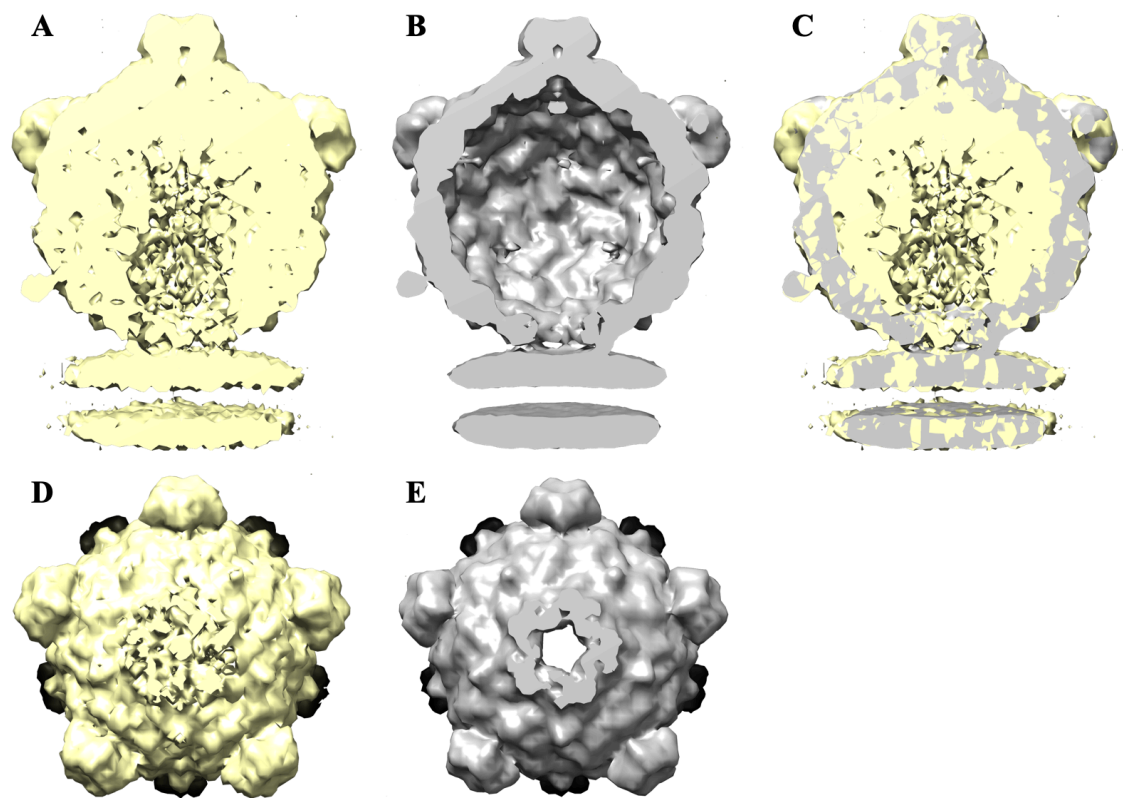


FIG 5.1 Cryo-EM reconstructions of eclipsing ϕ X174

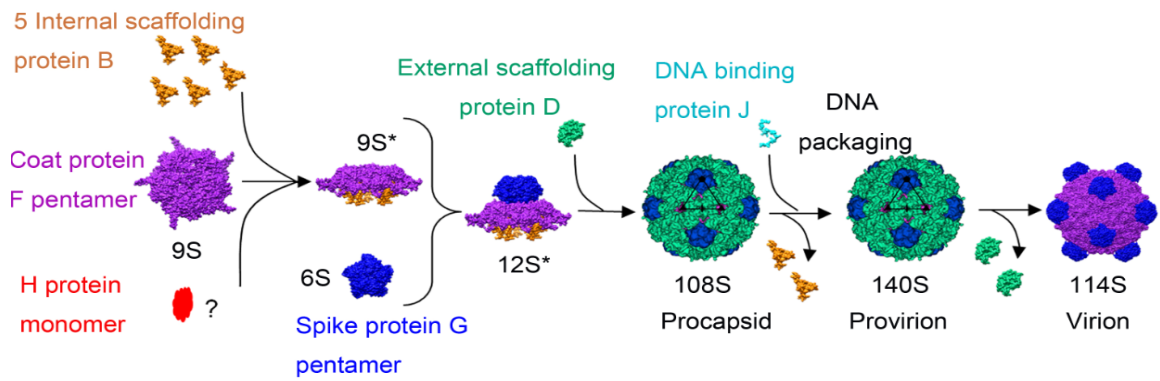


FIG 5.2 Φ X174 Morphogenetic pathway

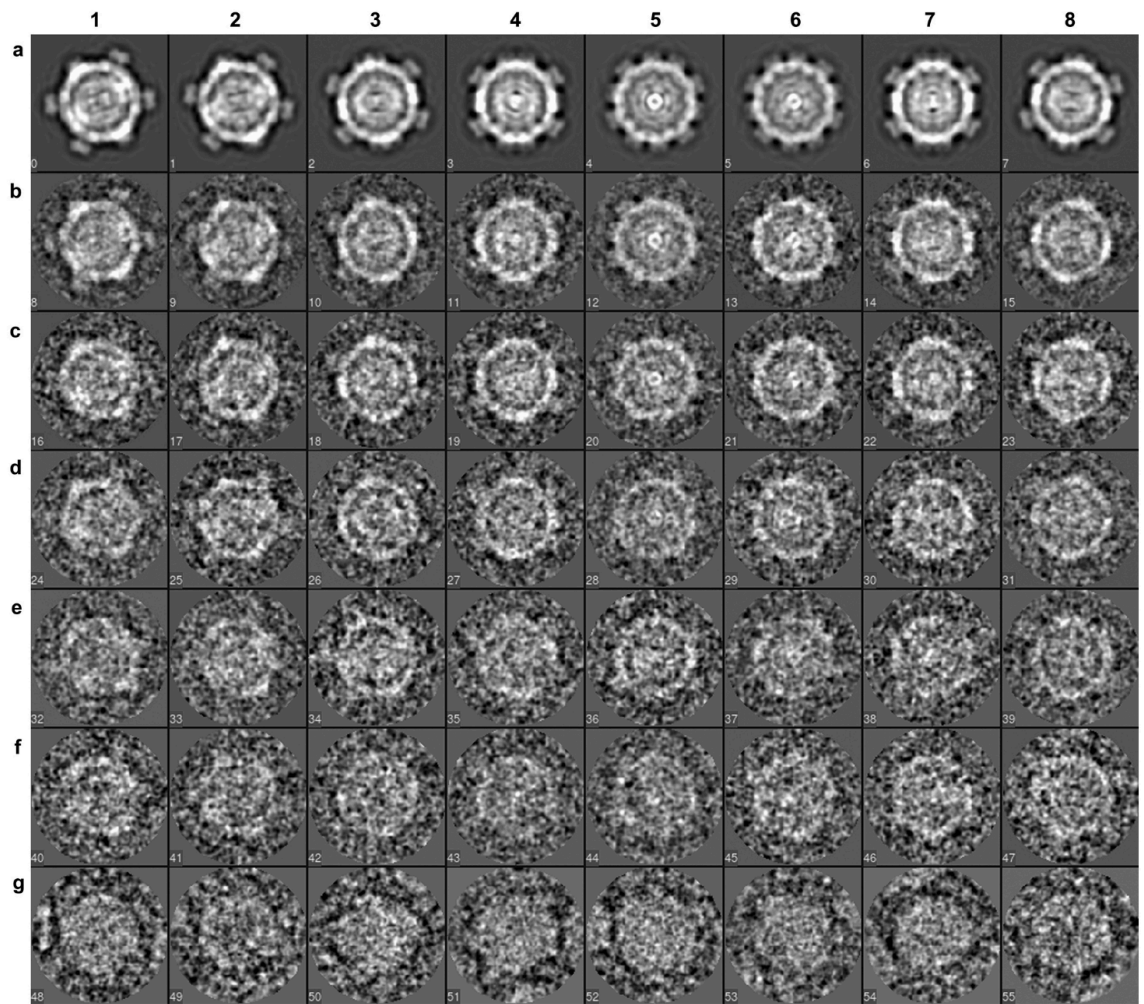


FIG 5.3 Simulation of cryo-electron micrographs

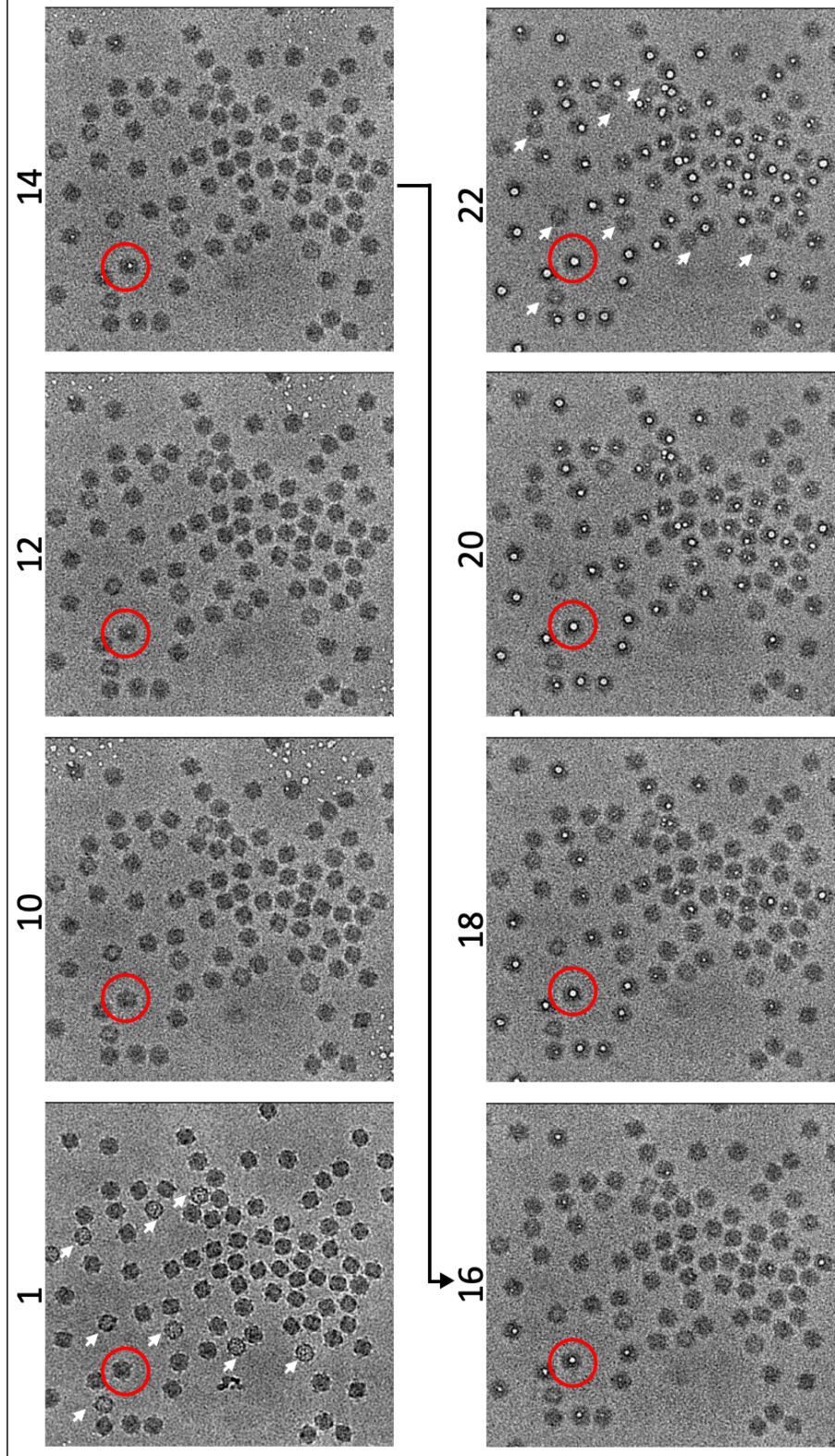


FIG 5.4 ST-1 Bubblegram analysis

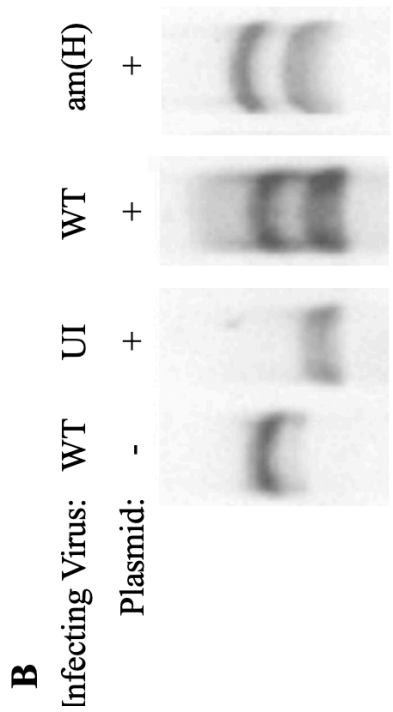
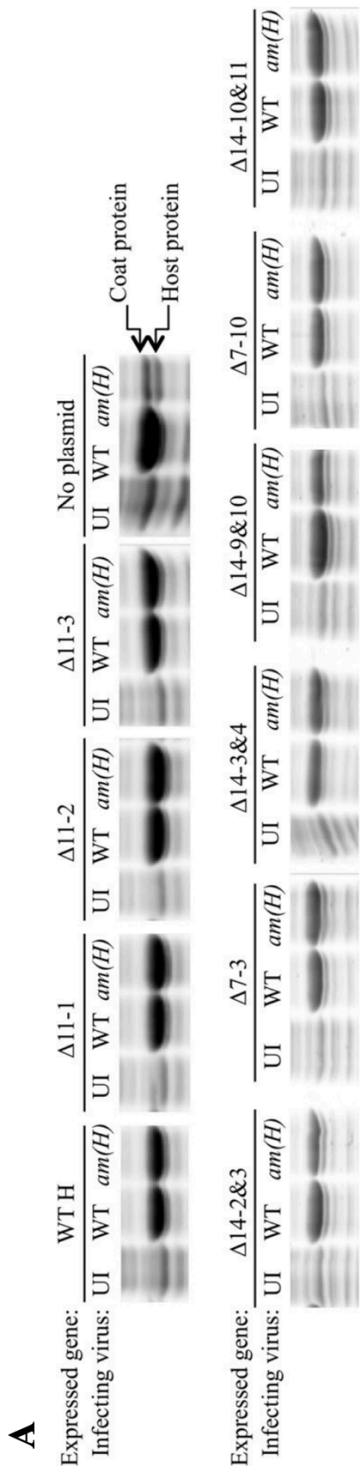


FIG 5.5 Viral protein and RF levels in wild-type and *am(H)* infected cells

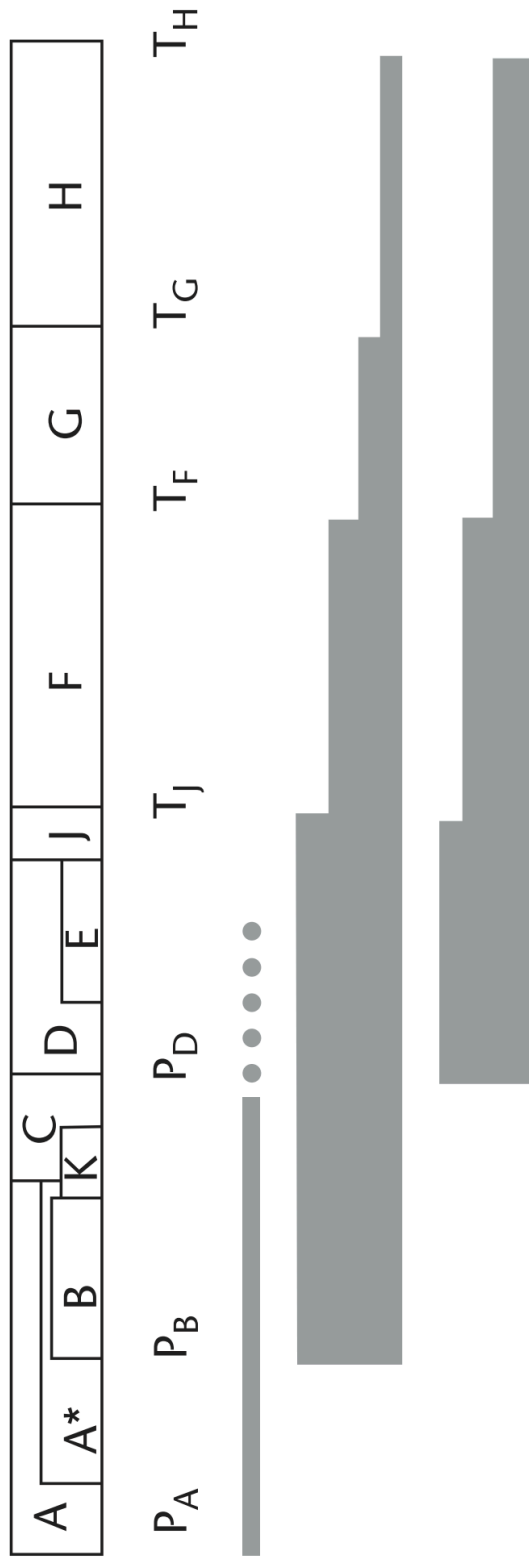


FIG 5.6 Linear depiction of the ϕ X174 genetic map

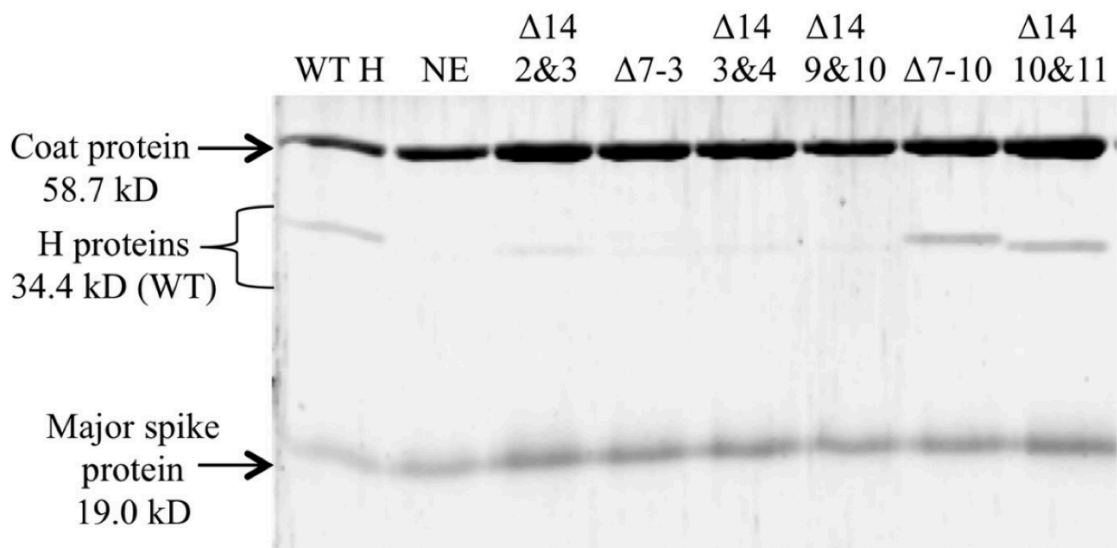


FIG 5.7 SDS-PAGE analysis of particles produced in am(H) mutant-infected cells expressing cloned H genes

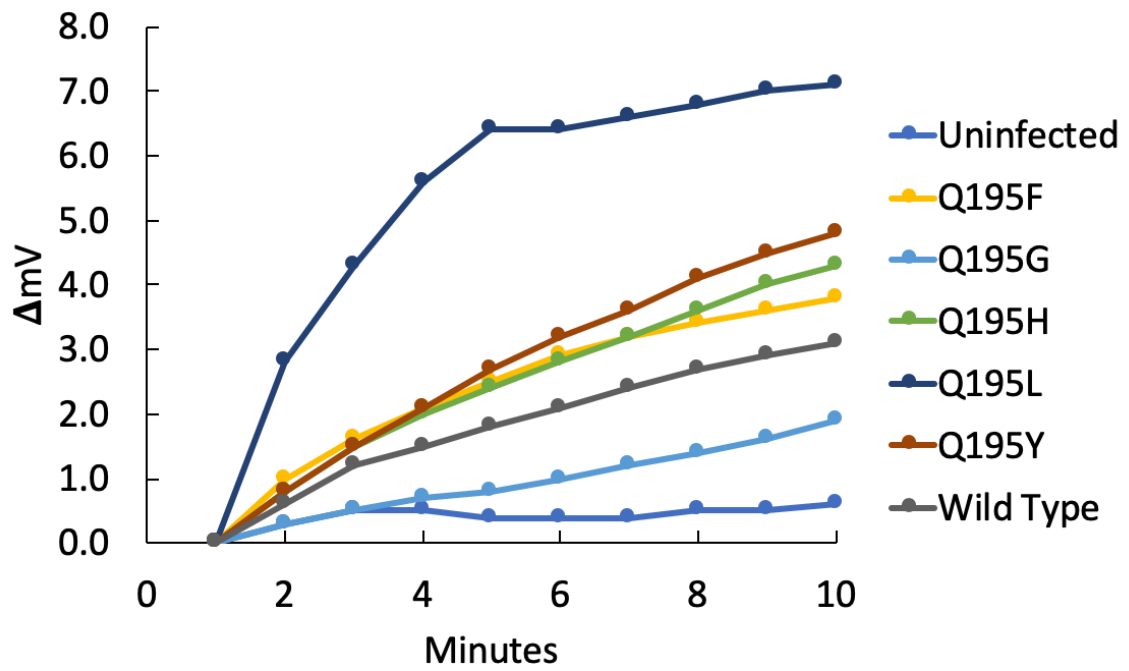


FIG 5.8 Potassium efflux curves from cells infected with Q195X mutants

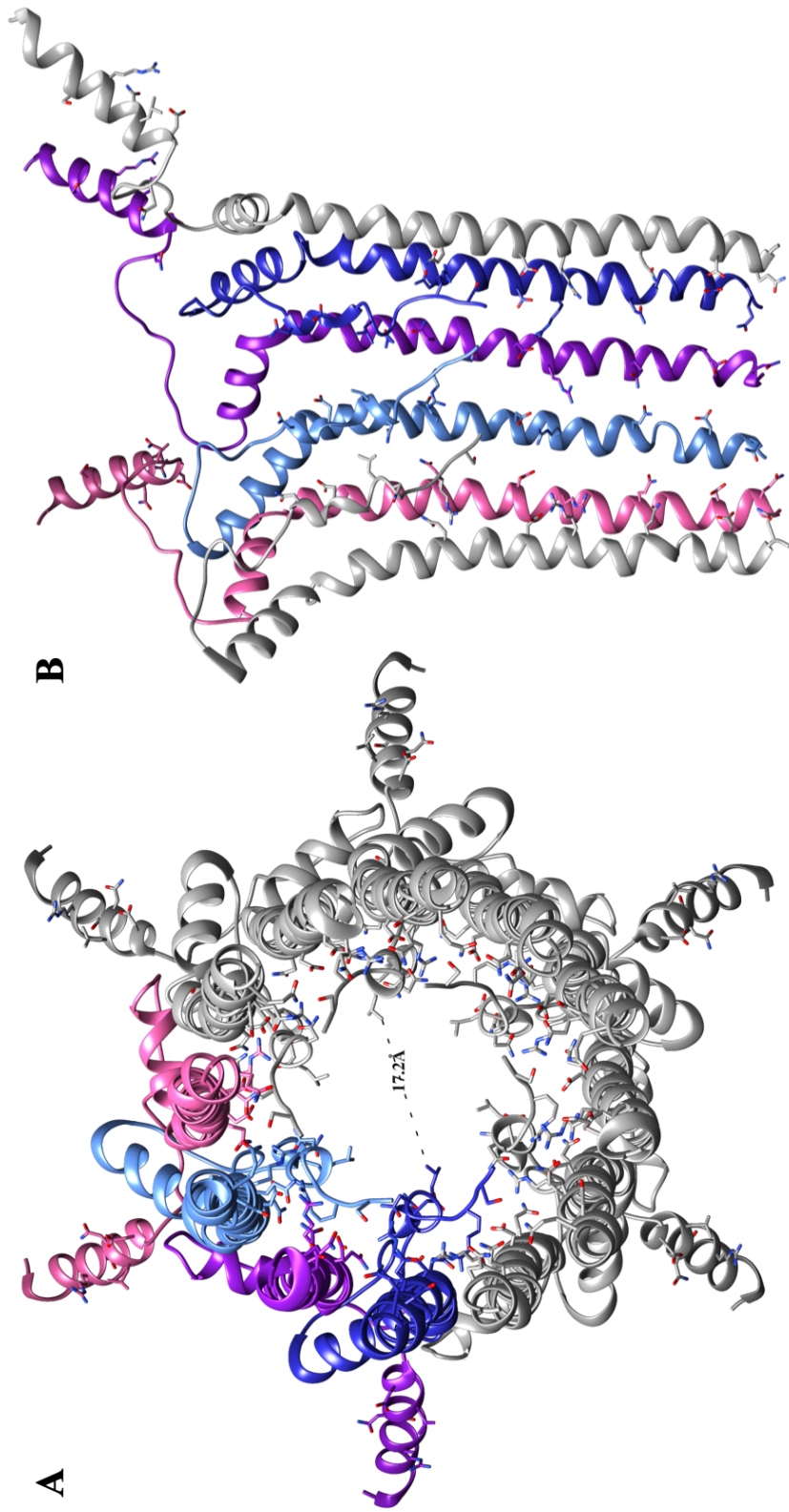


FIG 5.9 Ribbon depiction of the calicivirus VP2 structure

A

φX174_H	173	QKEIAGIQSAT-SRQNTKDQVYANEMLAYQQKESTARVASIMENTNLSKQQQVSEIMRQ	231
		Q E A Q T S Q V A Q N + + A R + A I N + L S K Q + E +	
P22_portal	619	QAE LAKAQNQTL SLQIDA AKVEAQNQL-----NAARIAE I FNMDLSKQSEFREFLKT	671
φX174_H	232	MLT-QAQTAGQYFTNDQI----KEMTRK VSAEV-DLVHQOTQNR YGS	273
		Q N + E T K + + + + Q Q N Q GS	
P22_portal	672	VASFQDRSEDARANAELLKGD EQTHKQRMDIANILQSQRQNQPSGS	719

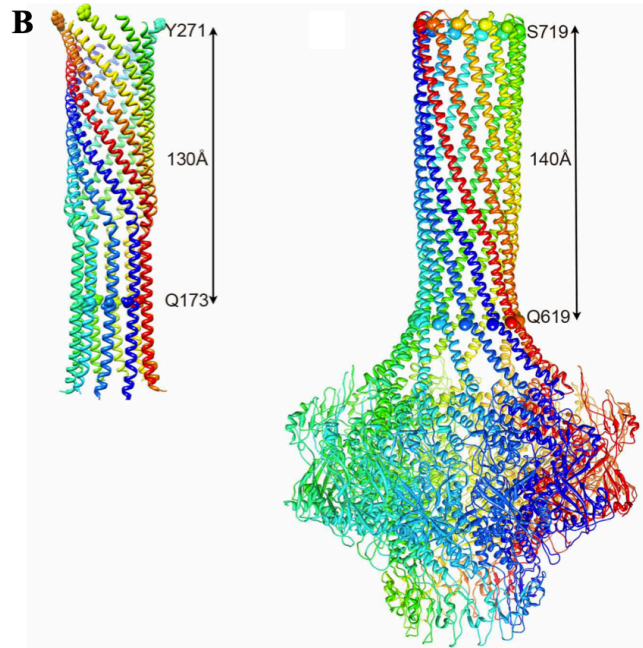


FIG 5.10 Comparison of the φX174 H-tube and the P22 portal structure

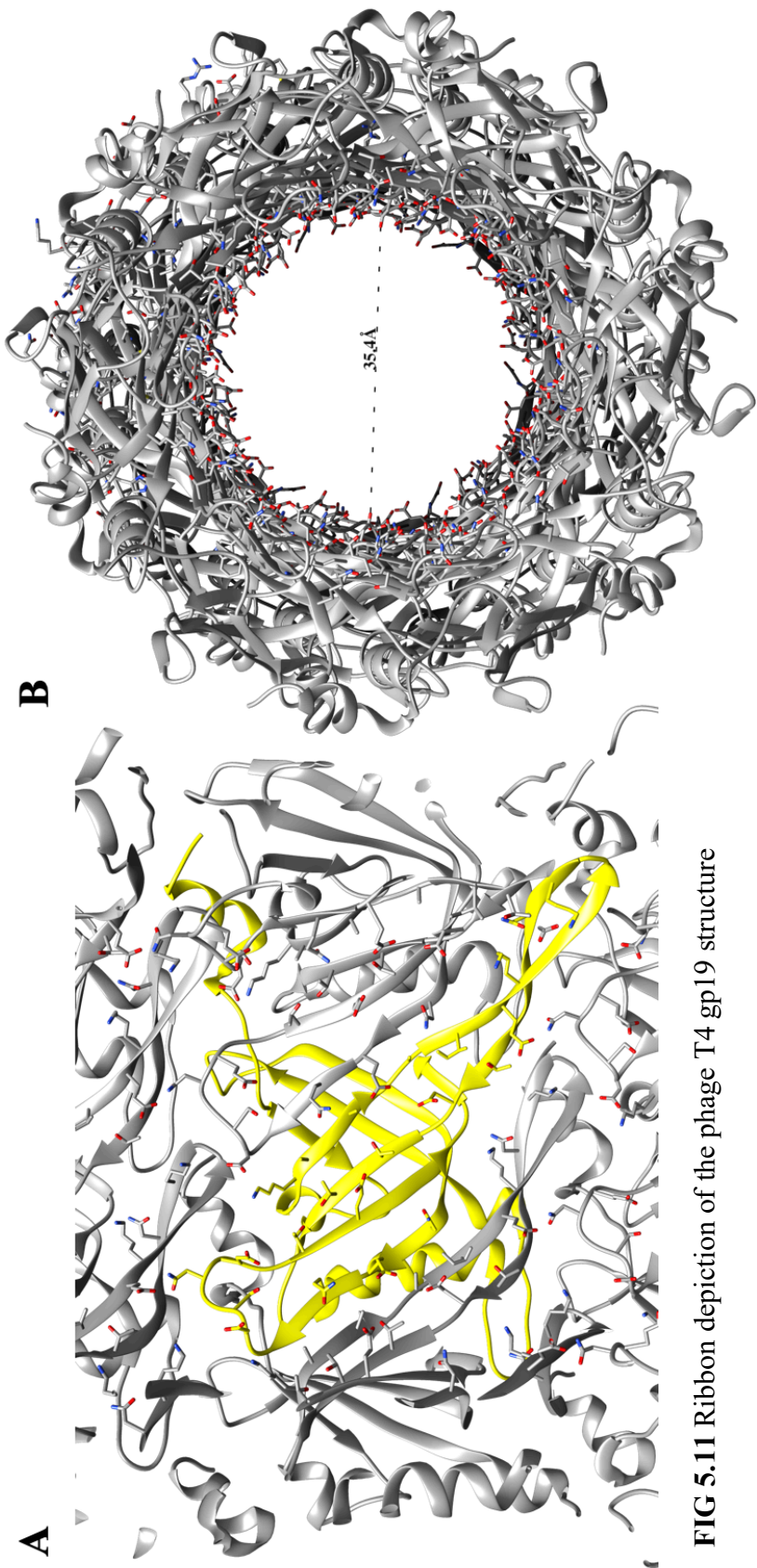


FIG 5.11 Ribbon depiction of the phage T4 gp19 structure

FULL DISSERTATION REFERENCES

Chapter 1

1. Wommack KE, Colwell RR. 2000. Virioplankton: Viruses in Aquatic Ecosystems. *Microbiol Mol Biol Rev* 64:69–114.
2. Kimura M, Jia ZJ, Nakayama N, Asakawa S. 2008. Ecology of viruses in soils: Past, present and future perspectives. *Soil Sci Plant Nutr* 54:1–32.
3. Suttle CA. 2005. Viruses in the sea. *Nature* 437:356–361.
4. Breitbart M, Rohwer F. 2005. Here a virus, there a virus, everywhere the same virus? *Trends Microbiol* 13:278–284.
5. Breitbart M, Hewson I, Felts B, Mahaffy JM, Nulton J, Salamon P, Rohwer F. 2003. Metagenomic Analyses of an Uncultured Viral Community from Human Feces. *J Bacteriol* 185:6220–6223.
6. Georgopoulos CP, Hendrix RW, Kaiser AD, Wood WB. 1972. Role of the Host Cell in Bacteriophage Morphogenesis: Effects of a Bacterial Mutation on T4 Head Assembly. *Nat New Biol* 239:38–41.
7. Georgopoulos CP, Hendrix RW, Casjens SR, Kaiser AD. 1973. Host participation in bacteriophage lambda head assembly. *J Mol Biol* 76:45–60.
8. Jazwinski SM, Lindberg AA, Kornberg A. 1975. The lipopolysaccharide receptor for bacteriophages ϕ X174 and S13. *Virology* 66:268–282.
9. Parent KN, Erb ML, Cardone G, Nguyen K, Gilcrease EB, Porcek NB, Pogliano J, Baker TS, Casjens SR. 2014. OmpA and OmpC are critical host factors for bacteriophage Sf6 entry in *Shigella*. *Mol Microbiol* 92:47–60.
10. Valentine RC, Strand M. 1965. Complexes of F-Pili and RNA Bacteriophage. *Science* 148:511–513.
11. Lovett PS. 1972. PBP1: A flagella specific bacteriophage mediating transduction in *Bacillus pumilus*. *Virology* 47:743–752.
12. Nicola A V., Aguilar HC, Mercer J, Ryckman B, Wiethoff CM. 2013. Virus Entry by Endocytosis. *Adv Virol* 2013:1–2.
13. Dáder B, Then C, Berthelot E, Ducouso M, Ng JCK, Drucker M. 2017. Insect transmission of plant viruses: Multilayered interactions optimize viral propagation. *Insect Sci* 24:929–946.

14. Bamford DH, Palva ET, Lounatmaa K. 1976. Ultrastructure and Life Cycle of the Lipid-containing Bacteriophage $\Phi 6$. *J Gen Virol* 32:249–259.
15. Hoogstraten D, Qiao X, Sun Y, Hu A, Onodera S, Mindich L. 2000. Characterization of $\Phi 8$, a Bacteriophage Containing Three Double-Stranded RNA Genomic Segments and Distantly Related to $\Phi 6$. *Virology* 272:218–224.
16. Vidaver AK, Koski RK, Van Etten JL. 1973. Bacteriophage $\Phi 6$: a Lipid-Containing Virus of *Pseudomonas phaseolicola*. *J Virol* 11:799–805.
17. Jääliñoja HT, Huiskonen JT, Butcher SJ. 2007. Electron Cryomicroscopy Comparison of the Architectures of the Enveloped Bacteriophages $\Phi 6$ and $\Phi 8$. *Structure* 15:157–167.
18. Huiskonen JT, de Haas F, Bubeck D, Bamford DH, Fuller SD, Butcher SJ. 2006. Structure of the Bacteriophage $\Phi 6$ Nucleocapsid Suggests a Mechanism for Sequential RNA Packaging. *Structure* 14:1039–1048.
19. de Haas F, Paatero AO, Mindich L, Bamford DH, Fuller SD. 1999. A symmetry mismatch at the site of RNA packaging in the polymerase complex of dsRNA bacteriophage $\phi 6$. *J Mol Biol* 294:357–372.
20. Mäntynen S, Laanto E, Kohvakka A, Poranen MM, Bamford JKH, Ravantti JJ. 2015. New enveloped dsRNA phage from freshwater habitat. *J Gen Virol* 96:1180–1189.
21. Romantschuk M, Bamford DH. 1985. Function of Pili in Bacteriophage $\Phi 6$ Penetration. *J Gen Virol* 66:2461–2469.
22. Bamford DH, Romantschuk M, Somerharju PJ. 1987. Membrane fusion in prokaryotes: bacteriophage $\phi 6$ membrane fuses with the *Pseudomonas syringae* outer membrane. *EMBO J* 6:1467–1473.
23. Hantula J, Bamford DH. 1988. Chemical crosslinking of bacteriophage $\phi 6$ nucleocapsid proteins. *Virology* 165:482–488.
24. Caldentey J, Bamford DH. 1992. The lytic enzyme of the *Pseudomonas* phage $\phi 6$. Purification and biochemical characterization. *Biochim Biophys Acta - Protein Struct Mol Enzymol* 1159:44–50.
25. Mindich L, Lehman J. 1979. Cell Wall Lysin as a Component of the Bacteriophage $\Phi 6$ Virion. *J Virol* 30:489–496.
26. Cvirkaite-Krupovic V, Poranen MM, Bamford DH. 2010. Phospholipids act as secondary receptor during the entry of the enveloped, double-stranded RNA

- bacteriophage $\Phi 6$. *J Gen Virol* 91:2116–2120.
27. Romantschuk M, Olkkonen VM, Bamford DH. 1988. The nucleocapsid of bacteriophage $\Phi 6$ penetrates the host cytoplasmic membrane. *EMBO J* 7:1821–1829.
 28. Krupovič M, Bamford DH. 2007. Putative prophages related to lytic tailless marine dsDNA phage PM2 are widespread in the genomes of aquatic bacteria. *BMC Genomics* 8:236.
 29. Leigh BA, Breitbart M, Oksanen HM, Bamford DH, Dishaw LJ. 2018. Genome Sequence of PM2-Like Phage Cr39582, Induced from a *Pseudoalteromonas* sp. Isolated from the Gut of *Ciona robusta*. *Genome Announc* 6.
 30. Abrescia NGA, Grimes JM, Kivelä HM, Assenberg R, Sutton GC, Butcher SJ, Bamford JKH, Bamford DH, Stuart DI. 2008. Insights into Virus Evolution and Membrane Biogenesis from the Structure of the Marine Lipid-Containing Bacteriophage PM2. *Mol Cell* 31:749–761.
 31. Camerini-Otero R., Franklin R. 1972. Structure and synthesis of a lipid-containing bacteriophage. *Virology* 49:385–393.
 32. Espejo RT, Canelo ES. 1968. Origin of Phospholipid in Bacteriophage PM2. *J Virol* 2:1235–1240.
 33. Kivelä HM, Männistö RH, Kalkkinen N, Bamford DH. 1999. Purification and Protein Composition of PM2, the First Lipid-Containing Bacterial Virus To Be Isolated. *Virology* 262:364–374.
 34. Cvirkaitė-Krupovič V, Krupovič M, Daugelavičius R, Bamford DH. 2010. Calcium ion-dependent entry of the membrane-containing bacteriophage PM2 into its *Pseudoalteromonas* host. *Virology* 405:120–128.
 35. Kivela HM, Daugelavicius R, Hankkio RH, Bamford JKH, Bamford DH. 2004. Penetration of Membrane-Containing Double-Stranded-DNA Bacteriophage PM2 into *Pseudoalteromonas* Hosts. *J Bacteriol* 186:5342–5354.
 36. Kivela HM, Madonna S, Krupovic M, Tutino ML, Bamford JKH. 2008. Genetics for *Pseudoalteromonas* Provides Tools To Manipulate Marine Bacterial Virus PM2. *J Bacteriol* 190:1298–1307.
 37. Berrier C, Bonhivers M, Letellier L, Ghazi A. 2000. High-conductance channel induced by the interaction of phage lambda with its receptor maltoporin. *FEBS Lett* 476:129–133.
 38. Shapira A, Giberman E, Kohn A. 1974. Recoverable potassium fluxes variations

- following adsorption of T4 phage and their ghosts on *Escherichia coli* B. *J Gen Virol* 23:159–171.
39. Boulanger P, Letellier L. 1992. Ion channels are likely to be involved in the two steps of phage T5 DNA penetration into *Escherichia coli* cells. *J Biol Chem* 267:3168–72.
 40. Koning RI, Gomez-Blanco J, Akopjana I, Vargas J, Kazaks A, Tars K, Carazo JM, Koster AJ. 2016. Asymmetric cryo-EM reconstruction of phage MS2 reveals genome structure in situ. *Nat Commun* 7:12524.
 41. Dent KC, Thompson R, Barker AM, Hiscox JA, Barr JN, Stockley PG, Ranson NA. 2013. The Asymmetric Structure of an Icosahedral Virus Bound to Its Receptor Suggests a Mechanism for Genome Release. *Structure* 21:1225–1234.
 42. Toropova K, Stockley PG, Ranson NA. 2011. Visualising a Viral RNA Genome Poised for Release from Its Receptor Complex. *J Mol Biol* 408:408–419.
 43. Rolfsson Ó, Middleton S, Manfield IW, White SJ, Fan B, Vaughan R, Ranson NA, Dykeman E, Twarock R, Ford J, Cheng Kao C, Stockley PG. 2016. Direct Evidence for Packaging Signal-Mediated Assembly of Bacteriophage MS2. *J Mol Biol* 428:431–448.
 44. Stockley PG, White SJ, Dykeman E, Manfield I, Rolfsson O, Patel N, Bingham R, Barker A, Wroblewski E, Chandler-Bostock R, Weiß EU, Ranson NA, Tuma R, Twarock R. 2016. Bacteriophage MS2 genomic RNA encodes an assembly instruction manual for its capsid. *Bacteriophage* 6:e1157666.
 45. Hung PP, Ling CM, Overby LR. 1969. Self-Assembly of Qbeta and MS2 Phage Particles: Possible Function of Initiation Complexes. *Science* (80-) 166:1638–1640.
 46. Date T. 1979. Kinetic Studies of the Interaction between MS2 Phage and F Pilus of *Escherichia coli*. *Eur J Biochem* 96:167–175.
 47. Krahn PM, O’Callaghan RJ, Paranchych W. 1972. Stages in phage R17 infection VI. Injection of A Protein and RNA into the Host Cell. *Virology* 47:628–637.
 48. Shiba T, Suzuki Y. 1981. Localization of A protein in the RNA-A protein complex of RNA phage MS2. *Biochim Biophys Acta - Nucleic Acids Protein Synth* 654:249–255.
 49. Leipold B, Hofschneider PH. 1975. Isolation of an infectious RNA-A-protein complex from the bacteriophage M12. *FEBS Lett* 55:50–52.
 50. Paranchych W, Krahn PM, Bradley RD. 1970. Stages in phage R17 infection V.

- Phage Eclipse and the Role of F Pili. *Virology* 41:465–473.
51. Silverman PM, Valentine RC. 1969. The RNA Injection Step of Bacteriophage f2 Infection. *J Gen Virol* 4:111–124.
 52. Danziger RE, Paranchych W. 1970. Stages in phage R17 infection III. Energy Requirements for the F-pili Mediated Eclipse of Viral Infectivity. *Virology* 40:554–564.
 53. Shiba T, Miyake T. 1975. New type of infectious complex of E. coli RNA phage. *Nature* 254:157–158.
 54. Rumnieks J, Tars K. 2017. Crystal Structure of the Maturation Protein from Bacteriophage Q β . *J Mol Biol* 429:688–696.
 55. Wang YA, Yu X, Silverman PM, Harris RL, Egelman EH. 2009. The Structure of F-Pili. *J Mol Biol* 385:22–29.
 56. Harrington LC, Rogerson AC. 1990. The F pilus of *Escherichia coli* appears to support stable DNA transfer in the absence of wall-to-wall contact between cells. *J Bacteriol* 172:7263–7264.
 57. Ou JT, Anderson TF. 1970. Role of Pili in Bacterial Conjugation. *J Bacteriol* 102:648–654.
 58. Babic A, Lindner AB, Vulic M, Stewart EJ, Radman M. 2008. Direct Visualization of Horizontal Gene Transfer. *Science* (80-) 319:1533–1536.
 59. Goldbourn A, Gross BJ, Day LA, McDermott AE. 2007. Filamentous Phage Studied by Magic-Angle Spinning NMR: Resonance Assignment and Secondary Structure of the Coat Protein in Pf1. *J Am Chem Soc* 129:2338–2344.
 60. Marvin DA, Welsh LC, Symmons MF, Scott WRP, Straus SK. 2006. Molecular Structure of fd (f1, M13) Filamentous Bacteriophage Refined with Respect to X-ray Fibre Diffraction and Solid-state NMR Data Supports Specific Models of Phage Assembly at the Bacterial Membrane. *J Mol Biol* 355:294–309.
 61. Marvin DA, Symmons MF, Straus SK. 2014. Structure and assembly of filamentous bacteriophages. *Prog Biophys Mol Biol* 114:80–122.
 62. Bradley DE, Whelan J. 1989. *Escherichia coli* tolQ Mutants Are Resistant to Filamentous Bacteriophages That Adsorb to the Tips, not the Shafts, of Conjugative Pili. *Microbiology* 135:1857–1863.
 63. Webster RE. 1996. Biology of the Filamentous Bacteriophage, p. 1–20. *In* *Phage Display of Peptides and Proteins: A Laboratory Manual*. Elsevier.

64. Lorenz SH, Jakob RP, Weininger U, Balbach J, Dobbek H, Schmid FX. 2011. The Filamentous Phages fd and IF1 Use Different Mechanisms to Infect *Escherichia coli*. *J Mol Biol* 405:989–1003.
65. Heilpern AJ, Waldor MK. 2003. PIII CTX, a Predicted CTXphi; Minor Coat Protein, Can Expand the Host Range of Coliphage fd To Include *Vibrio cholerae*. *J Bacteriol* 185:1037.
66. Endemann H, Bross P, Rasched I. 1992. The adsorption protein of phage IKe. Localization by deletion mutagenesis of domains involved in infectivity. *Mol Microbiol* 6:471–478.
67. Novotny CP, Fives Taylor P. 1974. Retraction of F pili. *J Bacteriol* 117:1306–1311.
68. Sun TP, Webster RE. 1986. fii, a bacterial locus required for filamentous phage infection and its relation to colicin-tolerant tolA and tolB. *J Bacteriol* 165:107–115.
69. Sun TP, Webster RE. 1987. Nucleotide sequence of a gene cluster involved in entry of E colicins and single-stranded DNA of infecting filamentous bacteriophages into *Escherichia coli*. *J Bacteriol* 169:2667–2674.
70. Heilpern AJ, Waldor MK. 2000. CTXphi Infection of *Vibrio cholerae* Requires the tolQRA Gene Products. *J Bacteriol* 182:1739–1747.
71. Cascales E, Buchanan SK, Duche D, Kleanthous C, Lloubes R, Postle K, Riley M, Slatin S, Cavard D. 2007. Colicin Biology. *Microbiol Mol Biol Rev* 71:158–229.
72. Clarke M, Maddera L, Harris RL, Silverman PM. 2008. F-pili dynamics by live-cell imaging. *Proc Natl Acad Sci* 105:17978–17981.
73. Lee S-W, Mao C, Flynn CE, Belcher AM. 2002. Ordering of Quantum Dots Using Genetically Engineered Viruses. *Science* (80-) 296:892–895.
74. Holliger P, Riechmann L, Williams RL. 1999. Crystal structure of the two N-terminal domains of g3p from filamentous phage fd at 1.9 Å: evidence for conformational lability 1 Edited by J. M. Thornton. *J Mol Biol* 288:649–657.
75. Eckert B, Martin A, Balbach J, Schmid FX. 2005. Prolyl isomerization as a molecular timer in phage infection. *Nat Struct Mol Biol* 12:619–623.
76. Rakonjac J, Feng J, Model P. 1999. Filamentous phage are released from the bacterial membrane by a two-step mechanism involving a short C-terminal fragment of pIII 1 Edited by M. Gottesman. *J Mol Biol* 289:1253–1265.

77. Bennett NJ, Rakonjac J. 2006. Unlocking of the Filamentous Bacteriophage Virion During Infection is Mediated by the C Domain of pIII. *J Mol Biol* 356:266–273.
78. Bennett NJ, Gagic D, Sutherland-Smith AJ, Rakonjac J. 2011. Characterization of a Dual-Function Domain That Mediates Membrane Insertion and Excision of Ff Filamentous Bacteriophage. *J Mol Biol* 411:972–985.
79. Smilowitz H. 1974. Bacteriophage f1 infection: fate of the parental major coat protein. *J Virol* 13:94.
80. Trenkner E, Bonhoeffer F, Gierer A. 1967. The fate of the protein component of bacteriophage fd during infection. *Biochem Biophys Res Commun* 28:932–939.
81. Abrescia NGA, Cockburn JJB, Grimes JM, Sutton GC, Diprose JM, Butcher SJ, Fuller SD, San Martín C, Burnett RM, Stuart DI, Bamford DH, Bamford JKH. 2004. Insights into assembly from structural analysis of bacteriophage PRD1. *Nature* 432:68–74.
82. Bamford D, McGraw T, MacKenzie G, Mindich L. 1983. Identification of a protein bound to the termini of bacteriophage PRD1 DNA. *J Virol* 47:311–6.
83. Bamford DH, Caldentey J, Bamford JKH. 1995. Bacteriophage Prd1: A Broad Host Range Dsdna Tectivirus With an Internal Membrane, p. 281–319. *In* *Advances in Virus Research*.
84. Cockburn JJB, Abrescia NGA, Grimes JM, Sutton GC, Diprose JM, Benevides JM, Thomas GJ, Bamford JKH, Bamford DH, Stuart DI. 2004. Membrane structure and interactions with protein and DNA in bacteriophage PRD1. *Nature* 432:122–125.
85. Rydman PS, Caldentey J, Butcher SJ, Fuller SD, Rutten T, Bamford DH. 1999. Bacteriophage PRD1 contains a labile receptor-binding structure at each vertex. *J Mol Biol* 291:575–587.
86. Davis TN, Muller ED, Cronan JE. 1982. The virion of the lipid-containing bacteriophage PR4. *Virology* 120:287–306.
87. Tuma R, Bamford JHK, Bamford DH, Thomas GJ. 1996. Structure, interactions and dynamics of PRD1 virus II. Organization of the viral membrane and DNA. *J Mol Biol* 257:102–115.
88. Santos-Pérez I, Oksanen HM, Bamford DH, Goñi FM, Reguera D, Abrescia NGA. 2017. Membrane-assisted viral DNA ejection. *Biochim Biophys Acta - Gen Subj* 1861:664–672.

89. Mindich L, Bamford D, McGraw T, Mackenzie G. 1982. Assembly of bacteriophage PRD1: particle formation with wild-type and mutant viruses. *J Virol* 44:1021–30.
90. Kotilainen MM, Grahn AM, Bamford JK, Bamford DH. 1993. Binding of an *Escherichia coli* double-stranded DNA virus PRD1 to a receptor coded by an IncP-type plasmid. *J Bacteriol* 175:3089–3095.
91. Grahn AM, Daugelavičius R, Bamford DH. 2002. Sequential model of phage PRD1 DNA delivery: Active involvement of the viral membrane. *Mol Microbiol* 46:1199–1209.
92. Rydman PS, Bamford DH. 2000. Bacteriophage PRD1 DNA entry uses a viral membrane-associated transglycosylase activity. *Mol Microbiol* 37:356–363.
93. Peralta B, Gil-Carton D, Castaño-Díez D, Bertin A, Boulogne C, Oksanen HM, Bamford DH, Abrescia NGA. 2013. Mechanism of Membranous Tunnelling Nanotube Formation in Viral Genome Delivery. *PLoS Biol* 11:e1001667.
94. Daugelavicius R, Bamford JK, Bamford DH. 1997. Changes in host cell energetics in response to bacteriophage PRD1 DNA entry. *J Bacteriol* 179:5203–5210.
95. Molineux IJ, Panja D. 2013. Popping the cork: mechanisms of phage genome ejection. *Nat Rev Microbiol* 11:194–204.
96. Casjens SR, Molineux IJ. 2012. Short Noncontractile Tail Machines: Adsorption and DNA Delivery by Podoviruses, p. 143–179. *In* Rossmann, MG, Rao, VB (eds.), *Viral Molecular Machines*. Springer US, Boston, MA.
97. Davidson AR, Cardarelli L, Pell LG, Radford DR, Maxwell KL. 2012. Long Noncontractile Tail Machines of Bacteriophages, p. 115–142. *In* Rossmann, MG, Rao, VB (eds.), *Viral Molecular Machines*. Springer US, Boston, MA.
98. Leiman PG, Schneider MM. 2012. Contractile Tail Machines of Bacteriophages, p. 93–114. *In* Rossmann, MG, Rao, VB (eds.), *Viral Molecular Machines*. Springer US, Boston, MA.
99. Taylor NMI, Prokhorov NS, Guerrero-Ferreira RC, Shneider MM, Browning C, Goldie KN, Stahlberg H, Leiman PG. 2016. Structure of the T4 baseplate and its function in triggering sheath contraction. *Nature* 533:346–352.
100. Hu B, Margolin W, Molineux IJ, Liu J. 2015. Structural remodeling of bacteriophage T4 and host membranes during infection initiation. *Proc Natl Acad Sci* 112:E4919–E4928.
101. Aksyuk AA, Leiman PG, Kurochkina LP, Shneider MM, Kostyuchenko VA,

- Mesyanzhinov V V., Rossmann MG. 2009. The tail sheath structure of bacteriophage T4: A molecular machine for infecting bacteria. *EMBO J* 28:821–829.
102. Leiman PG, Chipman PR, Kostyuchenko VA, Mesyanzhinov V V., Rossmann MG. 2004. Three-Dimensional Rearrangement of Proteins in the Tail of Bacteriophage T4 on Infection of Its Host. *Cell* 118:419–429.
 103. Guerrero-Ferreira RC, Hupfeld M, Nazarov S, Taylor NM, Shneider MM, Obbineni JM, Loessner MJ, Ishikawa T, Klumpp J, Leiman PG. 2019. Structure and transformation of bacteriophage A511 baseplate and tail upon infection of *Listeria* cells. *EMBO J* e99455.
 104. Browning C, Shneider MM, Bowman VD, Schwarzer D, Leiman PG. 2012. Phage Pierces the Host Cell Membrane with the Iron-Loaded Spike. *Structure* 20:326–339.
 105. Moak M, Molineux IJ. 2004. Peptidoglycan hydrolytic activities associated with bacteriophage virions. *Mol Microbiol* 51:1169–1183.
 106. Katsura I. 1976. Morphogenesis of bacteriophage lambda tail. Polymorphism in the assembly of the major tail protein. *J Mol Biol* 107:307–326.
 107. Vegge CS, Brondsted L, Neve H, Mc Grath S, van Sinderen D, Vogensen FK. 2005. Structural Characterization and Assembly of the Distal Tail Structure of the Temperate Lactococcal Bacteriophage TP901-1. *J Bacteriol* 187:4187–4197.
 108. Katsura I, Hendrix RW. 1984. Length determination in bacteriophage lambda tails. *Cell* 39:691–698.
 109. Katsura I. 1987. Determination of bacteriophage λ tail length by a protein ruler. *Nature* 327:73–75.
 110. Casjens SR, Hendrix RW. 1974. Locations and amounts of the major structural proteins in bacteriophage lambda. *J Mol Biol* 88:535–545.
 111. Schwartz M. 1975. Reversible interaction between coliphage lambda and its receptor protein. *J Mol Biol* 99:185–201.
 112. Heller K, Braun V. 1982. Polymannose O-antigens of *Escherichia coli*, the binding sites for the reversible adsorption of bacteriophage T5+ via the L-shaped tail fibers. *J Virol* 41:222–7.
 113. Baptista C, Santos MA, Sao-Jose C. 2008. Phage SPP1 Reversible Adsorption to *Bacillus subtilis* Cell Wall Teichoic Acids Accelerates Virus Recognition of Membrane Receptor YueB. *J Bacteriol* 190:4989–4996.

114. Boulanger P, Jacquot P, Plançon L, Chami M, Engel A, Parquet C, Herbeuval C, Letellier L. 2008. Phage T5 Straight Tail Fiber Is a Multifunctional Protein Acting as a Tape Measure and Carrying Fusogenic and Muralytic Activities. *J Biol Chem* 283:13556–13564.
115. Feucht A, Schmid A, Benz R, Schwarz H, Heller KJ. 1990. Pore formation associated with the tail-tip protein pb2 of bacteriophage T5. *J Biol Chem* 265:18561–18567.
116. Cumby N, Reimer K, Mengin-Lecreulx D, Davidson AR, Maxwell KL. 2015. The phage tail tape measure protein, an inner membrane protein and a periplasmic chaperone play connected roles in the genome injection process of *E. coli* phage HK97. *Mol Microbiol* 96:437–447.
117. Scandella D, Arber W. 1974. An *Escherichia coli* mutant which inhibits the injection of phage λ DNA. *Virology* 58:504–513.
118. Scandella D, Arber W. 1976. Phage λ DNA injection into *Escherichia coli* *pel*-mutants is restored by mutations in phage genes V or H. *Virology* 69:206–215.
119. Hu B, Margolin W, Molineux IJ, Liu J. 2013. The bacteriophage T7 virion undergoes extensive structural remodeling during infection. *Science* (80-) 339:576–579.
120. Lindberg AA, Sarvas M, Makela PH. 1970. The Tail Sheath of Bacteriophage N4 Interacts with the *Escherichia coli* Receptor. *Infect Immun* 1:88–97.
121. McPartland J, Rothman-Denes LB. 2009. The Tail Sheath of Bacteriophage N4 Interacts with the *Escherichia coli* Receptor. *J Bacteriol* 191:525–532.
122. Leiman PG, Battisti AJ, Bowman VD, Stummeyer K, Mühlenhoff M, Gerardy-Schahn R, Scholl D, Molineux IJ. 2007. The Structures of Bacteriophages K1E and K1-5 Explain Processive Degradation of Polysaccharide Capsules and Evolution of New Host Specificities. *J Mol Biol* 371:836–849.
123. Bayer ME, Takeda K, Uetake H. 1980. Effects of receptor destruction by *Salmonella* bacteriophages ϵ 15 and c341. *Virology* 105:328–337.
124. Schulz EC, Schwarzer D, Frank M, Stummeyer K, Mühlenhoff M, Dickmanns A, Gerardy-Schahn R, Ficner R. 2010. Structural Basis for the Recognition and Cleavage of Polysialic Acid by the Bacteriophage K1F Tailspike Protein EndoNF. *J Mol Biol* 397:341–351.
125. Porcek NB, Parent KN. 2015. Key residues of *S. flexneri* OmpA mediate infection by bacteriophage Sf6. *J Mol Biol* 427:1964–1976.

126. Xu J, Gui M, Wang D, Xiang Y. 2016. The bacteriophage ϕ 29 tail possesses a pore-forming loop for cell membrane penetration. *Nature* 534:544–547.
127. Hoffman B, Levine M. 1975. Bacteriophage P22 virion protein which performs an essential early function. II. Characterization of the Gene 16 Function. *J Virol* 16:1547–1559.
128. Hoffman B, Levine M. 1975. Bacteriophage P22 virion protein which performs an essential early function. I. Analysis of 16-ts mutants. *J Virol* 16:1536–46.
129. Jin Y, Sdao SM, Dover JA, Porcek NB, Knobler CM, Gelbart WM, Parent KN. 2015. Bacteriophage P22 ejects all of its internal proteins before its genome. *Virology* 485:128–134.
130. Perez GL, Huynh B, Slater M, Maloy S. 2009. Transport of phage P22 DNA across the cytoplasmic membrane. *J Bacteriol* 91:135–140.
131. Israel V. 1977. E Proteins of Bacteriophage P22. I. Identification and Ejection from Wild-Type and Defective Particles. *J Virol* 23:91–97.
132. Zhao H, Speir JA, Matsui T, Lin Z, Liang L, Lynn AY, Varnado B, Weiss TM, Tang L. 2016. Structure of a bacterial virus DNA-injection protein complex reveals a decameric assembly with a constricted molecular channel. *PLoS One* 11:1–16.
133. Inagaki M, Kawaura T, Wakashima H, Kato M, Nishikawa S, Kashimura N. 2003. Different contributions of the outer and inner R-core residues of lipopolysaccharide to the recognition by spike H and G proteins of bacteriophage ϕ X174. *FEMS Microbiol Lett* 226:221–227.
134. McKenna R, Xia D, Willingmann P, Ilag LL, Krishnaswamy S, Rossmann MG, Olson NH, Baker TS, Incardona NL. 1992. Atomic structure of single-stranded DNA bacteriophage phi X174 and its functional implications. *Nature* 355:137–43.
135. McKenna R, Ilag L, Rossmann M. 1994. Analysis of the Single-stranded DNA Bacteriophage PhiX174 Refined at a Resolution of 3.0Å. *J Mol Biol*.
136. Bernal RA, Hafenstein S, Esmeralda R, Fane BA, Rossmann MG. 2004. The ϕ X174 protein J mediates DNA packaging and viral attachment to host cells. *J Mol Biol* 337:1109–1122.
137. Ilag LL, Olson NH, Dokland T, Music CL, Cheng RH, Bowen Z, McKenna R, Rossmann MG, Baker TS, Incardona NL. 1995. DNA packaging intermediates of bacteriophage ϕ X174. *Structure* 3:353–363.

138. Ilag LL, McKenna R, Yadav MP, BeMiller JN, Incardona NL, Rossmann MG. 1994. Calcium Ion-induced Structural Changes in Bacteriophage ϕ X174. *J Mol Biol* 244:291–300.
139. Roznowski AP, Young RJ, Love SD, Andromita AA, Guzman VA, Wilch MH, Block A, McGill A, Lavelle M, Romanova A, Sekiguchi A, Wang M, Burch AD, Fane BA. 2018. Recessive Host Range Mutants and Unsusceptible Cells That Inactivate Virions without Genome Penetration: Ecological and Technical Implications. *J Virol* 93:1–16.
140. Sun Y, Roznowski AP, Tokuda JM, Klose T, Mauney A, Pollack L, Fane BA, Rossmann MG. 2017. Structural changes of tailless bacteriophage Φ X174 during penetration of bacterial cell walls. *Proc Natl Acad Sci* 114:13708–13713.
141. Jazwinski SM, Lindberg AA, Kornberg A. 1975. The gene H spike protein of bacteriophages ϕ X174 and S13. I. Functions in phage-receptor recognition and in transfection. *Virology* 66:283–293.
142. Jazwinski SM, Marco R, Kornberg A. 1975. The gene H spike protein of bacteriophages ϕ X174 and S13. II. Relation to synthesis of the parental replicative form. *Virology* 66:294–305.
143. Sun L, Young LN, Zhang X, Boudko SP, Fokine A, Zbornik E, Roznowski AP, Molineux IJ, Rossmann MG, Fane BA. 2014. Icosahedral bacteriophage Φ X174 forms a tail for DNA transport during infection. *Nature* 505:432–435.
144. Shepard W, Cruse WBT, Fourme R, De La Fortelle E, Prangé T. 1998. A zipper-like duplex in DNA: The crystal structure of d(GCGAAAGCT) at 2.1 Å resolution. *Structure* 6:849–861.
145. Mandel-Gutfreund Y, Schueler O, Margalit H. 1995. Comprehensive Analysis of Hydrogen Bonds in Regulatory Protein DNA-Complexes: In Search of Common Principles. *J Mol Biol* 253:370–382.
146. Luscombe NM. 2001. Amino acid-base interactions: a three-dimensional analysis of protein-DNA interactions at an atomic level. *Nucleic Acids Res* 29:2860–2874.
147. Luscombe NM, Thornton JM. 2002. Protein–DNA Interactions: Amino Acid Conservation and the Effects of Mutations on Binding Specificity. *J Mol Biol* 320:991–1009.
148. Suzuki M. 1994. A framework for the DNA–protein recognition code of the probe helix in transcription factors: the chemical and stereochemical rules. *Structure* 2:317–326.

149. Conley MJ, McElwee M, Azmi L, Gabrielsen M, Byron O, Goodfellow IG, Bhella D. 2019. Calicivirus VP2 forms a portal-like assembly following receptor engagement. *Nature* 565:377–381.

Chapter 2

1. Leiman PG, Schneider MM. 2012. Contractile Tail Machines of Bacteriophages, p. 93–114. *In* Rossmann, MG, Rao, VB (eds.), *Viral Molecular Machines*. Springer US, Boston, MA.
2. Hu B, Margolin W, Molineux IJ, Liu J. 2013. The bacteriophage T7 virion undergoes extensive structural remodeling during infection. *Science* (80-) 339:576–579.
3. Esquinas-rychen M, Erni B. 2001. Facilitation of Bacteriophage Lambda DNA Injection by Inner Membrane Proteins of the Bacterial Phosphoenolpyruvate:Carbohydrate Phosphotransferase System (PTS). *J Mol Microbiol Biotechnol* 3:361–370.
4. Russel M, Model P. 2006. Filamentous phage, p 146–160. *In* Calendar R (ed), *The bacteriophages*, 2nd ed. Oxford Press, London, United Kingdom.
5. Van Duijn J, Tsareva N. 2006. Single-stranded RNA phages, p 175–196. *In* Calendar R (ed), *The bacteriophages*, 2nd ed. Oxford Press, London, United Kingdom
6. Jazwinski SM, Lindberg AA, Kornberg A. 1975. The gene H spike protein of bacteriophages Φ X174 and S13. I. Functions in phage-receptor recognition and in transfection. *Virology* 66:283–293.
7. Jazwinski SM, Marco R, Kornberg A. 1975. The gene H spike protein of bacteriophages Φ X174 and S13. II. Relation to synthesis of the parental replicative form. *Virology* 66:294–305.
8. Sun L, Young LN, Zhang X, Boudko SP, Fokine A, Zbornik E, Roznowski AP, Molineux IJ, Rossmann MG, Fane BA. 2014. Icosahedral bacteriophage Φ X174 forms a tail for DNA transport during infection. *Nature* 505:432–435.
9. Sun L, Rossmann MG, Fane BA. 2014. High-Resolution Structure of a Virally Encoded DNA-Translocating Conduit and the Mechanism of DNA Penetration. *J Virol* 88:10276–10279.
10. Tang J, Lander GC, Olia A, Li R, Casjens S, Prevelige P, Cingolani G, Baker TS, Johnson JE. 2011. Article Peering Down the Barrel of a Bacteriophage Portal : The

Genome Packaging and Release Valve in P22. *Struct Des* 19:496–502.

11. Olia AS, Prevelige PE, Johnson JE, Cingolani G. 2011. Three-dimensional structure of a viral genome-delivery portal vertex. *Nat Struct Mol Biol* 18:597–603.
12. Egelman EH, Xu C, DiMaio F, Magnotti E, Modlin C, Yu X, Wright E, Baker D, Conticello VP. 2015. Structural Plasticity of Helical Nanotubes Based on Coiled-Coil Assemblies. *Structure* 23:280–289.
13. Pieters BJGE, van Eldijk MB, Nolte RJM, Mecinović J. 2016. Natural supramolecular protein assemblies. *Chem Soc Rev* 45:24–39.
14. Cherwa JE, Organtini LJ, Ashley RE, Hafenstein SL, Fane BA. 2011. In vitro assembly of the ϕ X174 procapsid from external scaffolding protein oligomers and early pentameric assembly intermediates. *J Mol Biol* 412:387–396.
15. Cherwa JE, Uchiyama A, Fane BA. 2008. Scaffolding Proteins Altered in the Ability To Perform a Conformational Switch Confer Dominant Lethal Assembly Defects. *J Virol* 82:5774–5780.
16. Ruboyianes M V, Chen M, Dubrava MS, Cherwa JE, Fane BA. 2009. The Expression of N-Terminal Deletion DNA Pilot Proteins Inhibits the Early Stages of Φ X174 Replication. *J Virol* 83:9952–9956.
17. Fane BA, Hayashi M. 1991. Second-site suppressors of a cold-sensitive prohead accessory protein of bacteriophage ϕ X174. *Genetics* 128:663–71.
18. Fane BA, Head S, Hayashi M. 1992. Functional relationship between the J proteins of bacteriophages ϕ X174 and G4 during phage morphogenesis. *J Bacteriol* 174:2717–2719.
19. Bernhardt TG, Struck DK, Young R. 2001. The Lysis Protein E of ϕ X174 Is a Specific Inhibitor of the MraY-catalyzed Step in Peptidoglycan Synthesis. *J Biol Chem* 276:6093–6097.
20. Sanger F, Coulson AR, Friedmann T, Air GM, Barrell BG, Brown NL, Fiddes JC, Hutchison CA, Slocombe PM, Smith M. 1978. The nucleotide sequence of bacteriophage ϕ X174. *J Mol Biol* 125:225–246.
21. Fane BA, Shien S, Hayashi M. 1993. Second-site suppressors of a cold-sensitive external scaffolding protein of bacteriophage ϕ X174. *Genetics* 134:1003–11.
22. Burch AD, Ta J, Fane BA. 1999. Cross-functional analysis of the Microviridae internal scaffolding protein. *J Mol Biol* 286:95–104.

23. Uchiyama A, Fane BA. 2005. Identification of an Interacting Coat-External Scaffolding Protein Domain Required for both the Initiation of Φ X174 Procapsid Morphogenesis and the Completion of DNA Packaging. *J Virol* 79:6751–6756.
24. Cherwa JE, Sanchez-Soria P, Wichman HA, Fane BA. 2009. Viral Adaptation to an Antiviral Protein Enhances the Fitness Level to Above That of the Uninhibited Wild Type. *J Virol* 83:11746–11750.
25. Hafenstein SL, Chen M, Fane BA. 2004. Genetic and functional analyses of the ϕ X174 DNA binding protein: the effects of substitutions for amino acid residues that spatially organize the two DNA binding domains. *Virology* 318:204–213.
26. McKenna R, Bowman BR, Ilag LL, Rossmann MG, Fane BA. 1996. Atomic structure of the degraded procapsid particle of the bacteriophage G4: Induced structural changes in the presence of calcium ions and functional implications. *J Mol Biol* 256:736–750.
27. Cherwa JE, Young LN, Fane BA. 2011. Uncoupling the functions of a multifunctional protein: The isolation of a DNA pilot protein mutant that affects particle morphogenesis. *Virology* 411:9–14.
28. Young LN, Hockenberry AM, Fane BA. 2014. Mutations in the N Terminus of the Φ X174 DNA Pilot Protein H Confer Defects in both Assembly and Host Cell Attachment. *J Virol* 88:1787–1794.
29. Mano Y, Sakai H, Komano T. 1979. Growth and DNA synthesis of bacteriophage ϕ X174 in a dnaP mutant of *Escherichia coli*. *J Virol* 30:650–6.
30. Harbury P, Zhang T, Kim P, Alber T. 1993. A switch between two-, three-, and four-stranded coiled coils in GCN4 leucine zipper mutants. *Science* (80-) 262:1401–1407.
32. Bayer ME, Starkey TW. 1972. The adsorption of bacteriophage Φ X174 and its interaction with *Escherichia coli*; a kinetic and morphological study. *Virology* 49:236–256.
33. Spindler KR, Hayashi M. 1979. DNA synthesis in *Escherichia coli* cells infected with gene H mutants of bacteriophage ϕ X174. *J Virol* 29:973–82.
34. Dokland T, McKenna R, Llag LL, Bowman BR, Incardona NL, Fane BA, Rossmann MG. 1997. Structure of a viral procapsid with molecular scaffolding. *Nature* 389:308–313.
35. McKenna R, Xia D, Willingmann P, Ilag LL, Krishnaswamy S, Rossmann MG, Olson NH, Baker TS, Incardona NL. 1992. Atomic structure of single-stranded DNA bacteriophage phi X174 and its functional implications. *Nature* 355:137–43.

Chapter 3

1. Bauer DW, Huffman JB, Homa FL, Evilevitch A. 2013. Herpes Virus Genome, The Pressure Is On. *J Am Chem Soc* 135:11216–11221.
2. Molineux IJ, Panja D. 2013. Popping the cork: mechanisms of phage genome ejection. *Nat Rev Microbiol* 11:194–204.
3. Aksyuk AA, Leiman PG, Kurochkina LP, Shneider MM, Kostyuchenko VA, Mesyanzhinov V V., Rossmann MG. 2009. The tail sheath structure of bacteriophage T4: A molecular machine for infecting bacteria. *EMBO J* 28:821–829.
4. Fokine A, Rossmann MG. 2014. Molecular architecture of tailed double-stranded DNA phages. *Bacteriophage* 4:e28281.
5. Hu B, Margolin W, Molineux IJ, Liu J. 2013. The bacteriophage T7 virion undergoes extensive structural remodeling during infection. *Science* (80-) 339:576–579.
6. Cumby N, Reimer K, Mengin-Lecreulx D, Davidson AR, Maxwell KL. 2015. The phage tail tape measure protein, an inner membrane protein and a periplasmic chaperone play connected roles in the genome injection process of *E. coli* phage HK97. *Mol Microbiol* 96:437–447.
7. Jin Y, Sdao SM, Dover JA, Porcek NB, Knobler CM, Gelbart WM, Parent KN. 2015. Bacteriophage P22 ejects all of its internal proteins before its genome. *Virology* 485:128–134.
8. Dent KC, Thompson R, Barker AM, Hiscox JA, Barr JN, Stockley PG, Ranson NA. 2013. The Asymmetric Structure of an Icosahedral Virus Bound to Its Receptor Suggests a Mechanism for Genome Release. *Structure* 21:1225–1234.
9. Krahn PM, O’Callaghan RJ, Paranchych W. 1972. Stages in phage R17 infection VI. Injection of A Protein and RNA into the Host Cell. *Virology* 47:628–637.
10. Toropova K, Stockley PG, Ranson NA. 2011. Visualising a Viral RNA Genome Poised for Release from Its Receptor Complex. *J Mol Biol* 408:408–419.
11. Webster RE. 1996. Biology of the Filamentous Bacteriophage, p. 1–20. *In Phage Display of Peptides and Proteins: A Laboratory Manual*. Elsevier.
12. Bennett NJ, Rakonjac J. 2006. Unlocking of the Filamentous Bacteriophage Virion During Infection is Mediated by the C Domain of pIII. *J Mol Biol* 356:266–273.
13. Bennett NJ, Gagic D, Sutherland-Smith AJ, Rakonjac J. 2011. Characterization of

- a Dual-Function Domain That Mediates Membrane Insertion and Excision of Ff Filamentous Bacteriophage. *J Mol Biol* 411:972–985.
14. Sun Y, Roznowski AP, Tokuda JM, Klose T, Mauney A, Pollack L, Fane BA, Rossmann MG. 2017. Structural changes of tailless bacteriophage Φ X174 during penetration of bacterial cell walls. *Proc Natl Acad Sci* 114:13708–13713.
 15. Sun L, Young LN, Zhang X, Boudko SP, Fokine A, Zbornik E, Roznowski AP, Molineux IJ, Rossmann MG, Fane BA. 2014. Icosahedral bacteriophage Φ X174 forms a tail for DNA transport during infection. *Nature* 505:432–435.
 16. Cherwa JE, Young LN, Fane BA. 2011. Uncoupling the functions of a multifunctional protein: The isolation of a DNA pilot protein mutant that affects particle morphogenesis. *Virology* 411:9–14.
 17. Dokland T, Bernal RA, Burch A, Pletnev S, Fane BA, Rossmann MG. 1999. The role of scaffolding proteins in the assembly of the small, single-stranded DNA virus ϕ X174. *J Mol Biol* 288:595–608.
 18. Dokland T, McKenna R, Llag LL, Bowman BR, Incardona NL, Fane BA, Rossmann MG. 1997. Structure of a viral procapsid with molecular scaffolding. *Nature* 389:308–313.
 19. Ilag LL, Olson NH, Dokland T, Music CL, Cheng RH, Bowen Z, McKenna R, Rossmann MG, Baker TS, Incardona NL. 1995. DNA packaging intermediates of bacteriophage ϕ X174. *Structure* 3:353–363.
 20. Novak CR, Fane BA. 2004. The functions of the N terminus of the ϕ X174 internal scaffolding protein, a protein encoded in an overlapping reading frame in a two scaffolding protein system. *J Mol Biol* 335:383–390.
 21. Azuma J, Morita J, Komano T. 1980. Process of Attachment of Φ X174 Parental DNA to the Host Cell Membrane. *J Biochem* 88:525–532.
 22. Mano Y, Sakai H, Komano T. 1979. Growth and DNA synthesis of bacteriophage ϕ X174 in a dnaP mutant of *Escherichia coli*. *J Virol* 30:650–6.
 23. Murakami Y, Nagata T, Schwarz W, Wada C, Yura T. 1985. Novel dnaG mutation in a dnaP mutant of *Escherichia coli*. *J Bacteriol* 162:830–2.
 24. Conley MJ, McElwee M, Azmi L, Gabrielsen M, Byron O, Goodfellow IG, Bhella D. 2019. Calicivirus VP2 forms a portal-like assembly following receptor engagement. *Nature* 565:377–381.
 25. Shepard W, Cruse WBT, Fourme R, De La Fortelle E, Prangé T. 1998. A zipper-like duplex in DNA: The crystal structure of d(GCGAAAGCT) at 2.1 Å

- resolution. *Structure* 6:849–861.
26. Luscombe NM. 2001. Amino acid-base interactions: a three-dimensional analysis of protein-DNA interactions at an atomic level. *Nucleic Acids Res* 29:2860–2874.
 27. Luscombe NM, Thornton JM. 2002. Protein–DNA Interactions: Amino Acid Conservation and the Effects of Mutations on Binding Specificity. *J Mol Biol* 320:991–1009.
 28. Mandel-Gutfreund Y, Schueler O, Margalit H. 1995. Comprehensive Analysis of Hydrogen Bonds in Regulatory Protein DNA-Complexes: In Search of Common Principles. *J Mol Biol* 253:370–382.
 29. Suzuki M. 1994. A framework for the DNA–protein recognition code of the probe helix in transcription factors: the chemical and stereochemical rules. *Structure* 2:317–326.
 30. Rokyta DR, Burch CL, Caudle SB, Wichman H a. 2006. Horizontal Gene Transfer and the Evolution of Microvirid Coliphage Genomes. *J Bacteriol* 188:1134–1142.
 31. Simossis VA, Heringa J. 2005. PRALINE: a multiple sequence alignment toolbox that integrates homology-extended and secondary structure information. *Nucleic Acids Res* 33:W289–W294.
 32. Simossis VA. 2005. Homology-extended sequence alignment. *Nucleic Acids Res* 33:816–824.
 33. Roznowski AP, Fane BA. 2016. Structure-Function Analysis of the Φ X174 DNA-Piloting Protein Using Length-Altering Mutations. *J Virol* 90:7956–7966.
 34. Young LN, Hockenberry AM, Fane BA. 2014. Mutations in the N Terminus of the Φ X174 DNA Pilot Protein H Confer Defects in both Assembly and Host Cell Attachment. *J Virol* 88:1787–1794.
 35. Ilag LL, McKenna R, Yadav MP, BeMiller JN, Incardona NL, Rossmann MG. 1994. Calcium Ion-induced Structural Changes in Bacteriophage ϕ X174. *J Mol Biol* 244:291–300.
 36. Ruboyianes M V, Chen M, Dubrava MS, Cherwa JE, Fane BA. 2009. The Expression of N-Terminal Deletion DNA Pilot Proteins Inhibits the Early Stages of Φ X174 Replication. *J Virol* 83:9952–9956.
 37. Boulanger P, Letellier L. 1992. Ion channels are likely to be involved in the two steps of phage T5 DNA penetration into *Escherichia coli* cells. *J Biol Chem* 267:3168–72.

38. Keweloh H, Bakker EP. 1984. Permeability changes in the cytoplasmic membrane of *Escherichia coli* K-12 early after infection with bacteriophage T1. *J Bacteriol* 160:347–353.
39. Roznowski AP, Young RJ, Love SD, Andromita AA, Guzman VA, Wilch MH, Block A, McGill A, Lavelle M, Romanova A, Sekiguchi A, Wang M, Burch AD, Fane BA. 2018. Recessive Host Range Mutants and Unsusceptible Cells That Inactivate Virions without Genome Penetration: Ecological and Technical Implications. *J Virol* 93:1–16.
40. Jazwinski SM, Marco R, Kornberg A. 1975. The gene H spike protein of bacteriophages ϕ X174 and S13. II. Relation to synthesis of the parental replicative form. *Virology* 66:294–305.
41. Morein S, Henricson D, Rilfors L. 1994. Separation of Inner and Outer Membrane Vesicles from *Escherichia coli* in Self-Generating Percoll Gradients. *Anal Biochem* 216:47–51.
42. Luria S, Delbrück M. 1943. Mutations of Bacteria from Virus Sensitivity to Virus Resistance. *Genetics* 28:491–511.
43. Fane BA, Hayashi M. 1991. Second-site suppressors of a cold-sensitive prohead accessory protein of bacteriophage ϕ X174. *Genetics* 128:663–71.
44. Fane BA, Shien S, Hayashi M. 1993. Second-site suppressors of a cold-sensitive external scaffolding protein of bacteriophage ϕ X174. *Genetics* 134:1003–11.
45. Gordon EB, Fane BA. 2013. Effects of an Early Conformational Switch Defect during Φ X174 Morphogenesis Are Belatedly Manifested Late in the Assembly Pathway. *J Virol* 87:2518–2525.
46. Gordon EB, Knuff CJ, Fane BA. 2012. Conformational Switch-Defective ϕ X174 Internal Scaffolding Proteins Kinetically Trap Assembly Intermediates before Procapsid Formation. *J Virol* 86:9911–9918.
47. Floor E. 1970. Interaction of morphogenetic genes of bacteriophage T4. *J Mol Biol* 47:293–306.
48. Sternberg N. 1976. A genetic analysis of bacteriophage λ head assembly. *Virology* 71:568–582.
49. Van Valen D, Wu D, Chen Y-J, Tuson H, Wiggins P, Phillips R. 2012. A Single-Molecule Hershey-Chase Experiment. *Curr Biol* 22:1339–1343.
50. García LR, Molineux IJ. 1995. Incomplete entry of bacteriophage T7 DNA into F plasmid-containing *Escherichia coli*. *J Bacteriol* 177:4077–4083.

51. Lanni YT. 1968. First-step-transfer deoxyribonucleic acid of bacteriophage T5. *Bacteriol Rev* 32:227–42.
52. Lanni YT. 1965. DNA transfer from phage T5 to host cells: dependence on intercurrent protein synthesis. *Proc Natl Acad Sci* 53:969–973.
53. Moffatt BA, Studier FW. 1988. Entry of bacteriophage T7 DNA into the cell and escape from host restriction. *J Bacteriol* 170:2095–2105.
54. Fane BA, Head S, Hayashi M. 1992. Functional relationship between the J proteins of bacteriophages ϕ X174 and G4 during phage morphogenesis. *J Bacteriol* 174:2717–2719.
55. Bernhardt TG, Struck DK, Young R. 2001. The Lysis Protein E of ϕ X174 Is a Specific Inhibitor of the MraY-catalyzed Step in Peptidoglycan Synthesis. *J Biol Chem* 276:6093–6097.
56. Burch AD, Ta J, Fane BA. 1999. Cross-functional analysis of the Microviridae internal scaffolding protein. *J Mol Biol* 286:95–104.
57. Uchiyama A, Fane BA. 2005. Identification of an Interacting Coat-External Scaffolding Protein Domain Required for both the Initiation of Φ X174 Procapsid Morphogenesis and the Completion of DNA Packaging. *J Virol* 79:6751–6756.
58. Cherwa JE, Sanchez-Soria P, Wichman HA, Fane BA. 2009. Viral Adaptation to an Antiviral Protein Enhances the Fitness Level to Above That of the Uninhibited Wild Type. *J Virol* 83:11746–11750.
59. Hafenstein SL, Chen M, Fane BA. 2004. Genetic and functional analyses of the ϕ X174 DNA binding protein: the effects of substitutions for amino acid residues that spatially organize the two DNA binding domains. *Virology* 318:204–213.
60. Karkhanis YD, Zeltner JY, Jackson JJ, Carlo DJ. 1978. A new and improved microassay to determine 2-keto-3-deoxyoctonate in lipopolysaccharide of gram-negative bacteria. *Anal Biochem* 85:595–601.

Chapter 4

1. Leiman PG, Chipman PR, Kostyuchenko VA, Mesyanzhinov VV, Rossmann MG. 2004. Three-dimensional rearrangement of proteins in the tail of bacteriophage T4 on infection of its host. *Cell* 118:419-29.
2. Belnap DM, Filman DJ, Trus BL, Cheng N, Booy FP, Conway JF, Curry S, Hiremath CN, Tsang SK, Steven AC, Hogle JM. 2000. Molecular tectonic model

- of virus structural transitions: the putative cell entry states of poliovirus. *J Virol* 74:1342-54.
3. Bubeck D, Filman DJ, Cheng N, Steven AC, Hogle JM, Belnap DM. 2005. The structure of the poliovirus 135S cell entry intermediate at 10-angstrom resolution reveals the location of an externalized polypeptide that binds to membranes. *J Virol* 79:7745-55.
 4. Hu B, Margolin W, Molineux IJ, Liu J. 2013. The bacteriophage t7 virion undergoes extensive structural remodeling during infection. *Science* 339:576-9.
 5. Cotmore SF, Tattersall P. 2007. Parvoviral host range and cell entry mechanisms. *Adv Virus Res* 70:183-232.
 6. Lee H, Shingler KL, Organtini LJ, Ashley RE, Makhov AM, Conway JF, Hafenstein S. 2016. The novel asymmetric entry intermediate of a picornavirus captured with nanodiscs. *Sci Adv* 2:e1501929.
 7. Hueffer K, Parker JS, Weichert WS, Geisel RE, Sgro JY, Parrish CR. 2003. The natural host range shift and subsequent evolution of canine parvovirus resulted from virus-specific binding to the canine transferrin receptor. *J Virol* 77:1718-26.
 8. Duffy S, Turner PE, Burch CL. 2006. Pleiotropic costs of niche expansion in the RNA bacteriophage phi 6. *Genetics* 172:751-7.
 9. Ford BE, Sun B, Carpino J, Chapler ES, Ching J, Choi Y, Jhun K, Kim JD, Lalloo GG, Morgenstern R, Singh S, Theja S, Dennehy JJ. 2014. Frequency and fitness consequences of bacteriophage phi6 host range mutations. *PLoS One* 9:e113078.
 10. Tetart F, Repoila F, Monod C, Krisch HM. 1996. Bacteriophage T4 host range is expanded by duplications of a small domain of the tail fiber adhesin. *J Mol Biol* 258:726-31.
 11. Yosef I, Goren MG, Globus R, Molshanski-Mor S, Qimron U. 2017. Extending the Host Range of Bacteriophage Particles for DNA Transduction. *Mol Cell* 66:721-728 e3.
 12. Bertozzi Silva J, Storms Z, Sauvageau D. 2016. Host receptors for bacteriophage adsorption. *FEMS Microbiol Lett* 363.
 13. Mindich L, Bamford D, McGraw T, Mackenzie G. 1982. Assembly of bacteriophage PRD1: particle formation with wild-type and mutant viruses. *J Virol* 44:1021-30.
 14. Mindich L, Sinclair JF, Cohen J. 1976. The morphogenesis of bacteriophage phi6: particles formed by nonsense mutants. *Virology* 75:224-31.

15. Mindich L, Sinclair JF, Levine D, Cohen J. 1976. Genetic studies of temperature-sensitive and nonsense mutants of bacteriophage phi6. *Virology* 75:218-23.
16. Stengele I, Bross P, Garces X, Giray J, Rasched I. 1990. Dissection of functional domains in phage fd adsorption protein. Discrimination between attachment and penetration sites. *J Mol Biol* 212:143-9.
17. Baptista C, Santos MA, Sao-Jose C. 2008. Phage SPP1 reversible adsorption to *Bacillus subtilis* cell wall teichoic acids accelerates virus recognition of membrane receptor YueB. *J Bacteriol* 190:4989-96.
18. McPartland J, Rothman-Denes LB. 2009. The tail sheath of bacteriophage N4 interacts with the *Escherichia coli* receptor. *J Bacteriol* 191:525-32.
19. Parent KN, Erb ML, Cardone G, Nguyen K, Gilcrease EB, Porcek NB, Pogliano J, Baker TS, Casjens SR. 2014. OmpA and OmpC are critical host factors for bacteriophage Sf6 entry in *Shigella*. *Mol Microbiol* 92:47-60.
20. Meyer JR, Dobias DT, Weitz JS, Barrick JE, Quick RT, Lenski RE. 2012. Repeatability and contingency in the evolution of a key innovation in phage lambda. *Science* 335:428-32.
21. Michel A, Clermont O, Denamur E, Tenaillon O. 2010. Bacteriophage PhiX174's ecological niche and the flexibility of its *Escherichia coli* lipopolysaccharide receptor. *Appl Environ Microbiol* 76:7310-3.
22. Weisbeek PJ, van de Pol JH, van Arkel GA. 1973. Mapping of host range mutants of bacteriophage phiX174. *Virology* 52:408-16.
23. Sinsheimer RL. 1968. Bacteriophage phi-X174 and related viruses. *Prog Nucleic Acid Res Mol Biol* 8:115-69.
24. Tessman ES. 1965. Complementation Groups in Phage S13. *Virology* 25:303-21.
25. Bone DR, Dowell CE. 1973. A mutant of bacteriophage phiX174 which infects *E. coli* K12 strains. I. Isolation and partial characterization of phiXtB. *Virology* 52:319-29.
26. Cox J, Putonti C. 2010. Mechanisms responsible for a PhiX174 mutant's ability to infect *Escherichia coli* by phosphorylation. *J Virol* 84:4860-3.
27. Newbold JE, Sinsheimer RL. 1970. The process of infection with bacteriophage phiX174. XXXII. Early steps in the infection process: attachment, eclipse and DNA penetration. *J Mol Biol* 49:49-66.

28. Sun L, Rossmann MG, Fane BA. 2014. High-resolution structure of a virally encoded DNA-translocating conduit and the mechanism of DNA penetration. *J Virol* 88:10276-9.
29. Sun L, Young LN, Zhang X, Boudko SP, Fokine A, Zbornik E, Roznowski AP, Molineux I, Rossmann MG, Fane BA. 2014. Icosahedral Φ X174 forms a tail for DNA transport. *Nature* 505:432-5.
30. Sun Y, Roznowski AP, Tokuda JM, Klose T, Mauney A, Pollack L, Fane BA, Rossmann MG. 2017. Structural changes of tailless bacteriophage PhiX174 during penetration of bacterial cell walls. *Proc Natl Acad Sci U S A* 114:13708-13713.
31. McKenna R, Ilag LL, Rossmann MG. 1994. Analysis of the single-stranded DNA bacteriophage phi X174, refined at a resolution of 3.0 Å. *J Mol Biol* 237:517-43.
32. McKenna R, Xia D, Willingmann P, Ilag LL, Krishnaswamy S, Rossmann MG, Olson NH, Baker TS, Incardona NL. 1992. Atomic structure of single-stranded DNA bacteriophage phi X174 and its functional implications. *Nature* 355:137-43.
33. Ilag LL, McKenna R, Yadav MP, BeMiller JN, Incardona NL, Rossmann MG. 1994. Calcium ion-induced structural changes in bacteriophage phi X174. *J Mol Biol* 244:291-300.
34. Rokyta DR, Burch CL, Caudle SB, Wichman HA. 2006. Horizontal gene transfer and the evolution of microvirid coliphage genomes. *J Bacteriol* 188:1134-42.
35. Sandulache R, Prehm P, Kamp D. 1984. Cell wall receptor for bacteriophage Mu G(+). *J Bacteriol* 160:299-303.
36. Bowes JM, Dowell CE. 1974. Purification and some properties of bacteriophage ST-1. *J Virol* 13:53-61.
37. Fane BA, Hayashi M. 1991. Second-site suppressors of a cold-sensitive prohead accessory protein of bacteriophage phi X174. *Genetics* 128:663-71.
38. Fane BA, Head S, Hayashi M. 1992. Functional relationship between the J proteins of bacteriophages phi X174 and G4 during phage morphogenesis. *J Bacteriol* 174:2717-9.
39. Bernhardt TG, Struck DK, Young R. 2001. The lysis protein E of phi X174 is a specific inhibitor of the MraY-catalyzed step in peptidoglycan synthesis. *J Biol Chem* 276:6093-7.
40. Moak M, Molineux IJ. 2000. Role of the Gp16 lytic transglycosylase motif in bacteriophage T7 virions at the initiation of infection. *Mol Microbiol* 37:345-55.

41. Daniel AS, Fuller-Pace FV, Legge DM, Murray NE. 1988. Distribution and diversity of hsd genes in *Escherichia coli* and other enteric bacteria. *J Bacteriol* 170:1775-82.
42. Kodaira K, Nakano K, Okada S, Taketo A. 1992. Nucleotide sequence of the genome of the bacteriophage alpha 3: interrelationship of the genome structure and the gene products with those of the phages, phi X174, G4 and phi K. *Biochim Biophys Acta* 1130:277-88.
43. Blackburn BJ, Li S, Roznowski AP, Perez AR, Villarreal RH, Johnson CJ, Hardy M, Tuckerman EC, Burch AD, Fane BA. 2017. Coat protein mutations that alter the flux of morphogenetic intermediates through the phiX174 early assembly pathway. *J Virol* doi:JVI.01384-17 [pii]
44. Cherwa JE, Jr., Sanchez-Soria P, Wichman HA, Fane BA. 2009. Viral adaptation to an antiviral protein enhances the fitness level to above that of the uninhibited wild type. *J Virol* 83:11746-50.
45. Hafenstein SL, Chen M, Fane BA. 2004. Genetic and functional analyses of the oX174 DNA binding protein: the effects of substitutions for amino acid residues that spatially organize the two DNA binding domains. *Virology* 318:204-13.
46. Cumby N, Reimer K, Mengin-Lecreulx D, Davidson AR, Maxwell KL. 2015. The phage tail tape measure protein, an inner membrane protein and a periplasmic chaperone play connected roles in the genome injection process of *E. coli* phage HK97. *Mol Microbiol* 96:437-47.
47. Boulanger P, Letellier L. 1992. Ion Channels Are Likely to Be Involved in the 2 Steps of Phage-T5 DNA Penetration into *Escherichia-Coli*-Cells. *Journal of Biological Chemistry* 267:3168-3172.
48. Letellier L, Plancon L, Bonhivers M, Boulanger P. 1999. Phage DNA transport across membranes. *Res Microbiol* 150:499-505.
49. Newbold JE, Sinsheimer RL. 1970. Process of infection with bacteriophage phi-X174. XXXIV. Kinetic of the attachment and eclipse steps of the infection. *J Virol* 5:427-31.
50. Boulanger P, Letellier L. 1992. Ion channels are likely to be involved in the two steps of phage T5 DNA penetration into *Escherichia coli* cells. *J Biol Chem* 267:3168-72.
51. A. ZA. 1972. Protein volume in solution. *Prog Biophys Mol Biol* 24:107-123.

52. Cherwa JE, Jr., Fane BA. 2009. Complete virion assembly with scaffolding proteins altered in the ability to perform a critical conformational switch. *J Virol* 83:7391-6.
53. Cherwa JE, Jr., Uchiyama A, Fane BA. 2008. Scaffolding proteins altered in the ability to perform a conformational switch confer dominant lethal assembly defects. *J Virol* 82:5774-80.
54. Doore SM, Baird CD, Roznowski AP, Fane BA. 2014. The evolution of genes within genes and the control of DNA replication in microviruses. *Mol Biol Evol* 31:1421-31.
55. Gordon EB, Knuff CJ, Fane BA. 2012. Conformational Switch-Defective ϕ X174 Internal Scaffolding Proteins Kinetically Trap Assembly Intermediates before Procapsid Formation. *J Virol* 86:9911-8.
56. Roznowski AP, Fane BA. 2016. Structure-Function Analysis of the φ X174 DNA-Piloting Protein Using Length-Altering Mutations. *J Virol* 90:7956-66.
57. Uchiyama A, Chen M, Fane BA. 2007. Characterization and function of putative substrate specificity domain in microvirus external scaffolding proteins. *J Virol* 81:8587-92.
58. Bernal RA, Hafenstein S, Olson NH, Bowman VD, Chipman PR, Baker TS, Fane BA, Rossmann MG. 2003. Structural studies of bacteriophage alpha3 assembly. *J Mol Biol* 325:11-24.
59. Holland JJ, de la Torre JC, Steinhauer DA, Clarke D, Duarte E, Domingo E. 1989. Virus mutation frequencies can be greatly underestimated by monoclonal antibody neutralization of virions. *J Virol* 63:5030-6.
60. Hutchison CA, 3rd, Sinsheimer RL. 1971. Requirement of protein synthesis for bacteriophage phi X174 superinfection exclusion. *J Virol* 8:121-4.
61. van der Avoort HG, van Arkel GA, Weisbeek PJ. 1982. Cloned bacteriophage phi X174 DNA sequence interferes with synthesis of the complementary strand of infecting bacteriophage phi X174. *J Virol* 42:1-11.
62. Crill WD, Wichman HA, Bull JJ. 2000. Evolutionary reversals during viral adaptation to alternating hosts. *Genetics* 154:27-37.
63. Pettersen EF, Goddard TD, Huang CC, Couch GS, Greenblatt DM, Meng EC, Ferrin TE. 2004. UCSF Chimera--a visualization system for exploratory research and analysis. *J Comput Chem* 25:1605-12.

Chapter 5

1. Sun L, Zhang X, Gao S, Rao PA, Padilla-Sanchez V, Chen Z, Sun S, Xiang Y, Subramaniam S, Rao VB, Rossmann MG. 2015. Cryo-EM structure of the bacteriophage T4 portal protein assembly at near-atomic resolution. *Nat Commun* 6:1–11.
2. Olia AS, Prevelige PE, Johnson JE, Cingolani G. 2011. Three-dimensional structure of a viral genome-delivery portal vertex. *Nat Struct Mol Biol* 18:597–603.
3. Casjens SR. 2011. The DNA-packaging nanomotor of tailed bacteriophages. *Nat Rev Microbiol* 9:647–657.
4. Rajagopala S V, Casjens S, Uetz P. 2011. The protein interaction map of bacteriophage lambda. *BMC Microbiol* 11:213.
5. Kikuchi Y, King J. 1975. Assembly of the tail of bacteriophage T4. *J Supramol Struct* 3:24–38.
6. Rochat RH, Liu X, Murata K, Nagayama K, Rixon FJ, Chiu W. 2011. Seeing the Portal in Herpes Simplex Virus Type 1 B Capsids. *J Virol* 85:1871–1874.
7. Bauer DW, Li D, Huffman J, Homa FL, Wilson K, Leavitt JC, Casjens SR, Baines J, Evilevitch A. 2015. Exploring the Balance between DNA Pressure and Capsid Stability in Herpesviruses and Phages. *J Virol* 89:9288–9298.
8. Newcomb WW, Juhas RM, Thomsen DR, Homa FL, Burch AD, Weller SK, Brown JC. 2001. The UL6 Gene Product Forms the Portal for Entry of DNA into the Herpes Simplex Virus Capsid. *J Virol* 75:10923–10932.
9. Chang JT, Schmid MF, Rixon FJ, Chiu W. 2007. Electron Cryotomography Reveals the Portal in the Herpesvirus Capsid. *J Virol* 81:2065–2068.
10. Connolly SA, Jackson JO, Jardetzky TS, Longnecker R. 2011. Fusing structure and function: a structural view of the herpesvirus entry machinery. *Nat Rev Microbiol* 9:369–381.
11. Ojala PM, Sodeik B, Ebersold MW, Kutay U, Helenius A. 2000. Herpes Simplex Virus Type 1 Entry into Host Cells: Reconstitution of Capsid Binding and Uncoating at the Nuclear Pore Complex In Vitro. *Mol Cell Biol* 20:4922–4931.
12. Padeloup D, Blondel D, Isidro AL, Rixon FJ. 2009. Herpesvirus Capsid Association with the Nuclear Pore Complex and Viral DNA Release Involve the Nucleoporin CAN/Nup214 and the Capsid Protein pUL25. *J Virol* 83:6610–6623.

13. Shahin V, Hafezi W, Oberleithner H, Ludwig Y, Windoffer B, Schillers H, Kuhn JE. 2006. The genome of HSV-1 translocates through the nuclear pore as a condensed rod-like structure. *J Cell Sci* 119:23–30.
14. Belnap DM, McDermott BM, Filman DJ, Cheng N, Trus BL, Zuccola HJ, Racaniello VR, Hogle JM, Steven a C. 2000. Three-dimensional structure of poliovirus receptor bound to poliovirus. *Proc Natl Acad Sci* 97:73–78.
15. Brandenburg B, Lee LY, Lakadamyali M, Rust MJ, Zhuang X, Hogle JM. 2007. Imaging Poliovirus Entry in Live Cells. *PLoS Biol* 5:e183.
16. Belnap DM, Filman DJ, Trus BL, Cheng N, Booy FP, Conway JF, Curry S, Hiremath CN, Tsang SK, Steven AC, Hogle JM. 2000. Molecular Tectonic Model of Virus Structural Transitions: the Putative Cell Entry States of Poliovirus. *J Virol* 74:1342–1354.
17. Strauss M, Schotte L, Karunatilaka KS, Filman DJ, Hogle JM. 2017. Cryo-electron Microscopy Structures of Expanded Poliovirus with VHHs Sample the Conformational Repertoire of the Expanded State. *J Virol* 91:1–22.
18. Gropelli E, Levy HC, Sun E, Strauss M, Nicol C, Gold S, Zhuang X, Tuthill TJ, Hogle JM, Rowlands DJ. 2017. Picornavirus RNA is protected from cleavage by ribonuclease during virion uncoating and transfer across cellular and model membranes. *PLOS Pathog* 13:e1006197.
19. Danthi P, Tosteson M, Li Q -h., Chow M. 2003. Genome Delivery and Ion Channel Properties Are Altered in VP4 Mutants of Poliovirus. *J Virol* 77:5266–5274.
20. Fricks CE, Hogle JM. 1990. Cell-induced conformational change in poliovirus: externalization of the amino terminus of VP1 is responsible for liposome binding. *J Virol* 64:1934–45.
21. Hogle J, Chow M, Filman D. 1985. Three-dimensional structure of poliovirus at 2.9 Å resolution. *Science* (80-) 229:1358–1365.
22. Sun Y, Roznowski AP, Tokuda JM, Klose T, Mauney A, Pollack L, Fane BA, Rossmann MG. 2017. Structural changes of tailless bacteriophage Φ X174 during penetration of bacterial cell walls. *Proc Natl Acad Sci* 114:13708–13713.
23. Ilag LL, Olson NH, Dokland T, Music CL, Cheng RH, Bowen Z, McKenna R, Rossmann MG, Baker TS, Incardona NL. 1995. DNA packaging intermediates of bacteriophage ϕ X174. *Structure* 3:353–363.

24. Dokland T, Bernal RA, Burch A, Pletnev S, Fane BA, Rossmann MG. 1999. The role of scaffolding proteins in the assembly of the small, single-stranded DNA virus ϕ X174. *J Mol Biol* 288:595–608.
25. Cheng N, Wu W, Watts NR, Steven AC. 2014. Exploiting radiation damage to map proteins in nucleoprotein complexes: The internal structure of bacteriophage T7. *J Struct Biol* 185:250–256.
26. Cheng N, Wu W, Steven AC, Thomas J, Black L. 2012. Bubblegrams reveal the inner body of bacteriophage phiKZ. *Microsc Microanal* 18:112–113.
27. Suzuki R, Inagaki M, Karita S, Kawaura T, Kato M, Nishikawa S, Kashimura N, Morita J. 1999. Specific interaction of fused H protein of bacteriophage ϕ X174 with receptor lipopolysaccharides. *Virus Res* 60:95–99.
28. Nishikawa S. 2000. Characterization of the Binding of spike H Protein of Bacteriophage phiX174 with Receptor Lipopolysaccharides 127:577–583.
29. Young LN, Hockenberry AM, Fane BA. 2014. Mutations in the N Terminus of the Φ X174 DNA Pilot Protein H Confer Defects in both Assembly and Host Cell Attachment. *J Virol* 88:1787–1794.
30. Bernal RA, Hafenstein S, Esmeralda R, Fane BA, Rossmann MG. 2004. The ϕ X174 protein J mediates DNA packaging and viral attachment to host cells. *J Mol Biol* 337:1109–1122.
31. Ruboyianes M V, Chen M, Dubrava MS, Cherwa JE, Fane BA. 2009. The Expression of N-Terminal Deletion DNA Pilot Proteins Inhibits the Early Stages of Φ X174 Replication. *J Virol* 83:9952–9956.
32. Hayashi M, Aoyama A, Richardson DL, Hayashi MN. 1988. Biology of the Bacteriophage ϕ X174, p. 1–71. *In* Calendar, R (ed.), *The Bacteriophages Volume 2*. Plenum Publishing Corporation, New York.
33. Molineux IJ, Panja D. 2013. Popping the cork: mechanisms of phage genome ejection. *Nat Rev Microbiol* 11:194–204.
34. Grayson P, Evilevitch A, Inamdar MM, Purohit PK, Gelbart WM, Knobler CM, Phillips R. 2006. The effect of genome length on ejection forces in bacteriophage lambda. *Virology* 348:430–436.
35. Lemay SG, Panja D, Molineux IJ. 2013. Role of osmotic and hydrostatic pressures in bacteriophage genome ejection. *Phys Rev E* 87:022714.
36. Aoyama A, Hayashi M. 1985. Effects of genome size on bacteriophage Φ X174 DNA packaging in vitro. *J Biol Chem* 260:11033–11038.

37. Russell PW, Muller UR. 1984. Construction of Bacteriophage phiX174 Mutants with Maximum Genome Sizes. *J Virol* 52:822–827.
38. Conley MJ, McElwee M, Azmi L, Gabrielsen M, Byron O, Goodfellow IG, Bhella D. 2019. Calicivirus VP2 forms a portal-like assembly following receptor engagement. *Nature* 565:377–381.
39. Sun L, Young LN, Zhang X, Boudko SP, Fokine A, Zbornik E, Roznowski AP, Molineux IJ, Rossmann MG, Fane BA. 2014. Icosahedral bacteriophage Φ X174 forms a tail for DNA transport during infection. *Nature* 505:432–435.
40. Lokareddy RK, Sankhala RS, Roy A, Afonine P V., Motwani T, Teschke CM, Parent KN, Cingolani G. 2017. Portal protein functions akin to a DNA-sensor that couples genome-packaging to icosahedral capsid maturation. *Nat Commun* 8:14310.
41. Zheng W, Wang F, Taylor NMI, Guerrero-Ferreira RC, Leiman PG, Egelman EH. 2017. Refined Cryo-EM Structure of the T4 Tail Tube: Exploring the Lowest Dose Limit. *Structure* 25:1436–1441.e2.